High throughput toxicity, physiological and metabolic studies for the characterization of hepatocytes and human embryonic stem cell derived hepatocyte-like cells

Dissertation
zur Erlangung des Grades
des Doktors der Ingenieurwissenschaften
der Naturwissenschaftlich-Technischen Fakultät III
Chemie, Pharmazie, Bio- und Werkstoffwissenschaften
der Universität des Saarlandes

von

Simone Beckers

Saarbrücken
2010

Tag des Kolloquiums: 18.03.2011

Dekan: Prof. Dr. S. Diebels

Berichterstatter: Prof. Dr. E. Heinzle

        Prof. Dr. C.-M. Lehr

Vorsitz: Prof. Dr. R.W. Hartmann

Akad. Mitarbeiter: Dr. N. Günnewich

"*A theory is something nobody believes, except the person who made it. An experiment is something everybody believes, except the person who made it.*"

Albert Einstein (1879 - 1955)

"*There is nothing like looking, if you want to find something. You certainly usually find something, if you look, but it is not always quite the something you were after.*"

John Ronald Reuel Tolkien (1892 - 1973)

Acknowledgements

Table of Content

Abstract

A dynamic respiration assay based on luminescence decay time detection of oxygen for high throughput toxicological assessment is presented. The method applies 24-well plates (OxoDishes). Dissolved oxygen concentration is measured by a SensorDishReader reading the oxygen sensor optodes immobilized in the centre of each well. This method allows LC_{50} calculations and recording of toxicokinetic profiles. Adherent primary rat hepatocytes and Hep G2 cell line were exposed to known toxic compounds. The novel assay showed to be robust, flexible and an improvement to current methods.

Three human embryonic stem cell (hESC) lines, which have been directed towards hepatocyte-like cells were characterized and compared to Hep G2 cells and primary human hepatocytes for evaluation of their application for predictive toxicity testing and drug metabolism studies. In multi-well plate formats, repeatedly cells were identified to be hepatocyte-like by morphologic evaluation. Gene expression of liver specific genes and hepatic lineage markers were evaluated. The cells showed functional hepatic characteristics, such as albumin secretion, glycogen storage and urea synthesis. Phase I and phase II metabolism of midazolam, phenacetin and diclofenac was detected for the respective metabolites and the toxicity to diclofenac was confirmed by a toxicodynamics study. The characterization results described here provide a unique overview of the functionality of hESC derived hepatocytes.

Multiple physiological and ^{13}C-labeling studies on hESC derived hepatocytes-like cells and primary human hepatocytes, exposed to sub-toxic diclofenac concentrations were performed to identify metabolic pathways. In addition, their response to drug treatment was evaluated. Glycolysis, TCA cycle, amino acid degradation, albumin synthesis and pyruvate (re)cycling were considered for a stoichiometric metabolic flux model. MFA analysis revealed influence of sub-toxic diclofenac concentrations on the oxidative phosphorylation pathway.

Zusammenfassung

Eine dynamische Hochdurchsatz-Methode zur Bestimmung von Toxizität mittels Messung der Respiration via Lumineszenz-Abklingzeit wurde in dieser Arbeit präsentiert. Hierfür wurden 24-well Platten (OxoDishes) verwendet, die mit Hilfe eines SensorDishReaders die Messung der Gelöst-Sauerstoffkonzentrationen in Kulturmedium mittels immobilisierten Sensoroptoden ermöglichen. Hierdurch konnten LC_{50}-Werte errechnet und toxikokinetische Profile erstellt werden. Es wurde gezeigt, dass diese neue Methode robust, flexibel und eine Verbesserung zu derzeitigen Methoden darstellt.

Drei von humanen embryonalen Stammzellen (hESC) abgeleitete Hepatozyt-ähnliche Zellenlinien wurden charakterisiert und mit Hep G2 Zellen und primären Humanhepatozyten verglichen. Diese Studie wurde durchgeführt um die Anwendung dieser Zellen für prädiktive Toxizitäts- und Metabolismusstudien zu evaluieren. Hepatozyt-ähnliche Zellen konnten anhand ihrer Morphologie wiederholt identifiziert werden. Leberspezifische Genexpression und typische hepatische Charakteristika wie Albuminsynthese, Glykogenspeicherung und Harnstoffsynthese wurden identifiziert. Funktionelle Biotransformation der Medikamente Midazolam, Phenacetin und Diclofenac wurde anhand ihrer Metaboliten gezeigt und Diclofenactoxizität wurde zudem durch eine toxikodynamische Studie belegt. Die Ergebnisse der hier gezeigten Charakterisierungsstudie bieten einen Überblick über die Funktionalität der von Stammzellen abgleitenden Hepatozyten.

Physiologische und ^{13}C-Markierungsstudien wurden an hESC abgeleiteten Hepatozyt-ähnlichen Zellen und primären Humanhepatozyten durchgeführt, die subtoxischen Konzentrationen von Diclofenac ausgesetzt waren, um metabolische Stoffwechselwege und deren Störung in Erwiderung zur Medikamentierung zu identifizieren. Glykolyse, TCA-Zyklus, Aminosäureabbau, Albuminsynthese und Pyruvatzyklen wurden für ein stoichiometrisches metabolisches Flussmodel verwendet. Mittels metabolischer Flussanalyse konnte der Einfluss von subtoxischen Diclofenac-Konzentrationen auf die Atmungskette gezeigt werden.

1 Introduction

1.1 General Introduction

Pharmaceutical companies invest up to $ 800 million prior to approval for each new drug developed (DiMasi et al., 2003). The high costs arise from the tedious development process and the high failure/attrition rate of chemical and biopharmaceutical entities in late clinical trial phases (DiMasi et al., 2003; Li, 2005). This high attrition rate results from a lack of both efficiency (about 30% of failure) as well as toxicological and clinical safety (accounting for further 30% of failure) (Kola and Landis, 2004). Drugs can also cause liver injuries, at which 20-40 % of all drug induced reported cases lead to fulminant hepatic failure. In this connection 75 % of idiosyncratic reactions lead to liver transplantation or death (Mehta et al., 2008). Since most pre-clinical test models used for predictability of drugs are of non-human origin, adverse effects of compounds in man are not revealed until late stage clinical phases or even after entering the market (Jensen et al., 2009). Some drugs, such as bromfenac and troglitazone, which caused idiosyncratic injuries, had to be withdrawn from the market after new drug application (NDA) approval. They caused liver injuries to patients and major losses to the companies due to loss of momentum in research after investments in late clinical phases (Alden et al., 2003; Jensen et al., 2009). Hence, there is a high demand for predictive pre-clinical *in vitro* tools and models that can reduce late-stage attritions as well as hinder potentially harming molecules from entering clinical phase studies (Jensen et al., 2009). Current *in vitro* models do not completely mimic the complexity of the liver. Even primary human hepatocytes are not the optimal *in vitro* model, since they lose their metabolic activity within days, are donor specific and their availability is scarce (Ek et al., 2007; O'Brien et al., 2006; Rodriguez-Antona et al., 2002). Hence, primary animal hepatocytes are used but they provide only limited predictability, are expensive and raise ethical issues. Recently, human embryonic stem cells have been targeted intensively as a promising source, since they are pluripotent and possess the capability of potential differentiation into any cell type in the human body. Thus they could be developed as source of functional human hepatocytes (Chiao et al., 2008; Duan et al., 2007; Ek et al., 2007;

Jensen et al., 2009; Sancho-Bru et al., 2009). A readily available and unlimited source of human embryonic stem cell (hESC) derived hepatocytes could revolutionize and shorten the early stages of the drug discovery process, by studying human hepatic metabolism of xenobiotics and drug-induced hepatotoxicity, and contribute to the development of stem-cell-based clinical trials (Ek et al., 2007; Soto-Gutierrez et al., 2008). Hence, for effective large-scale application of these cells, the demand exists for high-throughput method developments which provide dynamic information to get overall insight into pathological, physiological and metabolism based changes related to mechanism of toxicity (O'Brien et al., 2006; Xing et al., 2005).

1.2 Objectives and Contribution

1.2.1 Objectives of the VITROCELLOMICS project

The work presented in this thesis is part of the VITROCELLOMICS project. VITROCELLOMICS is a Specific Targeted Research Project (STREP, EU-Project No 018940) which started January 1st 2006 with duration of 36 months. The VITROCELLOMICS group addresses three major problems in current preclinical lead development; (1) the extensive use of animals, which is considered unethical; (2) the poor clinical relevance of the present *in vitro* drug metabolism studies; and (3) the time-consuming, unpredictable and laborious pre-validation protocols *in vivo*. Thus the objectives of VITROCELLOMICS are to establish clinically relevant and stable hepatocyte cell lines from human embryonic stem cells (hESC) that reliably mimic human hepatocytes. Instead of animal experimentations for selection and optimization of lead compounds before entering clinical phases, these *in vitro* cell models could be used in the pharmaceutical industry. In addition, human drug metabolism, uptake and efflux properties of compounds in the drug discovery and development processes could be tested and evaluated. To reach this goal a system involving 3D-hepatic cell culture and co-culture methods, which allow for maximal metabolic capacity and control of differentiation and growth conditions, is being developed for use in predictive studies of drug metabolism. In addition, a high-throughput micro-cultivation monitoring system for *in vitro* screening using an integrated optical oxygen sensing method was developed and evaluated. Genomic and metabolomic characteristics were studied and compared with established *in vitro* models, so that the new models and methods can be validated.

Successful completion can result in a new efficient *in vitro* pre-validation model, which significantly reduces the use of animal experimentation for prediction of human drug metabolism and disposition by an expected 60-80 %. Further, candidates chosen for later stages of the drug-discovery and development process can be assessed with increased safety and quality.

The members of the VITROCELLOMICS project are nine participants from four nations (Germany, Italy, Portugal and Sweden) within the European Union (EU). VITROCELLOMICS has the full title: Reducing animal experimentation in preclinical predictive drug testing by human hepatic *in vitro* models derived from embryonic stem cells. Research contributions are made by Linköping University, Saarland University, Karolinska Institute, Instituto de Biologia Experimental e Technológia, Charité University Hospital, Cellartis AB, Pharmacelsus GmbH, AstraZeneca R&D, and the European Centre for the Validation of Alternative Methods (ECVAM).

1.2.2   Contribution and objectives of this thesis

The objective of this thesis is three-fold. First, to establish a new high-throughput screening platform for drug candidates and initially determine culture conditions for cells using well known hepatic *in vitro* models (Hep G2 cells, primary rat hepatocytes), so that later validation of new models and methods can be performed. The high-throughput screening application is achieved by using 24-well SensorDishes® incorporated with oxygen sensors, up to 10 of which can be connected in series. Hence up to 240 samples can be monitored simultaneously.

Second, hepatocyte cultures from human embryonic stem cells (hESC) will be characterized and evaluated based on their morphology, their ability to secrete liver specific proteins, such as albumin, and their display of biotransformation function, as e.g. phase I and II biotransformation. In addition, toxicity studies on these cells will be performed and compared to current *in vitro* models. These results will be combined and discussed with achievements from other cooperation partners to gain an overall characterization of hESC derived hepatocytes and to judge if these cells can be used for preclinical drug testing studies.

Third, physiological and ^{13}C-labeling studies on cells exposed to sub-toxic concentrations of diclofenac will be performed to identify metabolic changes in hESC derived hepatocytes-like cells and primary human hepatocytes to evaluate subtle disturbances in biochemical pathways in response to drug treatment. Even in the absence of visible phenotype changes, metabolic changes, assessed using stable isotopic tracer studies, can possibly be directly related to the manifestation of toxicity. Therefore, hepatotoxicity, in case of hepatic cells, can be possibly identified by measuring these subtle changes. To measure these changes in the *in vitro* model developed, known techniques for quantitative physiological studies are adapted and implemented in the field of metabolic flux analysis (MFA).

1.3 Thesis Structure

The thesis is organized in three major parts. The central focus of the first chapter is the application of a high-throughput, non-invasive, dynamic toxicity platform with integrated optical sensors for oxygen measurement. The system is shown to be applicable for respiration monitoring and dynamic *in vitro* cytotoxicity testing. The second chapter deals with the characterization and application of embryonic stem cell derived hepatocytes, and evaluation of their metabolic and morphological competence. The third chapter addresses comparative, quantitative and qualitative physiological studies for primary human hepatocytes and hESC derived hepatocyte-like cells in response to sub-toxic diclofenac treatment.

2 High-Throughput, Non-Invasive and Dynamic Cytotoxicity Testing

Parts of this chapter are published as

Beckers S, Noor F, Muller-Vieira U, Mayer M, Strigun A, Heinzle E. 2010. High throughput, non-invasive and dynamic toxicity screening on adherent cells using respiratory measurements. Toxicol In Vitro 24(2):686-694.

2.1 Introduction

Billions of dollars are invested by hospitals and research institutes each year to combat adverse drug effects (Bennett et al., 2007). Moreover, newly synthesized drugs or therapeutic agents need to be tested for potential side effects on patients. In particular, these potential drugs must be tested for their hepatotoxicity, as the liver is the principal organ of biotransformation and elimination of xenobiotics (Guillouzo, 1998b). Due to safety regulations, clinical testing is only feasible if the safety of the compound has been demonstrated in both *in vitro* and *in vivo* animal toxicological studies. However, testing of substances to detect low incidence idiosyncratic toxicity requires large-scale animal studies which is difficult, expensive and evokes ethical issues. Moreover, *in vivo* studies have additional shortcomings, like difficulties to distinguish primary effects from secondary effects and species-specific responses (Uehara et al., 2008). Therefore, *in vitro* liver models, such as primary hepatocytes from animal origin and human hepatoblastoma-derived cell lines (e.g. Hep G2, Hep 3B, HepaRG) have been established to mimic human hepatocytes, which availability is scarce. Hep G2 cells, in particular, were established from liver tumor biopsies of a 15-year-old caucasian male (Argentina, 1975) and since being introduced by Aden et al. (1979) have raised hopes that they represent a suitable model (Javitt, 1990). Hep G2 cells are easy to cultivate and deliver reproducible results. These cells have been used as liver systems for organ-specific toxicity screening of compounds and for the investigation of drug metabolism as well as cytotoxic potential (Bort et al., 1999b; Brandon et al., 2005; Castell et al., 1997; Gomez-Lechon et al., 2001; Guo et al., 2006; Javitt, 1990; Nussler et al., 2001; Tirmenstein et al., 2002; Toyoda et al., 2001; Wang et al., 2002). However, it has been lately shown that Hep G2 cells have generally only very low cytochrome P450 activities and are thus not well suited for metabolism related toxicity studies (Kanebratt and Andersson, 2008b; Noor et al., 2009). Although there are permanent rat cell lines available (HTC, BRL 3A…), they are rarely used for toxicity testing, since they do not express the same cytochrome P450's as humans. Nevertheless, primary rat hepatocytes (PRH) are often compared to Hep G2 cells in toxicity studies (Bort et al., 1999b; McCarthy et al., 2004; Wang et al., 2002). Human primary hepatocytes are most relevant and often used, however contrary to primary rat hepatocytes; they show a much larger individual, donor specific drug response and are thus not as useful to test the new method. Their supply is

limited and costs are very high. PRH are readily available, very reproducible, display a higher metabolic competence and are thus used in addition to Hep G2 cells for method development. However, the trend towards cell-based screening assays requires not only adequate quantities of cells from primary and immortalized sources, but also demands parallel processing of multiple batches. Hence, parameters such as scale, flexibility, reproducibility, simplicity and costs are of significance (Slater, 2001). Thus, new powerful high throughput screening (HTS) tests combined with better cell lines promise a significant improvement. However, for further reduction of cell procurement and maintenance costs, high content screening (HCS) (Slater, 2001) using non-invasive pre-clinical toxicity assays is envisioned. Nevertheless, screening in HTS mode still requires improvement. Eventually, a whole set of tests should be analyzed together to cover the whole system response to an applied test compound adequately to get a more robust prediction of human *in vivo* toxicity (Dambach et al., 2005).

2.2 Motivation and Theoretical Background

Today, cell culture is a well known laboratory technique and regarded as core expertise in biological and medical science applications (Doyle and Griffiths, 1997; Ryan, 2008). Even though the method to grow animal cells outside the body had been established 1907-1910 by Ross Granville Harrison, it was not until the middle of the last century that cell culture was an easy available tool for scientists (Ryan, 2008; Schmitz, 2007). Pitfalls as bacterial contaminations, inadequate subculture techniques for continuous growth of cell lines and undefined media formulations had to be solved first (Ryan, 2008; Schmitz, 2007). Cell culture techniques were since advanced further and virus growth in cell culture systems and their purification allowed the first polio vaccine mass-production in the 1950's. Since the 80's mammalian cell culture is fundamental for production of many biological products by the recombinant DNA (rDNA) technology such as hormones, blood factors, interferons, monoclonal antibodies (MAb) and therapeutic enzymes. Today, therapeutic proteins are mainly produced in mammalian cell culture systems, since they possess correct conformation and post-translational modifications as demanded. In particular cell lines which keep their characteristics (liver, heart etc.) are in recent years used in the pharmaceutical industry to test for toxicity of chemicals and drugs and their adverse effects. This testing is nowadays mostly done by powerful high throughput screening (HTS) tests, a technique which was also implemented for lead

component screening in 1986 (Pereira and Williams, 2007). The HTS method is mostly performed in miniature reactors or microtiter plates, which offer the user high similarity between cultures. Thus, if a culture is disturbed, e.g. by supplemented drugs, growth parameter changes can be easily detected (Kumar et al., 2004). Only in the 80's of last century, HTS ADMET (Absorption, Distribution, Metabolism, Excretion, and Toxicity) concepts for chemical entities and lead target identification were introduced (Pereira and Williams, 2007). The applied methods used, were mostly colorimetric cytotoxicity assays, which are tetrazolium based (MTT, XTT and WST-1) and relay on the ability of living cells to reduce the tetrazolium to formazan crystals, or viability assays such as Sulfurhodamine B. These assays are used to determine end-points of these HTS ADMET experiments (Pauwels et al., 2003; Rubinstein et al., 1990). However, growth parameter such as oxygen, can give further valuable information about the cell viability, their mitochondrial function and their response to foreign chemicals (Hynes et al., 2003). Thus, electrochemical and later optical sensors have been developed to monitor these parameters (Schrenkhammer, 2008; Schröder, 2006). For oxygen determination in aqueous solutions the Clark electrode is often used. In the Clark electrode, two merged electrodes (platinum and silver in KCl solution) are separated from the sample solution by an oxygen permeable membrane. The polarized electric current flow between the electrodes is proportional to the oxygen partial pressure (pO_2) in the sample. Disadvantages of the Clark electrode however are, that membrane fouling and electronic inferences can occur and that the electrode consumes oxygen, thus inducing measurement errors. In addition, miniaturization to microplate format is difficult. Neither of these disadvantages is known for optical sensors, which have the further advantage that they can be easily miniaturized to HTS systems (Schrenkhammer, 2008; Schröder, 2006).

2.2.1   End-point high-throughput cytotoxicity assays

In vitro cytotoxicity assays rely on a number of end-points, such as cell component staining, release of constitutive cellular components and subsequent measurement of enzyme activity, as well as measurement of cellular metabolic functions. The assays function mainly by measurement of absorbtion and fluorescence (Slater, 2001). For HTS application, further, the use of cell culture robots is necessary.

2.2.1.1   Colorimetric assays

Cellular metabolic activity of viable cells can be measured by tetrazolium salt assays, such as MTT, XTT and WST-1. These assays are based on the principle that proliferating cells are more active than resting cells and thus can reduce more tetrazolium salts to blue colored formazans dye by their higher mitochondrial activity. Another common colorimetric assay is the lactate dehydrogenase (LDH) assay, in which the damage to the plasma membrane is quantified by release of the cytoplasmic protein LDH into the cell culture supernatant. The sulforhodamine B (SRB) assay, however, is based on cell density determination via proportional cellular protein content staining (Vichai and Kirtikara, 2006). All these assays can be measured in regular absorbance readers, however, for HTS screening, they are not well applicable, since they are either not considered to be homogeneous, or require multiple wash-steps and incubation steps, which is therefore not robot-friendly (Slater, 2001).

2.2.1.2   Fluorescence/Luminescent based assays

Compared to colorimetric assays, fluorescent or luminescent based cytotoxicity assays have the advantage to be simpler and more convenient in the procedure and to have higher sensitivities, due to light-emitting chemistries (Slater, 2001). A common fluorescent end-point assay is the quantification of adenosine 5'-triphosphate (ATP), which is regenerated from ADP if biosynthesis occurs and thus is a marker for cell proliferation. The detection of ATP is done by luciferase-driven bioluminescence which can be correlated to cell viability. Resazurin (trade name: Alamar Blue) is another fluorescent compound used for fluorescent based cytotoxicity assays. Blue colored Alamar Blue, which is a non-toxic metabolic indicator of viable cells, upon mitochondrial reduction changes its color to pink and also shifts in its fluorescence. Thus, having the advantage of being quantified either colorimetrically or fluorimetrically (Nociari et al., 1998). Many more fluorescent probes, such as ethidium homodimer-1, propidium iodide or ethidium bromide, have been widely used for membrane integrity based cytotoxicity assays (King, 2000). However, King (2000) pointed out, that while it is possible that a cell is mortally wounded, the cell membrane integrity can still be intact for relatively long time.

2.2.1.3   Dynamic high-throughput cytotoxicity assays

Due to the drawbacks of end-point assays, high-throughput systems based on oxygen as a growth parameter have been developed. These methods, using non-toxic fluorescent biosensors, measure the fluorescence of the dyes which are quenched in the presence of oxygen (Slater, 2001). By using fluorescence reader linked to computers, the dissolved oxygen concentration (DO) can be measured continuously in the culture supernatant and recorded online over the test period. Changes in dissolved oxygen concentrations can be correlated to exposed cytotoxic drug concentrations, and thus, these methods provide a rapid and dynamic cytotoxicity assay.

Several different biosensor and detection methods have been published over the last decade. Wodnicka et al. (2000) presented a novel fluorescence based method using one fluorescent dye (ruthenium based), immobilized within an oxygen-permeable silicone matrix, and measuring the fluorescence intensity over a certain time period. They could show a correlation in cell numbers between MTT assay and their method and further presented dose-response curves and IC_{50} values for bacteria exposed to antibacterial drugs. Deshpande et al. (2005) and Deshpande and Heinzle (2004) used microplates with integrated oxygen sensors (indicator and reference dye) for testing of oxygen uptake rate and culture viability measurement of Chinese Hamster Ovary (CHO) cells by measurement of the indicator fluorescence intensity that is quenched in the presence of oxygen and the non-oxygen-quenchable reference dye. In addition, Noor et al. (2009) showed the cytotoxicity application for adherent mammalian cells. Hynes et al. (2003; 2006) showed comparable applications using a phosphorescent porphyrin, water-soluble probe and measuring the time-resolved phosphorescence in microtiter plates over time.

In this part of the thesis a new SensorDish® reader (SDR) system (PreSens Precision Sensing GmbH, Regensburg, Germany) was used for the application of dynamic drug screening, thus it is explained more extensively.

The SensorDish® Reader (SDR) system, obtained from PreSens Precision Sensing GmbH (Regensburg, Germany), can be used in any commercially available humidified incubator. The system consists of three components: the central unit (splitter), the water proof 24-channel reader and the 24-well SensorDishes® with incorporated oxygen sensors (Figure 2.2.1). Up to ten reader modules, each comprising of 24 luminescence read-out

optics can be connected in series to a single splitter. Therefore, up to 240 samples can be monitored simultaneously (Figure 2.2.1 A).

The 24-well plates used for these experiments are sterile and disposable SensorDishes[®] (OxoDishes[®]). The SensorDish[®] is a polystyrene microplate in the common 24-well format with flat bottom. At the bottom centre of each well an oxygen sensor is immobilized (Ø ca. 4 mm). The SensorDish[®] is placed on the reader and read out is performed non-invasively through the transparent bottom of the multidish (depicted in Figure 2.2.1 B).

The OxoDishes[®] sensor contains an oxygen-sensitive, luminescent dye embedded in a tissue-compatible polymer. In the presence of oxygen the luminescence intensity as well as decay time of the oxygen-sensitive luminophore is quenched (Figure 2.2.1 C). In the SensorDish[®] Reader system the luminescence decay time is detected (Klimant and Wolfbeis, 1995).
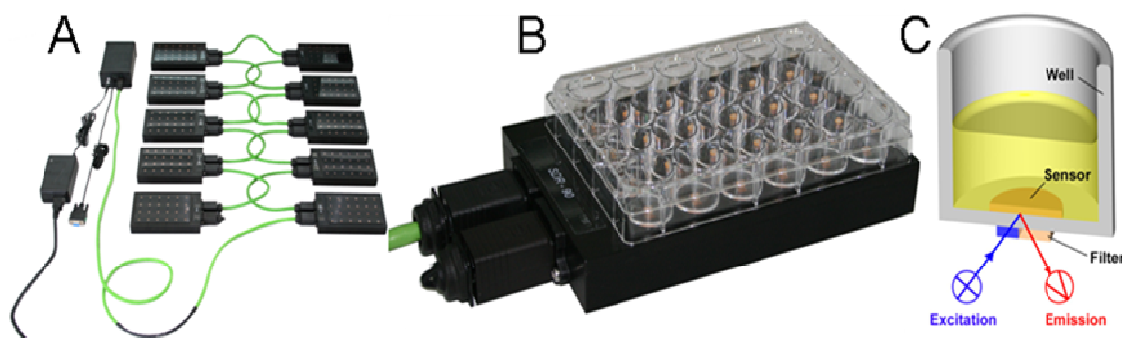
Figure 2.2.1: SensorDish[®] Reader System. A: Ten SensorDish Readers connected in series to the central unit (splitter) linked to a computer. B: SensorDish Reader with an 24-well OxoDish. C: Single well with oxygen sensor immobilised at the bottom of each well. The sensor is excited by the reader non-invasively through the transparent bottom of the multidish and its luminescence emission is detected from the bottom side.

The luminescence intensity and lifetime of an oxygen sensitive luminescent dye can be quantitatively related to the oxygen partial pressure of the solution in the well by the Stern-Volmer equation (Carraway, 1991; Klimant and Wolfbeis, 1995)

$$\frac{I_0}{I} = \frac{\tau_0}{\tau} = 1 + K_{SV}[O_2]$$
[Eq. 2.1]

11

where $[O_2]$ is the concentration of oxygen, I and I_0 are the quenched and unquenched luminescence intensities, τ_0 and τ are the luminescence decay times in absence or presence of oxygen and K_{SV} is the Stern-Volmer constant.

To evaluate the luminescence decay time, the sensor SensorDish® Reader system uses the phase-modulation technique, where the sensor is excited with a sinusoidal intensity modulated light and the decay time for an oxygen deprived system causes a delay in the emitted and measured signal. The sinusoidal reference signal and the decay induced phase shift (Φ) between the indicator (m) and the reference luminophore (m_0) are depicted in Figure 2.2.2.
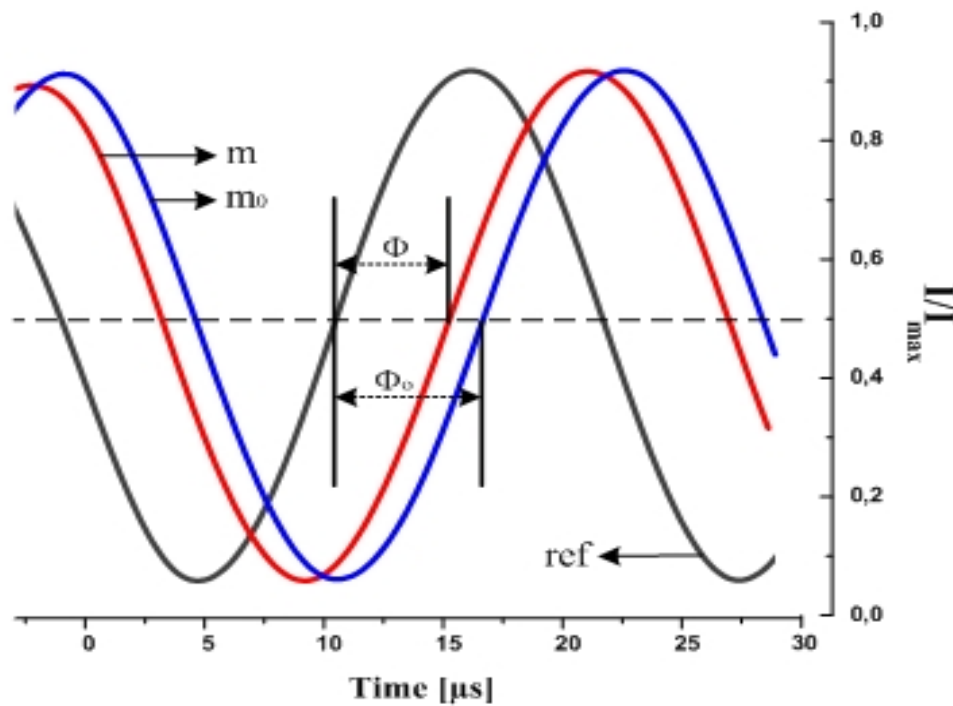
Figure 2.2.2:   Sinusoidal reference signal and decay induced phase shift (Φ), based on Bùrki (2008). The reference sinus signal (ref), the quenched indicator (m), and the reference luminophore (m_0) are denoted.

This delay is called the phase angle (Φ) and its tangent is correlated to the decay time τ, where f_{mod} is the modulation frequency of the excitation light. The relationship between the parameters is shown by solving equation [2.2].

$$\tau = \frac{\tan\Phi}{2\pi\cdot f_{mod}} \qquad\qquad \text{[Eq. 2.2]}$$

Collisional or dynamic quenching of the luminescence of the dye in the OxoDish[®] shows a distinct non-linearity in the Stern-Volmer plot but can be described with a modified Stern-Volmer equation [2.3]

$$\frac{\tan\Phi_0}{\tan\Phi} = \frac{\tau_0}{\tau} = \left(\frac{f_1}{1+K_{SV1}\times[O_2]} + \frac{1-f_1}{1+K_{SV2}\times[O_2]}\right)^{-1} \qquad\qquad \text{[Eq. 2.3]}$$

where K_{SV1} and K_{SV2} are the two quenching constants and f_1 is the weighting factor (Carraway, 1991; Klimant and Wolfbeis, 1995). This model is based on the assumption that the indicator is distributed in the polymer matrix at two different sites and each fraction (f_1, 1-f_1) shows a different quenching constant (K_{SV1}, K_{SV2}). Assuming one fraction of the indicator to be non-quenchable (K_{SV2}=0), equation [2.3] simplifies to

$$\frac{\tan\Phi_0}{\tan\Phi} = \left(\frac{f_1}{1+K_{SV1}\times[O_2]} + (1 - f_1)\right)^{-1} \qquad\qquad \text{[Eq. 2.4]}$$

The two parameters K_{SV1} and f_1 are obtained by calibration of the sensors which is carried out by the manufacturer for each production batch. All data are recorded online by a computer using PreSens SDR_v36 software. Dissolved oxygen concentration (% DO) in each well is automatically calculated based on equation [2.4] with additional modification for temperature compensation.

2.2.2   Objectives

The objective was to develop an application to monitor respiration changes online, caused by drugs. For this purpose, an optical sensor system, which measures the dissolved oxygen concentrations (DO) parallel in 24-well plates is applied (SensorDish® reader (SDR) system, PreSens Precision Sensing GmbH, Regensburg, Germany).

Since drug exposure was tested on adherent hepatic cell lines/types, first the necessary seeding and culture conditions have to be evaluated.

Second, the solvent influence of dimethyl sulfoxide (DMSO), in which the tested compounds are dissolved, on cell viability is tested.

Third, toxicity responses are monitored dynamically and drug-time dependencies for the cultured cells analyzed. The dynamic effects are also compared in regard to the cell types used.

Fourth, the reproducibility and the robustness of the respiration assay are tested and compared to (i) a sensitive *in vitro* toxicology assay (Sulforhodamine B) and (ii) to literature data.

2.3 Materials and Methods

2.3.1 Cell lines and culture conditions

2.3.1.1 Hep G2 cells

The human hepatoblastoma cell line Hep G2 was obtained from the German collection of microorganism and cell cultures (DSMZ, Braunschweig, Germany). Cells were routinely cultured in Williams Medium E (PAN Biotech GmbH, Aidenbach, Germany) supplemented with 100 U/ml penicillin, 100 µg/ml streptomycin and 2.5 % Panexin D (v/v) (PAN Biotech). The cells were maintained in 75 cm^2 culture flasks (Greiner Bio-One GmbH, Frickenhausen, Germany) at 37°C in an incubator (Memmert GmbH, Schwabach, Germany) with 95 % relative humidity in a 5 % CO_2 atmosphere. The medium was changed every 48 hours and cells were subcultured at 90 % confluency with a 1:4 split ratio. Cell density and viability were determined routinely during cell maintenance using the trypan blue exclusion method (Morris 1997) using a hemocytometer. Hep G2 cells were seeded in 24-well-OxoDishes at a density of 1.3 x 10^{5}cells/well and incubated for 30 hours prior to drug application.

2.3.1.2 Primary rat hepatocytes

Rat hepatocytes were provided by Pharmacelsus GmbH (Saarbrücken, Germany). In brief, hepatocytes were isolated from heparinised male Wistar rats (weighing > 250 g, purchased from Janvier, Le Genest-St-Isle, France) by the two-step collagenase perfusion method (Seglen, 1976). After the perfusion, the liver was transferred to WME I (Williams Medium E with 10% fetal calf serum (FCS) and 31.15 µg/ml Gentamycin) and the hepatocytes were unhinged from the connective-vascular tissue by hackling and shaking the liver. The cell suspension was filtered through sterile gauze (mesh width 280 µm) and washed three times at 50 × g (4°C, 5 min) in order to dilute out collagenase and to remove the non-parenchymal cells. Finally the pellet was resuspended and centrifuged at 150 × g (room temperature, 20 min) over a 40 % percoll gradient. The supernatant containing the dead cells was aspirated off and the pellet resuspended in WME II (Williams Medium E supplemented with 10 % FCS, 100 µg/ml streptomycin, 100 U/ml penicillin, 50 µg/ml gentamycin, 2 mM L-glutamine, 15 mM HEPES, 1 µM insulin and 1.4 µM hydrocortisone). The viability of the cells was determined by trypan blue exclusion. The primary hepatocytes were seeded in clear collagen-coated 24-well-

OxoDishes at a density of 1.25×10^5 cells/well and incubated for 20 hours prior to drug application.

2.3.1.3   Maintenance of cells in OxoDishes.

Approximately 1.3×10^5 Hep G2 cells per well were seeded in OxoDishes (PreSens Precision Sensing GmbH, Regensburg, Germany). The cells were allowed to adhere for 30 hours, after which the culture medium was replaced by fresh medium containing the tested chemical (drugs) at different concentrations. Measurements were continuously performed by the SDR reader every 15 min for 48 hours. For experiments with primary rat hepatocytes, OxoDishes were coated with 10 μg/cm^2 type I collagen solution (Sigma-Aldrich) and incubated overnight at 30°C. The excess fluid was then removed and the plates were allowed to dry at 30°C. Plates were rinsed with sterile tissue culture grade water before cell seeding. Isolated primary rat hepatocytes were seeded onto the prepared OxoDishes, allowed adhering and spreading for 20 hours. The morphology of primary rat hepatocytes was monitored during the cell attachment phase using an Olympus IX70 microscope connected to an Olympus CC12 Soft Imaging System (Münster, Germany). Pictures were recorded at the initial time point (t=0) and after 20 hours of seeding (t=0 drug) prior to drug application. The respiration measurements were performed as described for Hep G2 cells. Primary rat hepatocytes were treated with test compound in medium containing all supplements except FCS whereas Hep G2 cells were incubated in the presence of 2.5 % Panexin D supplement.

2.3.2   Cell viability assays

Cell density and viability were determined routinely during cell maintenance using the trypan blue exclusion method (Morris et al., 1997) using a Neubauer hemocytometer. Cell viability was also assessed using the Sulforhodamine B *in vitro* toxicology assay kit (Sigma-Aldrich, Taufkirchen, Germany), directly in OxoDishes after respiration measurements, according to the standard protocol with minor changes to adapt the assay to the 24-well plate format. The assay is based on proportional binding of Sulforhodamine B (SRB) dye to cellular proteins which is correlated to the total cell number (Skehan et al., 1990).
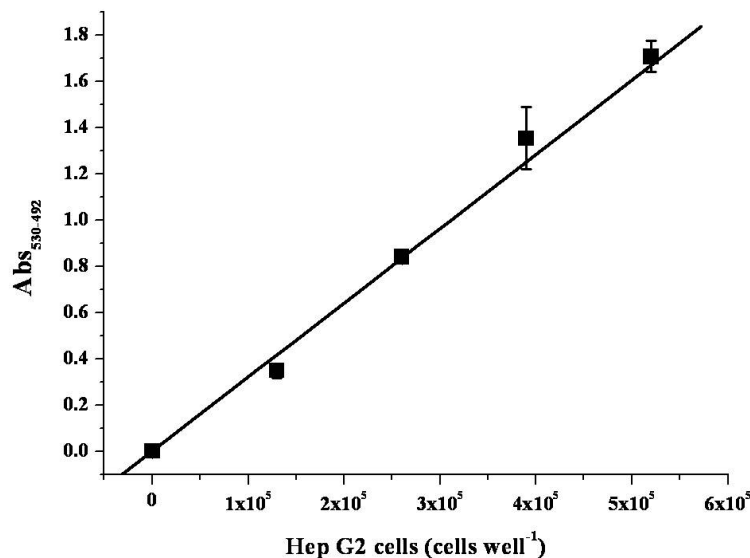
Figure 2.3.1: Linear relationship between SRB signal and cell numbers. The squares are the average values derived from the wells (n=4) for each cell number. The standard deviation is displayed as error bar. The R^2 is 0.995 (P<0.0001) and the equation results in: $SRB[A_{530}-A_{492}] = 3.2 \times 10^{-6}$ (Hep G2 cells) + 0.001. It was found to be linear till a cell density of 5.2×10^5 cells well^{-1} or the related seeding density of 3×10^5 cells cm^{-1}.

In brief, culture medium was aspirated off and cells were washed twice with serum and supplement free medium. One ml of protein-free medium was added to each well and the cells were fixed with 250 μl of 50 % trichloroacetic acid (TCA) solution. The plates were incubated for 1 hour at 4 °C, at the end of which the fixative was removed and after washing, 250 μl of 0.4 % (w/v) Sulforhodamine B solution was added. The cells were stained for 30 min followed by five washing steps with 1 % (v/v) acetic acid. The dye was solubilized in 500 μl of 10 mM Tris Base (Sigma) and transferred to a 96-well plate. Absorbance was measured at 565 nm against a background absorbance at 690 nm using an iEMS reader MF (Labsystems, Helsinki, Finland). Cell enumerations were performed by correlation of the signal of the protein binding dye Sulforhodamine B with defined cell numbers, e.g. five cell numbers ranging from 0 to 5.2×10^5 cells/well were seeded in multiple (n ≥ 4) and the average and standard deviation for each seeding cell number was calculated. The relationship between SRB signal and cell number is displayed in Figure 2.3.1. The linear regression plot resulted in a coefficient of determination > 0.99. For Hep G2 cells linearity was not ensured for cell numbers higher than 5.2×10^5 cells/well. It could be observed, by microscopic evaluation, that cell numbers higher than 5.2×10^5 cells/well resulted in confluency of approximately 100 %.

2.3.3   Hepatotoxic compounds

Test compounds were chosen based on their known hepatotoxicity and different mechanisms of hepatotoxic actions or their partly known drug metabolism, as described in the literature (Bort et al., 1999b; Deshpande et al., 2005; Guo et al., 2006; McCarthy et al., 2004; Thibault et al., 1992; Tirmenstein et al., 2002; Viau et al., 1993; Wang et al., 2002). The toxicity and its kinetics on cellular systems upon exposure to amiodarone, clozapine, diclofenac, glycerol, methotrexate (MTX), rifampicin, tacrine, troglitazone and verapamil were studied in order to obtain a better insight into the dynamic behavior of the cellular viability when exposed to these hepatotoxic agents. Additionally, data obtained using this new dynamic method was compared with the Sulforhodamine B assay for four test compounds (namely, diclofenac, MTX, sodium dodecyl sulphate (SDS) and troglitazone) and with those obtained by established cytotoxicity assay results taken from the literature.

All test compounds were dissolved in dimethyl sulfoxide (DMSO) (Sigma) except for glycerol and SDS, which were dissolved in growth medium. Stock solutions prepared in DMSO were diluted with William's medium E with or without Panexin D supplement for primary rat hepatocytes or Hep G2 cells, respectively, to yield the desired final concentrations of the test compounds. Final concentrations did not exceed 1 % DMSO (v/v) for all drug concentrations and controls. Control experiment were: (i) Medium containing no drug, (ii) medium containing the highest applied drug concentration (i.e. 1 mM), (iii) cells in medium containing no drug (untreated control) and (iv) cells in medium containing 1% DMSO. Eight or more concentrations of each compound were prepared and applied in triplicates to the cells in a volume of 1 ml per well.

2.3.4   LC$_{50}$ determination

LC$_{50}$ (lethal dose at which 50 % of subjects will die) was determined using a four-parameter sigmoidal concentration-response curve (OriginPro version 7.5G):

$$Y = \text{Bottom} + \frac{(\text{Top} - \text{Bottom})}{1 + 10^{(\text{LOG LC}_{50} - X)\,\text{x (HillSlope)}}} \qquad \text{[Eq. 2.5]}$$

where X is the logarithm of the applied substance concentration and Y is the response, i.e. dissolved oxygen concentration (DO) at selected time. Top is the maximum response

value, characterized by zero viability of cells. Bottom is the minimum response at maximum viability. The four parameters and the 95 % confidence intervals were computed with Origin Pro version 7.5G (OriginLabCorporation, Northampton, MA) using the Levenberg-Marquardt method.

2.3.5 Chemicals

All cell culture reagents were purchased from Sigma-Aldrich (Taufkirchen, Germany), except Williams medium E and Panexin D, which were obtained from PAN Biotech GmbH (Aidenbach, Germany) and FCS from PAA Laboratories GmbH (Pasching, Austria).

2.4 Results and Discussion

2.4.1 High-throughput dynamic respiration measurement

High throughput screening (HTS) systems have made assays cost and time efficient. Microtiter plates (MTP) provide a large number of parallel and miniaturized bioreactors with identical shape and fluid dynamics characteristics (Kumar et al., 2004) and have been widely used in the pharmaceutical industry. In aerobic prokaryotic and eukaryotic cells, oxygen is essential for central metabolic activity and indicates cell viability and mitochondrial function (Deshpande et al., 2004; Zitova et al., 2009). Thus, respiration can be considered as a useful parameter in *in vitro* cytotoxicity screening. 96-Well microtiter plates (MPTs) equipped with oxygen sensors have been shown to be an effective tool for cytotoxicity testing (Deshpande et al., 2005; Noor et al., 2009; Wodnicka et al., 2000). Recently, a phosphorescent porphyrin, water-soluble probe was applied for various toxicity experiments for up to 150 min. This method allows the detection of oxygen consumption, by reading the fluorescence intensities in a commercial fluorescence reader, even miniaturized to a 384-well microplate format (Hynes et al., 2003; Hynes et al., 2006; O'Riordan et al., 2000; Papkovsky et al., 2006). However, limitations of the current methods are that they require an external buffering system for long-term cultures and/or the transfer of the plates out of the incubator into the reader for measurement what may result in inaccurate results. Although it is technically feasible to maintain the pH outside a CO_2 incubator with HEPES as a buffer system, this system has not yet been shown to be as beneficial for long term experiments as the commonly applied bicarbonate buffer system. In addition, not all cell lines adapt to bicarbonate-free medium (Bonarius et al., 1995).

Sensor Dish readers (SDR), developed by PreSens Precisions Sensing GmbH (Regensburg, Germany), offer the possibility of monitoring the respiration of suspended and adherent cells on-line. This system is non-invasive, fully computerized and water-proof and hence can be used in humidified incubators. SDRs can also be adapted to a high throughput platform. The cells are grown in 24-well OxoDishes that are placed onto the SDR device. The dissolved oxygen in the well is measured with an oxygen sensor optode immobilized at the bottom of each well (Kocincova et al., 2008). Dissolved oxygen concentration can be correlated to the cell viability as described previously (Deshpande and Heinzle, 2004). This reported system is based on the measurement of

fluorescence intensity that is quenched in the presence of oxygen. The method showed high robustness and reliability, characterized by a Z' factor ("screening window coefficient", which compares the assay's dynamic range to data variation, hereby a Z`-factor equal to 1 indicates a perfect assay and > 0.5 for cell culture systems) of 0.74 indicating an excellent assay.

Using the SDR system, the luminescence lifetime instead of the luminescence intensity is measured. This is advantageous, since luminophores are intrinsically referenced and are therefore independent of fluctuations in light intensities due to variations in the optical properties of the samples including turbidity, color or refractive index (Huber et al., 2001). The intrinsic fluorescence of complex biological matrices (e.g. media and supplements) do not interfere with the luminescence decay time measurements for oxygen since fluorescence of biological materials usually decays within 100 ns (Kensy et al., 2005). Besides providing a controlled incubation environment, another major advantage of this system is that 24-well plates provide larger analyte samples than 96-well plates for additional analyses.

In the present study using the SDR system, the human hepatoblastoma cell line Hep G2 and freshly isolated primary rat hepatocytes were employed.

2.4.1.1 Seeding density optimization

Formation of a monolayer is one of the major preconditions for hepatocytes to maintain respiratory and metabolic activity in 2D cultures (Arnheiter, 1980; Deshpande et al., 2005; Wanson et al., 1977). Therefore it is essential for drug testing to identify optimal seeding concentrations of the non-dividing primary rat hepatocytes. This was done by recording dissolved oxygen concentration in the culture and by examining cell morphology.

Cell densities tested in triplicates ranged from 2.5×10^4 to 4.5×10^5 cells per well. The suspended rat hepatocytes settled quickly after seeding and adhered. Initially, cells were spherical in shape (Figure 2.4.1 A) but after approximately 12 to 16 hours the cells formed a monolayer of flat polygonal cells (Figure 2.4.1 B).
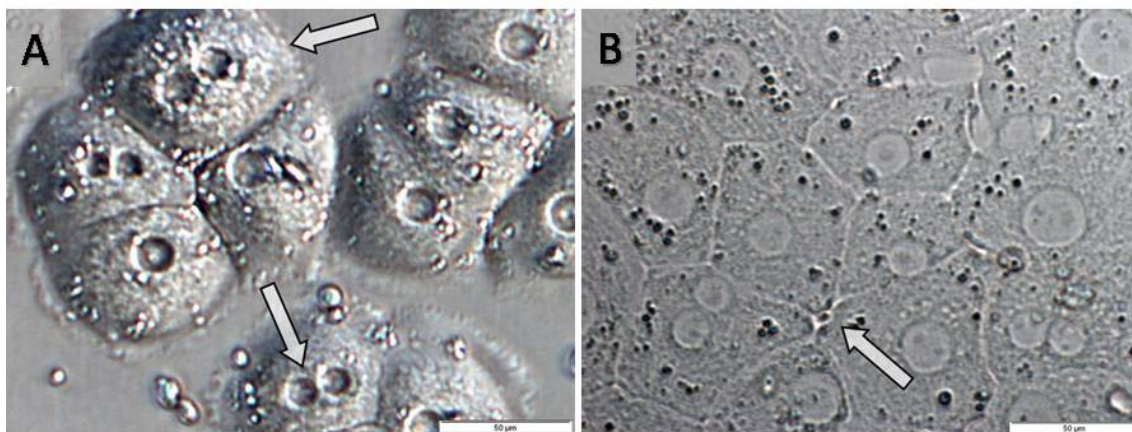
Figure 2.4.1: Morphology of primary rat hepatocytes. **A)** displays adhering primary rat hepatocytes five hours after seeding at a magnification of 40x. The scale bar of each figure measures 50 μm. **B)** is recorded 20 hours after seeding and immediately before drug addition.

This morphological transformation was observed under the light microscope and was consistent with results earlier described by Wang et al. (2004b). Moreover, binucleated cells were observed (Figure 2.4.1 A) in the primary rat hepatocyte cultures. After approximately 16 hours of cultivation the demarcation of hepatocytes was clear as displayed in Figure 2.4.1 B, showing also the formation and participation of bile canaliculi.

As depicted in Figure 2.4.2, dissolved oxygen concentration for primary rat hepatocyte cell densities from 10^5 to 2×10^5 cells/well decreased with increasing cell seeding density. Up to 2×10^5 cells/well, the signals were very similar. At cell densities above 2×10^5 cells/well, dissolved oxygen concentration increased with time indicating that the cells viability was decreasing with time probably due to oxygen and nutrition limitation. Cell densities of 1×10^5 and 1.25×10^5 cells/well reached a steady-state, indicating stable respiration for 48 hours. A cell density of 2.5×10^4 cells/well resulted in a stable respiration rate but DO difference of only 20 % compared to medium control. This difference is too small to allow an accurate estimation of LC_{50} since the accuracy of dissolved oxygen concentration is in the range of ± 5 percentage points. Hence 1.25×10^5 cells/well, corresponding to a cellular density of 0.74×10^5 cells/cm^2, were chosen for further experiments.
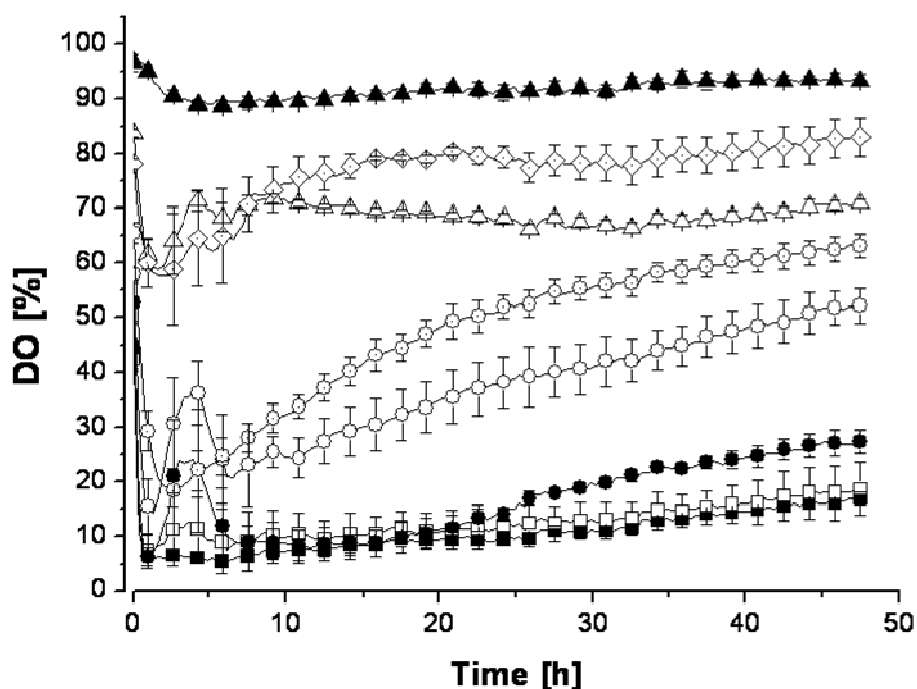
Figure 2.4.2: Dissolved oxygen concentration (DO) profiles at several seeding densities of primary rat hepatocytes versus time. Cells were seeded on OxoDishes (t=0). For primary rat hepatocytes, medium was aspirated off after 20 hours (t=0 drug), and replaced with medium without FCS but supplemented as described in Materials and Methods. Primary hepatocytes were seeded in the wells at 0 (▲), 2.5×10^4 (△), 1×10^5 (■), 1.25×10^5 ( ), 2×10^5 (●), 2.5×10^5 (○), 3×10^5 (☉), and 4.5×10^5 (◇) cells/well in triplicates and incubated for 48 hours. Dissolved oxygen concentration was recorded every 15 min, every fifth data point is displayed as average triplicate measurements with its standard deviation.

Cell seeding optimization for proliferating Hep G2 cells has to be performed due to doubling of cells and therefore decreasing availability of space and nutrition uptake from media (Figure 2.4.3). Measurements were carried out using the OxoDish system and respiration was recorded for 72 hours. As depicted in Figure 2.4.3, dissolved oxygen concentration for all cell densities decreased with increasing cell seeding density and time. Seeding of 2×10^5 to 3.5×10^5 cells/well resulted in sudden decreases in dissolved oxygen concentration at approximately 10 % air saturation, followed by a slow increase.

The sharp decrease indicates an increased oxygen consumption rate and the slight increase after the drop points to a decreasing the cell viability. Seeding cell densities of 1.3×10^5 cells/well and below showed a steady decreasing of DO over time without sharp

24

drop. The exact reason for the DO drop is not known, however, it can be surmised that it might be related to stress caused by oxygen depletion, nutrition or space limitations. Since the seeding density of 1.3×10^5 cells/well, corresponding to a cellular density of 0.76×10^5 cells/cm^2, showed the lowest DO without drop, allowing therefore the most accurate estimation of LC$_{50}$ values, it was chosen as optimal seeding density.
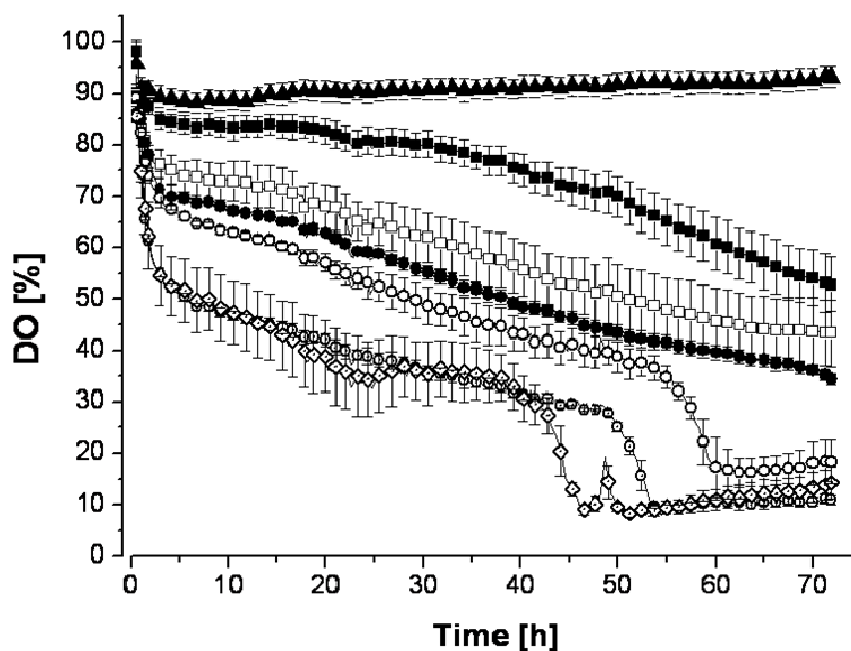
Figure 2.4.3:   Dissolved oxygen concentration (DO) profiles at several seeding densities of Hep G2 cells versus time. Cells were seeded on OxoDishes (t=0). Medium was aspirated off after 30 hours and replaced with medium without FBS but supplemented as described in Materials and Methods. Hep G2 cells were seeded in the wells at 0 (▲), 5×10^5 (■), 1×10^5 ( ), 1.3×10^5 (●), 2×10^5 (○), 2.5×10^5 (☉), and 3.5×10^5 (◇) cells/well in triplicates and incubated for 72 hours. Dissolved oxygen concentration was recorded every 15 min, every fifth data point is displayed as average triplicate measurements with its standard deviation.

The decrease in dissolved oxygen depends on the cell number and the specific respiration rate of the cells. For both cell types approximately the same number of cells was seeded. Rat primary hepatocytes, which do not proliferate, do however have a larger specific oxygen uptake rate per cell that can be explained by their larger size or their higher metabolism. Since the cells do not proliferate, the respiration per primary cell is nearly constant and thus the DO level remains nearly stable. Since Hep G2 cells, contrary to primary rat hepatocytes, are proliferating, the oxygen consumption increases with time and consequently DO decreases, as depicted in Figure 2.4.3.

2.4.1.2 Solvent influence

Since many drugs do not dissolve well in water, dimethyl sulfoxide (DMSO) is frequently added as a solvent for toxicity studies. The use of DMSO is mainly due to its polar aprotic characteristics and the low toxicity and environmental impact (Mortensen and Arukwe, 2006). However, Miret et al. (2006) have shown that if DMSO is cytotoxic to Hep G2 cells after 24 hours of incubation when applied at high concentrations (> 3 %, v/v).
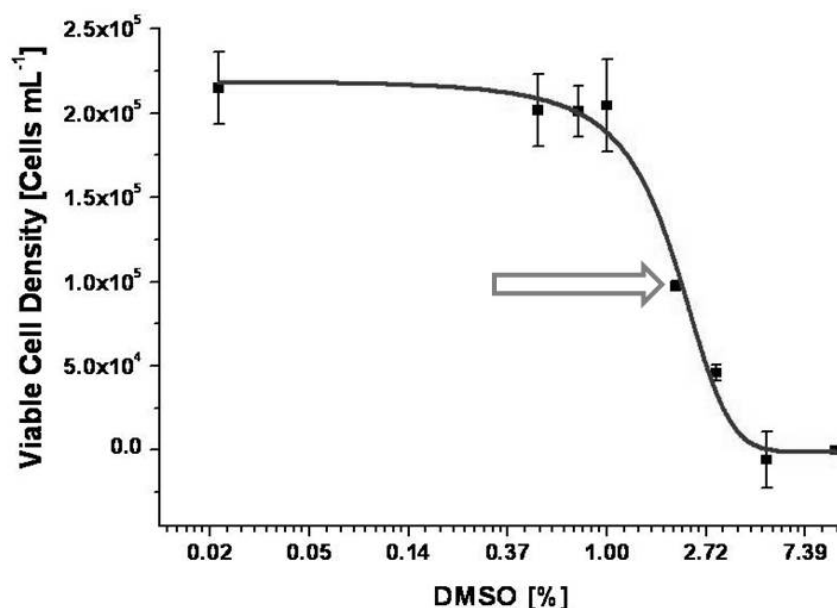
Figure 2.4.4:   Solvent influence on cell viability of Hep G2 cells. Cells were seeded on 24-well OxoDishes. Medium was aspirated off after 30 hours and replaced with medium without FCS but supplemented as described in Materials and Methods. The LC_{50} value of DMSO was determined after 48 hours of incubation with DMSO according to Eq. 2.5 using the SRB assay.

Hence, since a maximum of 1 % DMSO was applied for later drug studies, it had to be ensured, that no significant influence on viability and respiration is induced for the test period of 48 hours.

Therefore, Hep G2 cells were tested for the influence of DMSO on their viability and adhesion to the culturing surface by applying the Sulforhodamine B assay. As depicted in Figure 2.4.4, after 48 hours of DMSO exposure the LC_{50}-value resulted in approximately 2.2 % DMSO (depicted as arrow in Figure 2.4.4). However, no significant influence on viability and cell adhesion could be detected if 1 % DMSO was applied. Similar results

were found for the influence of DMSO on respiration of Hep G2 cells, as shown in Figure 2.4.5. The LC_{50} value detected by the respiration assay, applying OxoDishes, resulted in approximately 2.4 % DMSO.
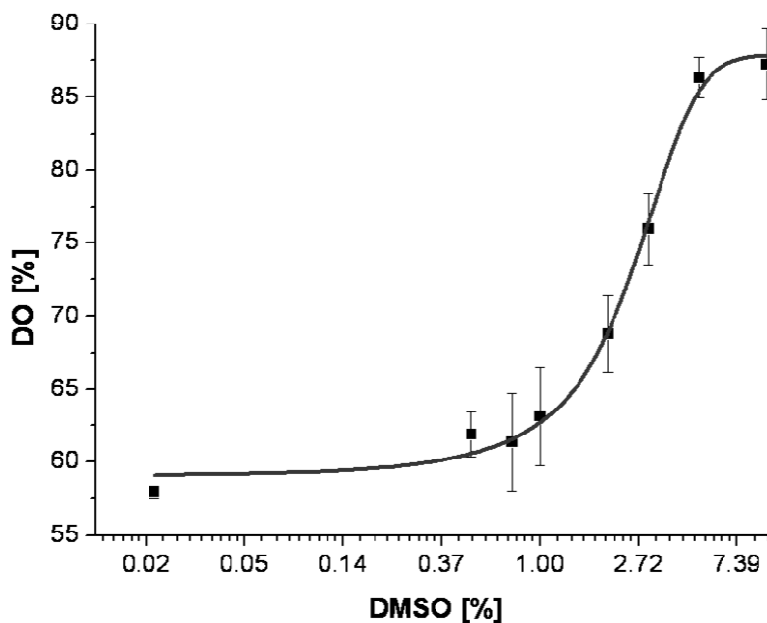
Figure 2.4.5: Solvent influence on respiration activity of Hep G2 cells. Cells were seeded on 24-well OxoDishes. Medium was aspirated off after 30 hours and replaced with medium without FCS, but supplemented as described in Materials and Methods. The LC_{50} value of DMSO was determined after 48 hours of incubation according to Eq. 2.5 using the SDR System.

In concordance with the literature (Liang and Akaike, 1997; Miret et al., 2006; Vesey et al., 1991) no significant influence of 1 % DMSO could be observed on respiration of Hep G2 cells or primary rat hepatocytes. Liang and Akaike (1997) and Vesey et al. (1991) even demonstrated that at doses up to 3 % DMSO there was no reduction of cell viability in Hep G2 and primary rat hepatocytes cultures for 48 hours of incubation. For concentration of 2 % DMSO compared to control cells Vesey et al. (1991) further did not find any optical-microscopic appearance differences.

2.4.1.3   Concluding remarks

It is essential to use an optimal seeding cell density to get a low dissolved oxygen concentration resulting eventually in reliable LC_{50} values, so that consistent data can be achieved in high throughput cytotoxicity studies.

For Hep G2 cells lower cell densities (2.5×10^4 cells/well) did not show a drop in dissolved oxygen probably due to slower growth, as the cells need a certain minimum density for growth support and cell-to-cell contact. Very high cell densities lead to oxygen and nutrition limitation resulting most probably in cell death as shown by an increase in the dissolved oxygen after 45 hours of culture (Figure 2.4.3). For Hep G2 cells it might be deduced that the observed DO drop at higher cell densities ($\geq 2 \times 10^5$ cells/well) starting at about 30 % air saturation is related to stress due to oxygen depletion, nutrition or space limitations and the associated increased oxygen consumption. Thus, for Hep G2 cells 1.3×10^5 cells/well, corresponding to an optimal seeding density of 0.76×10^5 cells/cm^2 was determined.

For primary rat hepatocytes, comparable responses could be observed (Figure 2.4.2). Very high or low cell seeding densities resulted in an increase in DO due to either nutrition or oxygen depletion or due to a lack of the required cell-to-cell contact. Hence 1.25×10^5 cells/well, corresponding to a cellular density of 0.74×10^5 cells/cm^2, were chosen for subsequent experiments for primary rat hepatocytes.

For toxicity studies, it has been shown that the solvent concentration of 1 % DMSO showed no influence on respiration and proliferation for Hep G2 cells and thus will be used for subsequent toxicity studies.

Further, it could be demonstrated that the introduced system can be adapted to any available, adherent cell line or cell type.

2.4.2   High-throughput cytotoxicity studies

The speed of screening new molecular targets and novel compounds for new drug-discovery and development has increased enormously due to the presence of high-throughput screening methods. The further a drug moves down the drug-discovery pipeline, the costs and challenges associated with its failure increase tremendously for the pharmaceutical industry (Slater, 2001). Hence, enormous efforts are taken to reduce identification failures and to discover toxicity by using high-throughput cell based assays. Widely used commercial viability and proliferation assays include membrane integrity assays (e.g. trypan blue exclusion) and assays based on metabolic markers such as (3-(4,5-Dimethylthiazol-2-yl)-2,5-diphenyltetrazolium bromide (MTT), 2,3-bis(2-methoxy-4-nitro-5-sulfophenyl)-2H-tetrazolium-5-carbox-anilide (XTT) or 4-[3-(4-Iodophenyl)-2-(4-nitrophenyl)- 2H-5-tetrazolio]-1,3-benzene disulfonate (WST-1). Proportional binding of Sulforhodamine B (SRB) dye to cellular protein, which is correlated to the total cell number, is also a common assay for viability testing. According to literature the SRB assay seems to be the most sensitive, robust and reproducible method with a large linear range with respect to cell number. Further, in contrast to the MTT assay, chemical compound interferences are rarely known in the SRB assay (Brandon et al., 2005; Hynes et al., 2003; Martin and Clynes, 1993; Rubinstein et al., 1990; Vichai and Kirtikara, 2006). Though these assays are easy to perform, they detect only highly specific changes, usually one cellular or metabolic parameter at a selected time point. Furthermore, since most of the current cytotoxicity assays are endpoint assays, they do not provide any dynamic information on the cell response during exposure to the applied substance unless multiple parallel experiments are carried out. However, dynamic information is mandatory to get overall insight into physiological and pathophysiological changes related to mechanism of toxicity (O'Brien et al., 2006; Xing et al., 2005) and thus, using a system as the SDR reader system, that monitors the behavior of cell-cultures exposed to test compounds in real-time is highly advantageous.

For the present cytotoxicity study, using the SDR system, the human hepatoblastoma cell line Hep G2 and freshly isolated primary rat hepatocytes were employed. Test compounds were chosen based on their known hepatotoxicity and different mechanisms of hepatotoxic actions or their partly known drug metabolism, as described in the literature (Bort et al., 1999b; Deshpande et al., 2005; Guo et al., 2006; McCarthy et al.,

2004; Thibault et al., 1992; Tirmenstein et al., 2002; Viau et al., 1993; Wang et al., 2002). The toxicity and its kinetics on cellular systems upon exposure to amiodarone, clozapine, diclofenac, glycerol, methotrexate (MTX), rifampicin, tacrine, troglitazone and verapamil was studied in order to obtain a better insight into the dynamic behaviour and viability of these cells after exposure to the hepatotoxic agents mentioned before. Additionally, toxicity data obtained using this new dynamic method was compared with the Sulforhodamine B assay for four drugs and from literature data obtained by established cytotoxicity assays for the others.

2.4.2.1   Dynamic toxicity measurement applying the SDR system

Previously published *in vitro* cytotoxicity studies have mainly applied ready-to-use endpoint assays, but provide only limited information on the tested cellular parameter. For the determination of a dynamic drug response, several identical assays have to be performed in parallel. Thus, using a system that monitors the behavior of cell-cultures exposed to test compounds in real-time is highly advantageous. In this part of the thesis the previously introduced 24-well respiration measurement system was used to monitor the toxicity of compounds in real-time for a defined seeding cell number.

The tested compounds were chosen due to their potential to induce hepatotoxicity by different mechanisms. The respiration profiles for primary rat hepatocytes and Hep G2 cells are depicted in Figure 2.4.6. Subplots A and B are showing concentration-dependent reaction to drug exposure, in this case diclofenac. Within three hours of incubation in presence of the drug, the dissolved oxygen in the media reaches a minimum or approaches a stationary state. This can be explained by means of the stationary liquid phase O_2 balance for cellular processes, which is shown in equation 2.6. Here, *DO* and *DO** denote the dissolved oxygen concentrations in the liquid phase and in equilibrium with the gas phase, respectively, and $k_L a$ is the volumetric liquid phase mass transfer coefficient. The specific oxygen uptake rate and the viable cell number are denoted by qO_2 and *X*, respectively.

$$\frac{d\,DO}{dt} = k_L a \cdot (DO^* - DO) - q_{O_2} \cdot X \qquad [2.6]$$

On the right hand side of the equation, the first term describes the transfer of oxygen into the medium, whereas the second term describes the oxygen uptake in cellular systems.

Since the media, in which diclofenac was dissolved, was fresh, it was oxygen-saturated in the initial incubation phase. It took 3 hours time until the DO reached a steady state. In this system, any time point after 3 hours can be chosen for LC_{50} calculations.

LC_{50} values for all tested drugs were calculated using the four-parameter sigmoidal concentration–response curve for Hep G2 cells and primary rat hepatocytes (Figure 2.4.6 C and D) at chosen time points. Addition of 1 % DMSO did not influence the respiration significantly for Hep G2 cells and primary rat hepatocytes as can be seen in Figure 2.4.6 A and B, respectively. With all drugs tested no significant impact on dissolved oxygen concentrations was observed if the drugs (e.g. in 1 mM concentration) were applied to the medium without cells, as depicted for diclofenac in Figure 2.4.6 A and B.

Figure 2.4.6 C and D show three concentration-response curves for primary rat hepatocytes and Hep G2, respectively, the calculated LC_{50} shifts from high to low over time thus indicating a toxicokinetic effect of diclofenac. By using several time points, toxicity dynamic for a given time-frame can be obtained (Figure 2.4.6 E and F). These dynamics combined with other cellular assays can provide more insight into the modes of toxicity.
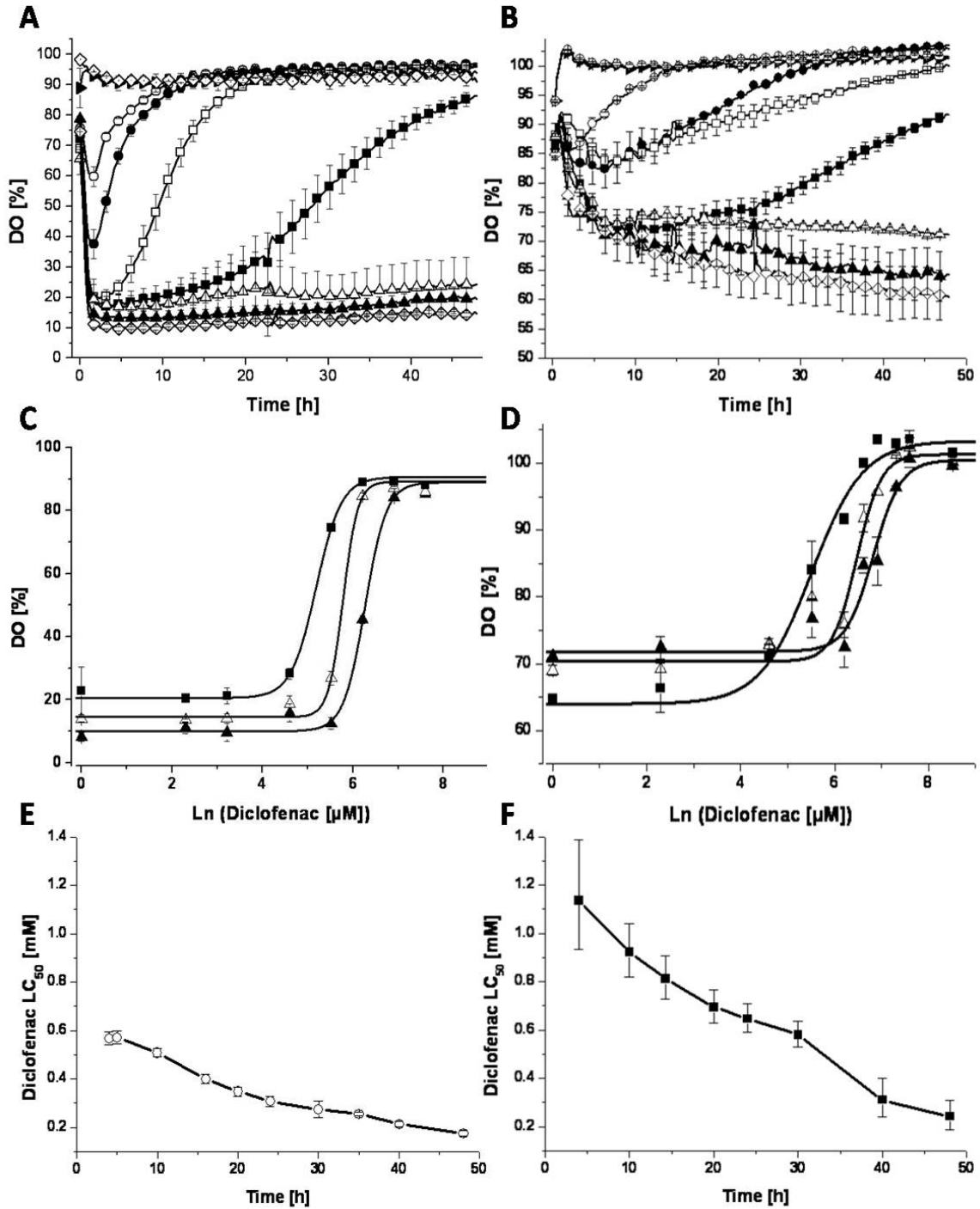
Figure 2.4.6: Kinetic effects of diclofenac on the respiration of primary rat hepatocytes (A, C, E) and Hep G2 cells (B, D, F). Dissolved oxygen concentration profiles (A & B). Diclofenac concentrations **A**: 0 mM (▲), 0.1 mM (Δ), 0.25 mM (■), 0.5 mM ( ), 0.75 mM (●), 1 mM (○) and controls; medium without cells but 1 mM diclofenac (⬦), medium without cells with 1 % DMSO (►) and cells with medium and 1 % DMSO (◊). **B**: 0 mM (▲), 0.1 mM (Δ), 0.5 mM (■), 0.75 mM ( ), 1 mM (●), 1.5 mM (○), medium without cells (⊙), medium with 1 mM diclofenac without cells (►) and cells with medium and 1 % DMSO (◊). **C:** Concentration-response curves of primary rat hepatocytes calculated at different time points: 10 h (▲), 24

h (Δ), 48 h ($\blacksquare$) using Eq. [2.5]. **D**: Concentration-response curves of Hep G2 cells calculated at different time points 10 h ($\blacktriangle$), 24 h (Δ), 48 h ($\blacksquare$) using Eq. 2.5. All measurements were carried out in triplicate. Corresponding mean values and standard deviations are displayed in A to D. LC_{50} values were determined using a four-parameter sigmoid concentration–response curve. E and F depict the LC_{50} time dependency for primary rat hepatocytes ($\circ$) and Hep G2 cells ($\blacksquare$), respectively, calculated from the LC_{50} diclofenac dissolved oxygen concentration. The error bars represent the coefficient of variance calculated from the standard error of the log estimate.

2.4.2.2   Dynamic effect of hepatotoxic drugs on different cell types

The SDR system was used to study the toxicodynamics of hepatotoxic drugs. As depicted in Figure 2.4.6, the death of cells with diclofenac, a commonly prescribed non-steroidal anti-inflammatory drug (NSAID), follows nearly first order kinetics. In Figure 2.4.6 E, the LC_{50} dynamics are shown for primary rat hepatocytes treated with diclofenac. Diclofenac toxicity is dependent on multiple factors such as a direct effect on the mitochondrial permeability transition (Lim et al., 2006; Masubuchi et al., 2000) as well as effects of the formed metabolites (Bort et al., 1999b; Tang et al., 1999). In case of primary rat hepatocytes the toxic effect, shown in Figure 2.4.6 C and Figure 2.4.6 E, is about twice as high as the effect on Hep G2 cells, shown in Figure 2.4.6 D and Figure 2.4.6 F. This may at least be due to the expected higher conversion into toxic metabolites due to higher expression of CYP 450 or glucuronation followed by protein adduct formation (Bailey and Dickinson, 1996; King et al., 2001; Poon et al., 2001). The curves seem to follow more or less a first order kinetics of reduction in LC_{50} values.

Comparison of the two cell types after treatment with diclofenac (Figure 2.4.6) and troglitazone (Figure 2.4.7) shows a higher LC_{50} at any specific time point for the human hepatoblastoma cell line Hep G2 than for the primary rat hepatocytes.
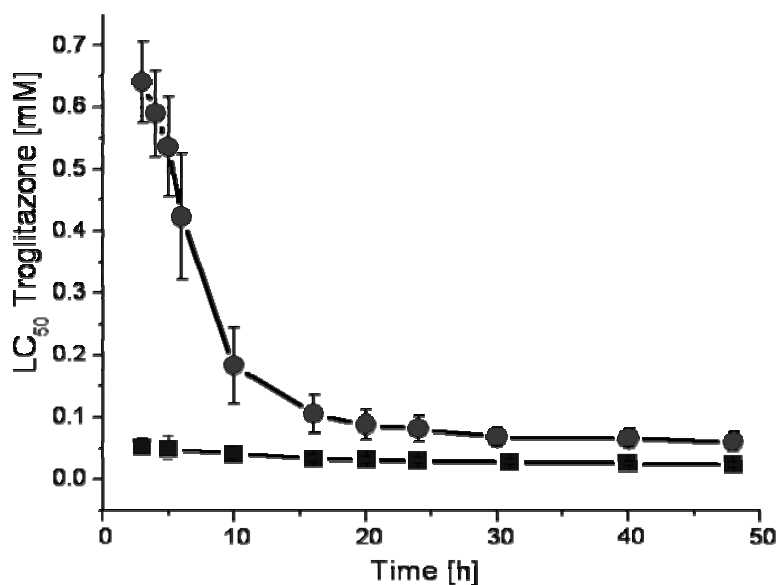
Figure 2.4.7: LC_{50} time dependency for primary rat hepatocytes (■) and Hep G2 cells (●) for troglitazone incubation. LC_{50}-values were determined using a four-parameter sigmoid concentration–response curve, calculated from dissolved oxygen concentration, using Eq. 2.5. Error bars indicate the error of the log estimates.

In contrast, Hep G2 cells were more sensitive to amiodarone treatment with respect to time and intensity of toxic effect (Figure 2.4.8). Verapamil and clozapine treatment on the other hand showed the same dynamics for both cells types (Table 2.4.1).
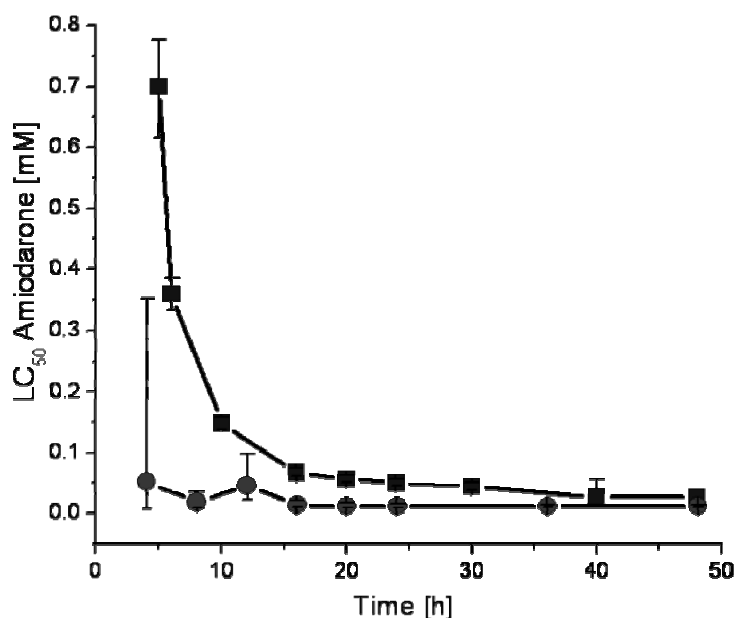
Figure 2.4.8: LC_{50} time dependency for primary rat hepatocytes (■) and Hep G2 cells (●) for amiodarone incubation. LC_{50}-values were determined using a four-parameter sigmoid concentration–response curve, calculated from dissolved oxygen concentration, using Eq. 2.5. Error bars indicate the error of the log estimates.

2.4.2.3   Reproducibility and robustness of the respiration assay

To test the reproducibility and robustness of this assay, some drugs were tested using different cell preparations from different rats at different time points or two Hep G2 cultivations.
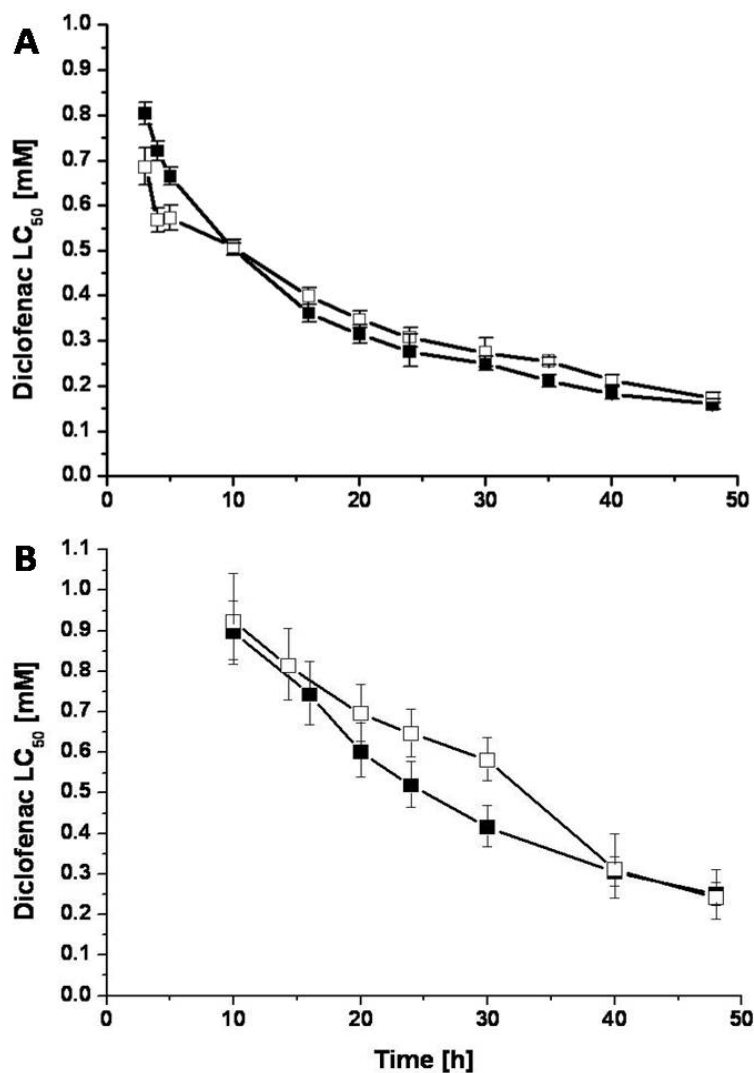
Figure 2.4.9: LC_{50}-values of two separate preparations of rat hepatocytes from two rats (A) and two separate Hep G2 seeding (B) after application of diclofenac. LC_{50}-values were determined using a four-parameter sigmoid concentration–response curve (Eq. 2.5). LC_{50} time dependency for primary rat hepatocytes and Hep G2 cells prepared at an interval of half a year, date 1 (■) and date 2 (□), for diclofenac incubation, respectively, calculated from dissolved oxygen concentration. Error bars indicate the error of the log estimates.

The time dependency for all applied test compounds was calculated in the same way as shown in Figure 2.4.6 for diclofenac. As depicted in Figure 2.4.9, the LC_{50} time

dependency derived from the respiration assay for primary rat hepatocytes (Figure 2.4.9 A) and Hep G2 cells (Figure 2.4.9 B), exposed to diclofenac, resulted in highly reproducible results.

Table 2.4.1: Time dependency of toxicity for all tested compounds. The compounds were tested in the respiration assay at concentrations up to 1 mM, except for diclofenac for which the highest tested concentration was 2.5 mM (n=3). Each LC_{50} value [µM] was determined from non-linear regression.

Compound	4h		16h		24h		48h	
	Hep G2	PRH	Hep G2	PRH	Hep G2	PRH	Hep G2	PRH
Amiodarone	53	> 1000	14	67	12	50	12	28
Clozapine	281	336	115	138	101	86	18	50
Diclofenac	1137	728	772	363	646	278	242	161
Glycerol	> 1000	> 1000	> 1000	> 1000	> 1000	> 1000	> 1000	> 1000
Methotrexate	> 1000	> 1000	> 1000	> 1000	> 1000	> 1000	> 1000	653
Rifampicine	> 1000	> 1000	> 1000	963	971	375	495	223
SDS	68	62	22	45	21	38	5	25
Tacrine	933	> 1000	393	> 1000	238	650	143	225
Troglitazone	590	50	105	32	81	28	60	22
Verapamil	311	464	321	219	299	160	100	105

Table 2.4.1 shows the toxicity of the compounds at drug exposure periods which are commonly used for assessing *in vitro* toxicity. All LC_{50} values in this study are calculated from a single run for each drug. For all the tested compounds the results were in good accordance with previously reported values. The time-dependency of toxicity was calculated similar to that of diclofenac, where three time points are shown in Figure 2.4.6 C and D.

2.4.2.4   Comparison of SDR system with literature data

The dynamic system allows calculation and comparison of LC_{50} values with literature data, without forcing of defined endpoints based on previously published time points. For example, Deshpande et al. (2005) calculated the LC_{50} for primary rat hepatocytes after 6 hours of treatment with diclofenac and clozapine using Oxoplates being 646 µM and 174 µM and testing via MTT assay to be 537 µM and 211 µM, respectively. Similar results were obtained here resulting in LC_{50} values of 632 (610-658) µM for diclofenac and 197 (153-253) µM for clozapine treatment, calculated after 6 hours of drug exposure for

primary rat hepatocytes. Bort et al. (1999) and Wang et al. (2002) published for Hep G2 cells and primary rat hepatocytes the LC_{50} values after 24 hours of diclofenac treatment. Bort et al. (1998) obtained LC_{50}-values of 762 ± 61 and 392 ± 43 μM, and Wang obtained as 50% lethal concentrations 399 ± 64 and 263 ± 43 μM for Hep G2 cells and primary rat hepatocytes, respectively. In this thesis, the 24 hour LC_{50} values (Table 2.4.1) match these published results.

Troglitazone, an anti-diabetic drug is associated with an idiosyncratic reaction leading to drug-induced hepatic injury in patients (Kostrubsky et al., 2000; Tirmenstein et al., 2002). Guo et al. (2006) estimated the LC_{50} for primary rat hepatocytes to be 217 and 54 μM after 2 and 16 hours drug exposure. Toyoda et al. (2001) calculated an LC_{50} value of 15 μM for 20 hour exposure. The SDR system is used to generate the dynamic concentration-response curves, observed average LC_{50} values for 2, 16 and 20 h were 113 (72-179) μM, 32 (26-38) μM to 30 (25-36) μM, respectively. Although the role of reactive metabolites contributing to troglitazone hepatotoxicity is controversial (Hewitt et al., 2002; Kostrubsky et al., 2000), troglitazone is reported to directly interfere with mitochondrial function (Bova et al., 2005; Masubuchi, 2006). Troglitazone also shows high serum protein binding (>99 %) (Loi et al., 1999). In the here presented system, primary rat hepatocytes were more sensitive to troglitazone exposure compared to Hep G2 cells, probably due to the fact that primary rat hepatocytes were treated in the absence of serum while the Hep G2 experiments were performed in presence of Panexin D, a defined serum replacement containing albumin, thus can bind to drugs. Therefore, the free troglitazone concentration was higher in the primary rat hepatocytes system leading to lower LC_{50} values.

Previous reports have indicated a concentration-dependent toxicity of amiodarone on the respiratory chain and on β-oxidation in Hep G2 cells and rat hepatocytes (Kaufmann et al., 2005; Spaniol et al., 2001). Hep G2 cells express phase I enzymes (Cytochrome P450) significantly less than primary human hepatocytes (Kanebratt and Andersson, 2008a) and are almost metabolically incompetent. Therefore they are likely to experience a direct cytotoxic effect due to mitochondrial interference (Waldhauser et al., 2006). As shown in Figure 2.4.8 and Table 2.4.1, Hep G2 cells are more sensitive towards amiodarone treatment in this system whereas primary hepatocytes, expressing higher

levels of metabolizing enzymes, might be able to detoxify the toxic parent compound by formation of less toxic metabolites.

2.4.2.5 Comparison of SDR system with Sulforhodamine B assay

For Hep G2 cells the dissolved oxygen method for determining drug toxicity was compared with the Sulforhodamine B assay for diclofenac, methotrexate, SDS and troglitazone (Table 2.4.2). The Sulforhodamine B (SRB) assay quantifies the protein content and was shown by Brandon et al. (2005) to be a sensitive and reproducible method compared to WST-1 and LDH release, at a specific endpoint. Hep G2 cells were exposed to the four compounds at eight different concentrations ranging from 0 to 1 mM. LC_{50} values were calculated after 48 hours using both methods described and are shown in Table 2.4.2.

Table 2.4.2: The 50 % lethal concentration (LC_{50}) values given in µM for reference compounds obtained in respiration and SRB assays on the human hepatoblastoma cell line Hep G2 after 48 hours of drug incubation. Data were determined using triplicate measurements for each drug concentration. The standard deviation was found to be < 10 % and the ranges were calculated from the standard error of the log estimate.

Compound	LC_{50} Hep G2 (OxoDish)	LC_{50} Hep G2 (SRB)
Diclofenac	242 (189-311)	239 (177-323)
Methotrexate	> 1000	> 1000
SDS	5 (4-7)	34 (30-39)
Troglitazone	60 (47-76)	70 (62-79)

LC_{50} values determined by the different methods were found to be comparable except for SDS. This difference is possibly caused by membrane or protein interference of SDS inhibiting respiration but keeping the integrity of the cells intact.

2.4.2.6 Concluding remarks

In this study, two different cell types from two species, primary rat hepatocytes and Hep G2 cells, were compared regarding their toxic effects using SensorDishes[®].

The results showed that the assay can be used for any cell type over a period longer than 48 hours.

A comparison of the respiratory data results with those obtained with the SRB endpoint assay for four test compounds showed a good accordance.

Using diclofenac as the model drug, the reproducibility and robustness of this assay was tested for different cell preparations from different rats and for Hep G2 cells seeded at different time points. As shown for the LC_{50} time dependency, the system resulted in highly reproducible results.

2.5 Conclusions

In conclusion, these results prove that the dynamic respiration assay presented here provides sensitive data in response to drug treatment. Using the ready-made, precalibrated 24-well SensorDishes® the experimental procedure is very simple, requiring considerably less manipulations compared to conventional assays.

It has been shown that it is of importance to acquire an optimal seeding density for adherent cell lines/types to test the system over a defined time period and, in addition, to test for solvent influence.

Further, for the here presented assay, reproducibility, robustness and comparability to other assays have been demonstrated.

In addition, for future drug development, the kinetic nature of online respiration monitoring is promising for providing an insight into toxicokinetics e.g. formation of toxic metabolites as from diclofenac or detoxification as for amiodarone. To obtain dynamics using conventional assays requires multiple parallel experiments, with associated higher cell and material requirements and therefore higher costs.

The new system has several further advantages; (i) it ensures complete online monitoring in a humidified CO_2 incubator (ii) the assay is non-invasive and therefore cells can be processed further (iii) no additional reagents are required (iv) by using 24-well plates it provides increased sample size for additional analyses compared to 96-well plates (v) for dynamic measurements less cell material has to be used compared to parallel experiments.

3 Metabolic Competence of Hepatocytes and Hepatocyte-Like Cells

3.1 Introduction

Hepatocytes are of interest as *in vitro* models for predictive drug toxicity testing and drug metabolism studies. Currently, primary liver cells from animal origin or human immortalized liver cell lines are commonly used in preclinical *in vitro* drug toxicity studies. However, due to their origin or immortalization they usually do not reflect human hepatocytes *in vivo* since they lack the presence and distribution of biotransforming systems needed for the biotransformation of drugs into toxic and reactive metabolites (Ek et al., 2007). Primary human hepatocytes are metabolically competent and naturally represent the human liver most suitably which makes them the most preferred model for drug metabolism and toxicity studies. However, they represent several drawbacks; 1) they exhibit donor–specific responses which can vary depending on the donor genotype; 2) their high pricing and limited availability; 3) despite high competence, the hepatocytes are jaded since the tissue is mostly derived from operations or from non-transplantable liver (physical damaged, pre-existing liver diseases, high fat content, high age etc. (Li, 2007)); 4), the drug detoxification capacity decreases over time and several transporter functions are either rapidly lost and/or altered when primary hepatocytes are in culture (Ek et al., 2007; Rodriguez-Antona et al., 2002); 5) it's difficult to stabilize the phenotype and avoid dedifferentiation which complicates high-throughput toxicity studies (O'Brien et al., 2006). As a result, human hepatoma cell lines, either from tumoral origin, or obtained by immortalization (i.e. Hep G2 cells), are often used. However, they lack expression of many liver-specific enzymes, especially cytochrome P450s (CYPs), important in phase I metabolism of xenobiotics (Kanebratt and Andersson, 2008a; Wilkening et al., 2003). Due to these reasons and despite the low concordance between animal and man, primary hepatocytes of animal origin are currently used for assessing the drug candidate's metabolism and safety (Ek et al., 2007; Jensen et al., 2009). This is suboptimal. Although primary animal hepatocytes are metabolically competent, they do not express the same P450's (CYP's) as human primary hepatocytes. In addition, to get statistically valid results a large number of animals must be used, which raises ethical issues. To conclude, no available cell type mirrors the complexity or the function of the human liver (Jensen et al., 2009). Hence, companies are investing in development of new hepatic cell types, which might overcome the before mentioned drawbacks of the current pre-clinical drug testing. Lately, human embryonic stem cells have been targeted

intensively as a source for hepatic cells. They are pluripotent and have the potential capability of differentiating into any cell type in the human body. Thus they can be developed, expanded and used as a source of functional human hepatocytes (Chiao et al., 2008; Duan et al., 2007; Ek et al., 2007; Jensen et al., 2009; Sancho-Bru et al., 2009). Having an available and unlimited source of human embryonic stem cell (hESC) derived hepatocytes could change the identification process of potentially liable drugs early in the drug discovery and development stage. By studying hepatic metabolism of xenobiotics and drug-induced hepatotoxicity in these cells as test systems, it could further lead to the development of stem-cell-based clinical trials (Ek et al., 2007; Soto-Gutierrez et al., 2008). Having hepatocyte-like cell lines from human origin, donor variability caused by homogeneous sourcing together with animal experiments, could be reduced. Also, a variety of different genotypes derived from multiple hESC cell lines could be used in order to mimic the variations among individuals in drug metabolism and distribution (Jensen et al., 2009).

In order to use hESC derived hepatocytes for compound testing or other *in vitro* pre-clinical studies, it has to be ensured that they display hepatocyte characteristics (Duan et al., 2007). The demand for characterization standards is increasingly requiring that hESC be tested for their ability to express and synthesize hepatocyte genes and proteins; satisfy in ultrastructural evaluation and display functional, secretory, storage and metabolism markers of the human liver (Sancho-Bru et al., 2009; Snykers et al., 2009). In addition, for future application, engraftment, differentiation and proliferation *in vivo* must also be tested (Sancho-Bru et al., 2009). In brief, they should be metabolically and morphologically competent. There are a few characterization studies on hESC-derived hepatocyte-like cells which address such metabolic markers, however, they have mostly focused on one or two criteria such as gene expression and phase I induction (Brolen et al., 2010; Cai et al., 2007; Ek et al., 2007; Lavon et al., 2004), protein expression (Cai et al., 2007; Soderdahl et al., 2007) or liver marker identification in combination with functional analysis (Baharvand et al., 2006; Li et al., 2008; Touboul et al., 2010). However, very little attention has been paid to the xenobiotic biotransformation activity of these cells. While phase I and II metabolism have been shown by PCR based methods (Brolen et al., 2010; Ek et al., 2007), phase II metabolism on the protein level was only addressed so far by Soderdahl et al. (2007). Only recently, complete characterization including drug metabolites and transport of pharmaceutical compounds in hESC derived

hepatocytes were shown by Duan et al. (2010). They were the first to show phase I and II biotransformation of bufuralol and phase I biotransformation for the three drugs diclofenac, midazolam and phenacetin in hESC derived hepatocytes.

The focus of this study was to characterize three human hESC cell lines which have been directed towards hepatocyte-like cells at Cellartis AB (Gothenburg, Sweden). This effort required a new culture protocol for reliable and reproducible differentiation, as well as characterization of these cell lines for their metabolic competence and morphological characteristics. For the characterization, several methods were applied and performed in cooperating partner labs. The Cytochrome P450 activity assay was performed at Saarland University. However, the analytics were carried out at Astra Zeneca (Gothenburg, Sweden) and Pharmacelsus GmbH (Saarbrücken, Germany). Gene expression identification via TaqMan low density array (LDA) cards was performed at Karolinska Institute (Stockholm, Sweden) and a quantitative Real-Time PCR (qRT-PCR) study at Cellartis AB. Fluorescence imaging (immunochemistry) for protein expression was performed at Cellartis AB. Cells from the same batches were seeded at Cellartis AB and shipped to Saarland University (Saarbrücken, Germany). Microscopic evaluation, enzyme activity assays, metabolic profiling and application as well as testing of the hESC derived hepatocytes for an *in vitro*, non-invasive toxicity assay were performed at Saarland University. This data provides a unique overview of characteristics of hepatic cells by comparing three hESC derived hepatic cell lines to freshly plated primary human hepatocytes and the human hepatoma cell line Hep G2.

3.2 Motivation and Theoretical Background

3.2.1 The liver

The liver is the second largest organ (weighting between 1.2 and 1.6 kg) in humans and the largest gland. It is situated beneath the diaphragm on the right side of the upper abdominal cavity. It is anatomically divided into two lobes, the left and the right lobe. The hepatic artery (20-25 % oxygenated blood) and the portal vein (75-80 % blood) supply the liver with blood (approx. 1500 mL/min) at the right lobe. The hepatic portal vein supplies the liver with metabolic substrates from the spleen, pancreas and small intestines, which are processed by the liver before reaching the systemic circulation. Both blood supply vessels subdivide into capillaries which lead to lobules. These lobules,

which are made up of thousands of hepatocytes, are structured as polyhedrons (pentagonal or hexagonal), in which hepatocytes are organized into unicellular plates, approximately 20 each separated by vascular, blood filled channels, the sinusoids (Alberts et al., 2002; Tzanakakis et al., 2000). The blood which flows through the sinusoids empties into the central vein of each lobule. The human liver consists of approximately 500.000 of those unicellular plates. The sinusoids have a fenestrated epithelial lining, lack a basement membrane and allow exchange of materials between the circulation and the space of Disse, where they have access to the hepatocytes (Tzanakakis et al., 2000). A schematic diagram of the structure of the liver is depicted in Figure 3.2.1. The central veins drain into the inferior vena cava, posterior from the liver.
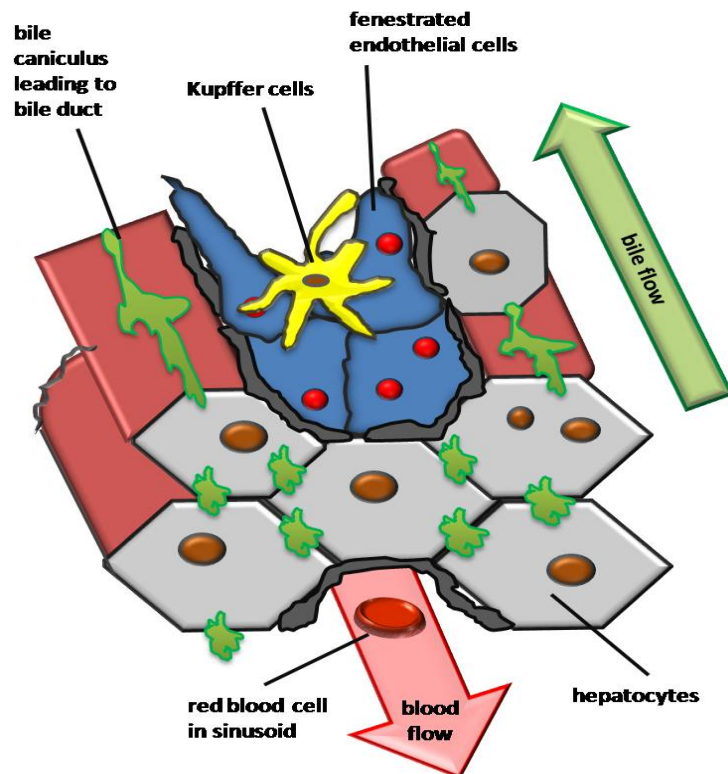
Figure 3.2.1: Schematic diagram of the structure of the liver based on Alberts et al. (2002). The hepatocytes are separated from small blood vessels (sinusoids) by a single thin layer of endothelial cells with interspersed Kupffer cells. Small holes in the capilla wall, called fenestrae, allow diffusion of molecules and small particles between the hepatocytes and the bloodstream. In the lobules, in opposite direction of the bloodstream, a system of bile canaliculi into which the hepatocytes secrete bile, is formed. Bile is released into the gut via the bile ducts.

Bile is produced by hepatocytes in the liver and flows via the biliary tree into the duodenum (Tzanakakis et al., 2000). In short, bile from the hepatocytes enters the common hepatic duct. This duct joins with the cystic duct from the gall bladder and forms the common bile duct. The bile duct combines with the pancreatic duct and drains into the duodenum.

The liver itself ranges from 2 % to 4 % of the body weight, and hepatocytes comprise approximately 70-80 % (approx. 2 billion hepatocytes) of the liver mass. Other cells which represent the liver cell population include endothelial cells, stellate (Ito cells), Kupffer cells and bile duct cells (Berg et al., 2003; Thews and Vaupel, 1999; Tzanakakis et al., 2000).

Since the liver is placed in-between the digestion tract and the systemic circulation, causing the so called "first-pass effect", it occupies a central role in major functions (Guillouzo, 1998a). The functions can be divided into four basic categories:

- Synthesis, regulation and secretion of blood clotting factors, transporter proteins, cholesterol, and bile components, which are of importance for maintenance of the body's normal state
- Uptake of nutrients (carbohydrates, amino acids, minerals) from systemic and portal blood.
- Storage of nutrients such as glucose in form of glycogen, fat soluble vitamins and minerals, such as copper and iron.
- Purification, transformation, metabolism and clearance of harmful substances such as ammonia, drugs, and toxins.

Disease or traumatic injury can greatly reduce the liver's ability to carry out these normal activities. Thus, most of the clinical manifestations of liver dysfunction are caused by cell damage and impairment of the normal liver capacities.

3.2.2   Drug metabolism

Drug metabolism, or biotransformation, is the metabolism of drugs and other foreign compounds (xenobiotics) by biochemical modification or degradation through specialized enzymatic systems to their metabolites. The liver is a major site of biotransformation and phase I reactions involve cytochrome P450 (CYP450) enzymes, which are localized in

the smooth endoplasmic reticulum of hepatocytes (Tzanakakis et al., 2000). However metabolizing enzymes are also present in other tissues, such as gut, kidney and brain. Drug metabolism often renders lipophilic and non-polar chemical compounds into more readily excreted polar and less lipid soluble products via oxidation, dealkylation and conjugation (Giron et al., 2008). Biotransformation is divided into two series of reactions (phase I and phase II), which mostly but not always occur sequentially.

3.2.2.1 Phase I

Phase I metabolic reactions convert substrates to more polar metabolites, so they can be readily excreted. This is done by either introducing or unmasking a functional group using catabolic reactions such as oxidation, reduction, hydrolysis, cyclization, or decyclization reactions and are mediated by either cytochrome P450, flavin-containing monoogygenase (FMO), esterases or amidases (Giron et al., 2008). The metabolites are sometimes more toxic than the parent drug, since they may be more chemically reactive (Giron et al., 2008). Cytochrome enzymes are bound to membranes of the smooth endoplasmatic reticulum. The cytochrome P450 (CYP) superfamily of enzymes are the major catalysts for phase I biotransformation reactions of xenobiotics and endobiotics. For drug metabolism the key human phase I CYP isoforms are CYP1A2, CYP2A6, CYP2E1, CYP2C9, CYP2C19, CYP2D6, CYP2E1 and CYP3A4. However, almost 50% of all known pharmaceuticals are oxidized by CYP3A4 (Li, 2001).

3.2.2.2 Phase II

Phase II reactions (non-cytochrome P450 mediated) are anabolic and since they conjugate with endogenous substrates such as glucuronic acid, sulfonates, glutathione or amino acids, known as conjugation reactions (Giron et al., 2008). The conjugates are usually detoxifying in nature and involve interactions of the polar functional groups of phase I metabolites. Sites on drugs where conjugation reactions occur include amino (NH_2), carboxyl (-COOH), hydroxyl (-OH), and sulfhydryl (-SH) groups. Key phase II enzymes and their multiple isoforms include UDP (Uridine 5'-diphospho)-dependent glucuronosyl transferase (UGT), phenol sulfotransferase (PST), estrogen sulfotransferase (EST) and gluthathione-S-transferase (GST) (Cantelli-Forti et al., 1998; Li, 2001).

3.2.2.3 Drugs transformed by phase I and phase II enzymes

After oral administration of a drug, it is absorbed by the digestive system and enters the hepatic portal system. In the liver the bioavailability of a drug is altered by metabolism (phase I and phase II biotransformation) before it enters the systemic circulation. This effect is called first-pass effect.

Diclofenac metabolism in hepatocytes

Diclofenac, a common non-steroidal anti-inflammatory drug (NSAID) with anti-inflammatory, antipyretic, and analgesic action, in humans undergoes an extensive hepatic metabolism involving two major biotransformation pathways, namely glucuronidation of the carboxylic acid group and aromatic hydroxylation (Bort et al., 1999a; Bort et al., 1999b; Ngui et al., 2000; Park et al., 2005).

Oxidative metabolites of diclofenac identified in humans include 4'-hydroxydiclofenac, 5'-hydroxydiclofenac, 4', 5'-di hydroxydiclofenac, 3'-hydroxydiclofenac and 3'-hydroxy-4'methoxy-diclofenac. However, they vary in their abundance (Bort et al., 1999a) and their cytochrome P450 (CYP) enzyme activities. In addition 4'- and 5-hydroxydiclofenac have been shown to be further metabolized via phase II, by formation of benzoquinone imine intermediates that react further with glutathione or microsomal proteins (Ngui et al., 2000). The main P450 (CYP) enzyme responsible for the 4'-hydroxylation and 3'-hydroxylation of diclofenac appears to be the cytochrome P450 (CYP) 2C9 enzyme, whereas the 5'-hydroxylation seems to be mediated by CYP2C and CYP3A4 enzymes (Hynninen et al., 2007).

Another phase II metabolite, which binds to hepatic protein and is thus recognized as foreign and reactive, is diclofenac glucuronide, conjugated directly by human UGT2B7 without being hydroxylated (King et al., 2001). This glucuronide can bind covalently to proteins (adduct formation) and is potentially the cause for the idiosyncratic toxicity of diclofenac (Bailey and Dickinson, 1996).
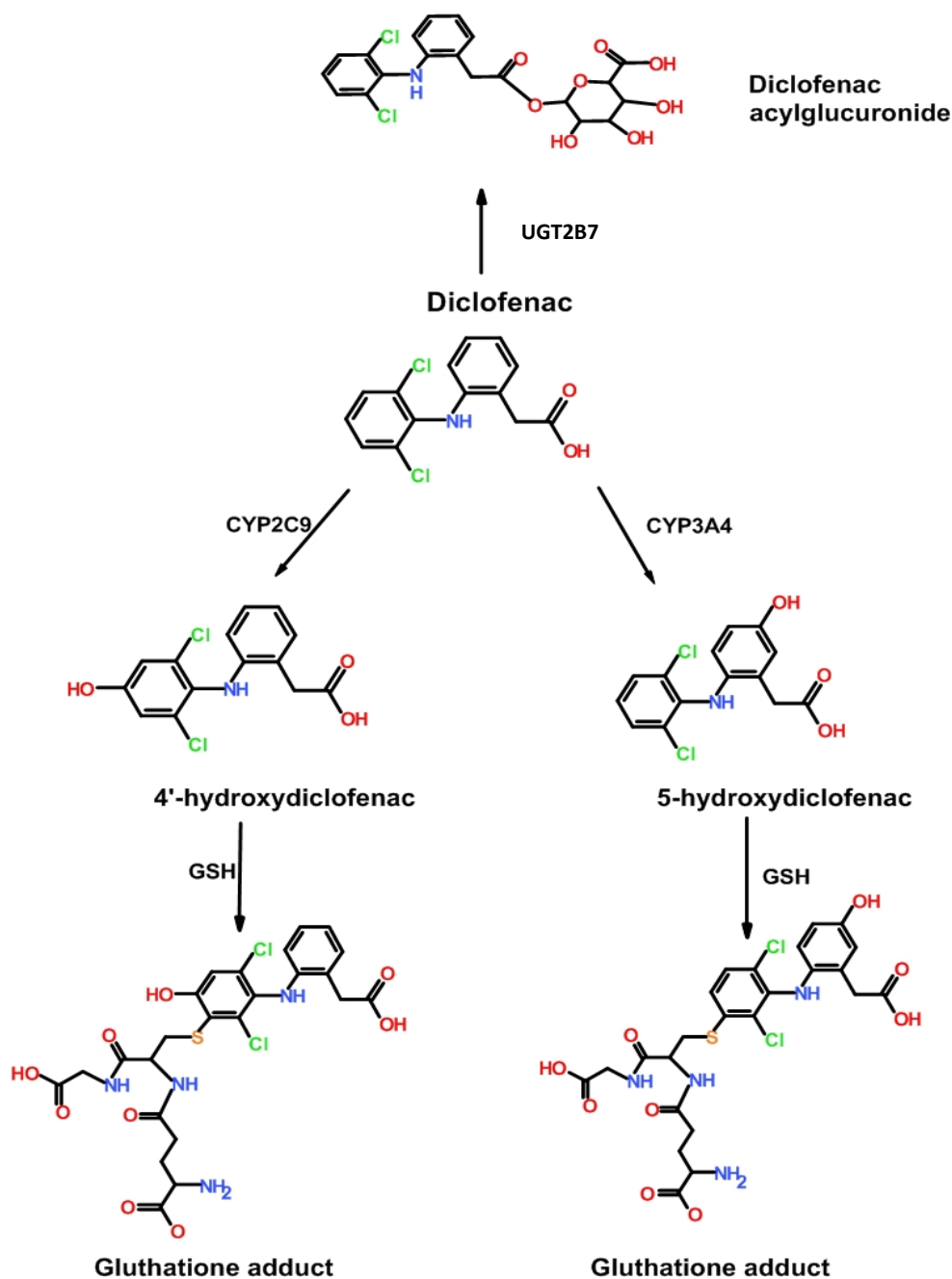
Figure 3.2.2: Schematic hepatic biotransformation of diclofenac based on Ngui et al. (2000), Boelsterli (2003) and Park et al. (2005). GSH = Glutathione catalyzed by glutathione S-transferase (GST)

Phenacetin metabolism in hepatocytes

Phenacetin is an antipyretic and analgesic drug which is metabolized in the liver by Cytochrome P4501A2 (CYP1A2) and hence phenacetin represents a suitable chemical entity for the assessment of human CYP1A2 activity *in vitro*. The major primary metabolite of phenacetin is the O-deethylated derivative acetaminophen (Polasek et al., 2006).
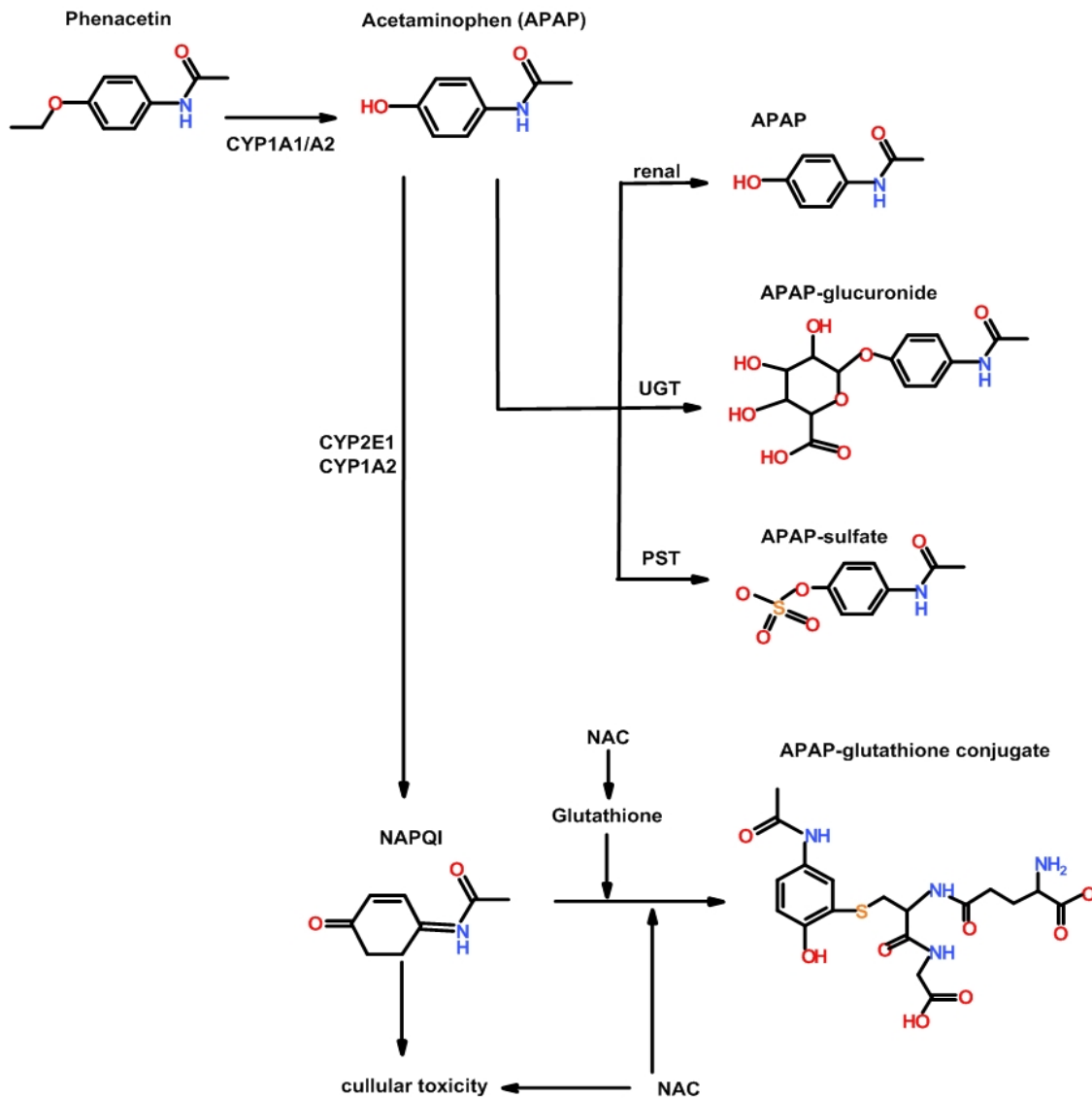
Figure 3.2.3: Schematic hepatic phenacetin metabolism in hepatocytes. Phenacetin is majorly metabolized to its acetaminophen derivative via CYP1A2. Bioactivation of acetaminophen undergoes further conversion to the chemically reactive species N-acetyl-p-benzoquinoneimine (NAPQI), which can oxidize and covalently modify proteins if glutathione depletion occurs. Figure based on Park et al. (2005) and Goldfrank's Toxicologic Emergencies - 8th Ed. (2006). UGT = UDP-Glucuronosyl transferase, NAC = N-acetylcysteine, PST = Phenol sulfotransferase

Acetaminophen (paracetamol), applied at therapeutic doses, is however, deactivated by glucuronylation (40-67 %) and sulphation (20-46 %) to metabolites, which are rapidly excreted in urine. Approximately 5% of the parent drug is excreted renally without being metabolized. Approximately 5-15 % of the drug undergoes bioactivation to N-acetyl-p-benzoquinoneimine (NAPQI) by P450 isoenzymes, namely: CYP2E1, CYP1A2, and CYP3A4 (minor contribution) (Park et al., 2005).

50

As explained above, acetaminophen applied in therapeutic doses is partly metabolized to NAPQI and rapidly quenched by a spontaneous reaction with hepatic glutathione. However, after a toxic dose, glutathione depletion results in NAPQI accumulation. Only then, NAPQI can covalently bind to proteins and nucleic acids. In consequence, accumulated NAPQI causes toxicity (Park et al., 2005). Formation of NAPQI is a marker for the isoenzymes cytochrome P450 activities and therefore a hepatic marker.

Midazolam metabolism in hepatocytes

Midazolam is a benzodiazepine derivative and has relaxant and sedative properties. It is extensively metabolized by CYP3A4 and CYP3A5, to 1'-hydroxymidazolam (40-100%) and 4-hydroxymidazolam, respectively. Since a large number of current and future drugs are metabolized via CYP3A subfamily, studies for inhibition and induction of CYP3A4 are of great scientific and clinical relevance (Klieber et al., 2008).
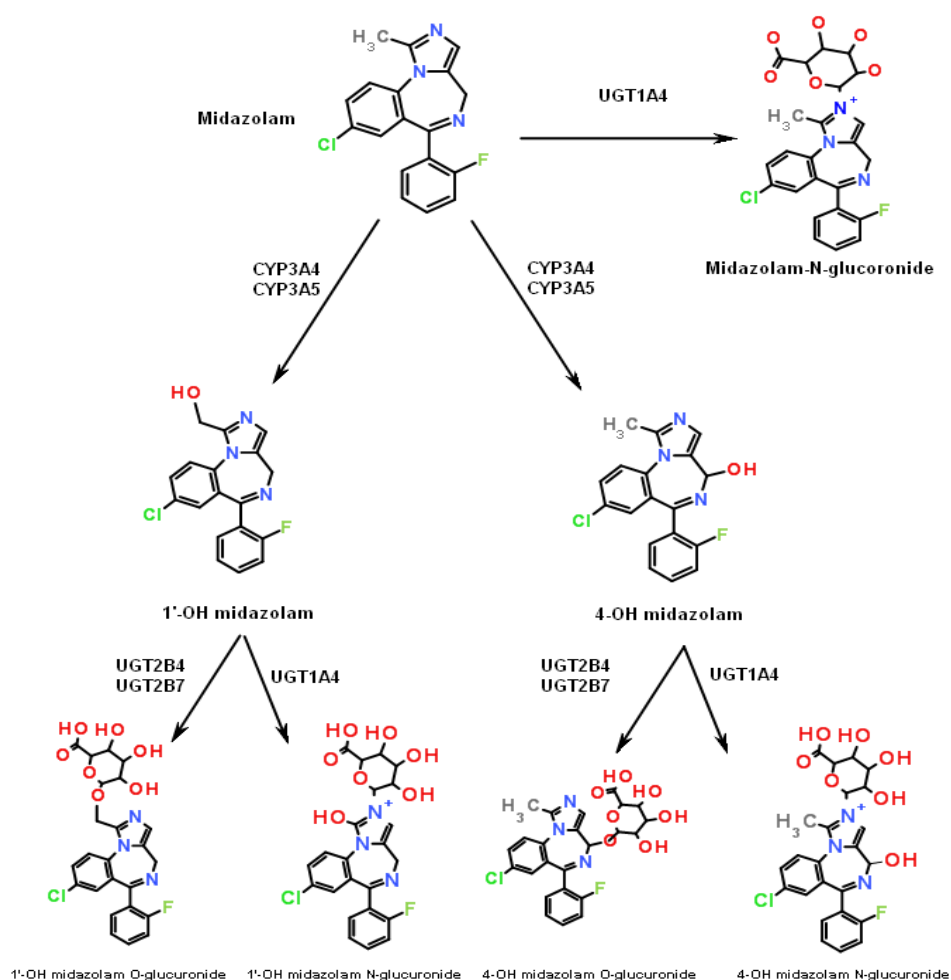

Figure 3.2.4: Metabolism of midazolam in human hepatocytes. The figure based on Hyland et al. (2009) and Klieber et al. (2008). UGT = uridine diphosphate glucuronosyl transferases

51

The hydroxylated metabolites can be further metabolized and conjugated, specially glucoronidation involving UGTs has been reported. (Hyland et al., 2009; Klieber et al., 2008). Recently it was found that the hydroxylated metabolites are mostly mediated by UGT2B4 and UGT2B7 (Hyland et al., 2009; Zhu et al., 2008). The hydroxylated metabolites are excreted by the liver as glucuronoconjugates (Klieber et al., 2008). N-glucuronation, however, can also occur directly from the parent compound and is mediated by phase II UGT1A4 (Hyland et al., 2009; Zhu et al., 2008). The assumed midazolam metabolism in human hepatocytes is depicted in Figure 3.2.4.

3.2.3 hESC derived hepatocytes/hepatocyte like cells

3.2.3.1 Stem cells

Stem cells have the ability to generate identical copies of themselves ("self-renewal") and to differentiate into several cell types ("stemness"). They can be classified into two major categories; embryonic stem (ES) cells and adult stem cells (ASCs), which include mesenchymal stem cells (MSCs) and multipotent adult progenitor cells (MAPCs) (Davila et al., 2004). ES cells are totipotent cells, which were first isolated by Thomson and colleagues (1998) from the inner cell mass (ICM) of a human blastocysts in 1998.

It has been shown that they differentiate into embryoid bodies (EBs) comprising all three germ layers and into somatic or somatic-like functional cells such as neurons, hepatocytes, cardiomyocytes and others and that they possess unlimited proliferation capability (Davila et al., 2004; Gepstein, 2002; Itskovitz-Eldor et al., 2000; Thomson et al., 1998). A schematic figure for the differentiation procedure towards functional cells is shown in Figure 3.2.5 A. Figure 3.2.5 B-E depicts the differentiation towards hepatocyte-like cells. ASCs can be found in several tissues as adipose tissue, liver and brain (Haridass et al., 2008). Unlike ES, they are specialized cells with the task for tissue homeostasis and repair (Davila et al., 2004). In addition, they are multipotent precursor cells which can be differentiated into several, however, not all cell types.
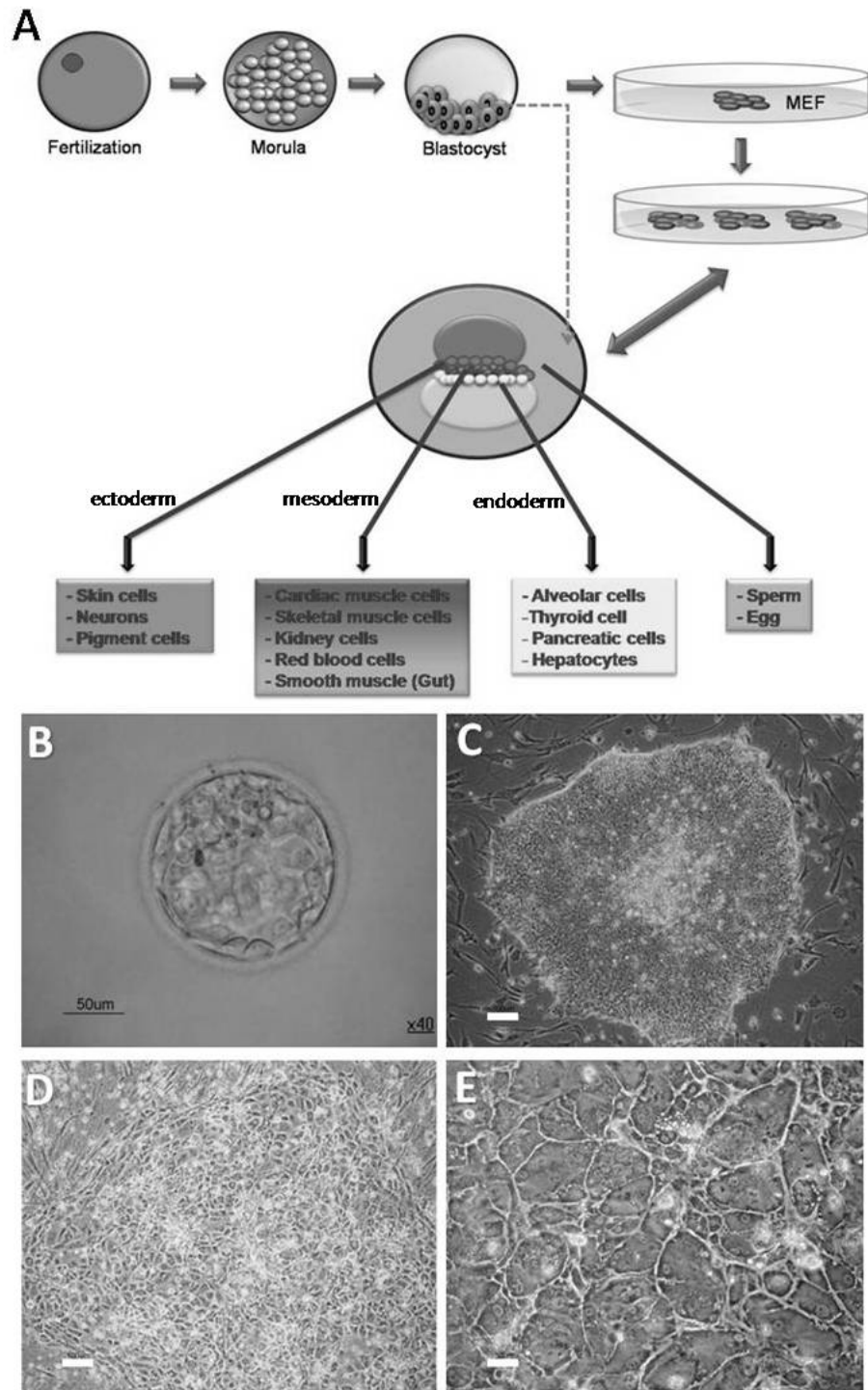
Figure 3.2.5: Mammalian development and derivation of the ES cell lines. **A)** Schematic development based on Gepstein (2002). After fertilization the blastocyst stage with ICM is formed. The figure depicts the three germ cell layers (ectoderm, mesoderm, and endoderm) formed within the inner cell mass. From the ICM all tissue types in the embryo are formed. ES cell lines are generated from the ICM and in general plated on mouse embryonic fibroblast (MEFs) feeder layers, on which they can be expanded. ES cells can differentiate into specialized cells, as shown above. **B)** Blastocyst at day 4 after fertilization **C)** hESC colony **D)** definite endoderm and **E)** hESC derived hepatocyte-like cells. Scale bar in **C)** and **D)** equals 100 µM, in **E)** 50 µm. Pictures **B-D** are courtesy of Cellartis AB.

53

3.2.3.2 Hepatogenic differentiation in ES cell culture

The inner cell mass of blastocysts can differentiate into all three germ layers, namely endoderm (internal layer), mesoderm (middle layer) and ectoderm (external layer). Several strategies are currently established and applied simultaneously for the purification of the endoderm and later differentiation from embryonic stem cells to ES cell-derived hepatocytes/hepatic progenitors. They include addition of soluble medium factors, reconstruction of *in vivo* cell-matrix, cell-cell interactions and genetic modifications (Snykers et al., 2009).

Activin A supplementation enriches ES cells for endodermal/definite endoderm populations. Fibroblast growth factors (FGFs) seem to mediate early hepatic differentiation and if hepatocyte growth factor (HGF) is supplemented, mid-late hepatic phenotypes have been reported. However, functional maturation is only achieved if a stepwise mixture of insulin-transferin-sodium selenite (ITS), dexamethasone and oncostatin M (OSM) are supplemented and the culture is coexposed to serum. However, serum-free conditions, e.g. the use of serum-replacement factors, is lately becoming a trend (Snykers et al., 2009).

For imitation of the *in vivo* cell-matrix, reconstruction of the ontogenic scaffold (collagen, matrigel…etc.) and cell-cell interactions by coculture with hepatic and non-hepatic cell types is the current method. Maintenance of hESCs is usually done on mouse embryonic fibroblast (MEFs) feeder layers (Lee et al., 2005). However, coculture with animal cells can result in cell-fusion and is associated with risks such as pathogen transmission and viral infection. Hence, MEF-conditioned culture media (MEF-CM) or feeder-free culture systems were introduced recently (Lee et al., 2005; Snykers et al., 2009).

Genetic modifications of ES cells, in form of HNF3β transfection and recombinant expression of E-cadherin have been shown to be an effective approach for acquisition of a hepatic phenotype, gene expression and functionality (Anouska et al., 2005; Tanaka et al., 2003). However, unintended gene upregulation is a major drawback. Hence epigenetic modification of the local chromatin structure by supplementation of the culture medium with 0.5-1 mM sodium butyrate has been introduced for enrichment. In combination with activin A it has been successfully shown to enrich cultures to the point of 70-90% purity (Gareth et al., 2009; Li et al., 2008; Snykers et al., 2009).

However, there are up till now, no reports of complete differentiation of stem cells towards adult human hepatocytes which show complete functional hepatic behavior (morphological, RNA expression, protein expression and activity levels) as human hepatocytes. Thus, to further obtain more information and increase the input of information, standardization of characterization protocols is required (Davila et al., 2004; Sancho-Bru et al., 2009; Snykers et al., 2009).

3.2.4   Objectives

Since stem cells are a readily available source of human cells; have the ability to proliferate unlimitedly and are totipotent so that all cell types important to toxicology testing can be generated, increased research effort has been put into developing stem cell-based systems recently. However, challenges remain in stem cell characterization, since they are poorly characterized.

Thus, in this part of the thesis, three hepatocyte cultures (hES-HEP^{TM} SA002, hES-HEP^{TM} SA167 and hES-HEP^{TM} SA461), which have been directed towards hepatocyte-like cells via definitive endoderm, are systematically characterized. Further, to evaluate their application, these cells are compared to the human hepatoma cell line Hep G2 and primary human hepatocytes.

First, the phenotype of the hESC derived hepatocyte-like cells will be evaluated by their microscopic appearance.

Second, gene expression of late stage maturation genes (AFP, ALB, G6P and A1AT), liver specific genes, as well as the expression of UDP-glucuronosyltransferases (UGTs), transporter and transcription factors and synthesis of hepatic lineage markers, including albumin, α-1-antitrypsin (A1AT), cytokeratin 8 (CK8) and cytokeratin 18 (CK18), as well as FoxA2 are evaluated. This part of the work is performed in collaboration with VITROCELLOMICS partners.

Third, functional hepatic characteristics, such as albumin secretion, glycogen storage and urea synthesis are quantified.

Fourth, phase I and phase II metabolism of midazolam, phenacetin and diclofenac is detected for the respective metabolites.

Fifth, these results will be combined with dynamic toxicity data and discussed with regard to future hESC derived hepatocyte-like cells applications.

3.3 Materials and Methods

3.3.1 Cell lines and culture conditions

3.3.1.1 Primary human hepatocytes

Primary human hepatocytes were plated and provided by Cellartis AB. For toxicity assessment cells were seeded in 24-well OxoDishes® (PreSens, Regensburg, Germany) on collagen I (Sigma Aldrich). Seeding cell density in collagen I pre-coated 24-well OxoDishes® was 1.7×10^5 cell/well. The seeded plates were shipped overnight in William's Medium E (Sigma Aldrich) medium supplemented with 10 % Fetal Calf Serum (FCS) (v/v), 100 U/mL penicillin and 100 µg/mL streptomycin. After arrival, medium was immediately replaced and cells were maintained at 37°C in an incubator (Memmert GmbH, Schwabach, Germany) with 95 % relative humidity in a 5 % CO_2 atmosphere for two days to adjust. For activity and toxicity experiments medium was switched to hES-HEP™ culture medium (Cellartis AB. Gothenburg, Sweden) supplemented with hES-HEP™ additive (Cellartis).

3.3.1.2 Human embryonic stem cells derived hepatocytes

Human embryonic stem cells (hESCs) were seeded and differentiated at Cellartis AB (Gothenburg, Sweden) towards hepatocyte-like cells (hES-HEP™, Cellartis). In brief, human embryonic stem cells were grown on mouse embryonic fibroblasts (MEFs) as feeder cells whose proliferation was arrested by Mitomycin C treatment. At day five of the differentiation protocol the hESCs were passaged to feeder-free, collagen I-coated 24-well OxoDishes® (for cell line and cell seeding density see Table 3.3.1).

Table 3.3.1: Cell lines and seeding cell numbers for the characterization of hESC derived hepatocytes and toxicity screening applying OxoDishes.

hESC Cell Line	Seeding Cell Number x 10^3 cm^{-2}
SA002	250
SA461	250
SA002	250
SA002	250
SA461	160
SA461	170
SA461	170
SA167	200
SA002	250

The fraction of the feeder cells was reduced compared to the starting material during further differentiation, as the MEF were growth arrested. Due to cell death and proliferation, estimated cell numbers were approximately 2 x 10^5 cells/well at day 25 of the proliferation. hES-HEP^{TM} cell lines chosen for the characterization and OxoDish study were SA002, SA167 and SA461 cells (which are derived from different donors). On day 21-22 the seeded 24-well OxoDishes$^®$ were shipped overnight in MEF preconditioned hES-HEP^{TM} culture medium (Cellartis) supplemented with hES-HEP^{TM} additive (Cellartis).

Shortly after arrival, cells were treated with MEF conditioned medium supplemented with hormones (not disclosed). The cells were maintained at 37°C in an incubator (Memmert GmbH, Schwabach, Germany) with 95 % relative humidity in a 5 % CO_2 atmosphere for one day to adjust. Growth-factor reduced Matrigel, phenol red free overlay was performed on day 23-24. Matrigel was kept at 8°C until shortly before overlay. It was supplemented to cold pre-supplemented medium in a concentration of 0.250 mg/mL. Immediately 1 mL of cold, well-mixed matrigel-containing-medium was distributed onto the plates with pre-cooled pipettes and pipette tips. Shortly after overlay treatment, cells were returned to the incubator. For the experiments, on day 25-26, medium was switched to serum-free conditions, but supplemented with specific concentrations of DMSO, hormones and growth factors such as human hepatocyte growth factor (hHGF), Oncostatin M (OSM), basic fibroblast growth factor (bFGF), however, without albumin and fatty acids.

3.3.1.3 Hep G2 cells

Hep G2 cells were seeded and maintained as explained previously (chapter 2). Seeding cell density in 24-well OxoDishes$^®$ (PreSens, Regensburg, Germany, surface area is 1.7 cm^2 w/o sensor spot) was 1.3 x 10^5 cells/well.

However, for the characterization study cells were cultured in serum-free conditions, supplemented as hESC derived hepatocytes.

3.3.2   Media preparation

3.3.2.1 Culture medium

MEF preconditioned hES-HEP^{TM} culture medium (Cellartis AB, Gothenburg, Sweden) was supplemented with hES-HEP^{TM} additive (depicted in Table 3.3.2) before application to stem cell derived hepatocytes. In addition hES-HEP^{TM} culture medium was further supplemented with other additives. Other medium supplement factors are completely defined, however, due to an ongoing patenting process are not disclosed.

Table 3.3.2: hES-HEP^{TM} additives supplied by Cellartis AB (Gothenburg, Sweden). Additives are supplemented in given concentrations to the media (Cellartis AB)

Additive	Concentration	Supplier	Order number
Oncostatin M	10 ng/mL	Promocell	C-65020
Basic fibroblast growth factor (bFGF)	2 ng/mL	Preprotech	C-100-18B
Human hepatocyte growth factor (hHGF)	10ng/ml	Promocell	C-64530
Dimethyl Sulfoxide (DMSO)	0.5 %	Sigma Aldrich	D2650

3.3.2.2 OxoDish experiment

For the OxoDish experiment completely defined medium and supplements were used as described for hESC derived hepatocyte-like cells. However, WME was not pre-conditioned, contained no phenol red and albumin was not supplemented. DMSO concentrations remained at 0.5 % (v/v) throughout the whole experiment.

3.3.2.3 Activity assay

Williams Medium E (w/o phenol red, w/o glutamine) was chosen as medium for substrate solution and it was supplemented with 0.1% Penicillin-Streptomycin, 2 mM glutamine and 25 mM HEPES Buffer (Pan Biotech, Aidenbach, Germany). Substrates chosen for CYP activity assay were phenacetin (CYP1A2), diclofenac (CYP2C9) and midazolam (CYP3A4) in final concentrations of 26, 9 and 3 µM, respectively.

3.3.3   Chemicals

All chemicals are described. Additional purchased additives and chemicals are depicted in Table 3.3.3:

Table 3.3.3:   Additional chemicals and supplements used for cell culture, characterization and hepatotoxicity studies.

Chemical	Supplier	Order number
HEPES Buffer	Pan Biotech	P05-01100
Penicillin-Streptomycin	Sigma-Aldrich	P4333
L-Glutamine	Sigma-Aldrich	G8540
L-Glutamine solution (200 mM)	Sigma-Aldrich	G7513
Matrigel, phenol red free	BD Biosciences	356231
Diclofenac sodium salt	Sigma-Aldrich	D6899
Midazolam hydrochloride	Sigma-Aldrich	UC429
Phenacetin	Sigma-Aldrich	77440

3.3.4   Microscopic analysis

3.3.4.1 Ultrastructural analysis

The morphology of the cells (seeded on collagen) at arrival and before and after matrigel overlay was monitored and recorded previous and afterwards to the activity, drug metabolism and toxicity studies using an Olympus IX70 microscope connected to an Olympus CC12 Soft Imaging System (Münster, Germany).

3.3.4.2 Immunocytochemistry for protein expression

Immunocytochemistry (ICC)-staining was performed in Cellartis AB (Gothenburg, Sweden). Differentiated hESC cultures were washed with PBS and fixed in 4 % (w/v) phosphate buffered paraformaldehyde (PFA) for 15 min at room temperature (RT). The cells were washed twice, permeabilised using PBS with 0.2 % Triton X-100 (PBST) and blocked by applying 5 % bovine serum albumin (BSA) for 30 min at room temperature. Primary antibodies against human AFP (mouse, Sigma-Aldrich, St Louis, MO), Foxa2 (goat) and CK 8 (mouse, both from Santa Cruz Biotech, Santa Cruz, CA), α-1-AT (rabbit), CK 18 (mouse), albumin (rabbit, all three from DAKO, Dako, Glostrup, Denmark), and Phalloidin (Alexa 488 conjugated, Invitrogen, Eugene, USA) and

Albumin (FITC conjugated, Bethyl Laboratories) were diluted 1:200 - 1:1000 in PBST with 1 % FCS and incubated with fixed samples overnight at 4°C. Secondary antibodies directed against mouse, rabbit or goat were conjugated with Alexa Fluor 488 (Molecular Probes, Eugene, OR, USA) and were incubated with the preparations for 2 hours at room temperature in a dark room. The nuclei were visualized by DAPI staining (Sigma Diagnostics, Stockholm, Sweden). DAKOCytomation Fluorescent Mounting Media (DAKO, Glostrup, Denmark) was used for mounting the specimens. Human primary hepatocytes were stained as controls. Stained samples were examined and recorded using a Nikon Eclipse TE2000-U fluorescence microscope and Nikon Act-1C for DXM1 200C software.

3.3.4.3 Periodic acid-Schiff (PAS) staining for glycogen storage

Glycols treated with periodic acid are oxidized to aldehydes. Addition of a mixture composed of pararosaniline and sodium metabisulfite (Schiff's Reagent), oxidized glycols (pararosaniline adducts) are stained pink to red. Differentiated hepatocyte-like hESC cultures (SA002 and SA461) were fixed for 15 min at room temperature (RT) in 4 % (w/v) PFA and subsequently washed three times with PBS. Negative control cultures were treated with α-amylase (human saliva) for 20 min at RT and subsequently also washed three times with PBS. 1 mL/well of periodic acid (PAS-kit, Sigma-Aldrich, St Louis, MO) was added to both treated and untreated cultures for 5 min at RT and immediately washed thrice. Consecutively, cultures were incubated in Schiff's reagent for 15 min resulting in a bright pink staining of the glycogen-containing cells. After repeatedly washing in PBS cells were counter-stained with haematoxylin for 90 s at RT and once again washed in PBS prior to mounting in mounting media (DAKO, Glostrup, Denmark). The protocol and the images for the PAS staining for glycogen storage were conducted at Cellartis AB.

3.3.5   TaqMan Low Density Array (LDA) gene expression analysis

Gene expression analysis was performed at Karolinska Institute (Stockholm, Sweden). Total RNA was extracted using RNeasy Midi Kit, including DNase treatment (Qiagen, Valencia, CA), according to the manufacturer's instructions. Quantity and purity of the RNA was determined, measuring the 260/280 ratio using a Varian Cary 400 Bio UV/Vis spectrophotometer (Agilent Technologies, Santa Clara, CA). Reverse transcription was

performed from 0.5 µg of total RNA in a final volume of 10 µl, using an oligo-dT primer and the M-MLV RT enzyme (Invitrogen, Carlsbad, CA).

The expression levels of 48 selected genes related to hepatic gene expression was analyzed using a custom made TaqMan Low Density Array (LDA; Applied Biosystems, Foster City, CA) as previously described (Ek et al., 2007). Three individual samples of undifferentiated SA002, differentiated hES-HEP^{TM} SA002, undifferentiated SA461 and differentiated hES-HEP^{TM} SA461 cells respectively were analyzed. Human primary hepatocytes (PHH, mix of 3) and HepG2 cells (mix of 3) were analyzed as control samples. Glyceraldehyde-3-phosphate dehydrogenase (GAPDH) was used as housekeeping gene. The relative gene expression values in comparison to expression levels in the HepG2 (relative expression value set to 1) were defined by the $2^{-\Delta\Delta CT}$ method as described by Livak and Schmittgen (2001).

3.3.6 Drug metabolism assays

After collection of supernatants from the OxoDish$^®$ experiment, cells which had not been exposed to any drug (controls) were carefully washed twice with phosphate buffered saline (PBS). 220 µL of activity assay medium (see chapter 3.3.2.3), supplemented with phenacetin (26 µM), diclofenac (9 µM) and midazolam (3 µM) was added to the three control wells in the 24-well OxoDishes$^®$. Cells were incubated with the activity assay medium for 16 hours. After the incubation, 200 µL of the activity assay medium was supplemented with 20 µL acetonitrile, transferred to a 0.5 mL Eppendorf tube and centrifuged at approx. 10.000 x g for 20 minutes at 4°C. 120 µL of the supernatant was transferred to a coned 96-well plate. Wells were sealed with tape and lid and the samples were stored at -20°C until shipment to Cellartis AB (Gothenburg, Sweden) and Pharmacelsus GmbH (Saarbrücken, Germany). Samples for subsequent measurements were transferred from Cellartis AB to Astra Zeneca (Gothenburg, Sweden).

3.3.6.1 Phase I metabolism -Cytochrome P450 activity assay

Subsequent sample preparation and liquid chromatography/mass spectrometry (LC/MS) HPLC detection were performed at Astra Zeneca according to recent publications (Kanebratt and Andersson, 2008a; Kanebratt and Andersson, 2008b). Samples were analyzed for their phase I metabolite formation as described by Kanebratt and Anderson (2008a) for the CYP1A2 metabolite acetaminophen, the CYP2C9 metabolite 4'-

hydroxydiclofenac, and the CYP3A4 metabolite 1'-hydroxymidazolam. The samples were analyzed by means of liquid chromatography/ mass spectrometry (LC/MS) HPLC. The multiple reaction monitoring (MRM) transitions chosen are displayed in Table 3.3.4:

Table 3.3.4: Cytochrome P450 activity measurement for phase I enzymes CYP2C9, CYP3A4 and CYP1A2, based on Kanebratt and Andersson (2008a; 2008b) and analyzed at Astra Zeneca (Gothenburg, Sweden).

Drug	Metabolite	Phase I enzyme	MRM (m/z)
Diclofenac	4'-hydroxydiclofenac	CYP2C9	309.9 > 265.9
Midazolam	1'-hydroxymidazolam	CYP3A4/A5	342.0 > 202.7
Phenacetin	paracetamol	CYP1A2	152.3 > 110.0

At Pharmacelsus samples were screened for phase I and phase II metabolites by means of liquid chromatography/tandem mass spectrometry (LC-MS/MS) HPLC. Potential metabolite formations were previously depicted for diclofenac, midazolam and phenacetin in Figures 3.2.2 – 3.2.4. Relative quantification of metabolites in respect to their parent compound was performed. Specific masses, measures by mass spectrometry, for the targeted metabolites of phase 1 biotransformation reactions are displayed in Table 3.3.5:

Table 3.3.5: Cytochrome P450 activity measurement for phase I enzymes CYP2C9, CYP3A4 and CYP1A2, analyzed at Pharmacelsus GmbH (Saarbrücken, Germany). NAPQI = N-acetyl-p-benzoquinoneimine, OH = Hydroxy, APAP = Acetaminophen,

Drug	Metabolite	Phase I enzyme	m/z
Diclofenac	OH diclofenac	CYP2C9/3A4	311.5 > 312.5
Midazolam	1'-OH midazolam	CYP3A4/A5	341.5 > 342.5
Midazolam	4 -OH midazolam	CYP3A4/A5	341.5 > 342.5
Phenacetin	APAP	CYP1A2	151.5 > 152.5
APAP	NAPQI	CYP2E1/1A2	151.5 > 152.5

3.3.6.2 Phase II metabolism

As pointed out by Cantelli-Forte et al. (1998) phase II enzymes are also important for the detoxification and activation of many xenobiotics. Thus, samples were further analyzed at Pharmacelsus GmbH using liquid chromatography/tandem mass spectrometry for their phase II metabolites. Specific masses, measured by mass spectrometry, of targeted metabolites are depicted in Figures 3.2.2 – 3.2.4 and in Table 3.3.6:

Table 3.3.6: Cytochrome P450 activity measurement for phase II enzymes analyzed at Pharmacelsus GmbH (Saarbrücken, Germany). GSH = Gluthatione, GST = glutathione S-transferase, UGT = Uridine-5'-diphosphoglucuronosyltransferase, NAPQI = N-acetyl-p-benzoquinoneimine, NAC = N-acetylcysteine, PST = Phenolsulfotransferase

Drug	Metabolite	Phase II enzyme	m/z
Diclofenac	4' -OH diclofenac-GSH	GST	616.5 > 617.5
Diclofenac	5 -OH diclofenac-GSH	GST	616.5 > 617.5
Diclofenac	Diclofenac acyl-glucuronide	UGT2B7	472.5 > 473.5
Diclofenac	Diclofenac O-glucuronide	UGT	487.5 > 488.5
APAP	APAP-glucuronide	UGT	327.5 > 328.5
APAP	APAP-sulfate	PST	231.5 > 232.5
NAPQI	APAP-GSH	GST	456.5 > 457.5
Midazolam	Midazolam-N-glucuronide	UGT1A4	502.5 > 503.5
OH midazolam	OH midazolam O-glucuronide	UGT2B4/B7	517.5 > 518.5
OH midazolam	OH midazolam N-glucuronide	UGT1A4	518.5 > 519.5

3.3.6.3 Diclofenac metabolites after test period

After 48 hours of cultivation with diclofenac, supernatant of samples which have been exposed to 50 µM diclofenac were collected after each OxoDish experiment. 200 µL of samples were separated and stored at -20°C until further processing. Diclofenac metabolites were identified. Samples were analyzed at Pharmacelsus GmbH using liquid chromatography/tandem mass spectrometry (LC/MS/MS).

3.3.7 Quantitative assays

3.3.7.1 Urea

Urea is one of the final degradation products of protein and amino acid metabolism of the liver. Catabolism of proteins breaks up the amino acids and deaminates them. Hereby ammonia is formed. To eliminate the excess of toxic ammonia, the liver metabolizes ammonia to urea, which can then be eliminated in the urine. Formation of urea is one important characterization factor to identify hepatocytes and their metabolic activity, since the liver is the sole location of urea production.

The assay used here (Fluitest UREA col, Analyticon, Lichtenfels, Germany) is based on Bertholot's indophenol assay (1859, Original Reference not available). The test principle is that urea, which is present in the media, is enzymatically deaminated (Urease) and ammonium ions are formed (see reaction 3.1).

$$CH_4N_2O + H_2O + 2H^+ \xrightarrow{\text{Urease}} 2NH_4^+ + CO_2 \qquad \text{[Eq. 3.1]}$$
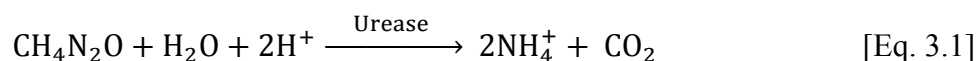
This formed ammonium ion reacts with the sodium salicylate and hypochloride which gives a green dye.

The change in absorbance is measured at a wavelength of 590 nm at 37°C using an iEMS reader MF (Labsystems, Helsinki, Finland). Samples and standards were prepared according to the manufactures recommendations, however the assay was adapted to a 96-well plate format and 20 µL of sample, instead of 10 µL were used to achieve higher absorbance changes. Urea (50 mg/dL = 8.325 mM), supplied with the kit, as well as an in-house compounded urea standard (range 100-0 mg/dl) served for quantification. The relationship between absorbance signal and urea concentration resulted in a coefficient of determination > 0.99.

3.3.7.2 Albumin

Albumin is synthesized in the liver and excreted via the kidney. Therefore, if albumin is synthesized and detected in the media, albumin is a further characterization factor for liver activity. The here used quantitative assay for albumin detection and quantification (Exocell Albuwell, Philadelphia, PA, USA) is an enzyme-linked immunosorbent assay (ELISA) following the conventional ELISA format, meaning using an antibody that recognizes a specific antigen (here albumin).

Samples and standards were prepared according to the manufactures recommendations. However, for the assay 20 µL of sample, instead of 10 µL were used to achieve higher absorbance changes.
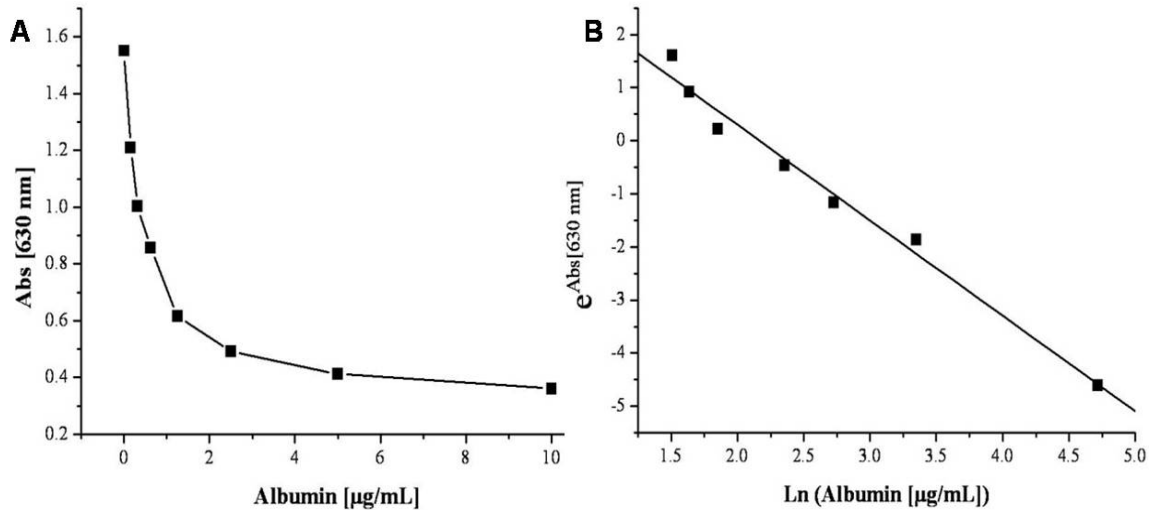
Figure 3.3.1: Albumin quantification using ELISA assay. **A**: Albumin concentration [µg/mL] measured at 630 nm. **B:** Inverse log function of obtained absorbance values over the natural log of albumin [µg/mL]. Linear regression resulted in R^2 being 0.992 and a linear equation; e^ABS(630nm)= -1.72 x Ln(Albumin[µg/mL])+3.59

An albumin concentration curve was obtained by recording the absorbance at 630 nm (Figure 3.3.1 A). By using the inverse log function the values were converted to raw µg/mL and linear regression was performed (Figure 3.3.2 B). The absorbance values of the samples were multiplied with the dilution factor (10) and albumin concentrations were calculated after normalization to the medium control.

3.3.7.3 Lactate dehydrogenase and aspartate amino transferase release

Lactate dehydrogenase (LDH) enzyme activity was measured in culture supernatants with a commercially available test kit (Fluitest[®] LDH-L, International Federation of Clinical Chemistry (IFCC), HITADO, Möhnesee, Germany). The assay was performed according to the manufacturer's instructions.

The test principle for the determination is that lactate dehydrogenase catalyses the conversion from pyruvate, the final product of glycolysis to lactic acid when oxygen is absent or in short supply.

$$\text{Pyruvate} + \text{NADH}^+ + \text{H}^+ \xleftrightarrow{\text{LDH}} \text{L} - \text{Lactate} + \text{NAD}^+ \qquad [\text{Eq. 3.2}]$$
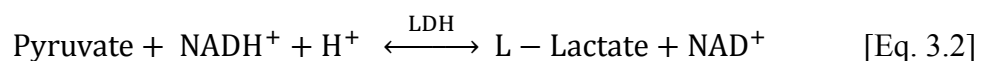
In this step NAD^+ is reduced $NADH^+$. The rate of NADH formation is directly proportional to the catalytic LDH activity and can be measured as change of absorbance over time at a wavelength of 340 nm using an iEMS reader MF (Labsystems, Helsinki, Finland). The relationship between change of absorbance signal and LDH activity resulted in a coefficient of determination > 0.99.

Aspartate aminotransferase (AST, glutamate-oxaloacetate-transaminase) enzyme activities were measured in culture supernatants with a commercially available test kit (Fluitest® GOT AST, International Federation of Clinical Chemistry (IFCC), HITADO, Möhnesee, Germany). The assay was performed according to the manufacturer's instructions.

The test principle is based on the release of AST if a cell disruption occurs. AST is present in the cytoplasm (mostly) and the mitochondria. Elevated levels of the aspartate aminotransferase can indicate tissue damage and diseases.

$$\alpha - \text{ketoglutarate} + \text{Aspartatic acid} \xleftrightarrow{\text{AST}} \text{Glutamamic acid} + \text{Oxaloacetic acid}$$

[Eq. 3.3]
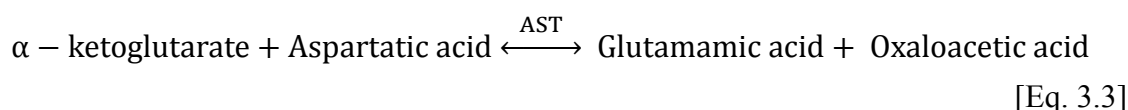
Oxaloacetic acid increases and is measured in a subsequent indicator reaction (catalyzed by malate dehydrogenase, MDH) by which NADH is oxidized to NAD.

$$\text{Oxaloacetic acid} + \text{NADH} + \text{H}^+ \xleftrightarrow{\text{MDH}} \text{Malate} + \text{NAD}^+ \qquad \text{[Eq. 3.4]}$$
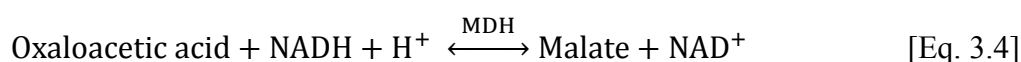
The rate of NADH reduction is directly proportional to the rate of oxaloacetic acid (OAA) formation, and thus the AST activity.

3.3.8 Analytics (Glucose, pyruvate and lactate quantification)

Quantification of glucose, pyruvate and lactic acid was performed by HPLC (Kontron Instruments, Neufarn, Germany) equipped with an Aminex HPX-87H column (300 × 7.8 mm; Bio-Rad, Hercules, CA, USA) at 40°C, with 7 mM H_2SO_4 as the mobile phase in an isocratic mode and a flow rate of 1 ml min^{-1}. Subsequent detection was performed via measurement of refraction indexes (RI) for sugars using an ERC-7515A detector (ERC Inc, Alteglofsheim-Regensburg, Germany) or UV absorption detection at 210 nm for organic acids (HPLC 535, Biotek, Neufahrn, Germany). Glucose (0-15 mM), lactate (0-15 mM) and pyruvate (0-5 mM) were tested for linearity and used as standard.

3.4 Results and Discussion

3.4.1 Microscopic morphology evaluation

Hepatocytes perform major functions associated with the liver. These functions are of exocrine and metabolic nature and are closely related to the architecture of the cells. Hepatocytes *in vivo* show a unique cellular and cell-to-cell architecture, they show three-dimensional, polygonal cell morphology and form aggregates of plates with regional polarization, which enhances polarized uptake and secretion (Arterburn et al., 1995). Dissociating of embryoid bodies early in the differentiation protocol (e.g. day five) and plating the cells as monolayer can result in multiple morphologies (Itskovitz-Eldor et al., 2000). However, addition of soluble medium factors, reconstruction of *in vivo* cell-matrix and cell-cell interactions (Snykers et al., 2009) can result in differentiation towards the hepatic lineage. Arterburn et al. (1995) showed for primary hepatocytes that dexamethasone and DMSO supplementation of the culture media and plating on collagen I coated dishes resulted in cell morphology very close to hepatocytes *in vivo*.

After about 20-22 days of differentiation towards hESC derived hepatocytes on collagen I coated plates, three batches of each SA cell line (except SA167, only once received) were shipped via overnight express to Saarland University, where their morphology was recorded immediately upon arrival. Morphology was also continuously recorded over the experiment time, including pictures before/after matrigel overlay (Figure 3.4.1 & 3.4.2 A-C). Cells upon arrival showed prominent cell aggregation and distinct cell-cell contacts. As can be seen in Figure 3.4.1 A-C cell populations of hESC derived colonies, SA002, SA167, SA461, display morphology characteristics for hepatocytes: they are large (up to 50 μm or more in diameter, Figure 3.4.1 B), they formed a monolayer of flat polygon shaped cells (rectangle in Figure 3.4.1 C), and were often bi-nucleated (arrows in Figure 3.4.1 A and B). Morphological characteristics for SA002 and SA167 cells were similar to those previously published by Soderdahl et al. (2007). The hepatic weblike-plate structure was visible (dashed square in Figure 3.4.1 A) and the demarcation among hepatocytes was clear and bright as shown in Figure 3.4.1, indicating the formation of bile canaliculi as suggested by Wang et al. (2004b). hESC cells, which were grown on collagen I gels were overlaid with growth factor reduced matrigel on day 25 (Figure 3.4.2 A-C). Hepatic characteristics could be observed after matrigel overlay (Figure 3.4.2 A-C).
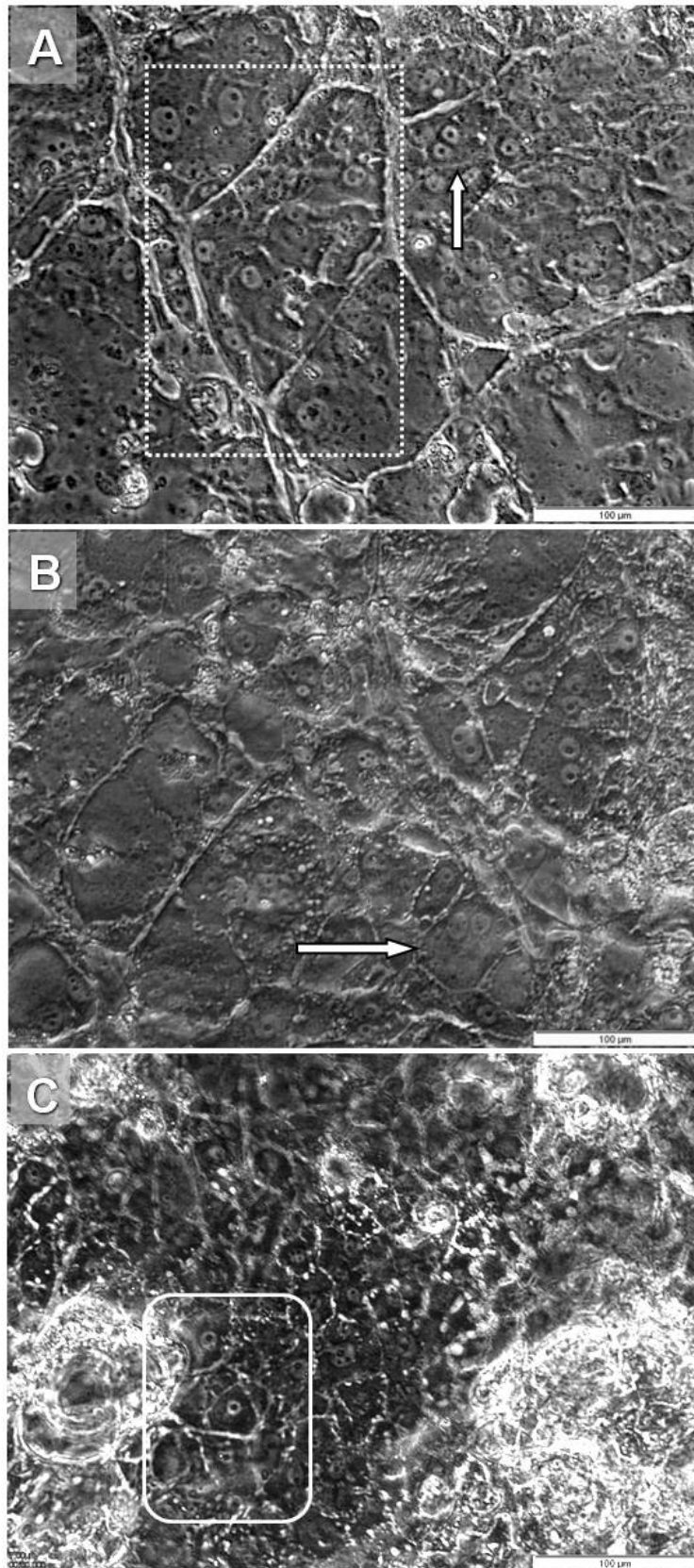
Figure 3.4.1: Cell lines SA002 **(A)**, SA461 **(B)** and SA167 **(C)** after 25 days of differentiation towards hepatic cells on Collagen I. The magnification of the pictures is 20X. The scale bar of each figure measures 100 μm. Photographs are representative for three experiments per cell line, except SA167 (only one batch).
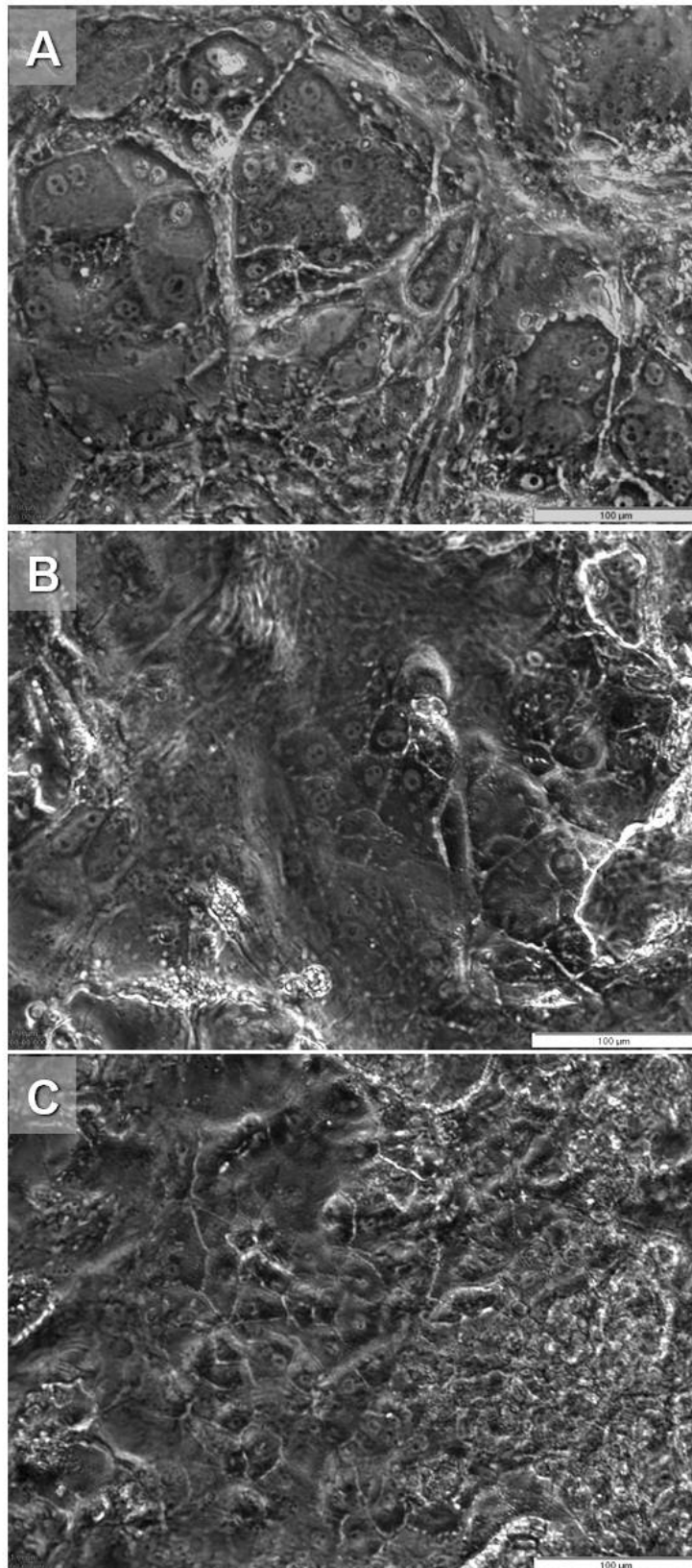
Figure 3.4.2: Cell lines SA002 **(A)**, SA461 **(B)** and SA167 **(C)** after 25-27 days of differentiation towards hepatic cells on Collagen I and matrigel overlay (sandwich culture). The magnification of the pictures is 20X. The scale bar of each figure measures 100 μm. Photographs are representative for three experiments per cell line, except SA167 (only one batch).

However, the cells, which were overlayed with matrigel (sandwich culture) appeared to be more cuboidal in shape and displayed more three-dimensional plate morphology, compared to the flat and spread polygonal cells, plated only on collagen I coated dishes.

Hepatocyte characteristics could be naturally observed in primary human hepatocytes (cubic cell shape, two nuclei, Figure 3.4.3 A, circle and arrows) but not for the hepatoma cell line Hep G2 (Figure 3.4.3 B). They displayed rather an epithelial-like morphology and contained always one nucleus.
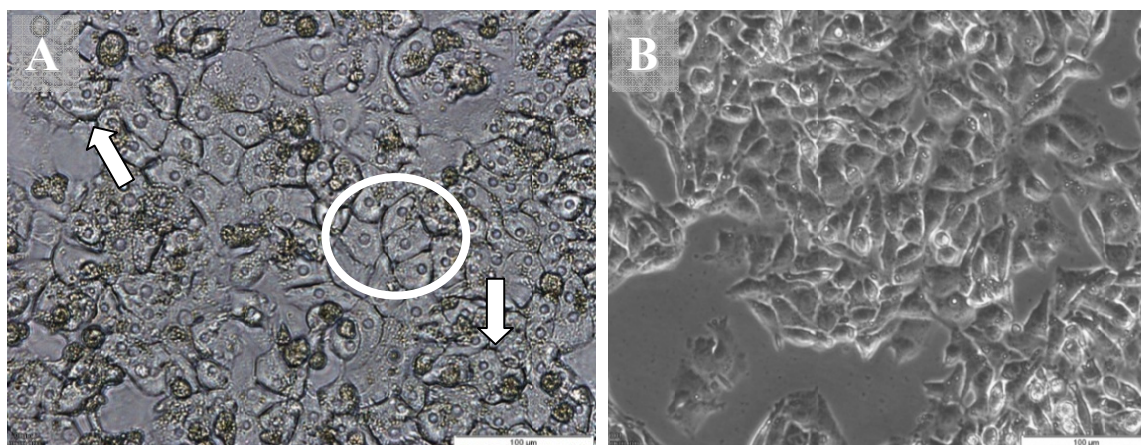
Figure 3.4.3: Morphology of primary human hepatocytes **(A)** plated on Collagen I and cultivated for two days after isolation. **(B)** Hep G2 cells 24 hours after plating. The magnification of the pictures is 20X. The scale bar of each figure measures 100 μm.

Though all hESC derived cells showed the required characteristics of adult hepatocyte-morphology, 100 % purity was not achieved for any hESC-derived cell line. The phenotype of the cell line SA002 suggested the most differentiation towards hepatic cells. However, only 70 % showed typical hepatic phenotype. Other proliferating cell types were additionally present and observed. The cell line SA461 differentiated into a mixed culture. Although cells with hepatocyte-morphology features could be detected, fibroblastic cells rapidly proliferated and represented the majority after 26 days of cultivation. These cells kept proliferating and after a culture period of 27 to 28 days the sandwich-cultured hepatocytes were dominated by the fibroblastic shaped cells. SA167 cells showed distinct hepatocyte-like structures but also presented with a large fraction of non-hepatic shaped cells. However, since the differentiation for SA167 cells seems to be a challenge (personal communication with J. Edsbagge, Cellartis AB) only one batch could be evaluated and no conclusion can be drawn.

The functionality of hepatocytes is closely related with their morphology (Arterburn et al., 1995). According to the ultrastructural observations, distinctive hepatocyte-like phenotype features for all three hESC derived hepatocyte-like cells could be observed, even though their population was mixed.

To further characterize the phenotype of the hESC-derived hepatocyte-like cell lines, protein expression was studied using immunofluorescence. Hepatic protein markers for early, mid-late and late stage of differentiation were investigated.
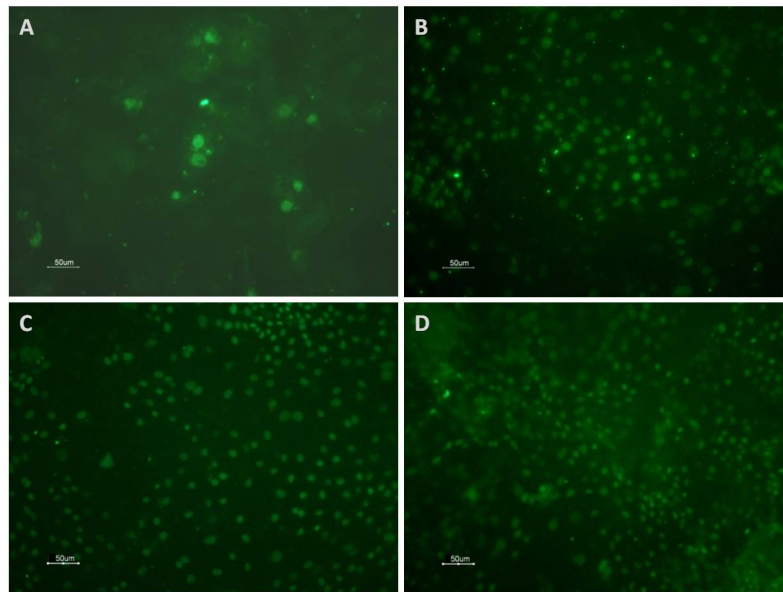
Figure 3.4.4:   Characterization of differentiated hESC derived cells, cultured in sandwich culture (collagen-matrigel). Expression of Foxa2 (HNF-3β; endoderm and hepatocyte marker) for **A)** Primary human hepatocytes **B)** SA002 **C)** SA461 and **D)** SA167 derived hepatocyte-like cells, subjected to immunofluorescence microscopy. The scale bar of each figure measures 50 μm. Images are courtesy of Cellartis AB.

As depicted in Figure 3.4.4, all tested cells (SA002, SA167, SA461 and PHHs as control) weakly expressed FoxA2 (HNF3β), which is a marker for the definite endoderm (yolk sac) as well as the fetal liver (Baharvand et al., 2006; Cai et al., 2007). The hESC-derived hepatocyte-like cells from the cell line SA002 and SA461 were further, as depicted in Figure 3.4.5, positive for the midlate/mature hepatic markers, the epithelial cytokeratins 8 (CK8) and 18 (Cho et al., 2008). For the SA002 cell line the hepatic weblike-plate structure with multiple bi-nucleated hepatocyte-like cells could be in addition very clearly visualized and the demarcation among hepatocytes was shown to be clear and bright. SA461 cells and PHHs, however, did not show such an organized morphology. The

SA461 cells seemed to be overgrown by proliferating non-hepatic cells, shown by DAPI-staining, which confirms previous suspicion.
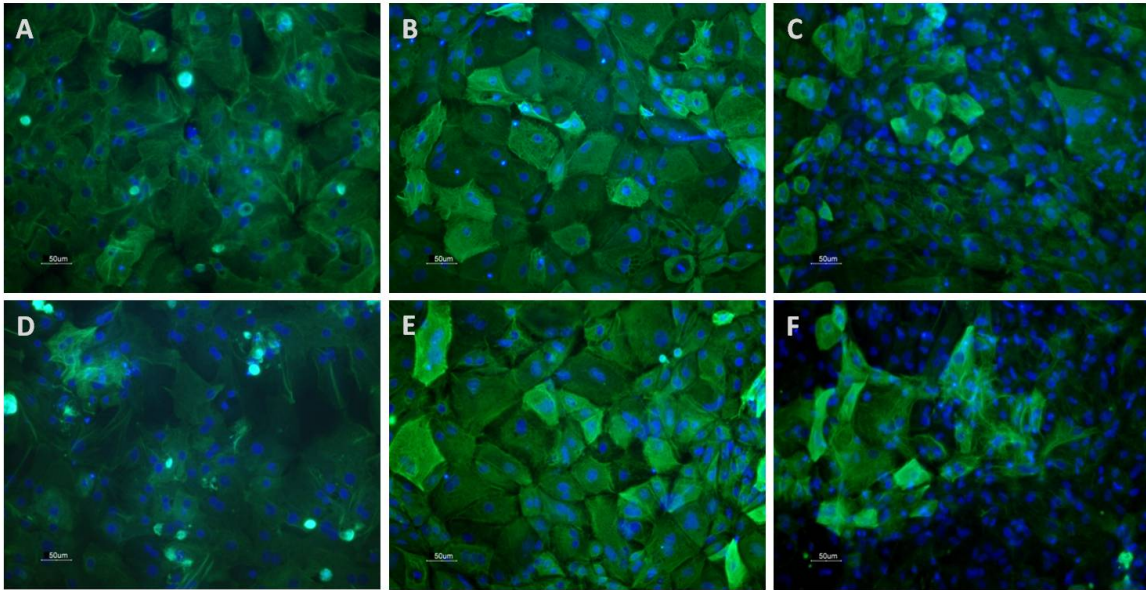
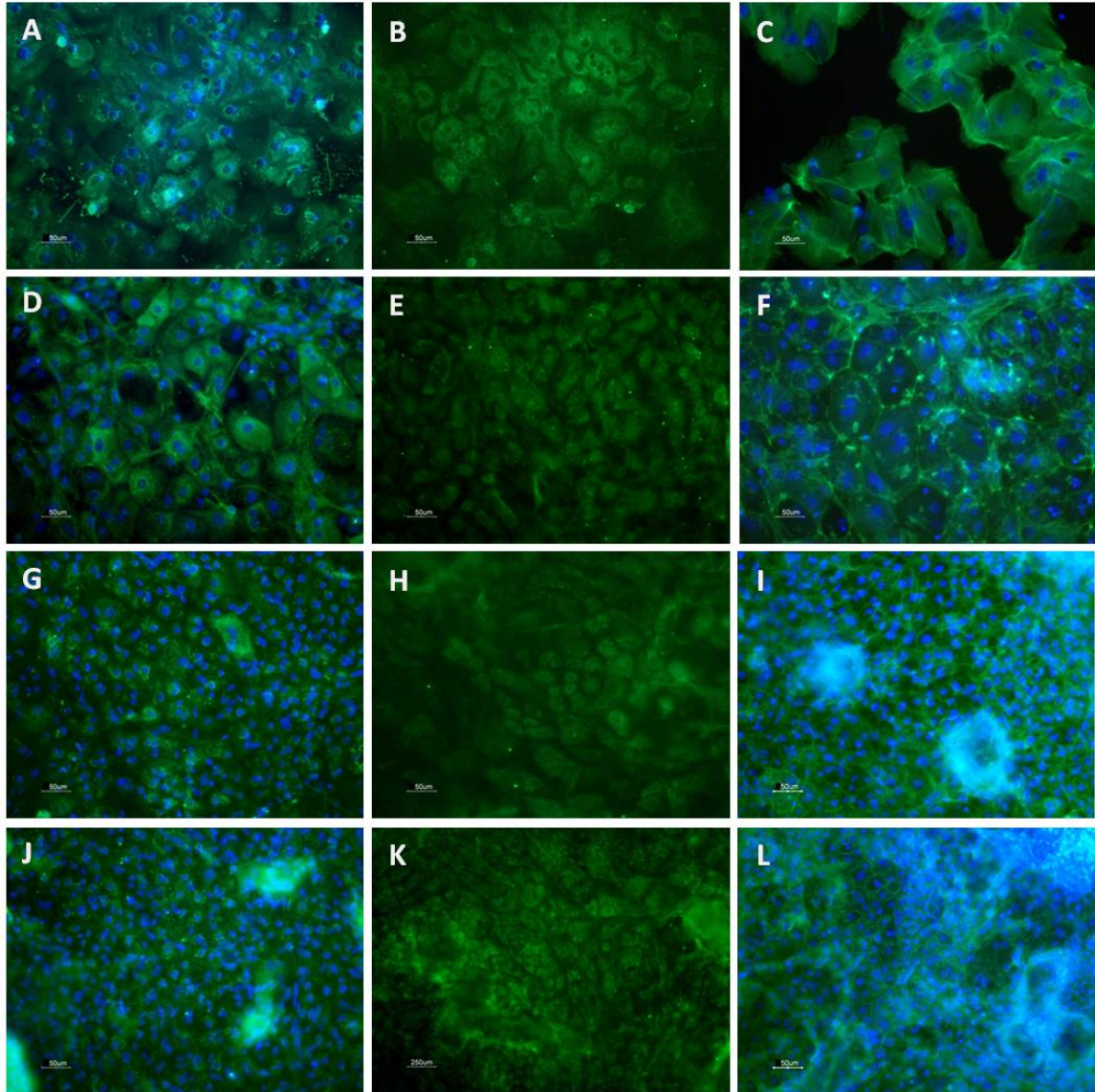**Figure 3.4.5**:   Characterization of differentiated hESC derived cells, cultured in sandwich culture (collagen-matrigel). Expression of cytokeratin 8 (CK8, indicated by FITC conjugated antibodies, pictures **A-C**) and cytokeratin 18 (CK18, indicated by FITC conjugated antibodies, pictures **D-F**) for primary human hepatocytes (**A&D**), hESC derived hepatocyte-like cell lines SA002 (**B&E**) and SA461 (**C&F**), subjected to immunofluorescence microscopy. The scale bar of each figure measures 50 μm. Images are courtesy of Cellartis AB.

α-Fetoprotein (AFP) expression, which is a very early hepatic marker expressed during the embryonic development (endoderm) but also expressed in the fetal stage, declines by proceeding down the hepatic lineage until its disappearance in adult hepatocytes. Albumin (ALB) on the other side is only expressed from early-midlate stage of liver organogenesis. However, both can be found in the yolk sac and the fetal liver (Baharvand et al., 2006). Therefore, based on AFP and ALB expression, a distinction between development stages can be performed, but not between tissues (Brewer and Tank, 1993; Snykers et al., 2009).
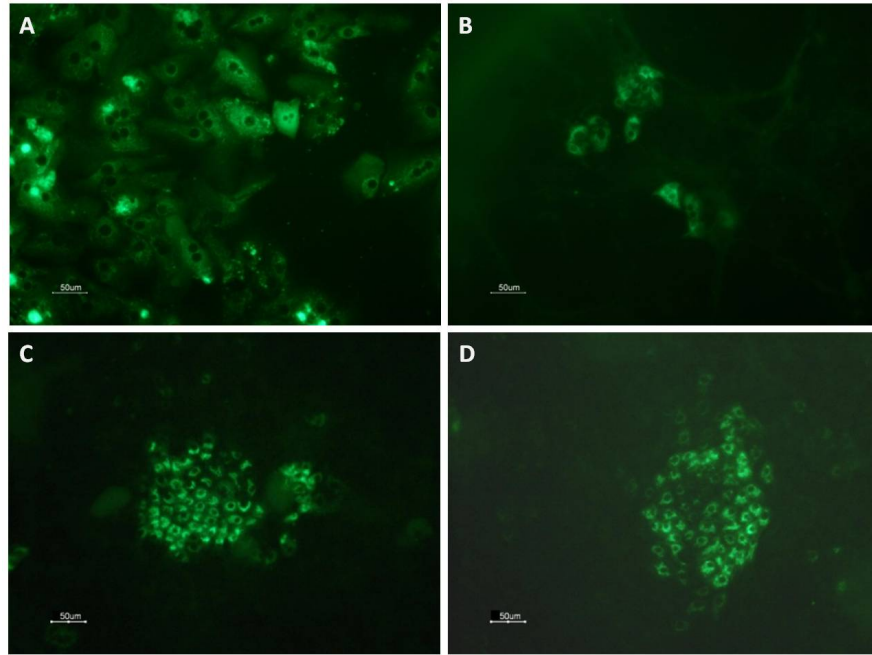
Figure 3.4.6: Characterization of differentiated hESC derived cells, cultured in sandwich culture (collagen-matrigel). Expression of albumin (marker for midlate stage of liver organogenesis), indicated by FITC conjugated antibodies against human albumin for **A)** Primary human hepatocytes **B)** SA002 **C)** SA461 and **D)** SA167 derived hepatocyte-like cells, subjected to immunofluorescence microscopy. The scale bar of each figure measures 50 μm. Images are courtesy of Cellartis AB.

For this study, α-Fetoprotein was either very weakly or not expressed (data not shown) for all tested cell lines/types, suggesting that the cells are in a more mature development stage. However, albumin was expressed, as depicted in Figure 3.4.6. While albumin could be prominently detected in the cytosol of primary human hepatocytes (Figure 3.4.6 A), only few hESC derived cells showed albumin expression and localized to hepatocyte islands and/or closer to the nucleus (Figure 3.4.6 B-D). This might be due to two reasons. First, hESC derived hepatocyte-like cells are smaller than PHHs or second, the culturing state is responsible. While PHH were trypsinized and seeded as a monolayer, the hESC derived hepatocyte-like cells were cultured in these wells. Due to this, proliferation and differentiation could be reason for the dense hepatocyte island and possibly for multiple cell layers. Based on the weak AFP and localized ALB serum protein staining, it can be presumed that the cells show endoderm commitment, however not the tissue (yolk sac or liver). One enzyme, however, CYP7A1, is only expressed in the liver and is thus a reliable marker for distinguishing yolk sac from liver cells (Baharvand et al., 2006). The CYP7A1 expression was thus performed via quantitative Real-Time PCR (qRT-PCR,

Figure 3.4.7). In comparison to PHH and Hep G2 cells, the CYP7A1 expression in SA-cell lines, although present, was weak, indicating *in vitro* liver organogenesis from definite endoderm for some cells in culture.
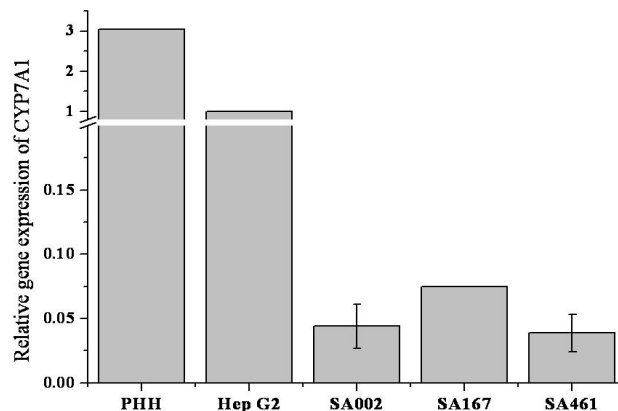
Figure 3.4.7: Relative gene expression of CYP7A1. The gene expression of Hep G2 cells is set as 1 and data are normalized to it. Data from SA002 and SA461 cells were combined from three or more experiments.

Development towards maturation could be further detected by Alpha-1-antitrypsin (A1AT) staining, a glycoprotein mostly synthesized in liver cells (Coakley et al., 2001). As displayed in Figure 3.4.8 (sub-images A, D, G & J), A1AT was distinctively expressed for SA002 and SA461 cells. Interestingly, the glycoprotein synthesis was weaker in the PHH cells, compared to the hESC derived hepatocyte-like cells. Immunofluorescence positive staining for the multidrug resistance protein 2 (Mrp2; *Abcc2*) (Pfandler et al., 2004), as depicted in Figure 3.4.8 (sub-images B, E, H & K), was also observed for all tested cell lines/types. Mrp2 is part of the ATP-binding cassette (ABC) transporter superfamily and together with the bile-salt export pump (BSEP; ABCB11) they provide the driving force for the bile flow within the bile caniculi (Pfandler et al., 2004). Although intracellular immunofluorescence was expressed for all tested cell lines/types, indicated by green staining in Figure 3.4.8 (sub-images A, D, G & J), only weak canalicular Mrp2 staining could be observed. Canalicular Mrp2 satining usually indicates maturation and correct polarization of functional hepatocytes. Similarly, no functional polarization (only canalicular Mrp2 staining) could be found for PH hepatocytes, which might be due to the trypsinization and plating procedure. However, for the hESC derived cell lines mainly Mrp2 transporters were found in the cytosol and thus further polarization factors as BSEP and basolateral transporters should be investigated on the protein level as previously shown by Pfandler et al. (2004). As can be

76

further seen in Figure 3.4.8 (sub-images C, F, I & L), for the hESC derived cell lines SA002, SA461 and SA167 phalloidin staining of F-actin bundles could be observed in the lumen of the cells, thus indicating polarity (Tanimizu et al., 2007). Primary human hepatocytes, however, did not only show phalloidin expression in the apical membrane but also in the cytosol, thus suggesting once again no correct polarization.

Figure 3.4.8: Characterization of differentiated hESC derived cells, cultured in sandwich culture (collagen-matrigel). Expression of alpha-1-antitrypsin (A1AT; ABcc2) is shown in sub-images A, D, G & J. MRP2 (ATP-binding cassette (ABC) transporter) expression (B, E, H & K) and phalloidin staining of F-actin (C, F, I & L) are shown for primary human hepatocytes (image A-C) and hESC derived hepatocyte-like cell lines SA002 (D-F), SA461 (G-I) and SA167 (J-K), subjected to immunofluorescence microscopy. All antibodies against specific proteins are FITC conjugated (green) and the nuclei are depicted by DAPI staining (blue). The scale bar of each figure measures 50 μm. Images are courtesy of Cellartis AB.

Based on the combined protein expression data, it can be surmised that the cells are derived from definite endoderm and are presumably in the mid-late hepatic development phase. However, they show signs of maturation. In addition, almost all hESC derived cells have been shown to express the expected hepatic proteins (ALB, CK8 & CK18, Foxa2, Mrp2, A1AT), indicating differentiation towards functional-hepatocyte-like cells. However, it should be pointed out, that during liver organogenesis, the final step of maturation takes place after birth and only then adult liver specific genes such as tryptophan oxygenase (TO) and as cytochrome P450s genes are expressed (Kamiya et al., 2002). Thus, to obtain a more detailed picture, gene expression profiling of metabolizing enzymes, transporters and transcription factors related to mature hepatocyte phenotype was performed.

3.4.2   Gene expression profiling via Low Density arrays (LDAs)

In this part of the characterization study the expression of late stage maturation genes (AFP, ALB, G6P and A1AT) and liver cell protein expressions, as well as UDP-glucuronosyltransferases (UGTs), transporter and transcription factors were evaluated using TaqMan low density array (LDA) cards approach as previously published by Ek et al. (2007). For each cell line (PHHs, Hep G2 cells, differentiated SA002 and SA461 cells, and undifferentiated SA002 and SA461 cells) 45 gene expressions were gathered and evaluated in Karolinska Institute (Stockholm, Sweden).

For three data sets, each, the gene expression was averaged for differentiated SA002 and SA461 cells and is depicted in Figure 3.4.9. The undifferentiated controls of SA002 and SA461 cells and Hep G2 cells were measured once. For PH hepatocytes the average of two data sets is depicted. A figure, including average values is attached in the appendix (Fig. 7.4.1).

As can be seen in Figure 3.4.9, the gene expression from the two differentiated hESC cell lines (SA002 and SA461) did not vary much from each other. CYP1A1, 1B1, 2A6, 2B6, 2C19, 2C8, 2D6, 2E1, 3A4 and 3A7 mRNA expression was detected in hepatocyte-like cell, whereas CYP2C9 was only expressed in SA461 cells. All cytochrome P450 genes which could not be detected in the SA cell lines (CYP1A2, 2C8 and 2C9) were also not present in Hep G2 cells, which served as the reference. Overall, the relative gene expression levels for the genes investigated were lower in hepatocyte-like cells from both lines, than in Hep G2 cells and primary human hepatocytes.

78
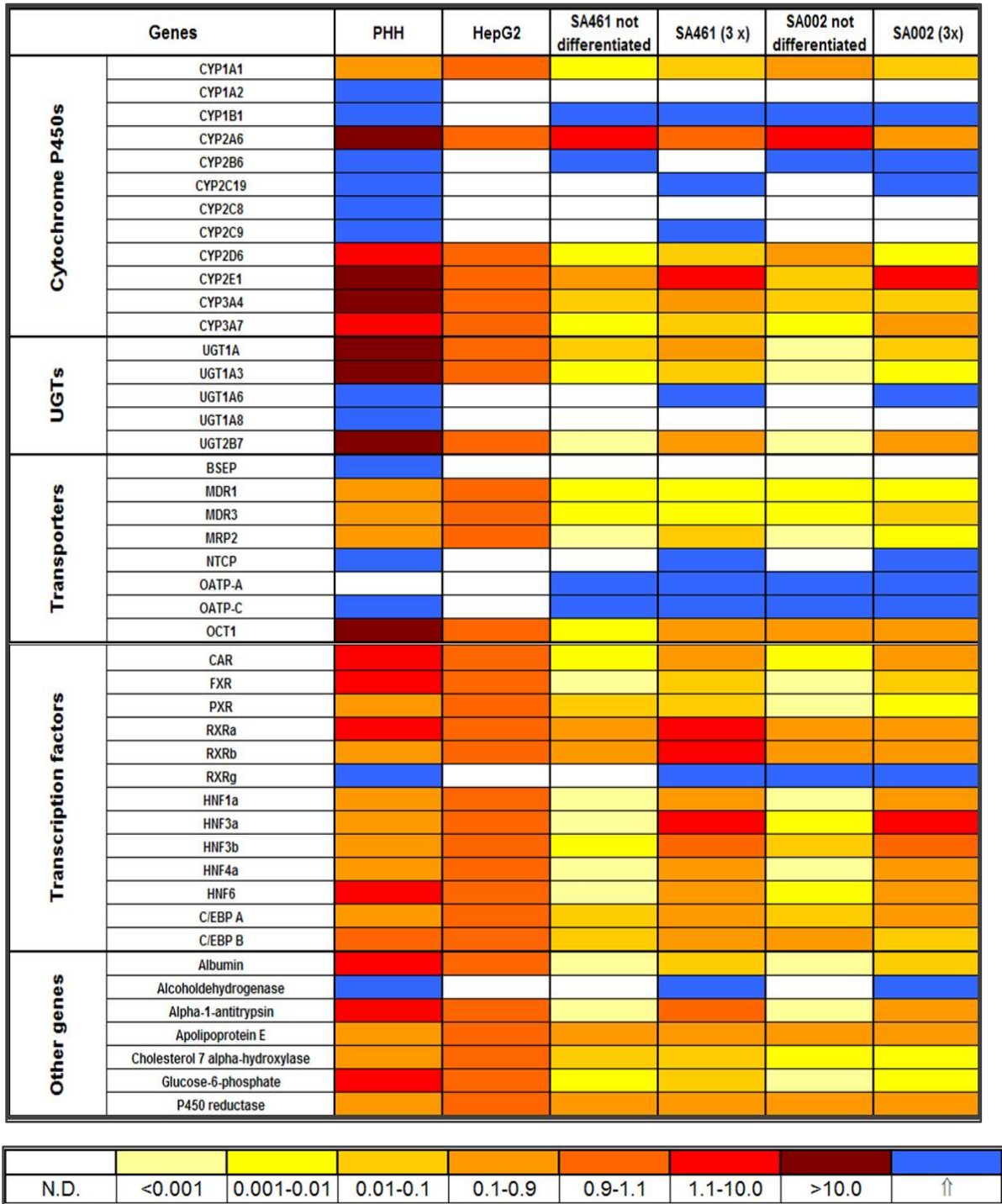
Figure 3.4.9: Relative gene expression for liver related genes as measured by LDA assay for PH hepatocytes, Hep G2 cells and SA002 and SA461 cell in undifferentiated and differentiated form. All samples were run on LDA cards containing different genes associated with liver drug metabolism. The expression for all genes is normalized against the expression of the gene for hypoxanthine phosphoribosyltransferase (HPRT) in each sample. The expression levels in each sample are compared to the expression levels in Hep G2 cells, which are set to 1.0 for all genes. UGTs: UDP-glucuronosyltransferases, N.D.: not detected, ↑: detected. Heat map was generated at Karolinska Institute.

However, more CYPs, UGTs, transcription factors and transporter were expressed in the hESC cell lines, compared to Hep G2 cells. Some gene expressions were even higher than in Hep G2 cells, such as CYP2E1 and the transcription factors RXRa and RXRb, as well as HNF3α and α1-antitrypsin. RXRb and HNF3α were even higher than in PH hepatocytes. In the undifferentiated hESC cell lines, only weak levels of liver specific genes were expressed. Only CYP2A6 was expressed more than in both differentiated hESCs. However, in general the relative gene expression levels were of the order undifferentiated hESC < differentiated cells < Hep G2 and PHH cells. Nevertheless, more complete liver specific gene expression was detected for the differentiated hESC cell lines, compared to Hep G2 cells. SA461 cells in comparison to SA002 cells appeared to show more relative gene expression, indicating more advanced differentiation. This is interesting, since the phenotype analysis revealed SA002 cells to be more hepatocyte-like.

However, on the transcriptome level, both hESC derived cell lines showed phase I and phase II (here seen by UGTs expressions) metabolism, which is important for biotransformation of chemical entities, especially drugs (Cantelli-Forti et al., 1998; Giron et al., 2008; Li, 2001; Tzanakakis et al., 2000). Both derived cell lines further showed expression of HNF4α, C/EBPa and C/EBPb, genes which suggest hepatic, immature, phenotype, comparable to PH hepatocytes (Li et al., 2000; Westmacott et al., 2006). Compared to Hep G2 their gene expression was even lower. Genes that indicate maturation (ALB, A1AT and G6PDH), were also elevated for the differentiated cells, compared to non-differentiated cells. α-1-antitrypsin, which is solely expressed in the liver (Coakley et al., 2001), was expressed for SA461 cells in amounts comparable to Hep G2 cells.

In conclusion, the data presented here indicate that the cell lines SA002 and SA461 differentiated towards functional hepatocytes. It was shown that the gene expression of differentiated cells, compared to undifferentiated cells, was elevated for almost all liver specific genes. However, overall gene expression profiles in comparison to Hep G2 cells and PH hepatocytes suggest that these cells are not yet mature, but start to show biotransformation capacities and functionality.

3.4.3 Functional analysis

The liver becomes a functional organ only in the terminal step of organogenesis and thus functional assays have to ascertain functional properties (Snykers et al., 2009) of hepatocytes, derived from stem cells. Functionality was tested by quantification of albumin secretion, urea metabolism (privileged for hepatocytes) and glycogen storage, as well as drug metabolism activity analyses. For all assays, cells were exposed to diclofenac in four different concentrations (0, 0.05, 0.10, 0.20 mM) to further determine drug metabolism activity and its influence onto hepatic functionality.

3.4.3.1 Urea production

Urea metabolism and secretion is a privileged function of hepatocytes and thus an important marker for hepatic metabolic function. As depicted in Figure 3.4.10, after 48 hours of incubation with and without diclofenac exposure, all cell lines/types showed functional urea metabolism, and thus hepatic functionality. However, cells derived from ES cells, did not reach the same urea metabolism activity as primary human hepatocytes or Hep G2 cells.
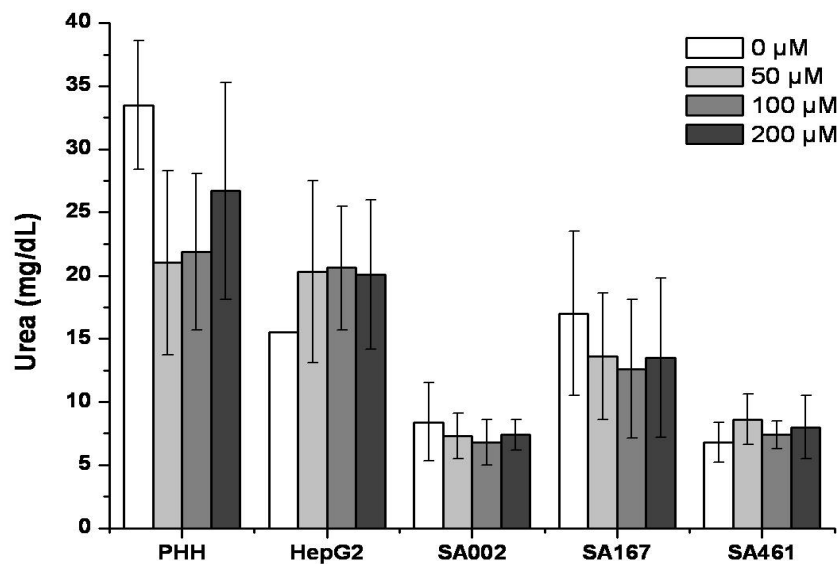
Figure 3.4.10: Urea secretion after 48 hours of cultivation for Hep G2 cells, primary human hepatocytes and hESC derived hepatocytes cell lines (SA002, SA167 and SA461) exposed to four concentrations of diclofenac, ranging from 0-200 μM in monolayer sandwich culture. Each column represents the mean of the results from three different cultures measured in duplicate.

Verma et al. (2007) reported that Hep G2 cells retain many liver specific functions, such as albumin secretion, urea synthesis, and glucose secretion. Similar results were also published recently (Guzzardi et al., 2009), which showed albumin secretion and urea synthesis for Hep G2 cells in static cultures. However, it also had been reported that Hep G2 have no functional urea cycle, since they lack ornithine transcarbamylase (OTC) as well as arginase I mRNA and protein (Mavri-Damelin et al., 2008a). However, Mavri-Damelin et al. (2008a) detected for C3A cells, a clonal derivative of Hep G2 cells, urea in the media and concluded that urea is produced via an urea cycle-independent mechanism, namely through arginase II. Since urea was quantified in the culture supernatant using a commercial assay, it was not determined which mechanism underlies urea synthesis. However, it is known, that functional PH hepatocytes maintain long-term urea synthesis, even in 2D culture (Katsura et al., 2002). In addition, urea was detected by GC/MS measurements (data not shown) in the media for all cell lines, which supports that urea is produced as depicted in Figure 3.4.10.

Li et al. (2008b) quantified urea synthesis in hESC derived hepatocytes as 70 $\mu g/(10^6$ cells x 24h) with a declining trend over time. For SA002 and SA167 and Hep G2 rates of 133, 125 and 138 $\mu g/(10^6$ cells x 24h), could be calculated based on approximately 2 x 10^5 cells/well at day 25 of the proliferation, respectively (cell enumeration performed at Cellartis AB). SA167 cells even showed an urea synthesis rate of 290 $\mu g/(10^6$ cells x 24h), which is half compared to primary human hepatocytes, showing 480 $\mu g/(10^6$ cells x 24h) as rate. Thus, these productions rates indicate urea metabolism to be active and functional, and further in the same order of magnitude as Hep G2 cells. Bahavand et al. (2006), obtained urea secretion concentrations for hESC derived cells, cultured in 24-well plates, of approximately 15-20 mg/dL after 22 to 28 days of differentiation in 2D cultures and higher values in 3D culture and thus concluded that hESC, differentiated in 3D culture systems, showed higher resemblance to *in vivo* conditions. They cultured five embryoid bodies and differentiated those towards hESC derived hepatocyte-like cell, however failed to enumerate the cell number for their functional analysis. Since for this study four embryoid bodies were used per well, their presented data are approximately in the same order of magnitude as the here obtained values. No distinctive influence on urea synthesis could be found, if diclofenac was supplemented for 48 hours to the culture medium.

3.4.3.2 Albumin synthesis

To further assess if the hESC derived hepatocyte-like cells possess liver-cell functionality, albumin secretion into the culture supernatant was measured after an incubation period of 48 hours. As depicted in Figure 3.4.11, PHHs synthesized 16.5 µg albumin in 48 hours if no drug was applied. Since the cell number was known, the albumin synthesis rate can be calculated and resulted in 47 µg/(10^6 cells x 24h). However if drug was present, the synthesized albumin concentration was reduced. Nahmias et al. (2006) reported an albumin synthesis rate of 35 µg/(10^6 cells x 24h) for PHH cells, which is in the same range as the values observed here.
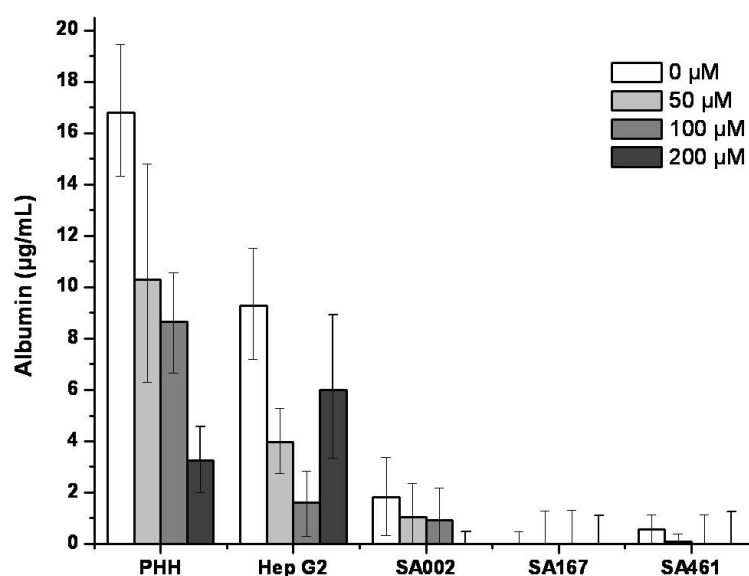
Figure 3.4.11: Albumin synthesis after 48 hours of cultivation of Hep G2 cells, primary human hepatocytes (PHH) and hESC derived hepatocytes cell lines (SA002, SA167 and SA461) exposed to four concentrations of diclofenac, ranging from 0-200 µM in monolayer sandwich culture. Each column represents the mean of the results from three different cultures measured in duplicate.

Hep G2 cells show synthesis of albumin (Guzzardi et al., 2009; Verma et al., 2007). However, the value of 6 µg/(10^6 cells x 24h) obtained in this study is higher than previously reported rates from Guzzardi et al. (1 µg/(10^6 cells x 24h)) and by Kinasiewicz et al. (2006) (2.5 µg/(10^6 cells x 24h)). As depicted in Figure 3.4.11, the hESC cell line SA002 produced approximately 2 µg/mL in 48 hours, resulting in an approximate rate of 3.3 µg/(10^6 cells x 24h), without drug supplementation. SA461 cells synthesized albumin in a rate of 1.67 µg/(10^6 cells x 24h) and SA167 cells secreted albumin into the culture medium with a rate of 0.5 µg/(10^6 cells x 24h) if no drug was supplemented. These

values, although lower than Hep G2 cells and primary human hepatocytes, are higher or comparable to reported results from hESC derived hepatocyte-like cells. Li et al. (2008b) reported albumin synthesis values below 0.5 µg/(10^6 cells x 24h). Bahavand et al. (2006) obtained albumin secretion concentrations of 1-2 µg/mL after 24 days of differentiation in 2D cultures, using more starting material than in this study.

All diclofenac concentrations induced an impaired albumin secretion for all cell types, indicating cells struggling with toxic effects. The impairment increased for increasing drug concentrations. Castell et al. (1997) showed for cultured primary rat hepatocytes that diclofenac concentrations of 70 µM induced a reduction of the albumin synthesis by approximately 50 %. These albumin responses to diclofenac exposure are similar to albumin production data of primary human hepatocytes, depicted in Figure 3.4.11.

3.4.3.3 Glycogen storage

Glycogen is stored in hepatocytes and thus assaying for glycogen is important for phenotype analysis. As depicted in Figure 3.4.12 most hESC derived hepatocyte-like cells, which also displayed hepatic morphological characteristics, showed glycogen accumulation, which is typical hepatic feature (Soderdahl et al., 2007), and thus indicating hepatic functionality. However, the intensities varied. While SA461 cells (Figure 3.4.12 C) showed a high glycogen storage, SA002 cells (Figure 3.4.12 B) only weakly showed glycogen staining, compared to control cells (Figure 3.4.12 A). Thus SA461 derived hepatocyte-like cells seemed to be superior and further differentiated than SA002 cells.
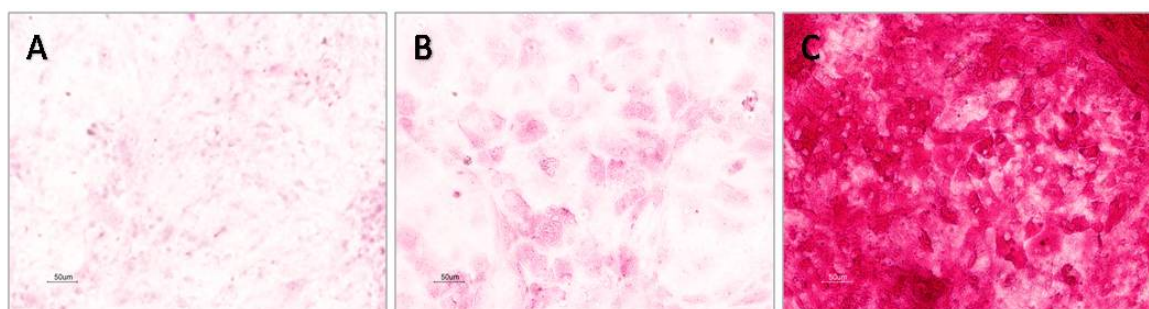
Figure 3.4.12: Periodic acid Schiff (PAS) staining for glycogen storage for **A)** control cells **B)** SA002 and **C)** SA461 cells after differentiation towards hepatocytes, subjected to light microscopy. The scale bar of each figure measures 50 µm. Images are courtesy of Cellartis AB.

Nevertheless, here, one cannot quantitatively compare glycogen staining, since the protocols were not performed at the same date and thus variability during staining might be the reason for the different intensities. However, both hESC cell lines showed distinct glycogen staining, thus indicating hepatic functionality.

3.4.3.4 Activity of drug metabolism

Presence of phase I and phase II drug metabolizing enzymes is a key factor for characterization of functional hepatocytes. Three drugs, namely diclofenac, phenacetin and midazolam, which are metabolized by both phases, thus were used to determine drug metabolism activity. Two approaches were used. After 16 hours of drug exposure the phase I (Astra Zeneca and Pharmacelsus) and phase II (Pharmacelsus) activities were determined by measurement of formed metabolites via LC-MS/MS. In another experiment diclofenac metabolites were measured in pooled samples (three wells per cell line) after 48 hours of 50 µM diclofenac exposure and biotransformation was analyzed.

Phase I activity assay after 16 hours of drug exposure

A drug cocktail with specific probe substrates, namely diclofenac, midazolam and phenacetin, was applied to all test cell lines/types to characterize phase I drug-metabolizing enzymes *in vitro*.
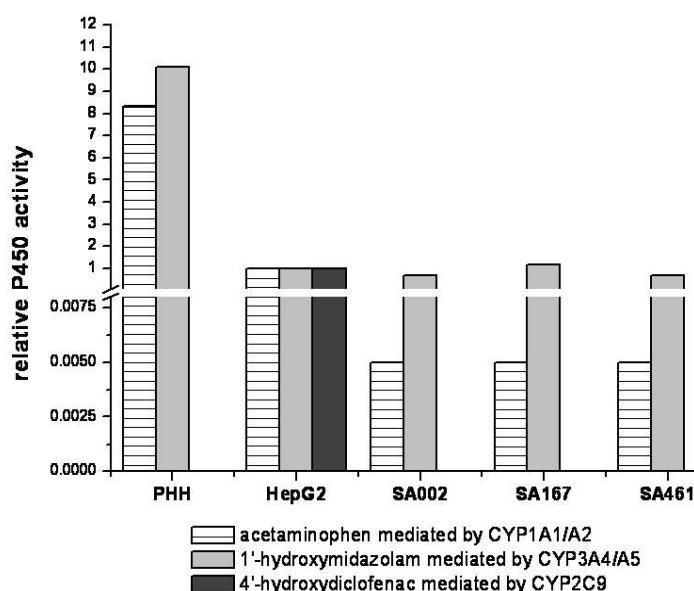
Figure 3.4.13: P450-selective activities using phenacetin, diclofenac, and midazolam in primary human hepatocytes (PHH), hESC derived hepatocyte like cells (SA002, SA167 and SA461) and Hep G2 cells. The activity levels in each sample are compared to the activity levels in Hep G2 cultures, which are set

to 1.0 for all cytochrome P450 activities. Samples were measured at Astra Zeneca (Gothenburg, Sweden).

As depicted in Figure 3.4.13, no CYP2C9 mediated diclofenac phase I metabolism towards 4'-hydroxydiclofenac could be detected for hESC derived cell lines, compared to Hep G2 (set to 1.0). Surprisingly, no 4'-hydroxydiclofenac was measured for primary human hepatocytes either. However, CYP2C9 metabolism for PHH is a well documented activity (Floby et al., 2004) and thus it can be speculated, that either a measurement problem existed, which is less likely, since CYP2CP activity could be found for Hep G2 cells, or that the metabolite was destroyed during storage or freezing. Formation of 1'-hydroxymidazolam, mediated by CYP3A4, was found for all cell lines/types. The hESC derived cell lines showed CYP3A4 activity comparable to Hep G2 cells; nevertheless, almost 10-fold less than PHHs. Based on these data activity for CYP3A4 for the hESC derived cell lines is relatively high. This is important, since CYP3A4 oxidizes approximately 50 % of all known pharmaceuticals (Li, 2001). Very little activity was found for CYP1A1 and CYP1A2 mediated biotransformation of phenacetin for the hESC derived cell lines, compared to Hep G2 or PHH cells. Thus, these data confirm the gene expression data, where expression of CYP1A2 was not detected and the expression of CYP1A1 was several fold less than Hep G2 cells (Figure 3.4.9).

Phase I and phase II activity assay after 16 hours of drug exposure

Diclofenac treatment has been associated with hepatocellular injury caused presumably by metabolic idiosyncracy and mediated by chemically reactive metabolites (Banks et al., 1995). Two major reactive metabolites that bind to hepatic protein and are thus recognized as foreign and likely to cause immune responses, seem to mediate potentially the idiosyncratic toxic responses; Glucuranation of diclofenac, catalyzed by human UGT2B7 (King et al., 2001), followed by covalent protein adduct formation (Bailey and Dickinson, 1996) and diclofenac CYP 450-mediated hydroxylation via CYP2C9, which is then further oxidized to reactive benzoquinone imine intermediates and trapped as glutathione adducts (Grillo et al., 2003; Ngui et al., 2000; Poon et al., 2001; Tang et al., 1999; Yan et al., 2005) are likely reasons for diclofenac-protein adduct formation and thus for hepatotoxicity.

As shown in Figure 3.4.14, diclofenac metabolites could only be detected for primary human hepatocytes after 16 hours of incubation in the activity assay medium. Phase I hydroxylation activity of CYP2C9 transformed the parent drug to its 4'-hydroxydiclofenac metabolite. Diclofenac-O-glucuronide formation was also detected which implies phase II UGT2B7 activity. It has to be pointed out, that no diclofenac-acylglucuronide formation could be detected after the culture period of 16 hours. In addition, no phase II glutathione adduct formation from 4'hydroxydiclofenac as intermediate could be observed for PHHs after the incubation period of 16 hours. Presumably either gluthathione S-transferase (GST), which catalyzes the conversion of 4' hydroxydiclofenac to the glutathione adduct, was not expressed, or, more likely, since no glutathione adduct formation could be detected for PH hepatocytes, it can be surmised that the adduct was damaged during storage and thus could not be detected.
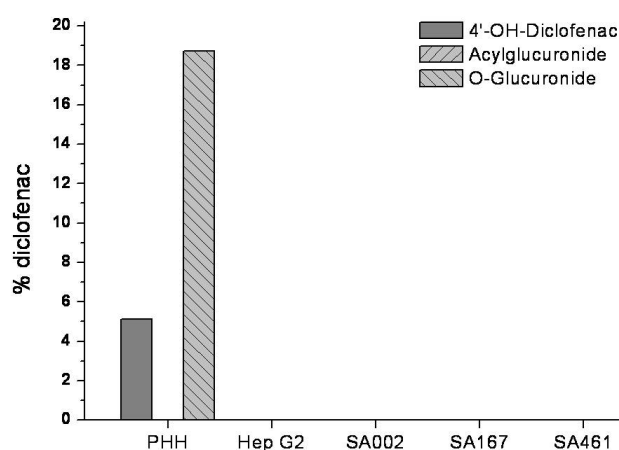
Figure 3.4.14: Metabolic fate of diclofenac after 16 hours of drug exposure. Tested cell lines/types were PHH, Hep G2 cells, and the hESC derived cell lines SA002, SA167 and SA461 medium. Only PHH cells showed any diclofenac metabolism capacity after 16 hours. Metabolites are depicted as % total diclofenac (9 μM). Samples were measured at Pharmacelsus GmbH (Saarbrücken, Germany).

In summary, and as shown in Figure 3.4.14, only primary human hepatocytes showed hydroxydiclofenac and diclofenac-O-glucuronide formation after 16 hours of diclofenac exposure, thus having the highest drug metabolizing activity towards the even more toxic metabolites (Seitz and Boelsterli, 1998). Neither for Hep G2 cells nor for any of the three hESC derived cell lines phase I or II diclofenac metabolism could be detected. However, as previously shown for the complimentary liver gene expression profiling (depicted in Figure 3.4.9), CYP2C9 and UGT2B7 genes were distinctively less expressed in these

cells compared to PH hepatocytes and thus high drug metabolism activity cannot be expected.

Midazolam undergoes extensive oxidative metabolism mediated by mainly CYP3A4, CYP3A5 and less CYP3A7 (fetal) to its equipotent 4-hydroxymidazolam and 1'-hydroxymidazolam (40-100%), which is further glucuronide conjugated followed by renal excretion (Hyland et al., 2009; Klieber et al., 2008; Zhu et al., 2008). N-glucuronation, however, can also occur directly from the parent compound and is mediated by phase II UDP-glucuronosyltransferase (UGT1A4). O-glucuronation from 1'-hydroxymidazolam however is mediated by UGT2B4 and UGT2B7 (Hyland et al., 2009).
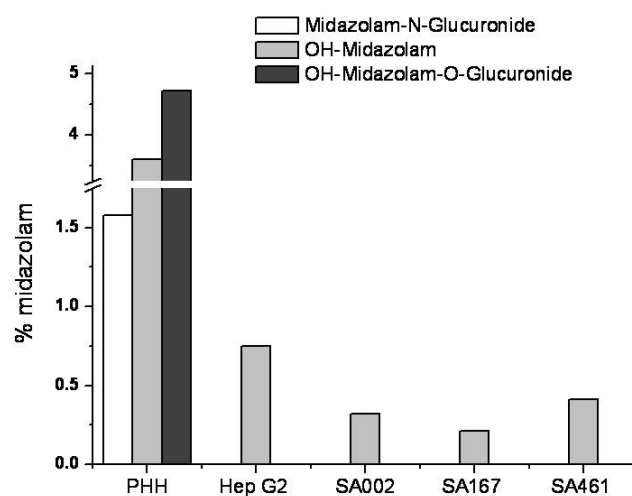
Figure 3.4.15: Metabolic fate of midazolam after 16 hours of incubation. Tested cell lines/types were primary human hepatocytes (PHH), Hep G2 cells, and the hESC derived cell lines SA002, SA167 and SA461. Metabolites are depicted as % total midazolam (3 μM). Samples were measured at Pharmacelsus GmbH (Saarbrücken, Germany).

As depicted in Figure 3.4.15, primary human hepatocytes showed distinct phase I biotransformation via CYP3A4/A5 to its 1'-hydroxymidazolam form (approx. 3.5% of total midazolam) and further glucuronidation to hydroxy-midazolam-glucuronide mediated by UGT2B4 and UGT2B7. Direct glucuronation via UGT1A4 (approx. 1.5% of total midazolam) could also be detected. Hep G2 cells and the hESC derived cells SA002, SA167 and SA461 showed CYP3A4/A5 activity indicated by 1'-hydroxymidazolam formation in comparable concentrations. These data are in concordance with previously shown activity data, measured at Astra Zeneca (Sweden) and depicted in Figure 3.4.13. However, no further glucuronation could be detected for the differentiated cells. Thus,

UGT2B4, UGT2B7and UGT1A4 did not seem to be active after 16 hours of incubation with midazolam.

Phenacetin is majorly metabolized via CYP1A2 to acetaminophen, which is followed by phase II metabolism to non-toxic metabolites APAP-sulfate, APAP-glucuronide or APAP-glutathione (Park et al., 2005; Polasek et al., 2006). Phase I phenacetin metabolism was detected by its CYP1A2 metabolite acetaminophen (APAP) for Hep G2 and PH hepatocytes. No unconjugated APAP could be found for the hESC derived hepatocyte-like cell lines SA002, SA167 or SA461. However, APAP-sulfate, which is a phase II metabolite of APAP, could be detected for all tested cell lines. Thus, CYP1A2 activity must have been present in the SA cell lines to deethylate phenacetin to acetaminophen, followed by phase II phenolsulphotransferase (PST) activity and its acetaminophen-sulfate metabolite (see Figure 3.4.16).
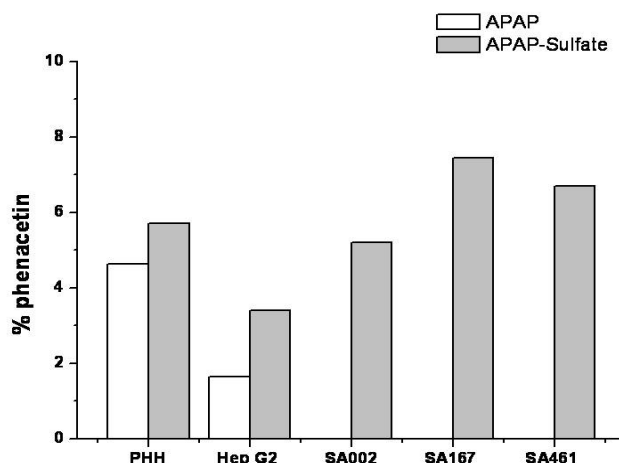
Figure 3.4.16: Metabolic fate of phenacetin after 16 hours of incubation. Tested cell lines/types were primary human hepatocytes (PHH), Hep G2 cells, and the hESC derived cell lines SA002, SA167 and SA461. Metabolites are depicted as % total phenacetin (26 µM). Samples were measured at Pharmacelsus GmbH (Saarbrücken, Germany).

No glutathione conjugate could be detected for any cell type. However, this was not unexpected, since NAPQI, the intermediate and toxic metabolite, is only approx. 5 % of parent drug (Park et al., 2005; Polasek et al., 2006), from which APAP-glutathione is mediated. However, most probably, the glutathione adduct formation could not be detected due to adduct damage during storage. The APAP-glucuronide, however, was expected to be found. While APAP-glucuronide peaks could be identified, high interference with the probe substrate cocktail, which served as control matrix, appeared

(see Appendix, Figure 7.4.3). Thus, no UGT activity could be validly confirmed here and for further phase II metabolism characterization studies, the measurements should be repeated.

Metabolic fate of diclofenac after 48 hours of exposure

As described previously, diclofenac is converted via two major biotransformation pathways, namely aromatic hydroxylation (Phase I, mainly CYP2C9) and glucuronidation (Phase II, mainly UGT2B7) of the carboxylic acid group (Bort et al., 1999a; Bort et al., 1999b; Ngui et al., 2000; Park et al., 2005). Phase I metabolites can further form benzoquinone imines which react with glutathione (Ngui et al., 2000).

As depicted in Figure 3.4.17, extensive phase I metabolism via diclofenac hydroxylation towards 4'hydroxydiclofenac (CYP2C9) could be observed for primary human hepatocytes. The formed 4'hydroxydiclofenac was the major metabolite with approx. 22 % of the parent compound. Hep G2 cells, which have been shown to express CYP2C9 very weakly compared to PH hepatocytes (see Figure 3.4.9), still hydrolyzed up to 2 % of diclofenac supplied towards 4'hydroxydiclofenac. On the contrary, none of the hESC derived hepatocytes showed CYP2C9 phase I metabolism after 48 hours.
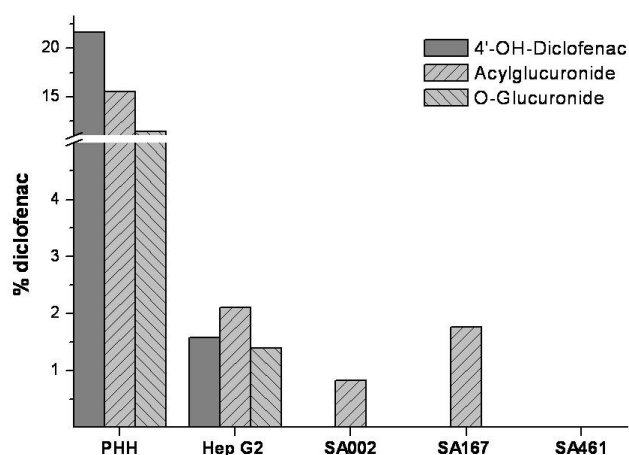
Figure 3.4.17: Metabolic fate of diclofenac after 48 hours of drug exposure, supplemented to primary human hepatocytes (PHH), Hep G2 cells, and the hESC derived cell lines SA002, SA167 and SA461. Metabolites are depicted as % total diclofenac (50 μM). Samples were analyzed at Pharmacelsus GmbH (Saarbrücken, Germany).

Direct phase II biotransformation of diclofenac could be observed by diclofenac acylglucuronide and O-glucuronide formation for PHH and Hep G2 cells. For PHH and

Hep G2 cells the summed concentration of glucuronation metabolites exceeded even the hydroxylation metabolism. hESC derived hepatocyte-like cells (SA002 and SA167) also showed diclofenac acylglucuronide formation. However no phase II metabolism was found for SA461 cells.

Detection of excreted diclofenac glucuronide has been reported to depend on the MRP2 transporter. Thus if the cells lack this transport protein, no diclofenac glucuronide can be transported outside the cells (Seitz et al., 1998). As previously shown in Figure 3.4.8 H, MRP2 was weaker visualized for SA461 cells using immunohistological stainings compared to SA002 and PHH cells. In addition, no polarization was found for SA461 cells. Therefore, the data presented here are in consistence with Seitz's findings. In addition, it has been reported by Seitz and Boelsterli (1998) that diclofenac glucuronides are more toxic than their free parent drug. Since they are the main metabolites (sum of Acyl- and O-glucoronide), it can be expected, that the toxicity should be the highest for cell types transforming diclofenac to its glucuronide forms. Hence, the toxic responses should be in the order, PH hepatocytes > Hep G2 cells > SA cell lines. In addition, it should be noted, that no glucuronide formation could be found for either Hep G2 or hESC derived cell lines after 16 hours of diclofenac exposure; however, it could be detected after 48 hours, indicating a delayed biotransformation activity and thus a later toxicity onset. Thus, the toxicodynamics responses to diclofenac treatment were tested (see Chapter 3.4.4) and will be addressed there more extensively.

3.4.3.5 Energy metabolism

As previously described, the liver has the important task to metabolize and biotransform energy-generating substances, such as amino acids, fatty acids, lactate, pyruvate and sugars (Alberts et al., 2002; Xu and Purcell, 2006). In this part of the study it was investigated if hESC derived hepatocyte-like cells can be used as an *in vitro* model to evaluate the status of energy metabolism under diclofenac exposure. In addition, the functionality after exposure to diclofenac was tested. This is based on the hypothesis that energy metabolic pathways, which are interrelated with mitochondria via the key intermediate pyruvate (which can either form acetyl-CoA to produce ATP in the mitochondria or is used for biosynthesis of e.g. lactate and other substances), will be disturbed if a test agent is supplied (Xu and Purcell, 2006). It is presumed, that with this screening approach response patterns or indicators for toxicity can be identified.

The glucose consumption and lactate production were calculated from the average concentration of triplicate cultures in duplicate measurement after 48 hours (Figure 3.4.18 A and B). For all cell lines, the control (no diclofenac supplementation) glucose uptake and lactate secretion were set to 100 %.

As displayed in Figure 3.4.18 A, for all cell lines and experiments the glucose consumption was reduced if diclofenac was supplied at a concentration of 50 µM or more compared to control (0 µM). Only PHH did not show any distinct responses to the increasing diclofenac concentrations for diclofenac exposure up to 100 µM (the 200 µM value was not available).
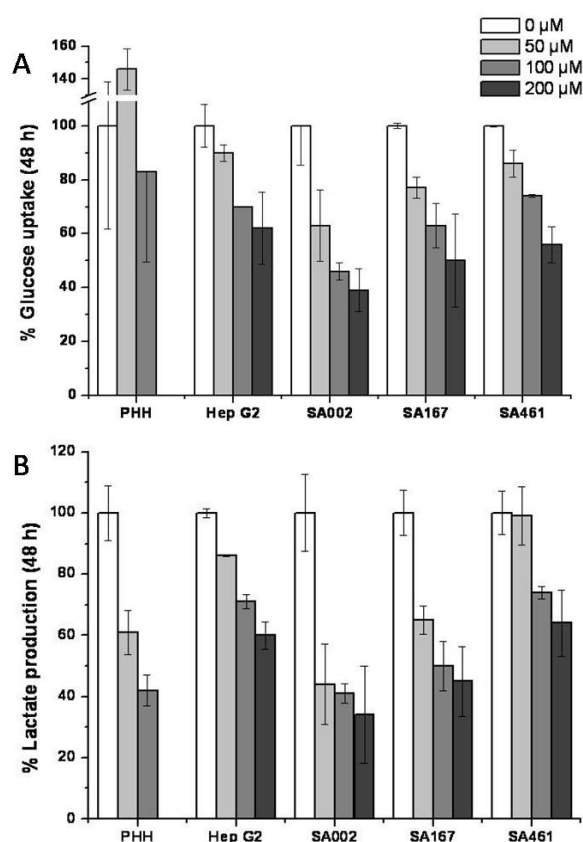
Figure 3.4.18: A) Glucose consumption and **B)** Lactate production after 48 hours of exposure to diclofenac for all cell lines/types (SA002, SA167, SA461, PHH and Hep G2). DMSO concentration in all samples was 0.5 %. Each column represents the mean of the results from three different cultures measured in duplicate.

Lactate was released for all cell lines/types if the drug was present (Figure 3.4.18 B), however, the lactate production reduced as the diclofenac concentration increased.

Pyruvate uptake/release was also analyzed; however, the concentration differences after the culture period were not significantly different.

Anyway, as can be seen in Figure 3.4.19, the lactate/glucose (L/G) ratio also decreased if the drug was present at low concentrations of 50 µM – 100 µM. Further, as in addition depicted in Figure 3.4.19, with increasing concentrations of diclofenac in the culture medium, the L/G ratio decreased somewhat for all groups.

In addition, as observed from Figure 3.4.19, the L/G ratio for some cell lines/experiments neared or exceeded two. This could be explained by the "Warburg effect" (rapid glucose consumption, with most of glucose derived carbons secreted as lactate), which is also considered a marker for tumor aggressiveness. However, hepatocytes are known to be able to synthesize glucose, since their main function is glucose homeostasis (Klover and Mooney, 2004). Hence, other substrates, such as amino acids (e.g. glutamine), could be auxiliary responsible for the high lactate production. Nevertheless, a reduction of the L/G ratio could be detected if diclofenac was present in the media compared to control (0 µM), which can be probably explained by the decreased lactate release (see Figure 3.4.18 B).
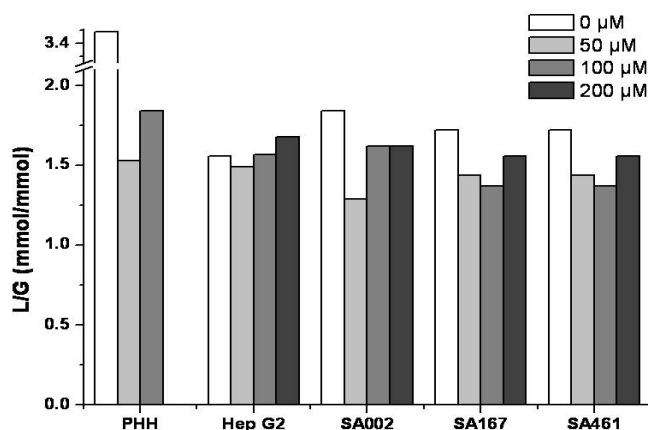
Figure 3.4.19: Lactate/glucose ratios for sampling time points after 48 hours exposure to diclofenac for all cell lines/types tested (SA002, SA167, SA461, PHH and Hep G2). DMSO concentration in all samples was 0.5 %. Each column represents the mean of the results from three different cultures measured in duplicate.

The influence of diclofenac on the changes of energy metabolism was examined. It has been previously published that diclofenac can injure and affect mitochondria and their function, and thereby impairing ATP synthesis by inhibiting the rate of oxidative

phosphorylation in the mitochondria (Bort et al., 1999b; Moreno-Sánchez et al., 1999; Xu and Purcell, 2006). This results in an immediate effect on the energy balance of cells (Castell et al., 1997). In concordance with reduced albumin synthesis, the changes in lactate and glucose suggest disturbances in hepatocyte functionality and energy metabolism. However, hESC derived hepatocyte-like cells did not behave distinctly different compared to Hep G2 or PHH cells when exposed to diclofenac. Thus, while a concentration dependant influence onto the energy metabolism could be observed by this screening, no further characterization factor could be obtained.

3.4.3.6 LDH and AST release

To determine cell damage and the loss of cell viability, analysis of release of intracellular enzymes was measured. In this set of experiments the hepatotoxic dose response effects of diclofenac treatment were tested. All cell lines/types were exposed to 0.05, 0.1 or 0.2 mM diclofenac for an incubation period of 48 hours. Subsequently the LDH and AST leakage was measured and is depicted in Figure 3.4.20.

An increase of cytosolic LDH release (Figure 3.4.20 A) could be observed with increasing drug concentration, for all cell lines/types tested, compared with untreated control. The data suggest that concentrations of 0.1 mM only mildly affected primary human hepatocytes. However, Hep G2 cells and all SA cell lines released LDH in higher amounts even at drug concentrations as low as 0.05 mM.
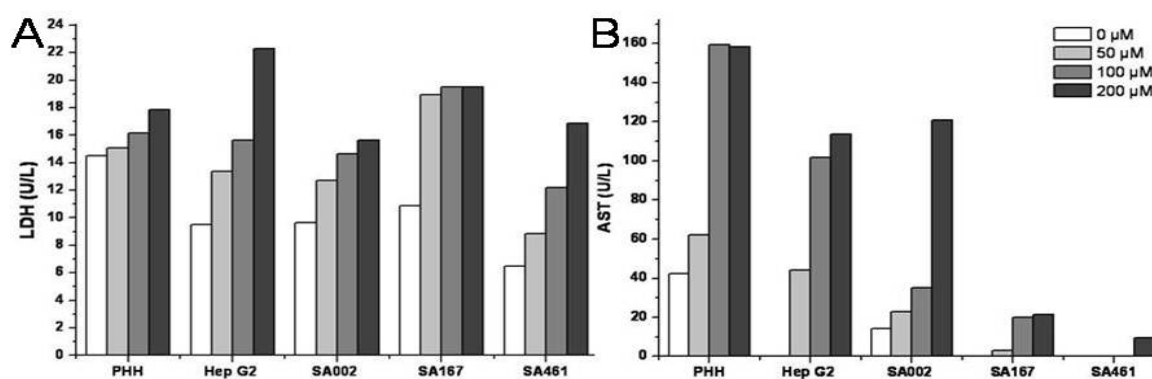
Figure 3.4.20: **A)** Lactate dehydrogenase (LDA) and **B)** aspartate amino transferase (AST) release for Hep G2 cells, PHH and hESC derived hepatocytes cell lines exposed to four concentrations of diclofenac. DMSO concentration in all samples was 0.5 %. Each column represents the mean of the results from three different cultures measured in duplicate.

In addition to the LDH release, aspartate amino transferase concentrations (Figure 3.4.20 B) also increased with increasing diclofenac concentrations. These findings were observed for all cell types. Interestingly, Hep G2, SA167 and SA461 released no AST if they were not exposed to diclofenac, suggesting no mitochondrial stress during the culture period of 48 hours. However, primary human hepatocytes and SA002 cells, released AST even if no drug was present.

It has been previously described, that LDH is mostly released from the cytosol and AST is localized in mitochondria to 80 % (Wang et al., 2004a; Washizu et al., 2005). The data shown in Figure 3.4.20 A thus suggest, that PHH cells show less membrane damage compared to the other cell types. In combination with the activity assay, it can be concluded that the PH hepatocytes depict higher drug metabolizing capacity and thus reduction of cytotoxic effects. Further, in was observed that the cells released AST into the culture medium after diclofenac exposure for 48 hours. Thus, one can surmise that the permeability of mitochondria was reduced and damaged due to diclofenac exposure. SA002 cells, which showed the highest purity and appeared to be non-proliferating and hence be affected in the same way as PH hepatocytes.

It has been published recently, that the enzyme activity of cells is related to their energy metabolism (Washizu et al., 2005). As depicted in Figure 3.4.18 B (lactate synthesis) and 3.4.20 A (LDH release) and B (AST release), the enzyme release and the lactate synthesis of PHH cells seemed to behave most related in response to diclofenac exposure to that of the hESC derived cell line SA002. However, more energy related enzymes, such as hexokinase (HK), malate dehydrogenase (MDH) or pyruvate kinase (PK) should be tested to better localize and evaluate energy production.

Additionally, it has to be noted that the highest drug concentration was close to the 50 % lethal concentration (see Table 3.4.1); hence the increase of enzyme leakage with rising drug concentrations was expected. However, for both enzyme assays these drug response effects are also used to identify drug concentrations which cause 50 % of cell population to die (LC_{50}). Nevertheless, the advantage of these assays is getting hints to the localization of the damage (mitochondrial and membrane). Thus, the use of this assay is of also of interest for dynamic studies and for monitoring the viability of cells (Wang et al., 2004a).

3.4.4   Respiration toxicity assay

To evaluate drug effects on hESC derived hepatocyte-like cells, they were exposed to diclofenac, while measuring their respiration in comparison to PHHs and Hep G2 cells.

Hep G2 cells, primary human hepatocytes and hESC derived hepatocytes were exposed to diclofenac in seven concentrations, ranging from 0 - 1 mM (0 mM, 0.05 mM, 0.1 mM, 0.2 mM, 0.5 mM, 0.75 mM and 1.0 mM). Each experiment was performed twice (different batches) to assure repeatability and each diclofenac concentration was applied in triplicate. Dissolved oxygen concentration (DO) was recorded online, continuously for 48 hours in 15 min intervals and LC_{50} values were calculated as previously described (Chapter 1) and published (Beckers et al., 2010).
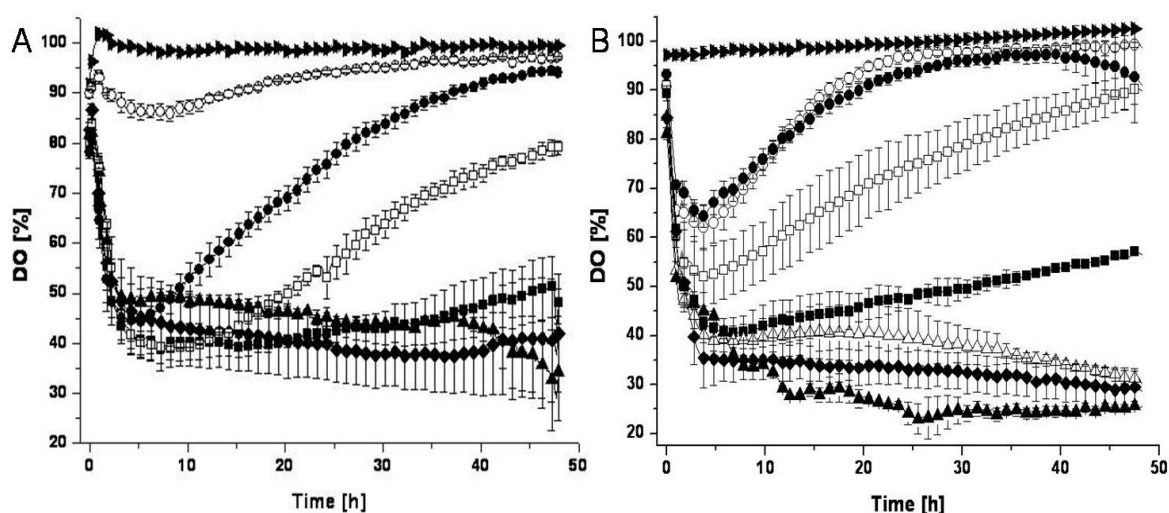
Figure 3.4.21: Dissolved oxygen concentration profiles of **(A)** SA002 cells (EXP 54) and **(B)** primary human hepatocytes. Diclofenac concentrations: 0 mM (▲), 0.05 mM (♦), 0.1 mM (Δ), 0.2 mM (■), 0.5 mM ( ), 0.75 mM (●), 1 mM (○) and medium without cells with 0.5 % DMSO (►). DO values of 0.1 mM (Δ) are not depicted in **(A)** due to unexpected recording errors. Dissolved oxygen concentration was recorded every 15 min. All measurements were carried out in triplicate and corresponding mean values are displayed. Every fifth data point is depicted.

As shown in Figure 3.4.21, the hESC derived cell lines SA002 (Figure 3.4.21 A) and primary human hepatocytes (Figure 3.4.21 B), as well as SA167 (data not shown, however similar profile as SA002 cells), showed stable DO values over the time period of 48 hours when not exposed to diclofenac. In addition, no drug influence on the cell respiration could be observed for concentrations below 0.1 mM diclofenac. Dissolved oxygen concentration values for cells which were exposed to concentrations of 0.1-0.2

mM diclofenac increased slowly over the test period. Cells which were exposed to higher diclofenac concentrations (e.g. 0.5-1 mM) showed concentration dependant DO increase responses, indicating cell-death.
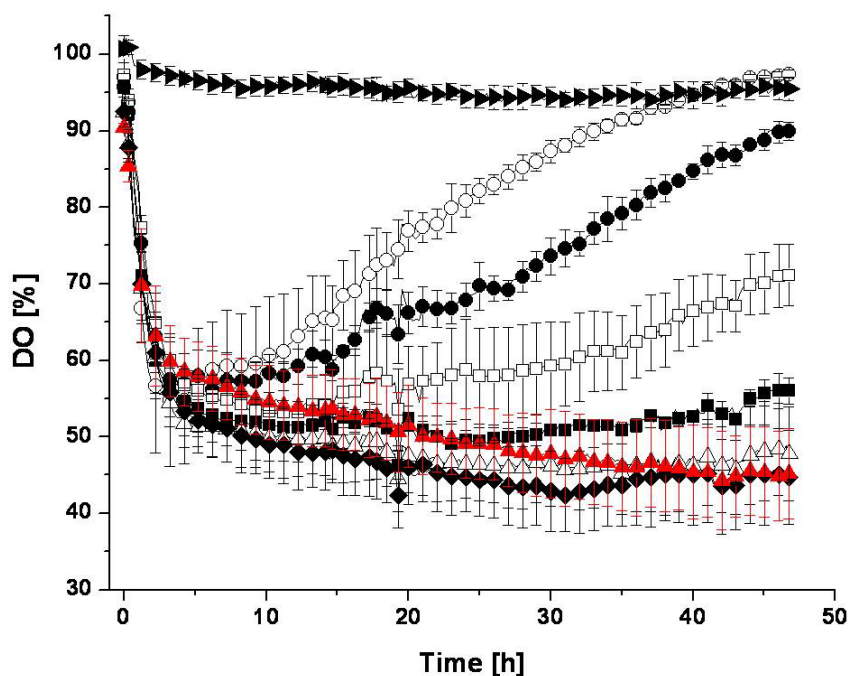
Figure 3.4.22: DO profile of SA461 cells (EXP 42). Diclofenac concentrations: 0 mM (▲), 0.05 mM (♦), 0.1 mM (Δ), 0.2 mM (■), 0.5 mM ( ), 0.75 mM (●), 1 mM (○) and medium without cells with 0.5 % DMSO (►). Dissolved oxygen concentration was recorded every 15 min. Measurements were carried out in triplicate and corresponding mean values are displayed. Every fifth data point is depicted.

Comparable respiration and drug responses could be observed for SA461 cells. However, as depicted in Figure 3.4.22 (red triangular symbol), the DO values for cells, which were not exposed to diclofenac decreased over time. Thus, as previously described (phenotype, Chapter 3.4.1), the mixed SA461 cell population presumably proliferated and was dominated by fibroblastic shaped cells after 28 days (end of respiration assay).

The inflection point of the non-linear regression curve (LC_{50}) was computed for all dose-response curves for all tested cell lines/types after 48 hours, for each experiment, with a 95 % confidence interval and R^2 being higher than 0.99 and is exemplary depicted for SA002 and PH hepatocytes in Figure 3.4.23 A and B.
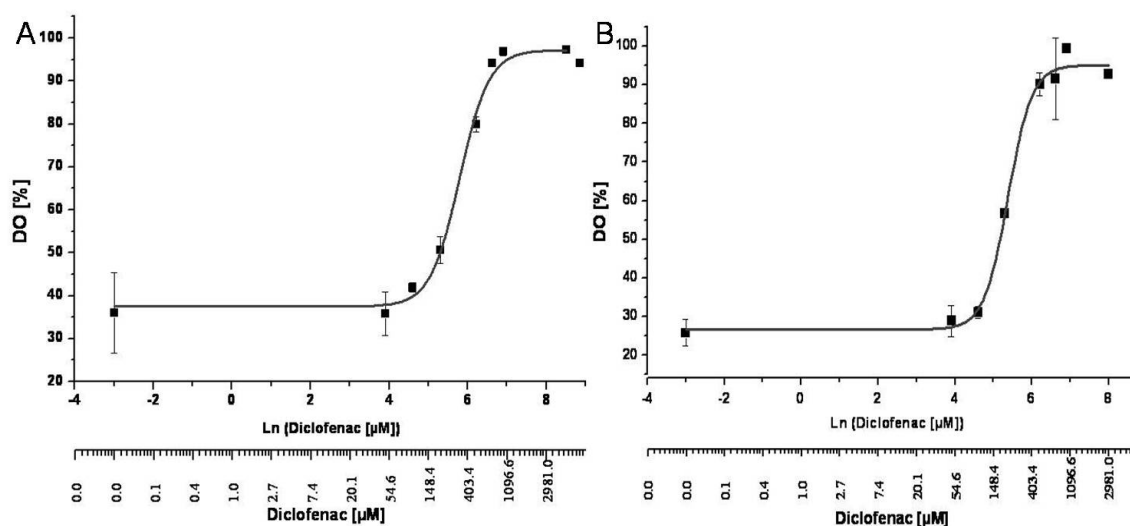
Figure 3.4.23: Diclofenac concentration-response curves of **(A)** hESC derived hepatocytes, SA002 (EXP54), and **(B)** primary human hepatocytes, calculated at 48 hours. The inflection point of the non-linear regression curve (LC_{50}) was computed to be 5.79 ± 0.075 and 5.38 ± 0.07 with a 95 % confidence interval and R^2 being > 0.99 for SA002 cells and PHH cells, respectively. The LC_{50} values are calculated using equation [2.5], resulting in 325 (303-353) µM diclofenac for SA002 cells and 217 (201-236) µM diclofenac for PHH cells.

As shown for the LC_{50} values after 48 hours of incubation (Table 3.4.1), the system resulted in reproducible results. For primary human hepatocytes only one batch was available for this assay. Nevertheless, for primary human hepatocytes Bort et al. (1999b) reported after 24 hours of diclofenac exposure LC_{50} values of 331 (324-338) µM and Castell et al. (1997) reported values of 392 (358-426) µM, respectively. These data are very similar to the data shown in Table 3.4.1. The higher toxic effects for Hep G2 cells and primary human hepatocytes may at least be due to the expected higher conversion into toxic metabolites due to PHH's higher expression of CYP 450 (see chapter 3.4.2, "Gene expression profiling via Low Density arrays (LDAs) ") and their capability of higher phase II transformation into even more toxic metabolites than the parent compound (see chapter 3.4.3.4, "Activity of drug metabolism").

Table 3.4.1: The 50 % lethal concentration (LC_{50}) values given in µM for diclofenac obtained in respiration assays on the human hepatoblastoma cell line Hep G2, primary human hepatocytes and hESC derived hepatocytes after 24 and 48 hours of drug incubation. Data were determined using triplicate measurements for each drug concentration. The ranges were calculated from the standard error of the log estimate.

$$LC_{50} \ [\mu M]$$

Cell Line	24 hours		48 hours	
	Experiment 1	Experiment 2	Experiment 1	Experiment 2
Hep G2	518 (464-578)	567 (493-652)	250 (224-279)	154 (140-171)
Primary Human Hepatocytes	321 (281-365)	N.A.	217 (201-236)	N.A.
hES-HEP™ SA002	1141 (900-1520)	1236 (934-1636)	441 (351-558)	327 (303-353)
hES-HEP™ SA461	665 (596-742)	781 (728-837)	420 (351-503)	441 (403-483)

As further shown in Figure 3.4.24, the kinetic time dependency for all hESC derived hepatocyte-like cells was recorded and calculated (Figure 3.4.24, SA167 (A) and SA002 (B). This dynamic can be compared to the dynamic curves of Hep G2 cells and primary human hepatocytes (Figure 3.4.24 C and D). As depicted in Figure 3.4.24, cell death kinetics of diclofenac are nearly first order type. However, even though all cell types tested showed a LC_{50} decrease over time, the onset of toxicity is delayed for the SA cell lines, compared to PHH and Hep G2 cells. SA002 and SA167 cells only showed LC_{50} values below 1 mM (highest tested concentration) after 20 hours. However, diclofenac toxicity is dependent on multiple factors such as a direct effect on the mitochondrial permeability transition (Lim et al., 2006; Masubuchi et al., 2000) as well as effects of the formed metabolites (Bort et al., 1999b; Tang et al., 1999).

In case of primary human hepatocytes the toxic effect, shown in Figure 3.4.24 C, is earlier and slightly higher than the effect on Hep G2 cells, shown in Figure 3.4.24 D and approximately twice higher compared to the hESC cell lines SA002 and SA167 (Figure 3.4.24 A and B) after 30 hours. Thus, according to the metabolic activity data (see Chapter 3.4.3.4, "Activity of drug metabolism") and the time-dependant drug responses, metabolism capacity can be directly related to the cytotoxic response if exposed to diclofenac. Castell et al. (1997) and Bort et al. (1999b) found comparable results. They

found higher cytotoxicity for drug metabolizing rat and human primary cultured cells exposed to diclofenac compared with Hep G2, FaO cells and non-hepatic cells (MDCK), which they considered as nonmetabolizing.
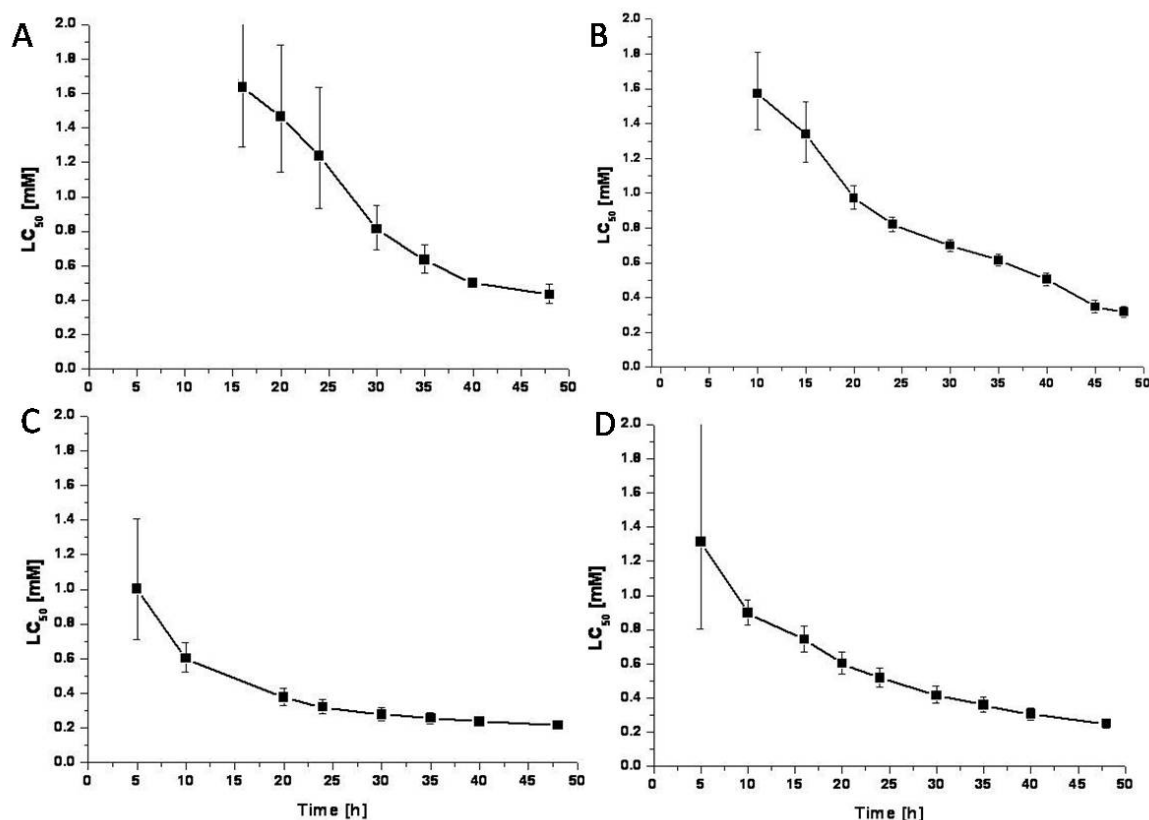
Figure 3.4.24: LC_{50} time dependency for **(A)** SA002 cells, **(B)** SA167 cells, **(C)** PHH cells and **(D)** Hep G2 cells calculated from the LC_{50} diclofenac dissolved oxygen concentrations. The error bars represent the coefficient of variance calculated from the standard error of the log estimate.

Based on the toxicity data in combination with previously presented gene expression and activity data, it can be assumed that SA002 and SA167 cells are capable of Phase II drug metabolism and according to the LDA data, show CYP activity (Phase I biotransformation), even if reduced in comparison to Hep G2 and PHHs.

3.5 Conclusions

To determine if the hESC derived hepatocyte-like cells can be used for future pharmacological and toxicological studies hepatic morphology, gene expression, protein expression of functional proteins, energy metabolism and drug biotransformation metabolism was evaluated.

The results illustrate that the hESC cells can be repeatedly differentiated towards a phenotype similar to hepatocyte-like cells. In addition it was shown that these cells responded comparably to diclofenac exposure.

Typical hepatocyte morphology could be demonstrated and characteristic hepatic protein expression of FoxA2 (HNF-3β), CK8, CK18, AFP, ALB and A1AT was observed. However, it has to be pointed out, that all these markers are also expressed in the late embryonic liver development stage.

Hepatic functions as glycogen storage, urea metabolism and albumin secretion were detected for all three cell lines, thus indicating hepatic functionality.

Even though the phase I and phase II biotransformation system was weaker compared to primary human hepatocytes and the human hepatoblastoma cell line Hep G2, specific biotransformation metabolites were detected. Confirmation for phase I and phase II metabolism was shown by complementing hepatic gene expression profiling.

Hence, it can be concluded these cells are developing towards functional hepatocytes. Nevertheless, they do not yet show sufficient hepatic biotransformation functionality and thus are not yet applicable in the pharmaceutical industry for drug metabolism studies. Regardless, these cells show the potential to provide an alternative source of primary human hepatocytes for drug metabolism and toxicity studies in the future. As soon as these cells become fully functional, both animal studies and demand for liver donations can be reduced. However, as previously pointed out, the efficiency of the differentiation protocols, the purity of the end-culture and their functionality should be further improved in future research studies to finally obtain a valid hepatic *in vitro* model.

4   Physiological Studies at Sub-Toxic Drug Concentrations

4.1 Introduction

Currently many cellular and organism-based methods are available and widely accepted for assessment of acute toxicity. Though these assays are easy to perform, they detect only highly specific changes, such as one cellular or metabolic parameter at a selected time point. Furthermore, most of the current cytotoxicity assays are end point assays and do not provide dynamic information on the cell response after exposure to the applied substance and are therefore not likely to provide an overall insight into the mechanism of toxicity (O'Brien et al., 2006; Xing et al., 2005). Although these methods are quite sensitive, sub-toxic effects are difficult to identify. In this study, drug concentrations were considered as sub-toxic, if neither an influence on cell growth, morphology or respiration as determined by dissolved oxygen concentration measurements, were identified. However, serious adverse drug reactions (ADR) and sub-toxic effects can contribute to the later failure of the drugs due to toxicity when the drug already went into clinical phase and tremendous amount of money was spent (Schuster et al., 2005). Studies in sub-toxic range are advisable, since biological systems are considered robust; they have the ability to use alternative metabolic pathways, bidirectional reactions, isoenzymes and alternative substrates (Christensen and Nielsen, 2000; Wiechert, 2001; Wittmann, 2002). Further, metabolic systems might change if their biochemical pathways are subtly disturbed (Heinloth et al., 2004) without visible phenotype changes. In addition, there is the possibility that metabolic changes can be directly related to the manifestation of toxicity, and therefore can identify toxicity and in case of hepatic cells hepatotoxicity. Several different approaches have been published for identification of (predictive) toxicity using methods as diverse as toxicogenetics (Heinloth et al., 2004), proteomics and genomics (Craig et al., 2006; Ruepp et al., 2002) or tracer based metabolomics (Harrigan et al., 2006). The studies of metabolic network activities using metabolic flux analysis in the sub-toxic range can contribute to the identification and understanding of such effects. Computational modeling in combination with experimental measurements of hepatic metabolism is increasingly used to understand and control the performance of hepatocytes under adverse culture conditions (Yang et al., 2009). MFA analysis has been used to determine metabolic profiles of perfused liver systems (Lee et al., 2000) and to screen cell lines (Balcarcel and Clark, 2003). In addition, MFA has been applied to determine flux distributions in hepatocytes exposed to plasma or to amino acid supplemented plasma (Chan et al., 2003a; Chan et al., 2003b) and to define amino acid supplementation strategies for culturing (Yang et al., 2009). Using GC/MS for identification of positional tracer incorporation into metabolites

produced by pathways as glycolysis, pentose phosphate pathway (PPP) or tricarboxylic acid (TCA) cycle and then secreted into the culture medium can help to gain a more detailed picture of metabolism of mammalian cells. With more complex labeling studies using ^{13}C isotopes, circular, reversible and alternative pathways can be identified which might be involved in the drug metabolism. Furthermore, anabolic and catabolic pathways of metabolites can be researched and also flux parameters, as split ratios, can be calculated and applied. Using the isotopomers to further investigate specific rates, molar enrichment (ME) or so called summed fractional labeling (SFL) can be used (Wittmann, 2007). Changes in specific uptake or production rates might be an indicator for later toxicity.

4.2 Motivation and Theoretical Background

4.2.1 Basic mammalian metabolism

Metabolism enables cells to acquire and utilize energy for growth, reproduction, response to foreign substances and maintenance of structure. Metabolism has two major functions; production of energy by breakdown of substrates (catabolism) and to provide precursor molecules (anabolism). This energy and precursor molecules are used to synthesize complex components of cells for e.g. biomass formation. Energy provided through the breakdown of substrates (carbohydrates, amino acids, fats) is partly stored in form of adenosine-5'-triphosphate (ATP) in the cells. This energy can be released by exergonic conversion of ATP to adenosine diphosphate (ADP) and is coupled to many endergonic reactions (Browne et al., 1999) to enable them to run. In addition, during this oxidative breakdown a release of electrons occurs, which are stored in the reduced forms of nicotinamide adenine dinucleotide (NADH) and flavin adenine dinucleotide (FADH$_2$). As reducing power the reducing equivalents NADH and FADH$_2$ are used to form ATP via the respiratory chain, while nicotinamide adenine dinucleotide phosphate (NADPH) is mostly used for anabolic reactions (Browne et al., 1999). The chemical reactions for the breakdown of substrates, the energy transfer and biosynthesis are linked and organized into metabolic pathways. Oxidative breakdown of glucose or amino acids to gain useful energy, in form of e.g. ATP, usually involves glycolysis, PPP, pyruvate metabolism and the TCA cycle. Thus these pathways are referred to as central or primary metabolism. NADH and FADH$_2$ are the main reducing agents, primarily synthesized in the TCA cycle and are needed for oxidative phosphorylation in the mitochondria of mammalian cells to form further ATP. Besides glucose, glutamine is considered as a major energy source in mammalian cells (Reitzer et al., 1979; Stumvoll et al.,

1999). However, all other amino acids also interact with the central metabolism for anabolic or catabolic purpose (see Figure 4.2.1). In addition to this hepatocytes are responsible for sugar homeostasis and elimination of ammonia. In this respect the urea cycle, gluconeogenesis and glycogenesis are important and briefly described in the following chapters.

4.2.1.1   Glycolysis and gluconeogenesis

The transport of glucose across the plasma membrane into non-cancerous liver cells (GLUT 2 transporter; K_M = 15-20 mM (Berg et al., 2003)) is not coupled to energy-requiring components (Gould and Holman, 1993), however the transporter is a key rate-limiting factor in the metabolism of glucose (Amann et al., 2009). The glycolysis is the first pathway glucose enters to produce energy in form of ATP and NADH, before finally being oxidized to water and CO_2. Glycolysis is the series of enzymatic reactions and the anaerobic catabolism of the 6-carbon molecule glucose to the 3-carbon molecule pyruvate.

The overall net reaction of the glycolysis is:

$$\text{glucose} + 2\ \text{NAD}^+ + 2\ \text{ADP} + 2\ P_i \rightarrow 2\ \text{pyruvate} + 2\ \text{NADH} + 2\ H^+ + 2\ \text{ATP} + 2\ H_2O$$

[Eq. 4.1]
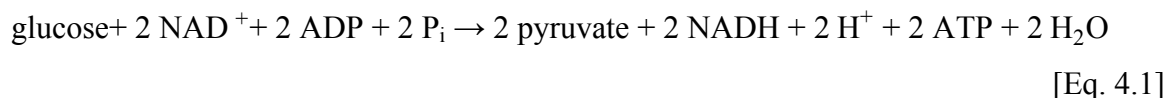
During glycolysis, which is a series of cytosolic reactions in mammalian cells, the cells gain 2 mol ATP per mol glucose. The control of the glycolysis is quite comparable between all other cell types, however, hepatocytes do not synthesize the enzyme hexokinase, but glucokinase (high glucose specificity and high K_M-value) to ensure high glucose supply for brain and muscles (Rehm and Hammar, 2008). The end product of the glycolysis is pyruvate. Under aerobic conditions pyruvate can enter the TCA cycle for complete oxidation and production of CO_2, ATP, NADH and $FADH_2$. Under anaerobic conditions it can be converted to the waste product lactate under regeneration of NAD^+, which is required for continuing glycolysis.

$$\text{pyruvate} + \text{NADH} + H^+ \xrightarrow{LDH} \text{lactate} + NAD^+ \qquad \text{[Eq. 4.2]}$$
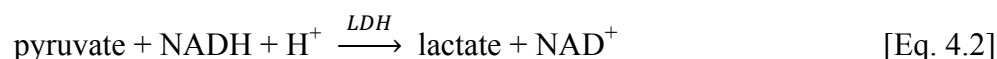
In the mitochondria, pyruvate can also be carboxylated to oxaloacetate. Oxaloacetate is the starting point of the gluconeogenesis; however, it can also react with acetyl-CoA to form citrate. This depends on the ATP concentration inside the cells. Hence, if there is an ATP overflow and citrate excess, fructose-1,6-bisphosphatase is activated and gluconeogenesis initiated (Rehm and Hammar, 2008). Lactate can also be converted into pyruvate using the

enzyme lactate dehydrogenase and glucose can be synthesized by gluconeogenesis. This metabolic pathway, between e.g. muscle and liver, is referred to as Cori Cycle (Rehm and Hammar, 2008). Another way to maintain blood sugar homeostasis is the storage of glucose in form of glycogen (glycogenesis) and release of it (glycogenolysis) when the body is in a catabolic state. For this, a liver specific enzyme, glucose-6-phosphatase, catalyses the dephosphorylation of glucose 6-phosphate back to glucose, thus increasing the glucose level in the blood stream.

4.2.1.2 Pentose phosphate pathway (PPP)

The pentose phosphate pathway also takes place in the cytosol of mammalian cells and is closely connected to the glycolysis. The PPP is an alternative route to the glycolysis with the major purpose to generate reducing equivalents in form of NADPH and to produce pentose and erythrose carbon units for biosynthetic demands of e.g. RNA and DNA. The PPP is divided into two distinct phases; the oxidative phase, in which NADPH and ribulose 5-phosphate are generated, and the non-oxidative, responsible for inter-conversion of sugars and connection of PPP with glycolysis. The overall net reaction for the oxidative phase is shown in equation 4.3 and of the non-oxidative phase in equation 4.4.

Glucose 6-phosphate + 2 $NADP^+$ + H_2O → ribulose 5-phosphate + 2 NADPH + 2 H^+ + CO_2

[Eq. 4.3]

3 ribose 5-phosphate → 2 fructose 6-phosphate + glyceraldehye 3-phosphate   [Eq. 4.4]
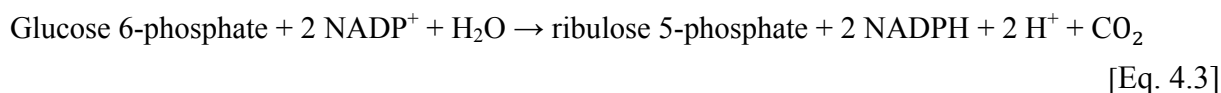
The activity of the PPP depends strongly on the cellular demand for energy (ATP), reducing equivalents in form of NADPH and on biosynthetic molecules (Berg et al., 2003). However, the activity of the enzyme glucose 6-phosphate dehydrogenase (G6PD), the regulatory enzyme of the PPP, has been found to be low in mammalian cells. This is probably due to the small growth rates, and thus the low demand for synthesis of nucleic acids.
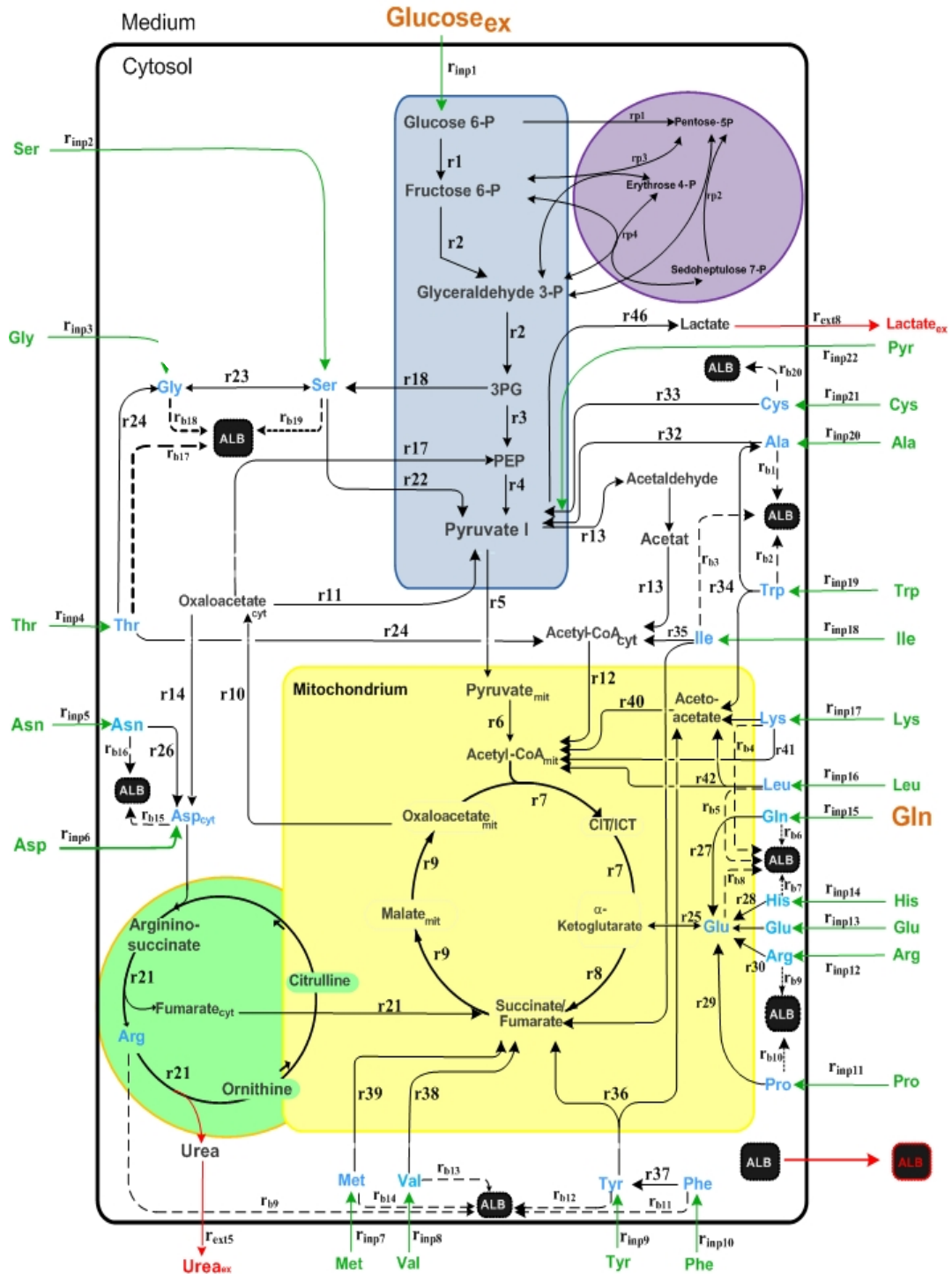
Figure 4.2.1: Mammalian cell metabolism. The network is comprised of intracellular metabolite balances, extracellular fluxes (22 uptake fluxes of amino acids, pyruvate and glucose, indicated by green arrows), 3 fluxes which indicate secretion (red arrows)) and 20 anabolic fluxes (albumin synthesis, dashed arrows). Arrows indicate the direction of reaction assumed in the model. Abbreviations used: CIT citrate, ICT isocitrate, ALB albumin. The amino acids have the standard 3 letter abbreviation. The subscripts "mit" indicate mitochondrial metabolites and "cyt" cytosolic. The subscripts "inp" and "ext" indicate input and export fluxes, respectively.

4.2.1.3   Tricarboxylic acid (TCA) cycle and oxidative phosphorylation

The citric acid or tricarboxylic acid (TCA) cycle is a series of enzyme reactions active under aerobic condition. During the cycle biosynthetic precursors are produced and most of the reducing equivalents (NADH and $FADH_2$) needed by oxidative phosphorylation and thus for ATP formation, are generated by oxidation of carbons. The overall net reaction for one turn of the TCA cycle is given below (Berg et al., 2003).

$$\text{Acetyl-CoA} + 3\ NAD^+ + FAD + GDP + P_i + 2\ H_2O \rightarrow$$

$$\text{CoA} + 3\ NADH + 2\ H^+ + FADH_2 + GTP + 2\ CO_2 \qquad \text{[Eq. 4.5]}$$
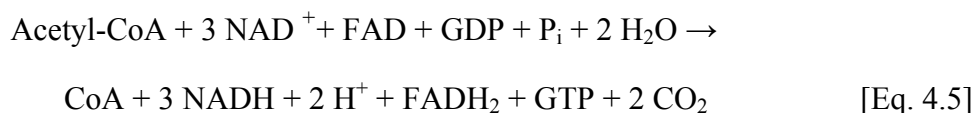
Pyruvate formed during glycolysis is transported into the mitochondria after decarboxylation to acetyl-CoA by the pyruvate dehydrogenase complex (PDC). Acetyl-CoA reacts with oxaloacetate to form citrate.

$$\text{pyruvate} + CoA + NAD^+ \rightarrow \text{Acetyl-CoA} + NADH + CO_2 \qquad \text{[Eq. 4.6]}$$

$$\text{Acetyl} - CoA + \text{oxaloacetate} + H_2O \rightarrow CoA - SH + \text{citrate} \qquad \text{[Eq. 4.7]}$$
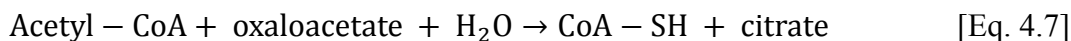
Fatty acids, glycogen and amino acids are also converted to Acetyl-CoA and subsequent oxidation of these in the TCA cycle supplies the cells with energy (Berg et al., 2003). In addition to the macromolecules, glutamine, an important substrate for mammals, feeds into the TCA cycle. For mammalian cells it has been described by Reitzer et al. (1979) that glutamine is the major energy source, not glucose. The main task of the citric acid cycle is the production of NADH and $FADH_2$. To assure that enough oxaloacetate is available for the condensation with acetyl-CoA, anaplerotic reactions replenish the pools of metabolic intermediates in the TCA cycle (Owen et al., 2002). For example, oxaloacetate can be generated from phosphoenolpyruvate (PEP) by use of phosphoenealpyruvate carboxykinase (PEPCK). Further, oxaloacetate can be directly formed from aspartate and α-ketoglutarate from glutamate. Malate can be formed from pyruvate in presence of PEP carboxylase and under oxidation of reduced nicotinamide adenine dinucleotide phosphate (NADPH) in the cytosol and thus can replenish the TCA cycle. The opposite reaction by malic enzyme catalysis leads to complete oxidation of e.g. glutamine and provides thus efficient use of carbons for the production of ATP.

The TCA cycle, which provides 3 moles of NADH and 1 mole of $FADH_2$, generated during each round of the cycle, is followed by oxidative phosphorylation in the mitochondria. This

process extracts the energy from NADH and FADH$_2$, oxidizing them to NAD$^+$ and FAD and transfers the electrons to oxygen. Thereby, oxygen is reduced to H$_2$O and the released energy is utilized to transfer protons through the inner mitochondrial membrane into the mitochondrial inter-membrane space, thereby generating energy in form of a pH gradient and an electrical potential across the membrane. Protons can flow back over the inner membrane into the matrix and by conversion of ADP + P$_i$, by the enzyme ATP synthase, ATP is generated. During this reaction, each mole of FADH$_2$ results in about 1.5 moles of ATP and each mole of NADH in about 2.5 moles of ATP (Berg et al., 2003; Rehm and Hammar, 2008).

In eukaryotic cells the complete breakdown of a molecule of glucose by glycolysis, TCA cycle and oxidative phosphorylation provides approximately 30 ATP. However, the highest contribution to this total energy gain is accomplished by oxidative phosphorylation, generating 26 out of the 30 ATP molecules (Berg et al., 2003).

4.2.1.4   Amino acid and nitrogen metabolism

Mammalian cells, as opposed to plants and microorganisms, are dependent on supply of essential amino acids for protein synthesis and nine of the twenty amino acids are considered essential. However, they do possess the capability of synthesizing non-essential amino acids, amino acid remodeling and conversion of non-amino acid molecules into amino acids. In this process, derivates are generated that contain nitrogen. While the carbon backbones of amino acids are catabolized, ammonia, which is highly toxic to the body is formed and has to be eliminated. This is accomplished by transamination, amidation or urea formation. In the human body, the liver with its urea cycle is the major site capable of this process. The remaining carbon skeletons are either conserved (e.g. glycogen via gluconeogenesis) or are used to generate fatty acids. Thus amino acids can be categorized for their glucose precursor ability into three categories; glucogenic (all amino acids, except lysine and leucine, are partly glucogenic), ketogenic (lysine and leucine) or both (isoleucine, phenylalanine, threonine, tryptophan and tyrosine). The amino acid catabolism, synthesis and their interactions with mammalian central metabolism are well researched (Berg et al., 2003; Browne et al., 1999) and are briefly described.

The synthesis of non-essential amino acids follows relative simple pathways by conversion of intermediates from the central metabolism. Serine can be synthesized from 3-phosphoglycerate and can then be the precursor of glycine and cysteine. Serine itself is

111

utilized for the biosynthesis of proteins and phospholipids, glycine for proteins and nucleotide biosynthesis. During glycine synthesis, a methylene group from the side-chain of serine is transferred to tetrahydrofolate (THF), which is an important coenzyme for biosynthesis intermediates and a transport molecule for one carbon atoms (Berg et al., 2003). Synthesis of glutamine and glutamate is done by the addition of ammonia; asparagine and aspartate can be synthesized by direct transamination of its corresponding α-ketoacid. Formation of alanine is mostly done by transamination to pyruvate using glutamate. Since this reaction is reversible, alanine can be also catabolized to pyruvate and further converted in metabolic pathways such as glycolysis, gluconeogenesis, and the TCA cycle. It acts as a transporter of amino groups to the liver via a pathway called the glucose-alanine-cycle (Browne et al., 1999).

In mammalian cells most of the amino acid catabolism takes place in the liver. Here, all catabolic pathways converge to form only six major products (α-ketoglutarate, acetyl-CoA, succinyl-CoA, fumarate, oxaloacetate and partly pyruvate), all of which enter the TCA cycle (Browne et al., 1999). One important metabolic fuel in mammalian cells is glutamine. It is the major nitrogen provider and primary fuel for the TCA cycle and thus for energy production. The major conversion of glutamine to α-ketoglutarate takes place via the phosphate-dependant mitochondrial enzyme glutaminase (Kovacevic and McGivan, 1983).

$$\text{Glutamine} + H_2O \longrightarrow \text{Glutamate} + NH_4^+ \qquad \text{[Eq. 4.8]}$$

The formed glutamate is converted to α-ketoglutarate, making glutamine a glucogenic amino acid. α-Ketoglutarate can be formed by conversion of glutamate using several enzymes;

Glutamate dehydrogenase:

$$\text{Glutamate} + NAD(P)+ \rightarrow \alpha\text{-Ketoglutarate} + NAD(P)H + NH_3 \qquad \text{[Eq. 4.9]}$$

The ammonia produced is routed to the urea cycle. Alanine and aspartate can be formed by alanine or aspartate aminotransaminase reactions from glutamate with pyruvate or oxaloacetate, respectively. Arginine, proline and histidine can be also converted into glutamate, which can then produce α-ketoglutarate. Isoleucine, methionine, threonine and valine can be catabolized to succinyl-CoA and phenylalanine and tyrosine into fumarate. Asparagine and aspartate can also directly feed into the TCA cycle by conversion to oxaloacetate. Alanine, tryptophan, cysteine, serine, glycine and threonine can be converted to pyruvate, which in turn can be either converted to acetyl-CoA or oxaloacetate. Leucine, lysine, phenylalanine, tryptophan and tyrosine are converted to acetoacetyl-CoA and then can

either be transformed into acetyl-CoA or directly converted into ketone bodies. However, the branched-chained amino acids (leucine, valine and isoleucine) cannot be catabolized in the liver (Browne et al., 1999).

As previously described, during catabolism of amino acids, toxic ammonia is formed. Reductive amination of α-ketoglutarate to glutamate or glutamine synthesis from glutamate are important pathways for the disposal of ammonia. However, pathways of ammonia removal have side-effects on the cells. Increased levels of glutamine, an osmolyte, triggers the uptake of water into the cells and causes swelling. In addition, the glutamine synthesis can cause glutamate and γ-aminobutyrate (GABA) depletion, which are important neurotransmitters required in the brain (Browne et al., 1999). Thus the ammonia formed is removed in animals by means of the urea cycle in the hepatocytes. In the urea cycle, 1 mol ammonia in the mitochondrial matrix reacts with CO_2 (HCO_3^-) and forms carbamoyl phosphate using 2 mol ATP and enters the urea cycle, where it donates its carbamoyl group to ornithine to form citrulline that leaves the mitochondria. Citrulline reacts with the amino group of aspartate to form argininosuccinate, which requires 2 equivalents of ATP, followed by cleavage to form fumarate (interconnection to the TCA cycle) and arginine. Arginine in turn is then cleaved by arginase into urea and ornithine. While ornithine is transported back into the mitochondria to initiate another round of the urea cycle, urea is released into the cytosolic pool (Browne et al., 1999; Rehm and Hammar, 2008). The hepatocytes secrete the urea into the blood stream, from where it is excreted by the kidneys into the urine.

4.2.2 Metabolic flux analysis

Since the beginning of the nineties, metabolic flux analysis (MFA) emerged as a standard tool for bioprocess optimization in connection with metabolite production and analysis of metabolism (Genolet et al., 2005; Martens, 2007; Nielsen, 1998). The aim of the MFA is to accurately quantify and study intracellular metabolic fluxes (reaction rates) within the central metabolism in the cell (Deshpande, 2007; Wahl, 2002). The central metabolism has been briefly explained in the previous section. By using detailed information of the pathways, a stoichiometric model for all the major reactions can be set up and mass balances can be applied around the intracellular metabolites for the calculation of the fluxes (Nielsen, 1998).

4.2.2.1 Metabolite balancing

For metabolite balancing certain constraints have to be considered to generate flux distribution maps; the biochemistry of the desired model, a pseudo-steady-state (PSS) approximation for the intracellular metabolites and the measured rates of the extracellular metabolites (Vallino and Stephanopoulos, 1993).

Hence, to set-up a stoichiometric model of the central metabolism, mass balances for all participating metabolites have to be compiled. The accumulation rate of one metabolite is equal to the sum of all reactions leading to the metabolite minus the sum of all reactions consuming that metabolite (Vallino and Stephanopoulos, 1993):

$$ar_{met}(t) = \sum_{i=1}^{n} s_{i,in} r_{i,in}(t) - \sum_{o=1}^{m} s_{o,out} r_{o,out}(t) \qquad \text{[Eq. 4.10]}$$

Where $ar_{met}(t)$ is the accumulation rate of metabolite met, $r_{i,in}(t)$ is the flux towards the metabolite through reaction i, $r_{o,out}(t)$ the flux from the metabolite through reaction o, and s being a stoichiometric coefficient. For balancing each metabolite, linear equations for each biochemical reaction are compiled and thus a set of linear equations (model) can be obtained. After set-up of the stoichiometric model of interest, substrate uptake rates, metabolite secretion rates and biomass synthesis rates are typically used as input for the calculations (Vallino and Stephanopoulos, 1993). The fluxes through each of the reactions in the network are then calculated by applying matrix algebra.

$$ar(t) = A \cdot x(t) \qquad \text{[Eq. 4.11]}$$

Where A is a $m \times n$ stoichiometric matrix, with m columns and n rows, for which m is the number of reactions and n the number of considered metabolites in the network, $x(t)$ an n-dimensional flux vector and $ar(t)$ is the m-dimensional metabolite accumulation rate vector (Heinzle, 2006; Vallino and Stephanopoulos, 1993). By applying the pseudo-steady-state approximation (assumption that the metabolite concentrations in a cell are maintained by metabolic control directives of the cell in an approximate constant level) equations 4.10 and 4.11 can be simplified to

$$0 = \sum_{i=1}^{n} r_{i,in}(t) - \sum_{o=1}^{m} r_{o,out}(t) \qquad \text{[Eq. 4.12]}$$

and
$$0 = A \cdot x(t) \qquad \text{[Eq. 4.13]}$$

Based on this, measurable and non-measurable reactions can be separated, resulting in equation 4.14.

114

$$0 = A_{m} \cdot x(t)_m + A_{nm} \cdot x(t)_{nm} \qquad \text{[Eq. 4.14]}$$

Where *m* denotes measurable and *nm* non-measurable reaction rates. If A_{nm} is existent in a quadratic and invertible matrix form, the non-measurable rates can be estimated directly by reformulating equation 4.14 in equation 4.15.

$$x(t)_{nm} = A_{nm}^{-1} \cdot \; [-A_m \cdot x(t)_m] \qquad \text{[Eq. 4.15]}$$

However, if the system is overestimated, i.e. the number of in the network considered metabolites is higher than the number of the computable reactions, the least square method to resolve the system of equations and the intracellular fluxes is applied (Heinzle, 2006; Vallino and Stephanopoulos, 1993), described in equation 4.16

$$x(t)_{nm} = (A_{nm}^T \cdot A_{nm})^{-1} \cdot A_{nm}^T \; \cdot (-A_m \cdot x(t)_m) = A_{nm}^{\#} \cdot (-A_m \cdot x(t)_m)$$
$$\text{[Eq. 4.16]}$$

Where *T* is assigned to be the transpose of the matrix and # is its pseudo inverse. Thus this way of calculation can be applied for e.g. mammalian metabolic flux analysis, due to the many measurable extracellular metabolites in the culture medium (Heinzle, 2006). However, if the system is still underdetermined, additional co-metabolites such as ATP and NADH can in principle be balanced to generate additional constraints (Bonarius et al., 1998). It however has been shown that the ATP balance in mammalian cells can generally not be closed (Martens, 2007) and that redox balanced are subject to uncertainties (Christensen and Nielsen, 2000), particularly concerning the specificity of enzymatic reactions for NADH and NADPH. However, electron balances are usable as an additional constraint. Nevertheless, cyclic metabolic pathways, reversibility and parallel reactions with similar stoichiometry can in addition cause linear dependency of the reaction and thus can be cause for generation of singular (underdetermined) metabolic networks (Bonarius et al., 1998).

4.2.2.2   ^{13}C-Metabolic flux analysis

To overcome the problems of the metabolite balancing approach in underdetermined systems (energy, redox and pathway related) additional information can be gained by applying isotopic-tracer techniques (Bonarius et al., 1998; Christensen and Nielsen, 2000). By combinational use of metabolite balancing and tracer studies, metabolic networks can be identified in detail, with respect to metabolite channeling, pathway identification, compartmentation, flux partitioning ratios and bidirectional fluxes (Christensen and Nielsen,

2000; Wittmann, 2002). Both stable and radioactive isotope labeled compounds have been applied as substrate. The detection of the labeled metabolites for the so called metabolic network analysis is achieved by analytical techniques such as mass spectrometry (MS) or nuclear magnetic resonance (NMR) spectroscopy. However, MS techniques, in particular gas chromatography-mass spectrometry (GC-MS), have emerged as superior since they provide higher sensitivity and faster data generation, compared to NMR (Wittmann, 2002; Wittmann and Heinzle, 1999) and also provide the user with mass isotopomers. Carbon isotopomers are molecules that can be ^{13}C labeled or unlabeled at each carbon atom position. With n carbon atoms 2^n different positional isotopomers exist. Thus, if a molecule has three carbons, eight different isotopomers for the isotopomer distribution exist, which are characterized by percentage of each isotopomer within the metabolite pool (Wiechert, 2001) and the corresponding mass isotopomer fractions *m*, *m+1*, *m+2* and *m+3* (Wittmann, 2007) obtained by GC-MS. This labeling information can be used for the computer based metabolic flux analysis, by comparing simulated labeling distributions with experimentally achieved data (Schmidt et al., 1997). However, isotopomer distribution alone accounts for too many positional isotopomers, which demands high computing power. Thus isotopomer simulation was restricted to relatively small metabolic networks. Only the introduction of metabolite activity vectors (MAVs) and atom mapping matrices (AMMs) by Zupke and Stephanopoulos (1994) significantly advanced the estimation of isotopomers. Schmidt et al. (1997) extended the concept by introducing isotopomer distribution vectors (IDVs) in combination with isotopomer mapping matrices (IMMs) for the handling of the complex equation system.
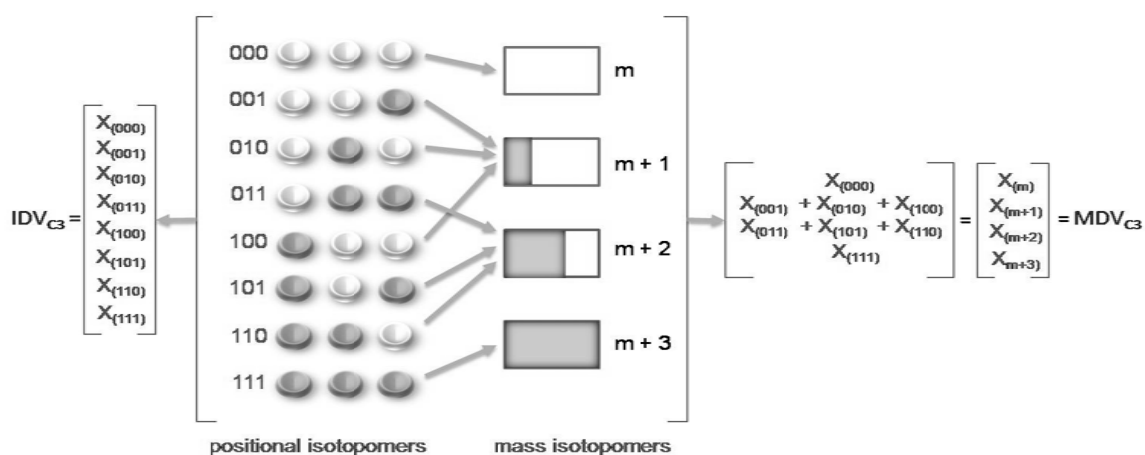
Figure 4.2.2: Pools of positional isotopomers and mass isotopomer based on Wittmann (2002) three carbon molecule, as e.g. lactate or pyruvate.

116

Thus by using the IMM's and IDV's, which also include the transfer of carbons for each of the reactions, created for the metabolic network in combination with the compiled mass balances for all participating metabolites, metabolic flux analysis can be carried out. Then flux values are adjusted by numerical optimization protocols minimizing the differences between computed and experimental mass isotopomer distributions. For the computation of the fluxes, random initial values are fed into the model for the free fluxes and computationally the dependant fluxes and labeling pattern of the metabolites of the supplied fluxes are hereby obtained. The best fit of the simulated and experimental data sets are obtained by further demanding computational tasks to supply the absolute carbon flux through the network (Young et al., 2008). However, as pointed out, a large amount of data sets are generated, which demand computer time and are complicated to solve for big metabolic networks. Thus, a decomposition method, which identifies the minimum amount of information demanded for the simulation of the labeling pattern of metabolites within the reaction network by using the atomic transitions knowledge which occurs in the network was introduced by Antoniewicz et al. (2007b). The so called elementary metabolite unit (EMU) framework generates the EMUs by using the decomposition algorithm, which then are used for the generation of new systems equations that give the relationship between fluxes and stable isotope measurements (Antoniewicz et al., 2007b). By applying the EMU framework the number of equations needed for solving a typical ^{13}C-labeling system is reduced by approx. one order-of-magnitude compared to isotopomer methods and the computation time is significantly reduced (Antoniewicz et al., 2007b).

4.2.2.3 ^{13}C-Metabolic flux analysis in mammalian cells

Metabolic flux analysis (MFA) based on ^{13}C carbon labeling experiments has been successfully applied for quantification of fluxes in microorganisms *in vivo* and emerged as a quantitative tool for characterization and prediction of cell types exposed to various substrates-production strategies, effect of genetic manipulations and in case of mammalian cells for medium optimization (Deshpande et al., 2009; Noh and Wiechert, 2006; Wiechert and Noh, 2005; Yang et al., 2009). To calculate these fluxes in central metabolic and biosynthesis pathways, certain requirements have to be met; 1) for cultured cells, the fluxes and the intracellular pool sizes have to be in a metabolic stationary state for the whole time period of the experiment and 2) to fulfill the demands for MFA based on ^{13}C carbon labeling, isotopic steady-state of all intra-cellular intermediates and pools is required as well (Noh and Wiechert, 2006; Wiechert and Noh, 2005). By sampling extracellular metabolites, which are

closely related to the intermediates in the cells and by calculating the extracellular fluxes, MFA can then be applied (Goel et al., 1993; Stephanopoulos et al., 1998; Wiechert and de Graaf, 1997). With more complex labeling studies using ^{13}C isotopes, circular, reversible and alternative pathways can be identified, based on known biochemical network and pathways. Using mass spectrometry (MS) or nuclear magnetic resonance (NMR) spectrometry measurements for identification of positional tracer information of selected metabolites and of amino acids from proteins, one can obtain a more detailed picture of the metabolism of mammalian cells. For mammalian cell cultures one cannot assume steady-state, but a pseudo-steady state, due to very high turnover of the pools of most metabolites when cells grow with a constant specific growth rate (μ) (Deshpande et al., 2009; Stephanopoulos et al., 1998). Moreover for adherent mammalian cell lines, both the basic requirements, (1) flux and pool size steady state and (2) isotopic steady state, for ^{13}C carbon based stationary MFA are difficult to achieve, since they mostly never reach exponential growth due to their surface growth, varying limitations in substrates and space. Primary hepatocytes, in addition, do not proliferate at all. Another drawback for using MFA with this type of cells is that for reaching a isotopic steady state where the precursor-product relationship is in equilibrium demands long culturing times, due to possible storage pools (glycogen in hepatocytes) and protein turnover (Wiechert and Noh, 2005). For adherent mammalian fibroblasts it has been shown that certain intracellular metabolites remain unlabelled after transferring to a labeled media even after two doubling times, indicating a very long turnover rate (Bennett et al., 2008). However, Deshpande et al. (2009) showed that ^{13}C-labeling patterns of extracellular metabolites reached or asymptotically approached isotopic steady state for the suspension cell line CHO. However, for glutamate, the culturing time was longer than 60 hours, which also equates two doublings or more. Due to this equilibrium problem several groups have started to use dynamic or isotopic instationary labeling strategies (Maier 2009; Provost and Bastin, 2004; Wiechert and Noh, 2005). However, these also enhance the computational demands, since the linear equations required for steady state calculations are now replaced by high dimensional sets of nonlinear differential equations (Noh and Wiechert, 2006; Wiechert and Noh, 2005). Also for hepatocytes and hepatocyte-like cells, further additional challenges exist in extensive bidirectional reaction steps, recycling, gluconeogenesis (GNG) and dilution of the tricarboxylic acid (TCA) cycle by glyconeogenic substrates as lactate, glycerol and glycogenic amino acids which result in an unknown degree of isotopic exchange (Haymond and Sunehag, 2000). Further, these glycogenic amino acids and several other carbon sources besides glucose, are usually supplemented in the culture medium to assure survival/growth

118

(Deshpande et al., 2009). Moreover, growth required supplementation is often performed by using fetal calf serum (FCS), which is a complex mixture of proteins and peptides, containing various other factors, such as hormones and attachment factors, needed for proliferation of cells in culture (Bai and Cederbaum, 2006; Van der Valk, 2004). The disadvantage from the pathway modeling view is that serum is ill-defined and therefore an ambiguous factor. In addition, it is known that individual batches display quantitative and qualitative variations in their composition (Van der Valk, 2004). Therefore there is a trend in cell culture related carbon based MFA experiments to change to either chemical completely defined serum substitutes or to serum free conditions, since characterization of metabolic changes is more straightforward (Deshpande et al., 2009). However, the situation is further complicated by the fact that non-essential amino acids, as alanine, aspartate, serine, proline and glutamate are not only net consumed/produced, as usually assumed using MFA, but reversibly exchanged between the cells and the culture medium. Therefore net rates calculated by ordinary flux analysis would introduce an overall mistake to the isotopomer balance.

Despite all of these complexities, specific information regarding the pathway fluxes can still be obtained. Choosing specific labels which give carbon fate information about certain pathways and by calculating the molar enrichment (ME) of those in the synthesized metabolites, information can be gained. However, as pointed out by Rantanen et al. (2008) these fluxes or flux ratio equations depend heavily on the topology of the metabolic network, precise measurements and the substrate labeling distribution.

4.2.3 Objectives

To identify if sub-toxic effects can contribute to the later failure of drugs due to toxicity, diclofenac, a commonly prescribed non-steroidal anti-inflammatory drug (NSAID) used for treatment of rheumatic and arthritic diseases was used. In previous studies diclofenac has been associated with liver injury and hepatitis. Although there are some indications how and where diclofenac acts, the entire mechanism of action and pathways involved are not known. Labeled substrates can be applied to give a more detailed picture of the diclofenac metabolism and its effect on glucose and amino acid metabolism.

For this study, using a single experimental setup for each cell type, multiple analyses are carried out to gain an overall view of the system.

First, since the adherent cells cannot be cultured continuously, several time points are chosen to follow the incorporation of carbons dynamically. Labeled substrates ($[U-^{13}C_6]$glucose, $[1,2-^{13}C_2]$glucose or $[U-^{13}C_5]$glutamine) are applied onto primary human hepatocytes and hESC derived hepatocyte-like cells. In addition, cells are exposed to three sub-toxic concentrations of diclofenac. The influence of diclofenac is tested by comparing medium substrates and synthesized metabolites over a time period of 48 hours.

Second, metabolic profiles of primary human hepatocytes and hESC derived hepatocyte-like cells are analyzed with respect to diclofenac exposure. In addition, the cell types are tested to be in a metabolic steady state.

Third, a stoichiometric model is set up to determine intracellular fluxes and their possible changes due to diclofenac administration. The goal for this part of the thesis is that the results of this study can improve insight into the effect of changes in glucose and amino acid metabolism on diclofenac metabolism. In addition, by evaluating these metabolic responses to sub-toxic concentrations, prediction of toxicity might be obtained before these drugs enter the clinical phase.

Fourth, analysis of fractional enrichment data is performed to elucidate activity of glycolysis, gluconeogenesis, pentose phosphate pathway and TCA cycle.

120

4.3 Materials and Methods

4.3.1 Cell lines and culture conditions

The cell line and culture conditions are similar to those described in the previous parts under materials and methods. The only differences were for primary human hepatocytes and hESC derived hepatocyte-like cells the seeding in 48-well plates instead of 24-well plates. Primary human hepatocytes and hESC derived hepatocyte-like cells (cell line SA002) were provided by Cellartis AB (Gothenburg, Sweden) and seeded on collagen I in 48-well plates with a cell density of 1×10^5 cells/cm^2 and 2.5×10^5 cells/cm^2, respectively.

4.3.1.1 Primary human hepatocytes

For the labeling study primary human hepatocytes were provided by Cellartis AB (Gothenburg, Sweden) and seeded on collagen I (Sigma Aldrich) in 48-well plates with a cell density of 1×10^5 cells/cm^2. The seeded plates were shipped overnight in William's Medium E (Sigma Aldrich) medium supplemented with 10% Fetal Calf Serum (FCS) (v/v), 100 U/ml penicillin and 100 µg/ml streptomycin. Shortly after arrival, medium was renewed and cells were maintained at 37°C in an incubator (Memmert GmbH, Schwabach, Germany) with 95 % relative humidity in a 5 % CO_2 atmosphere for two days to adjust. For the labeling experiment medium was switched to serum-free conditions, however supplemented with specific concentrations of hormones, induction and growth factors as described for hESC derived hepatocyte-like cells in chapter 3.3.1.3.

4.3.1.2 Human embryonic stem cells derived hepatocytes

Human embryonic stem cells derived hepatocytes were differentiated in Cellartis AB (Gothenburg, Sweden) for 20 days, followed by resuspension and seeding on collagen I. For the ^{13}C-labeling studies, SA002 cells were chosen as model system. The seeded 48-well plates were shipped overnight in William's Medium E (Sigma Aldrich) medium supplemented with additives (Single Quots). Shortly after arrival, medium which was pre-conditioned on mouse feeder cells, supplemented with hormones, was added to the cells. The cells were maintained at 37°C in an incubator (Memmert GmbH, Schwabach, Germany) with 95 % relative humidity in a 5 % CO_2 atmosphere for one day to adjust. Matrigel overlay was performed on day 23. For the experiments on day 25-26 medium was switched to serum-free conditions as described previously in Chapter 3.3.1.3.

121

4.3.2 Choosing sub-toxic concentrations based on OxoDish results

Based on the LC_{50} results, obtained for cryopreserved primary human hepatocytes and an earlier batch of hESC derived hepatocyte-like cells (both experiments performed at Cellartis, March 2009), sub-toxic concentrations for primary human hepatocytes and SA002 cells were chosen. The highest sub-toxic concentration (ST) was chosen to be slightly toxic (approx. LC_{25}), meaning after 48 hour of exposure a slight respiration decrease could be observed. All sub-toxic diclofenac concentrations are listed in Table 4.3.1.

Table 4.3.1:   Sub-toxic diclofenac concentrations chosen for labeling study for primary human hepatocytes (PHH) and SA002 cells based on previous experimental results. LC_{50} values are given in µM and calculated using equation [2.5] after 48 hours of exposure to diclofenac.

Concentration	Cryopreserved PHH	SA002 (EXP 19)
LC_{50}	183 (170-221)	639 (580-720)
Control (C)	0	0
Sub-toxic 1 (ST1)	10	100
Sub-toxic 2 (ST2)	25	200
Sub-toxic 3 (ST3)	50	400

4.3.2.1   Media and sampling

As depicted in Figure 4.4.3, four sub-toxic concentrations of diclofenac and three labeled substrates were applied in combination. In addition, five time points were chosen for sampling.

Williams Medium E (PAN Biotech GmbH, Aidenbach, Germany) without glucose, glutamine and phenol red but supplemented as described previously was used for the labeling study exposing the cells further to subtoxic diclofenac concentrations. [U-$^{12}C_6$]-, [U-$^{13}C_6$]- or [1,2 -$^{13}C_2$]-glucose (Cambridge Isotope Laboratories, Andover, USA) were added in three parallel preparations with the same molar composition as the normal culture medium. Total glucose concentration was 10 mM. For the fourth preparation 4 mM glutamine [U-$^{12}C_5$]glutamine (PAA, Düsseldorf, Germany) or [U$^{13}C_5$]glutamine (Cambridge Isotope Laboratories, Andover, USA) was supplemented to the culture

medium. For both cell types (primary human hepatocytes and hESC derived hepatocyte-like cells) it was previously positively tested (Gothenburg, March 2009) that they survived the time period without any increase in dissolved oxygen concentrations in the serum-free media.
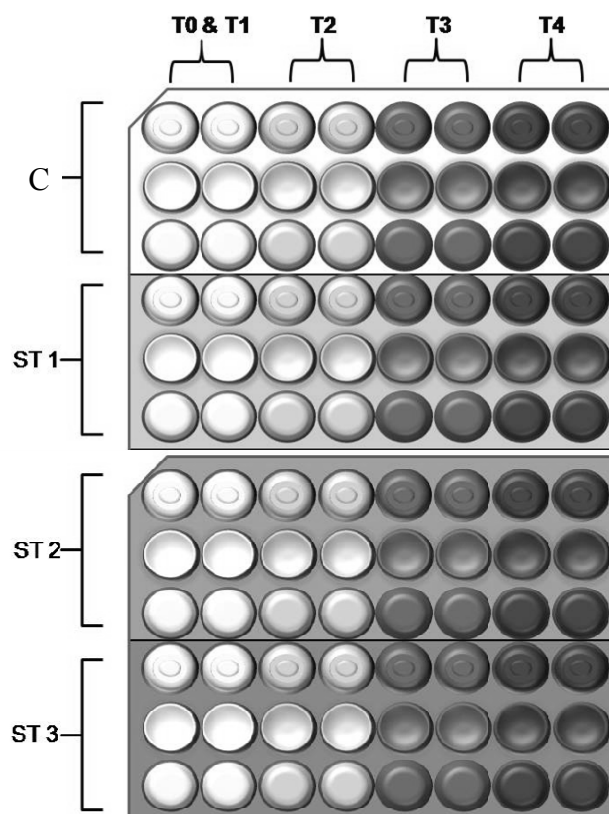
Figure 4.3.1: Experimental plan: Sampling time points (T0-T4) and diclofenac concentration (Control-ST3). The dotted convex symbol represent [U-^{13}C6]glucose as substrate, the plain concave symbol shows the [1,2-^{13}C$_2$]glucose used as substrate and the plain convex symbol indicates samples for which glutamine was substituted as [U-^{13}C$_5$]glutamine. Sub-toxic concentrations (C-ST1) were chosen according to respiration experiments. Time points (T0-T4) were chosen to be in a time frame of 48 hours.

The cells were cultured in media, as described above. Shortly before the labeling experiment, cells were washed twice with PBS and overlaid with the prepared media containing the sub-toxic diclofenac concentrations and labeled substrates in parallel as depicted in Figure 4.3.1. Thus, for each time point, four concentrations of diclofenac exposed media were collected, whereas for each diclofenac concentration, six replicates for the media concentration assessment (three times equally concentrated media

preparations) and two replicates for the each labeling were assessed. Thus, for each time point 24 samples were collected.

The initial samples were taken directly after the addition of the media, containing the labeled substrates and the diclofenac concentrations. Hence, the initial time represented by time "0" (T0) is after the addition of the media. For primary human hepatocytes and hESC derived hepatocyte-like cells extracellular samples for determination of mass isotopomers were collected in triplicate and samples were immediately frozen after collection for later analytical processing. Sample collection time points are depicted in Table 4.3.2:

Table 4.3.2: Sample collection time points for primary human hepatocytes (PHH) and human embryonic stem cell derived hepatocyte-like cells (SA002).

Sample Name	Time Point [h]	
	PHH	SA002
T0	0	0
T1	12	16
T2	24	24
T3	35	36
T4	48	48

4.3.3 Tracers used for study

Three isotopic substrates were chosen for the labeling approach. The Williams medium E media used for this experiment was specially designed for this experiment and was neither supplemented with glucose, glutamine or phenol red (Pan Biotech, Aidenbach, Germany).

$[U-^{13}C_6]$glucose can be used to identify all metabolites which are generated from glucose as carbon source. In addition, fully labeled metabolites, as alanine, serine, glycine and lactate can be identified derived directly via glycolysis and pentose phosphate pathway (PPP). Further, the minimum concentrations present in the media can be calculated.

$[1,2-^{13}C_2]$glucose allows determination of the contribution of the non-oxidative and the oxidative pathways of the pentose phosphate cycle to obtain macromolecules (Lee et al., 1998).

124

Besides glucose, glutamine is a major carbon source in mammalian cells and provides more than half of the cell energy even if glucose is present in high concentration (Neermann and Wagner, 1996; Reitzer et al., 1979). Therefore [U-^{13}C$_5$]glutamine which feeds into the TCA cycle can give an idea about the synthesis of metabolites as glutamate and aspartate, but also of gluconeogenic activities.

4.3.4 Chemicals

All chemicals used are similar to those described in the previous parts under materials and methods. The tracer substrates used were purchased from Cambridge Isotopes, Inc. (Andova, MA, USA).

4.3.5 Quantification of extracellular metabolites

4.3.5.1 Amino acids analysis

Amino acids in the culture media were analyzed by reversed phase high performance liquid chromatography (RP-HPLC) (Agilent 1100, Agilent Technologies, Waldbronn, Germany), utilizing a C$_{18}$-Gemini column (Phenomenex, Aschaffenburg, Germany) with automated online derivatization (*o*-phtaldialdehyde (OPA) and 3-mercaptopropionic acid) at a flow rate of 1 ml/min, column temperature at 40 °C and fluorescence detection (340 nm excitation, 450 nm emission). OPA only reacts with primary amines in the presence of thiol compounds and forms highly fluorescent isoindole products. Hence, the quantification of L-proline demands an additional derivatization step, since it exists as secondary amine. Therefore, L-proline was derivatized with N-(9-fluorenyl) methoxycarbonyl (FMOC) and quantified using the fluorescence detector by switching after 43.5 min of each run to 266 nm excitation and 305 nm emission. All samples were diluted 1:2 with 225 μM α-aminobutyric acid (ABU), which served as internal standard for the quantification. Two eluents were used and the eluent time profile is depicted in Table 6.6.3. Eluent A (40 mM NaH$_2$PO$_4$ (pH=7.8, NaOH)) for the polar phase and eluent B (Acetonitril-Methanol-Water (45:45:10)) as the non-polar phase. The resulting peaks were integrated and the quantification was computed from the known internal standard concentration and the dilution factor.

Table 4.3.3: Eluent time profile for amino acid separation via reversed phase high performance liquid chromatography (RP-HPLC). Eluent A = 40 mM NaH$_2$PO$_4$ (pH=7.8, NaOH) and eluent B = (Acetonitril-Methanol-Water (45:45:10).

Time [min]	Eluent A [%]	Eluent B [%]
0	100	0
41.0	59	41
46.0	19	81
46.5	0	100
49.0	0	100
49.5	100	0
52.0	100	0

4.3.5.2 Glucose, pyruvate and lactate quantification

Quantification of glucose, pyruvate and lactic acid was performed as described previously in Chapter 3.3.8.

4.3.6 Gas chromatography-mass spectrometry analysis

For quantification of ^{13}C-labeling patterns, such as fractional ^{13}C enrichment and mass isotopomer distribution, gas chromatography-mass spectroscopy (GC-MS) analysis was carried out on a Hewlett-Packard 6890 gas chromatograph (Hewlett Packard, Paolo Alto, CA, USA) connected to a quadrupole mass selective detector (MS 5937, Agilent Technologies, Waldbronn, Germany) with electron impact ionization at 70 eV, and an HP-5MS column (95 % dimethyl–5 % phenyl-methyl-siloxane-diphenylpolysiloxane; 30 m × 0.251-mm × 0.25 µM, Agilent) was used with a column head pressure of 70 kPa and helium (0.8 mL/min) as the carrier gas.

4.3.6.1 Amino acids and lactate

Approximately 50 µL of cultivation supernatant from samples and controls (extracellular amino acids) was lyophilized. To the lyophilizate 50 µL of dimethylformamide (DMF) (0.1% pyridine) was added and amino acids were converted to their t-BDMS derivative by adding 50 µL of *N*-(*t*-butyldimethylsilyl)-*N*-methyltrifluoroacetamide (MBDSTFA, Macherey and Nagel, Düren, Germany), and one hour of incubation at 80 °C.
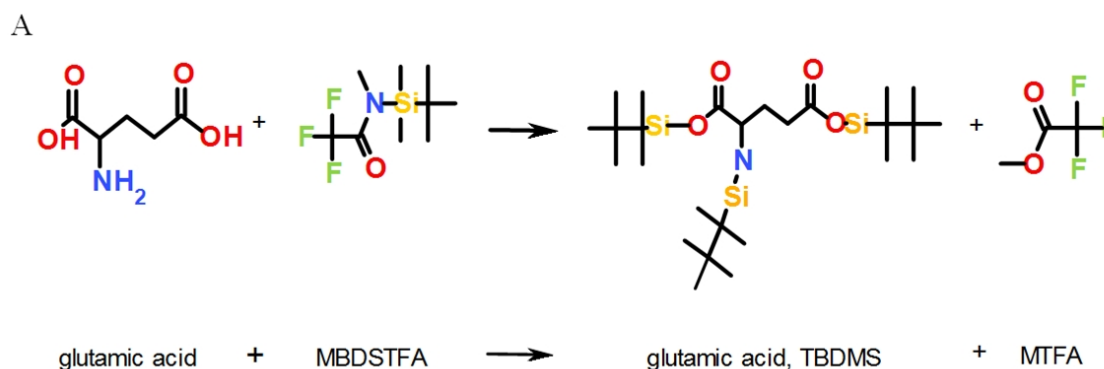
Figure 4.3.2: Schematic depiction of glutamic acid conversion to its silyl derivative (L-Glutamic acid, N-(tert-butyldimethylsilyl)-, bis(tert-butyldimethylsilyl) ester). For other metabolites, rest groups besides -OH or -NH$_2$ can also be –COOH, =NH or –SH for silation.

The derivatized samples were centrifuged in 0.5 ml Eppendorf tubes to remove debris and 40 µL of the supernatant was transferred to HPLC vials with inserts. The analyte volume for GC-MS analysis was 1 µL. The temperature program was as followed: The column temperature was initially kept at 100°C for 1 min, subsequently increased by 3°C/min up to 175°C, then switched to a second ramp with 10°C/min up to 325°C and maintained at that temperature for 1 min. Other temperature settings were 290°C (inlet), 280°C (interface), and 280°C (quadrupole). The total run time was 42 min. For identification of metabolites, based on their mass spectrum, mass spectra were analyzed in the range of 30-650 atom mass to charge (m/z) ratio at a rate of 90 scans/min for a run time of 42 min. Operation of a GC/MS in selected ion monitoring (SIM) mode allows for detection of specific analytes with increased sensitivity relative to full scan mode. In SIM mode the MS gathers data for masses of interest. Mass isotopomer distribution in SIM mode was always measured in duplicate. All measured metabolites exhibited high signal intensity for a fragment ion obtained via mass loss of m-57, due to a *t*-butyl group release from the derivatization residue. Ions corresponding to the whole carbon backbones + 1 were monitored in SIM mode. Relevant ion clusters for SIM analysis in electron impact ionization (EI) mode: lactate (m/z 261), alanine (m/z 260), glycine (m/z 246), urea (m/z 231), proline (m/z 286), methionine (m/z 320), serine (m/z 390), aspartate (m/z 418) and glutamate (m/z 432).

For the integration of the GC/MS peaks and for the calculation of the mass isotopomer distribution a program for Matlab 2007B (The MathWorks, Natick, MA, USA) was used, which was written by E. Heinzle, T. H. Yang und N. Lakshmanaperumal and applied for the upper listed fragments.

4.3.6.2   Glucose

The aldonitrile penta–acetate derivative of glucose was assayed by GC-MS according to the method described by Szafranek et al. (1974). [U-^{13}C]glucose (99 %) was purchased from Cambridge Isotopes (Andova, MA, USA) and naturally labeled glucose (Sigma-Aldrich, Taufkirchen, Germany) were utilized as standards. Samples and standards were lyophilized as described previously. Hydroxylamine hydrochloride in pyridine solution (20 mg/mL pyridine) was freshly prepared and 50 µL was added to the samples. The mixture was incubated in a 100°C oven for 30 min. Subsequently, 50 µL of acetic anhydride was added and the solution was heated at 100°C for 1 hour to create aldonitrile penta-acetate. After cooling, samples were diluted with 50 µL ethyl acetate shortly before GC-MS analysis. The analyte volume for GC-MS analysis was 1 µL. The applied temperature program was as followes: The column temperature was initially kept at 160°C for one minute, subsequently increased by 11.5°C/min up to a final temperature of 320°C and maintained for 1 min. Other temperature settings were 280°C (inlet), 280°C (interface), and 280°C (quadrupole). The total run time was 16 min. Relevant ion clusters for SIM analysis in electron impact ionization mode of the aldonitrile derivative were chosen based on preserving the whole carbon structure of glucose: m/z 328 cluster for the C1-C6 fragment.
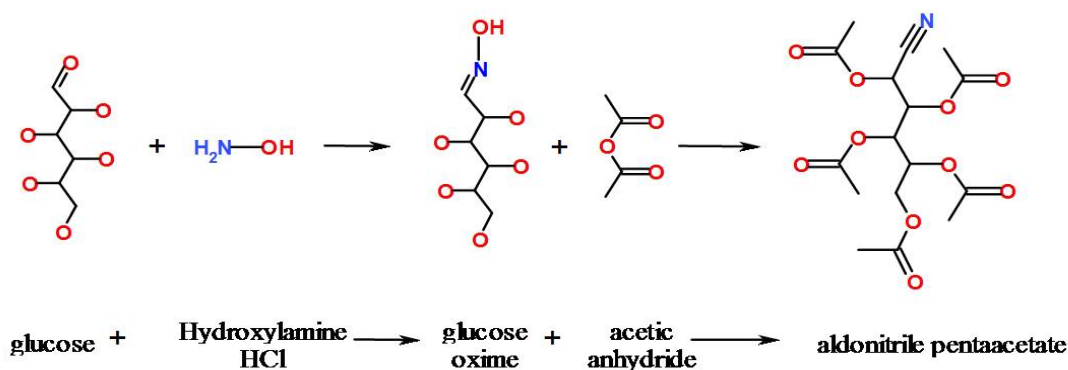
Figure 4.3.3:   Schematic depiction of glucose conversion to glucose oxime after incubation with hydroxylamine hydrochloride and further conversion to its aldonitrile penta–acetate derivative by incubation with acetic anhydride.

4.3.1 Metabolic flux analysis

The estimation of intracellular fluxes was carried out using ^{13}C-labeled substrates for the calculation of all determinable extracellular substrate uptake and product building rates. The mathematical model for the hepatocytes main metabolism included here the glycolysis, the citric acid cycle, anaplerotic carboxylation and all amino acid degradation pathways. In addition, since albumin is the major protein produced in hepatocytes and the cells did not proliferate, for the anabolic demand, amino acids consumption for albumin synthesis, was used according to Equation 4.17 (Chan et al., 2003a).
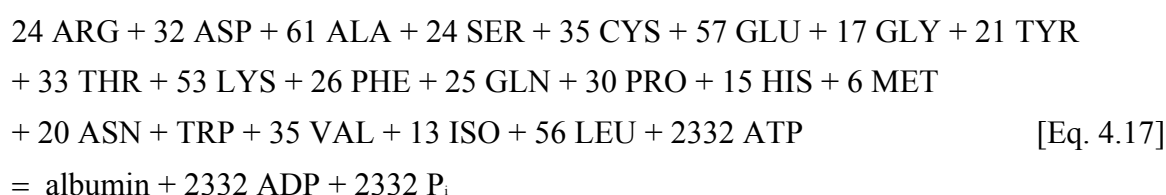
$$24 \text{ ARG} + 32 \text{ ASP} + 61 \text{ ALA} + 24 \text{ SER} + 35 \text{ CYS} + 57 \text{ GLU} + 17 \text{ GLY} + 21 \text{ TYR}$$
$$+ 33 \text{ THR} + 53 \text{ LYS} + 26 \text{ PHE} + 25 \text{ GLN} + 30 \text{ PRO} + 15 \text{ HIS} + 6 \text{ MET}$$
$$+ 20 \text{ ASN} + \text{TRP} + 35 \text{ VAL} + 13 \text{ ISO} + 56 \text{ LEU} + 2332 \text{ ATP} \qquad [\text{Eq. 4.17}]$$
$$= \text{ albumin} + 2332 \text{ ADP} + 2332 \text{ P}_i$$

By multiplication of the anabolic demand of amino acids for the albumin synthesis [$\text{mmol}_{\text{amino acid}} \cdot \text{mg}_{\text{Albumin}}^{-1}$] with the yield [$\text{mg}_{\text{Albumin}} \cdot \text{mmol}_{\text{substrate}}$] the values were normalized to the defined substrate uptake and implemented into the stoichiometric flux model for the estimation of specific uptake or production rates. The major substrate for the hESC derived hepatocyte-like cells was hereby glucose. The specific rates were calculated as mmol metabolite per 1 mg albumin synthesis in 24 hours and are referred to as r [$\text{mmol}_{\text{metabolite/precursor}}/(\text{mg}_{\text{Albumin}} \times 24 \text{ hours})$].

4.4 Results and Discussion

4.4.1 Physiological studies on hepatic model systems

The present study was performed to improve the current understanding of the mechanism of diclofenac hepatotoxicity and its impact on the metabolic pathways of hepatocytes exposed to sub-toxic concentrations of diclofenac. The influence of the non steroidal anti-inflammatory drug (NSAID) diclofenac was tested for control cells and cells exposed to sub-toxic concentrations by comparing medium substrates and synthesized metabolites over a time period of 48 hours. Further, we aimed to characterize and deepen the understanding of the diclofenac mechanism of toxicity by means of flux balance analysis (FBA). However, to perform reliable FBA the requirement of metabolic steady state has to be tested and validated first.

4.4.1.1 Metabolic characteristics in sub-toxic diclofenac range

For any metabolic characterization, the parameters involved had to be analytically determined. For humans, usually 50 mg to 150 mg of diclofenac are prescribed for treatment of pain. The free plasma concentration after administration ranges thus from $35 \, \mu M$ to $100 \, \mu M$ (MW 318.15 and five liter blood). It was tested for primary human hepatocytes (PHH) and hESC derived hepatocyte-like cells (SA002) if the changes occurring after exposure to sub-toxic concentrations of diclofenac would be in analytical detectable range in a metabolic profile over a culture period of 48 hours.

Earlier (as shown in the previous chapter) it was determined which concentrations are sub-toxic using the OxoDish for an exposure period of 48 hours. For the PHH cells (Figure 4.4.1 A) all chosen sub-toxic concentrations were clearly below the LC_{50} value ($217 \, \mu M$, range 201-236 μM) and the dissolved oxygen concentrations (DOs) of the drug exposed samples were the same as the control. For the hESC derived hepatocyte-like cells the LC_{50} value was determined to be 441 (351-558) μM (Figure 4.4.1 B). Here, three concentrations were chosen to be in the sub-toxic range and one close to the LC_{50} value after 48 hours of diclofenac exposure. This higher concentration was chosen based on previous results (see Table 4.3.1), where the estimated LC_{50} value was 639 (580-720) μM. Since the amount of cells was scarce, all sub-toxic concentrations for the extracellular metabolic profiles had to be chosen before the experiments. Due to an improvement of the differentiation protocols, the hESC derived hepatocyte-like cells

130

improved their drug metabolism compared to previous experiments and thus, the highest concentration applied here was chosen too high to be considered as sub-toxic.
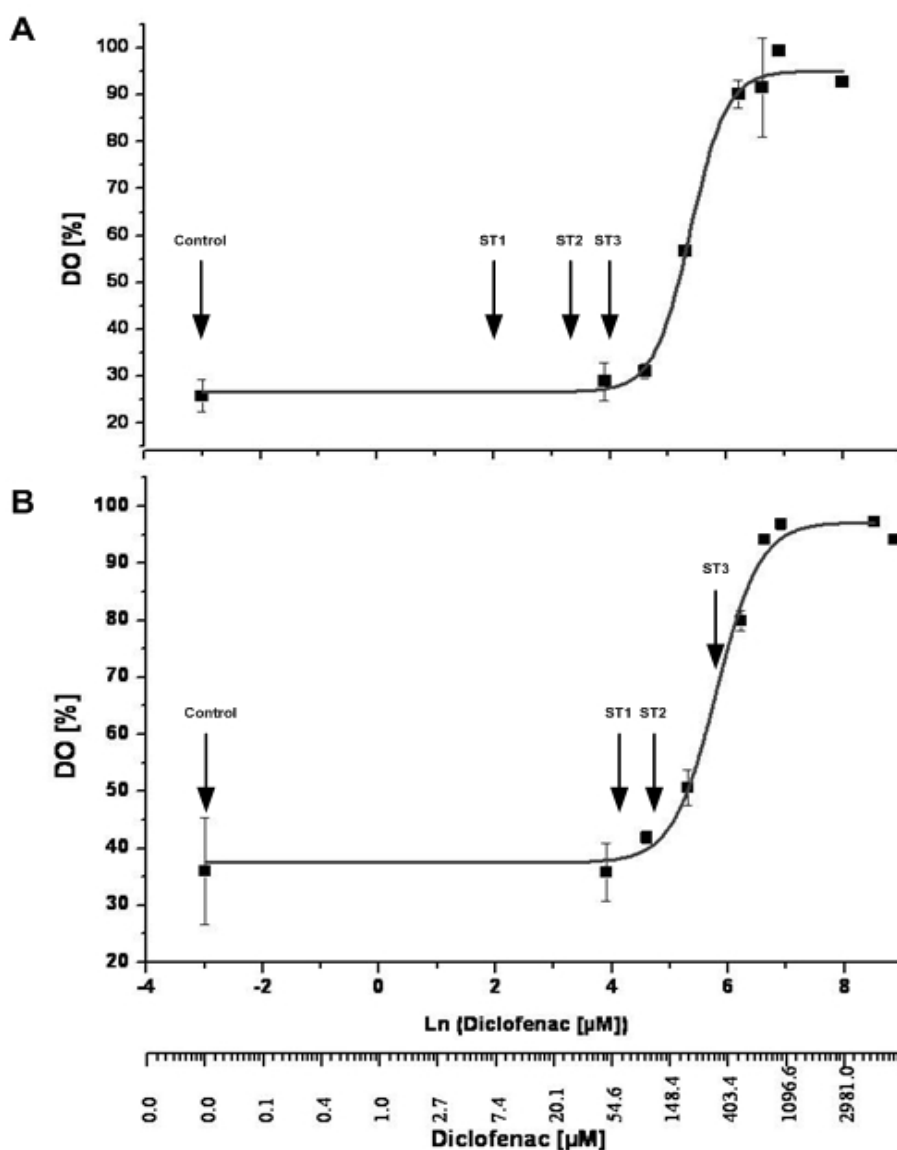
Figure 4.4.1: Concentration-response curves of **(A)** PHH and **(B)** SA002 cells measured after 48 hours of exposure to diclofenac. The arrows depict the control sample (C = 0 µM) and chosen sub-toxic diclofenac concentrations (ST1-ST3) from left to right. All measurements were carried out in triplicate. Corresponding mean values and corresponding standard errors are give in **(A)** and **(B)**. LC_{50} values were determined using a four-parameter sigmoid concentration–response curve using Eq. 2.5.

The extracellular metabolic profile for primary human hepatocytes is shown in Figure 4.4.2. The influence of the three sub-toxic diclofenac concentrations on the metabolism of primary human hepatocytes had no major impact compared to the control

medium. Nevertheless, some interesting changes in the metabolic profile for the ketogenic amino acids that can give rise to ketone bodies or fatty acids (Berg et al., 2003) could be observed and are briefly discussed.
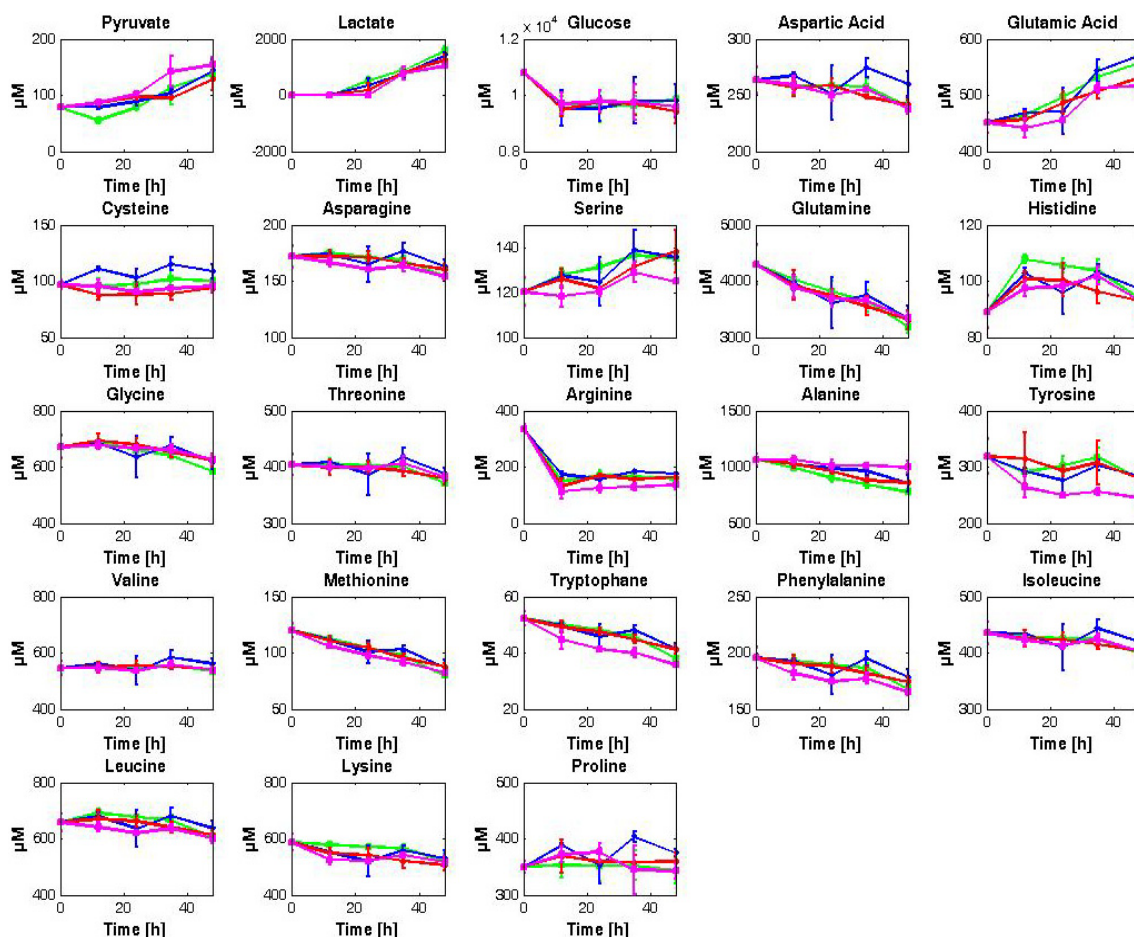
Figure 4.4.2: Concentrations of amino acids, glucose, pyruvate and lactate over time [h] for primary human hepatocytes. Sampling time points were 0, 12, 24, 35 and 48 hours after exposure to 0 μM [control, green line], 10 μM [ST1, blue line], 25 μM [ST2, red line] and 50 μM [ST3, magenta line] diclofenac. Measurements for each sample time point correspond to six parallel cultures, measured in duplicate. The mean values and standard deviations are given.

The ketogenic and glucogenic aromatic amino acids, which contain a benzene ring (phenylalanine, tyrosine and tryptophan), can be either degraded to acetoacetate and acetyl-CoA or are used for the synthesis of more complex molecules (Berg et al., 2003; Michal, 1999). Here, these amino acids were consumed slightly more in the presence of diclofenac. Since degradation of aromatic ring structures mostly occurs in the liver to synthesize more complex molecules by using their benzene and indole rings, it can be

132

surmised, that diclofenac exposure stimulated their uptake. This is in concordance with the literature.
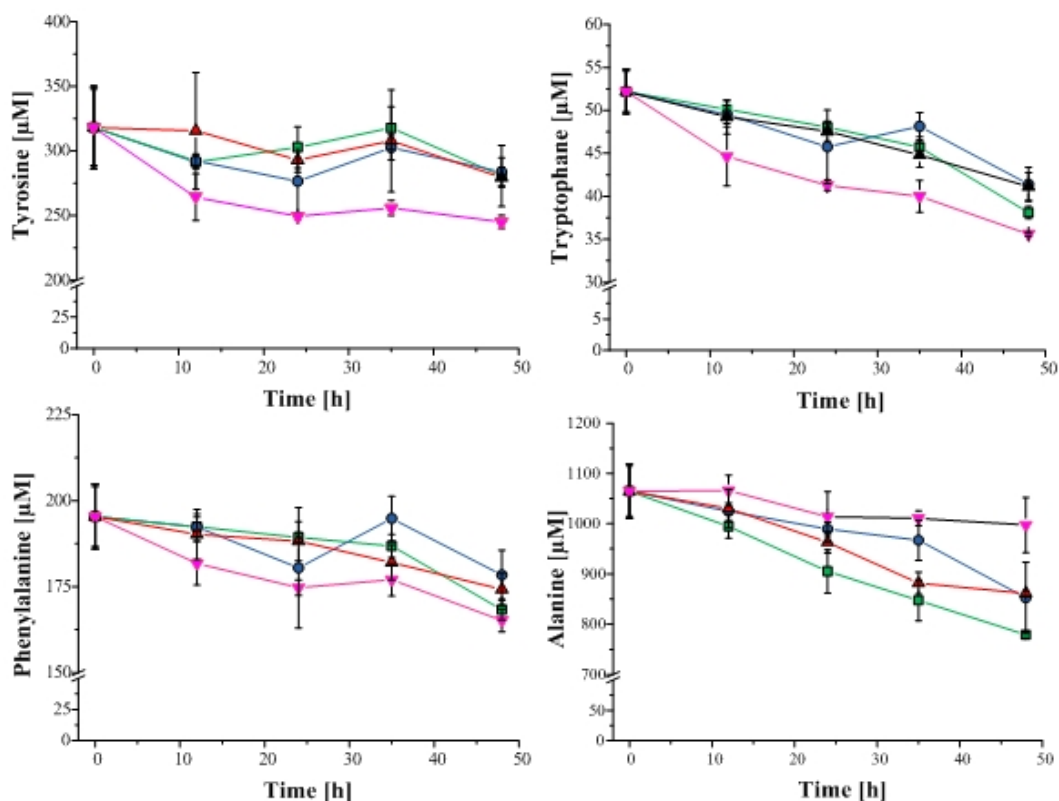
Figure 4.4.3: Concentration of tyrosine, tryptophane, phenylalanine and alanine over time [h] for primary human hepatocytes. Sampling time points were 0, 12, 24, 35 and 48 hours after exposure to 0 μM [control, green line], 10 μM [ST1, blue line], 25 μM [ST2, red line] and 50 μM [ST3, magenta line] diclofenac. Measurements for each sample time point correspond to six parallel cultures, measured in duplicate. The mean values and standard deviations are given.

Further, an increased uptake of tryptophan was observed. Tryptophane is a precursor of niacin, which can be converted to the coenzymes NAD and NADP. Hence, the increased uptake could be further explained by the demand of the cells to generate reducing equivalents in form of NADPH for the detoxification (in form of reduction) of oxidized gluthathione (GSH) by P450-monooxygenases (Berg et al., 2003). For the increased tyrosine uptake, one possible explanation could be catecholamine (dopamine, norepinephrine and epinephrine) demand, which are derivatives of tyrosine (Michal, 1999).

Further, for the sole ketogenic amino acids (degradation products are acetoacetate and acetyl-CoA), such as leucine (involved in cholesterol synthesis) and lysine (β-oxidation),

a trend for the increased degradation could be detected if the cells were exposed to diclofenac. Further, a reduced consumption of the amino acid alanine was found for the primary human hepatocytes when exposed to diclofenac and compared to control cells (see Figure 4.4.3). This can be explained by three mechanisms: 1. In the presence of diclofenac, more alanine is synthesized for secretion of NH_3; or 2. alanine uptake is reduced in presence of diclofenac; or 3. a reduced activity of alanine aminotransferase (due to the diclofenac treatment) could explain the lower degradation of alanine in presence of diclofenac.

The extracellular metabolic profile for the hESC derived hepatocyte-like cells (SA002) is shown in Figure 4.4.4. The influence of exposure to diclofenac showed a different response in the metabolic profiles than primary human hepatocytes. These responses can be attributed to the higher concentrations applied. The diclofenac exposure influenced the pyruvate, lactate and glucose profiles. For the glucose consumption a change in uptake after 24 hours of culture was observed for the control cells. While the consumption was high in the first 24 hours, glucose uptake was reduced when the glucose concentration in the culture medium was less than approximately 4 mM. The glucose concentration in humans, which normally ranges from about 4.4 - 6.7 mM (Berg et al., 2003), determines either the synthesis or release of glucose from liver. Thus, here the glucose concentration in the media could have been maintained by the cells by gluconeogenic activity. In addition to the decreased glucose uptake change, a decreased lactate and pyruvate production was observed before 24 hours for the control cells. In addition, pyruvate was completely depleted from the culture medium within the first 16 hours when diclofenac was present at 400 μM.

In addition, aspartate and glutamate were completely consumed within 24 hours. Interestingly up to 24 hours of culture the profiles of the other amino acids were similar. However, after that time point, distinct differences in uptake or degradation were observed. Major changes were detected for the aromatic amino acids phenylalanine and tyrosine, the branched-chain amino acids (BCAAs) leucine, isoleucine, and valine and further arginine (part of the urea cycle). For all these amino acids, the control cells displayed a distinctly different profile than cells exposed to diclofenac, which did not show much variability between each other. Contrary to the PHHs, for the hESC derived

134

hepatocyte-like cells alanine was net produced and no major difference between control and diclofenac treated cells was observed for the alanine synthesis.
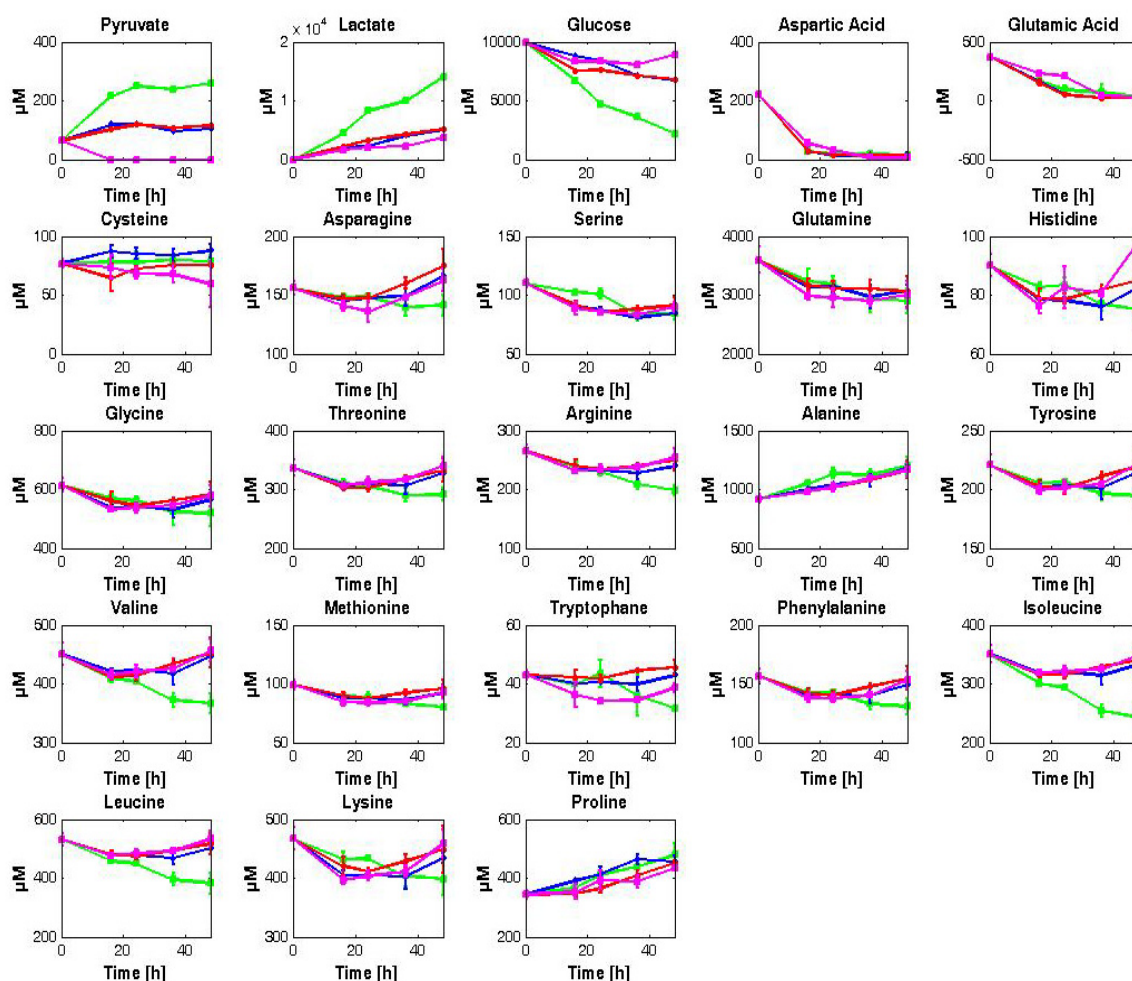
Figure 4.4.4: Concentrations of amino acids, glucose, pyruvate and lactate over time [h] for human embryonic stem cell derived hepatocytes (hESC cell line SA002). Sampling time points were 0, 16, 24, 36 and 48 hours after exposure to 0 μM [control, green line], 100 μM [ST1, blue line], 200 μM [ST2, red line] and 400 μM [ST3, magenta line] diclofenac. Measurements for each sample time point correspond to six parallel cultures, measured in duplicate. The mean values and standard deviations are given.

4.4.1.2 Testing for metabolic steady state

As previously explained (chapter 4.4.2), in order to perform MFA for cultured cells, the fluxes and the intracellular pool sizes must be in a metabolic steady state or in a pseudo steady state. This means that all concentrations of the metabolites in the model are constant, i.e. change over time will be zero.

For primary human hepatocytes (PHH) and hESC derived hepatocyte-like cells, which were both cultured in serum-free conditions, no growth was observed over 48 hours and the DO profiles remained constant (see Figure 3.4.21). Metabolic steady state can be determined by examining the relationship between the extracellular metabolite concentrations with the main carbon sources for each of the five sample time points (Deshpande, 2007). For mammalian cells, glucose and glutamine are the major carbon substrates. Linearity between the metabolites with the major carbon substrates therefore indicates metabolic steady state.

Primary Human Hepatocytes

As shown for primary human hepatocytes (Figure 4.4.5), none of the tested metabolites (glutamine, pyruvate, lactate and alanine) showed a linear relationship with glucose. However, this was not surprising, since glucose utilization was only observed in the first twelve hours after supplementation with fresh media. Glutamine was however degraded over the culture period. It has been shown that glutamine is often the main energy substrate for mammalian cultures (Kovacevic et al., 1991) and thus the metabolites were tested for their linear relationship to glutamine degradation. However, no linear relationship of pyruvate, lactate or arginine to glutamine degradation is observable (Figure 4.4.5). Nevertheless, alanine and glutamate showed a linear relationship to the glutamine degradation. This is probably due to their relation at the biochemical level. When the glucogenic amino acid glutamine is converted by glutaminase to glutamate and further to α-ketoglutarate, alanine is produced from pyruvate via alanine transaminase (ALT). In addition, no linearity between glutamate and aspartate was seen (see Figure 4.4.5), even though one can expect that, due to both their involvement in the malate-aspartate shuttle. Further, serine and glycine did not correlate, even though they are related by the enzyme serine hydroxymethyltransferase. Asparagine and aspartate, further, also did not correlate.

136
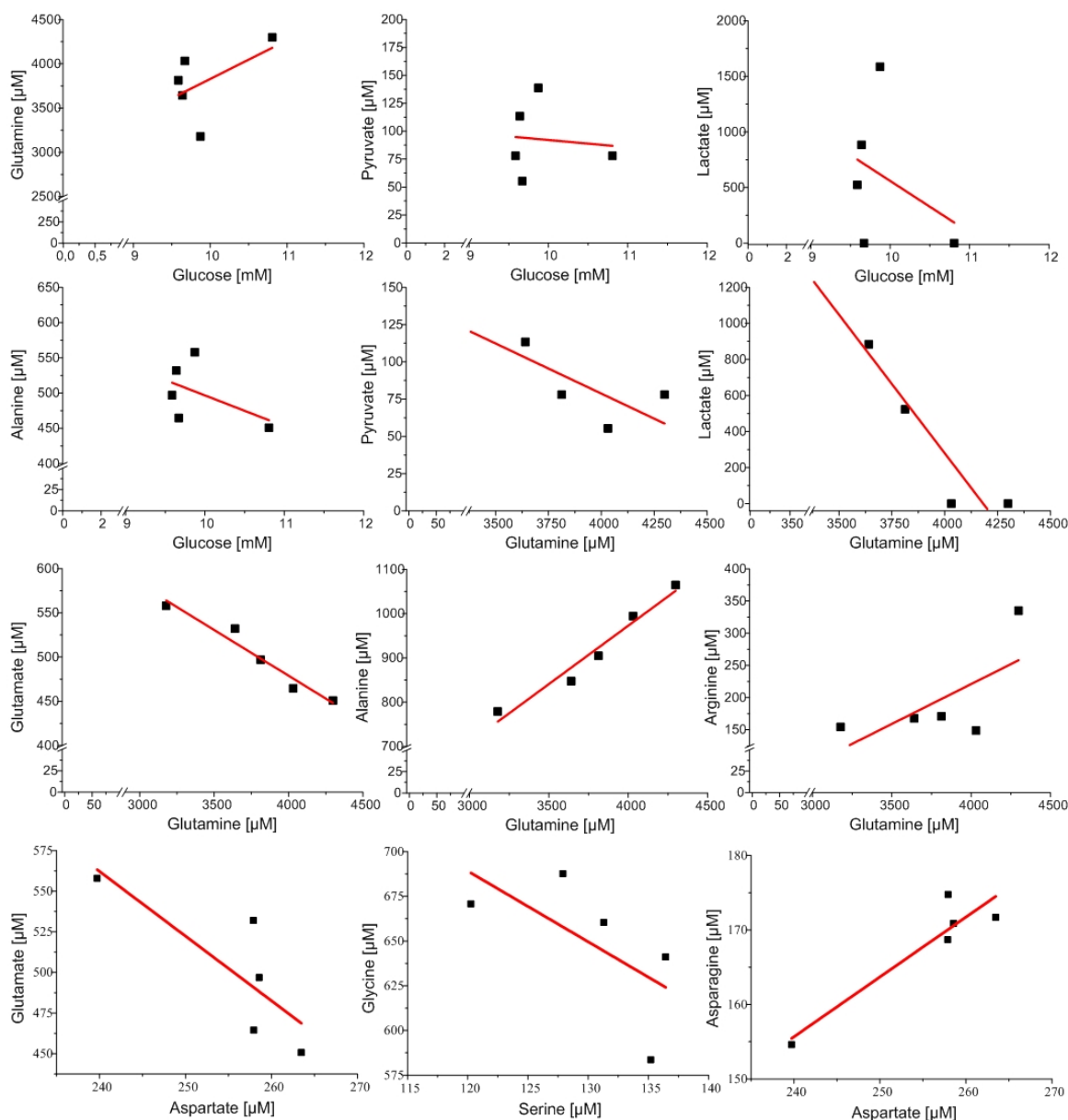
Figure 4.4.5: Selected metabolite concentrations plotted each other for primary human hepatocytes. Linear regression was performed for each of the metabolites.

Since for primary human hepatocytes no direct correlation was found between the major carbon sources with the metabolites or the metabolites over time, it can be surmised for the cells that there is an extensive and varying exchange of amino acids or other metabolites with the surrounding media; i.e. there is no metabolic (pseudo) steady state existing under these conditions.

Alanine, aspartate, glutamine and glutamate are among the amino acids involved the most in the central metabolism acting as both substrates and sinks (Kovacevic et al., 1991). It

has been reported that due to these exchanges for proliferating mammalian batch cultures no metabolic steady state could be found (Deshpande et al., 2009; Provost and Bastin, 2004). Here, for the non-proliferating primary hepatocytes no metabolic (pseudo) steady state was detected, either. Hence, since the reaction rates cannot be assumed to be constant, non-stationary models should be applied for further flux calculations. In addition ^{13}C substrates should be applied for these experiments. However, the combination of ^{13}C-experiments with non-stationary models enhances the computational demands, since no longer linear equations, but high dimensional sets of nonlinear differential equations have to be applied (Noh and Wiechert, 2006; Wiechert and Noh, 2005).

hESC derived hepatocyte-like cells

As shown for hESC derived hepatocyte-like cells in Figure 4.4.6, glutamine uptake, lactate production and alanine production correlated well with the glucose consumption. In addition, the correlation of glutamate, alanine and lactate production to glutamine uptake showed an acceptable metabolic steady state. Thus a metabolic (pseudo) steady state can be assumed. However, no linear relationship of aspartate to glutamine degradation could be observed. Further, for the hESC derived hepatocyte-like cells no correlation between glutamate and aspartate was seen.

It has been previously shown (see Figure 4.4.4) that aspartate is completely degraded after 24 hours of cell culture. However, since aspartate is only consumed in small quantities, compared to glucose consumption, one can still assume the hESC derived hepatocyte-like cell culture to be in a metabolic steady state.
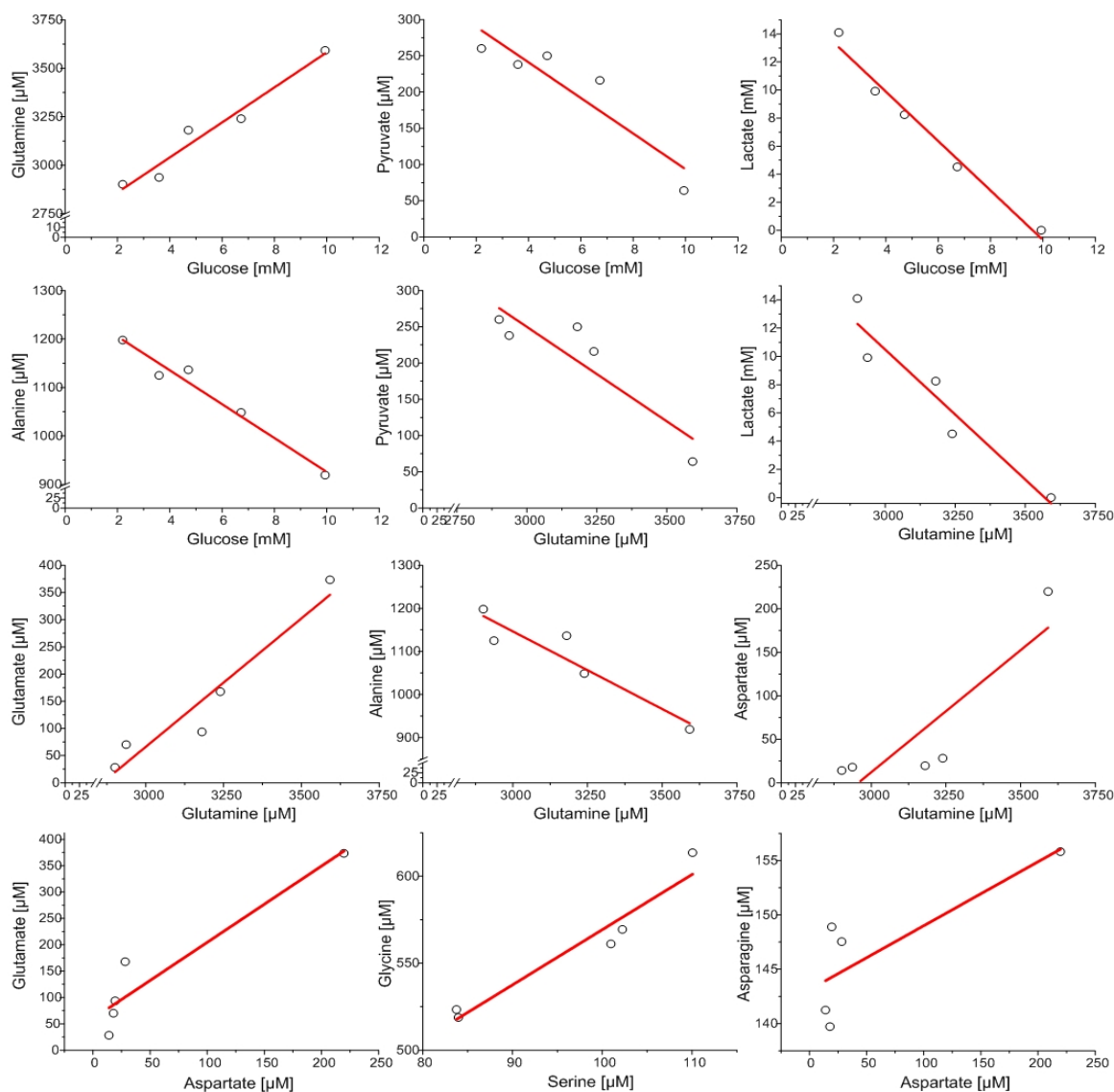
Figure 4.4.6: Selected metabolite concentrations plotted each other for hESC derived hepatocyte-like cells. Linear regression was performed for each of the metabolites.

4.4.1.3 Metabolic flux analysis of hESC derived hepatocyte-like cells

Metabolic flux analysis (MFA) analysis was applied to gain further insight into the cellular function of hESC derived hepatocyte-like cells, exposed to sub-toxic concentrations of diclofenac and its metabolism. Here, experimental measurements of substrate inputs and product outputs were applied to a pseudo-steady-state stoichiometric model to determine intracellular flux distributions between metabolite pools.

In the present study, MFA was used to characterize the effect of sub-toxic supplementation of diclofenac on the metabolic state of hepatocytes. First, extracellular

fluxes were determined based on substrate uptake and product output of each supplemented amino acid. Next, a model for hepatocyte metabolism was created based on the known stoichiometry of the hepatic metabolic network. Finally, intracellular fluxes were calculated using this metabolic model.
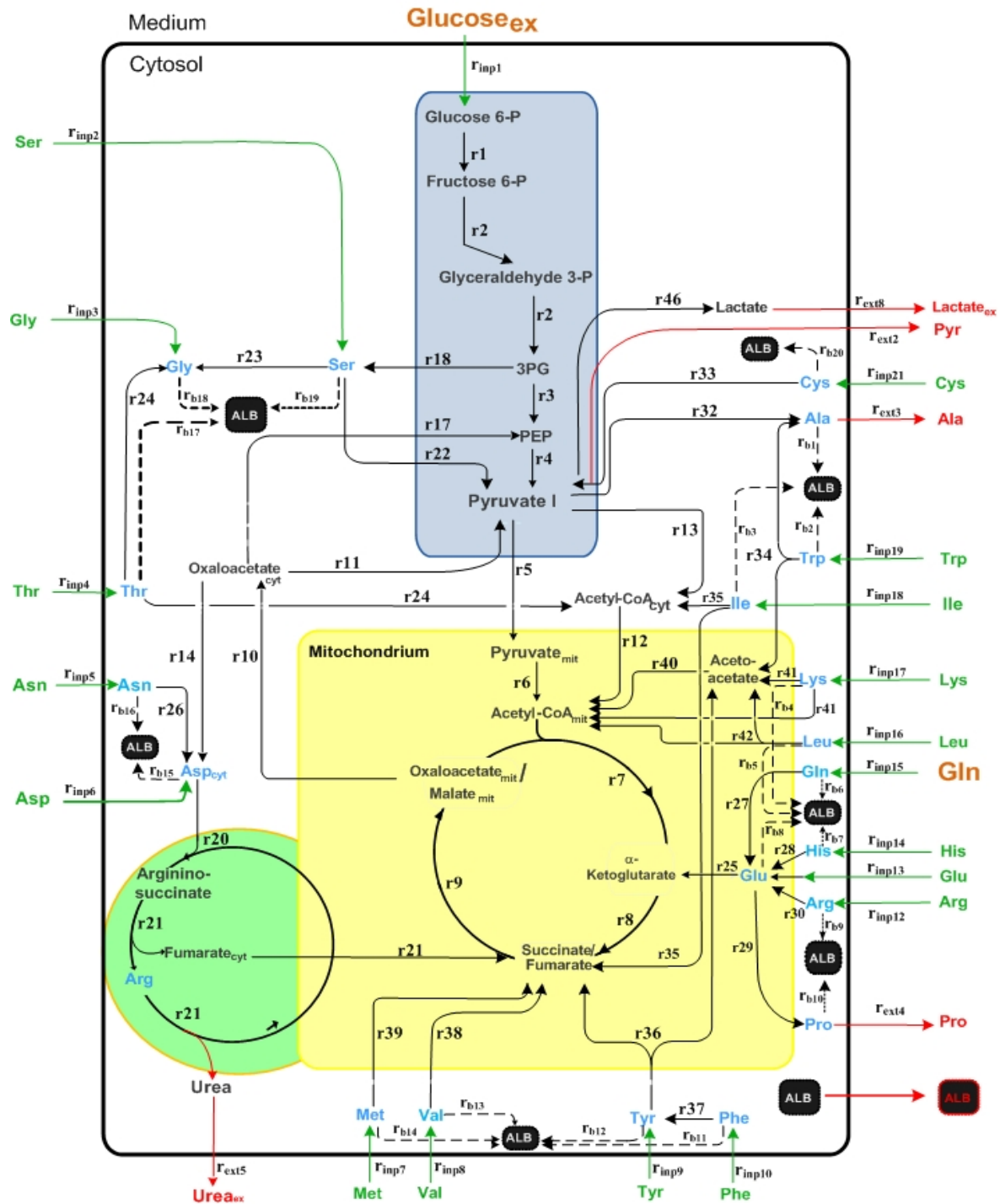
Figure 4.4.7: Mammalian cell metabolism. The network is comprised of intracellular metabolite balances, extracellular fluxes (19 uptake fluxes of amino acids and glucose, indicated by green arrows), 5 fluxes which indicate secretion (red

arrows)) and 20 anabolic fluxes (albumin synthesis, dashed arrows). Arrows indicate the direction of reaction assumed in the model. Abbreviations used: CIT citrate, ICT isocitrate, ALB albumin. The amino acids have the standard 3 letter abbreviation. The subscripts "mit" indicate mitochondrial metabolites and "cyt" cytosolic. The subscripts "inp" and "ext" indicate input and export fluxes, respectively.

The constructed stoichiometric network was additionally based on previous observations, obtained from the metabolic profile, to generate a working mathematical description of the hepatic metabolism. Pathways included were, glycolysis, the TCA cycle, the urea cycle, amino acid oxidation and albumin synthesis (see Figure 4.4.7 and Appendix 7.5.2). Glycogen synthesis and fatty acid production were not considered, since both were not quantified. Since SA002 cells do not proliferate, other definitions, regarding the pseudo-steady-state metabolic network had to be defined and are given in Appendix 7.5.1.

Since there is no biomass formation and the cells are not proliferating, the extracellular fluxes were calculated as metabolite consumed/produced per milligram albumin produced within 24 hours using the stoichiometric model and are depicted for hESC derived hepatocyte-like cells in Figure 4.4.8. Interestingly, with increasing drug concentrations the uptake for aspartate and glutamate was increased. In addition, alanine synthesis was also visibly increased. Lactate, urea and pyruvate synthesis were reduced in presence of diclofenac and glucose uptake was also reduced. For all the other amino acids (except serine) the uptake was decreasing with increasing diclofenac concentrations. However, due to the high variability, these amino acid uptake changes are not significant.

While the glutamine uptake was not distinctively changing with increasing diclofenac concentrations, aspartate and glutamate were increasingly required for presumably anaplerotic demand of the TCA cycle. Glucose uptake and lactate production were decreased in presence of diclofenac, which suggests decreased glycolysis. All the other amino acid uptake/release rates were decreased with increasing diclofenac concentrations. Hence, even sub-toxic concentrations of diclofenac (100 μM) appear to interfere with the metabolism of amino acids and/or with albumin synthesis. A reduced albumin synthesis in presence of diclofenac was previously observed in chapter 3.4.3.2. There, it was shown, that the presence of 50 μM of diclofenac, induced impairment of albumin synthesis by approximately 50 %.
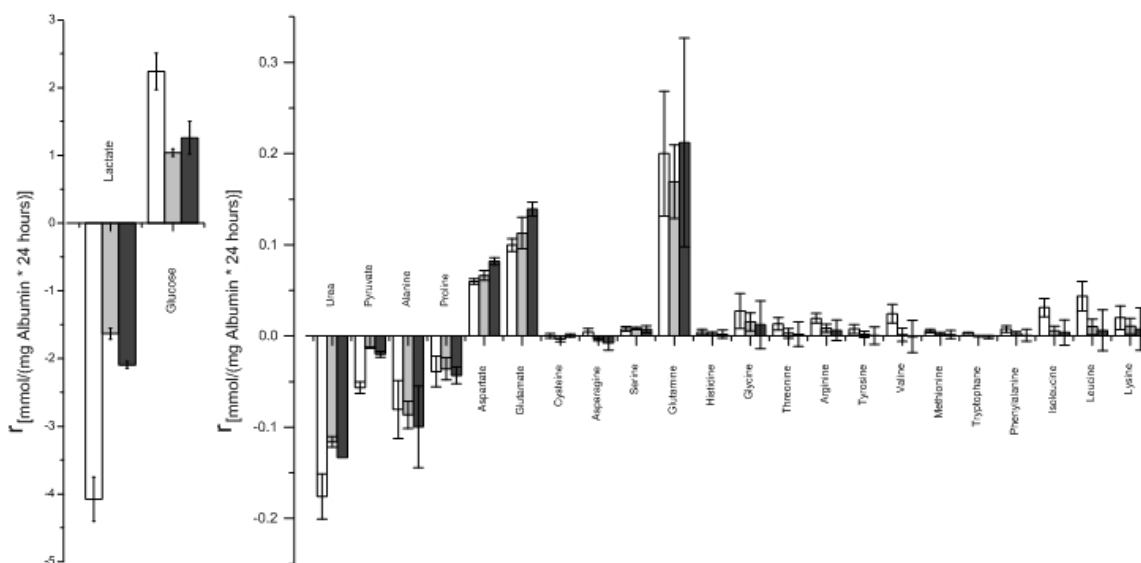
Figure 4.4.8: Extracellular fluxes, expressed as [mmol/(mg Albumin x 24 hours)] for hESC derived hepatocyte-like cells, exposed to sub-toxic concentrations of diclofenac. The white column indicates the control [0 µM Diclofenac], the light gray column ST1 [100 µM Diclofenac] and the dark grey column ST2 [200 µM Diclofenac]. The production fluxes (efflux) are depicted as negative columns and the consumption fluxes as positive columns.

In order to elucidate the mechanism by which diclofenac reduces the amino acid metabolism and impairs albumin synthesis (possibly to restore or maintain hepatocellular functions) the intracellular flux distributions was examined by MFA. For this, the assumption of only glycolytic activity, opposed to gluconeogenesis, was chosen. In addition, no fatty acid synthesis or oxidation was included, since no lipids or fatty acids were supplied in the culture media and no distinct fatty acid synthesis was observed in the GC-MS measurements. The stoichiometric balances for the intracellular metabolites were defined according to biochemical knowledge and are provided in the Appendix (Table 7.5.1).

For hESC derived hepatocyte-like cells a decreased uptake of glucose and less lactate secretion was previously observed in presence of diclofenac (Figure 4.4.8). However, here the glycolytic fluxes (from glucose to pyruvate, r1-r4) did not change significantly. Further, the flux towards lactate (r46) appeared to be only slightly reduced. The pyruvate influx into the TCA cycle, however, was slightly enhanced for both sub-toxic diclofenac concentrations (see reactions r6 and r7, PYR_mit → Acetyl-CoA_mit+ OAA$_{mit}$/Malate$_{mit}$ → α-Ketoglutarate, and r13, r12 and r7, PYR → Acetyl-CoA_cyt → Acetyl-CoA_mit +

142

$OAA_{mit}/Malate_{mit} \rightarrow \alpha$-Ketoglutarate, in Figure 4.4.9). Thus, one can surmise increased anaplerosis for the hESC derived hepatocyte-like cells. This hypothesis is further confirmed by enhanced oxidation of glutamate (r25, Glutamate $\rightarrow \alpha$-Ketoglutarate), which feeds into the TCA cycle (Figure 4.4.9). However, most amino acids, which feed into the TCA cycle, were used to maintain the synthesis of albumin and not for anaplerosis if diclofenac was present. This is apparent by reduced metabolization of these amino acids as can be seen in reactions r30 and r35-r42.
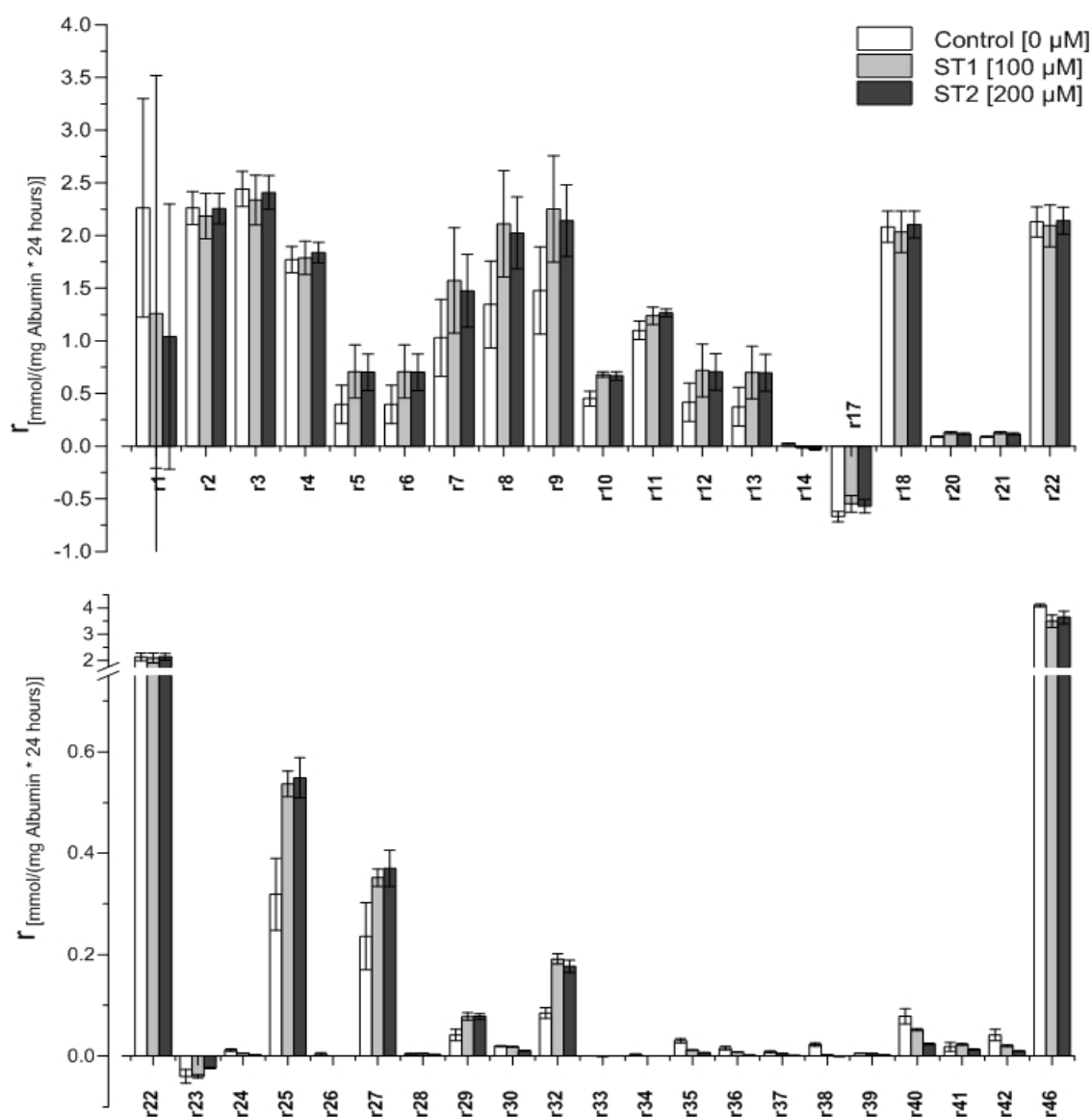
Figure 4.4.9: Intracellular fluxes, calculated as demand of metabolite in order to produce 1 mg albumin in 24 hours for hESC-derived hepatocyte-like cells, exposed to sub-toxic concentrations of diclofenac. Depicted are the calculated fluxes of glycolysis, TCA and urea cycle and the amino acid degradation towards metabolism. The rates are depicted in Figure 4.4.7 and defined in the Appendix (*S_C*, chapter 7.5.2).

In addition, urea secretion (see r20 and r21, ASP_cyt + Citrulline → ARGSucc → Urea + Succinate/Fumarate) and the flux from Succinate/Fumarate to OAA were slightly increased with increasing diclofenac concentrations. Thus, removal of free ammonia was enhanced, which increase was probably caused by the increased flux of glutamine and glutamate into the TCA cycle (r25 and r27), whereby one NH_4^+ is released in each intermediate step. However, ammonia removal by alanine synthesis was also increased and could also account for the produced NH_4^+ (Figure 4.4.9, r32: Pyr → Alanine).

The action of diclofenac and its toxicity are not yet completely understood. However, diclofenac toxicity has been associated with protein adduct formation with reactive acyl-glucuronide or quinone imine and is linked to oxidative stress. The latter is induced via formation of diclofenac cation radicals or nitroxide and quinone imine associated redox cycling. In addition, diclofenac was found to injure mitochondria by uncoupling of oxidative phosphorylation (Bort et al., 1999a; Bort et al., 1999b; Masubuchi et al., 2006; Masubuchi et al., 1998; Masubuchi et al., 2002; O'Connor et al., 2003; Vickers, 2009). As reviewed by Davies et al. (2000) NSAIDs can inhibit the glycolytic and TCA cycle activity, which results in inhibition of oxidative phosphorylation and thus ATP depletion.

Here, metabolic responses of hESC derived hepatocyte-like cells indicated no change of glycolytic activity in response to diclofenac. The TCA cycle activity appeared to be increased when the cells were exposed to diclofenac (see r7 and r8 in Figure 4.4.9). Thus, there is no indication that the oxidative phosphorylation pathway of the hESC derived hepatocyte-like cells is inhibited by the drug. An explanation for this could be the lower expression of phase I and phase II enzymes (chapter 3), compared to primary human hepatocytes. These metabolic products can cause an effect on mitochondria and lead to inhibition of oxidative phosphorylation. In addition, for the hESC derived hepatocyte-like cells an increased flux from pyruvate into the TCA cycle was observed, which is most probably due to anaplerosis or ATP demand.

It has been reported by Niklas et al. (2009), who applied MFA analysis that the glycolysis is reduced after administration of the non-steroidal anti-inflammatory drug (NSAIDs) diclofenac to Hep G2 cells. Here, only a minor decrease or no glycolytic effect was observed for the hESC derived hepatocyte-like cells. It has been reported by several groups, that NSAIDs, containing a carboxyl group, such as diclofenac and mefenamic,

uncouple oxidative phosphorylation. Diclofenac, since it is weakly acidic and lipophilic hereby acts as a proton translocator across the inner mitochondrial membrane (Boelsterli, 2003), leading to a collapse of the mitochondrial inner transmembrane potential ($\Delta\Psi_m$). In order to increase cytosolic ATP generation to account for the ATP loss, due to uncoupled oxidative phosphorylation, stimulation of glycolysis and glycogenolysis and reduction of gluconeogenic activities is induced by the cells (Kemmelmeier and Bracht, 1989; Lim et al., 2006; Moreno-Sánchez et al., 1999; Petrescu and Tarba, 1997; Porter et al., 2000) and not the other way around. Thus, one can surmise that both Hep G2 cells and hESC derived hepatocyte-like cells do not respond to the diclofenac exposure as has been previously shown for primary human hepatocytes.

4.4.1.4 Concluding remarks

From examination of the metabolic profiles of primary human hepatocytes and hESC derived hepatocyte-like cells common biological themes emerged. For each cell type, primary human hepatocytes and hESC derived hepatocyte-like cells, the influence of the applied sub-toxic diclofenac concentrations could be observed over the tested time period for all pathways involving ketogenic amino acid degradation. Here dose-dependent changes in the global metabolic profiles for aromatic amino acids (tryptophan, phenylalanine and tyrosine) seemed to be influenced the most by diclofenac exposure. However, observable metabolic changes for the primary human hepatocytes were subtle and mostly within the error range, compared to the other samples. For hESC derived hepatocyte-like cells, higher differences could be observed.

In addition, it can be assumed for primary human hepatocytes that extensive exchange of amino acids with the surrounding culture media is present. Both steady state and pseudo steady state assumptions could not be verified at these conditions and thus no metabolic balance analysis was performed.

For hESC derived hepatocyte-like cells, metabolic steady state could be assumed and thus stationary metabolic balance analysis was performed. Hereby, it was observed that diclofenac increases the activity of the TCA and the urea cycle even at sub-toxic concentrations. However, the expected increase in glycolysis to balance the ATP depletion due to uncoupling of the oxidative phosphorylation pathway was not observed.

Hence, ^{13}C labeled substrates have to be applied to further investigate a possible amino acid exchange of primary human hepatocytes and hESC derived hepatocyte-like cells with the culture medium and to obtain a better insight into the central carbon metabolism and to investigate whether sub-toxic concentrations of diclofenac have an influence on the metabolism.

4.4.2 Studies of central carbon metabolism employing ^{13}C isotopes

Carbon isotopes offer an elegant method to investigate the central metabolism of microorganisms and mammalian cells. In the previous chapter it was determined that no stationary metabolic flux analysis is feasible for primary human hepatocytes (PHHs). However, ^{13}C substrates were used to further compare both cell types (PHHs and hESC derived hepatocyte-like cells) and to investigate the influences of diclofenac exposure to the cellular physiology of the hepatocytes and the involved metabolic pathways.

The use of ^{13}C or ^{14}C labeled substrates for pathway identification has been successfully employed by many researchers (Bonarius et al., 1998; DeBerardinis et al., 2007; Katz and Wood, 1960; Kelleher, 1999; Lee et al., 1998; Lu et al., 2002). They mostly used universally or positional labeled glucose for their research, since glucose is the primary substrate for the cellular metabolism. Lee et al. (1998) have used [1,2-^{13}C$_2$]glucose to quantify the oxidative pentose-phosphate activity and Sibson et al. (2001) measured fluxes of neurotransmitter glutamate cycling, anaplerosis and TCA cycle employing [2-^{13}C]- and [5-^{13}C]glucose. In addition to positional or fully labeled glucose, labeled amino acids have been shown to improve the understanding of mammalian metabolism. Glutamine has been shown to be the main energy source in mammalian cells. It is to be used by the cells for biosynthetic pathways (e.g. fatty acids synthesis) and to provide an anaplerotic source of oxaloacetate (DeBerardinis et al., 2007; Kovacevic et al., 1991; Kovacevic and McGivan, 1983; Reitzer et al., 1979; Waagepetersen et al., 2008). By feeding fully labeled glutamine and glutamate, Des Rosiers et al. (1994) were able to determine reversibility of the isocitrate dehydrogenase reaction in liver cells. Other carbon substrates have been used further to investigate certain aspects of metabolism; Sherry et al. (2004) used [2-^{13}C]acetate and [3-^{13}C]- and [U-^{13}C]propionate to investigate substrate oxidation, multiple pyruvate cycles and gluconeogenesis in human liver cells and Peuhkurinen et al. (1983) employed [1-^{14}C]pyruvate and [1-^{14}C]lactate to investigate metabolic compartmentation of pyruvate in the isolated perfused rat heart.

Thus, these applications of ^{13}C or ^{14}C labeled substrates for pathway identification suggest that mammalian cells utilize various different substrates and that the carbon requirement cannot be fulfilled by a single substrate. However, in many bacteria glucose can be used as single substrate. In the previous chapter, it was demonstrated that no metabolic flux analysis was feasible for primary human hepatocytes. In this chapter, we

aimed for more informative insight into the uptake/production of metabolites and the involved metabolic pathways while the cells were exposed to sub-toxic diclofenac concentrations. Hence, the hepatic cells were cultured in parallel on [U-^{13}C$_6$]glucose, [1,2-^{13}C$_2$]glucose and [U-^{13}C$_5$]glutamine and simultaneously exposed to sub-toxic concentrations of diclofenac.

4.4.2.1 Glucose and glutamine metabolism

In hESC-derived hepatocytes-like cells and primary human (PH) hepatocytes the presence of a functional glycolysis and tricarboxylic acid (TCA) cycle was tested using [U-^{13}C$_6$]glucose and [U-^{13}C$_5$]glutamine as substrates. Both cell types showed uptake of the supplemented substrates and labeling in synthesized metabolites from the glycolysis (alanine, lactate and serine, glycine) and the TCA cycle (glutamate, proline and aspartate). A more detailed analysis for each cell type, while cultivated on isotopic labeled substrates and co-subcultured with sub-toxic diclofenac concentrations, is given below.

Primary human hepatocytes

As shown in Figure 4.4.10, primary human hepatocytes consumed glucose and glutamine, which was supplemented in the media. As can be seen in the time course, glucose was only consumed in the beginning of the cultivation (Figure 4.4.10 A) and glutamine was continuously taken up from the culture media (Figure 4.4.10 B).

Glucose, which was supplemented (10 mmol/L) in the culture medium, was rapidly metabolized in the beginning of the cultivation for all four co-supplemented diclofenac concentrations (Control, ST1-ST3). This can be explained by the presence of insulin and dexamethasone in the culture medium, which promote glucose uptake and glycogen synthesis (Klein et al., 2002; Swagell et al., 2006). However, since only small concentrations of insulin and dexamethasone were supplemented, no further glucose metabolization took place after 12 hours.

According to DeBerardinis et al. (2007), an increased glutamine uptake can be linked to an increased energy related demand, since glutamine metabolism (glutaminolysis) is a robust source of NADPH via malic enzyme. They also pointed out that glutamine degradation can be used for replenishment of TCA cycle intermediates (anaplerosis).

148

Here, however, glutamine consumption was highest for the primary human hepatocytes, which were not exposed to diclofenac (control) at the end of the cultivation (after 48 hours). Nevertheless, a slightly higher glutamine uptake can be presumed for the highest sub-toxic concentration in the first 12 hours of cultivation (Figure 4.4.10 B), even though the differences are not significant.
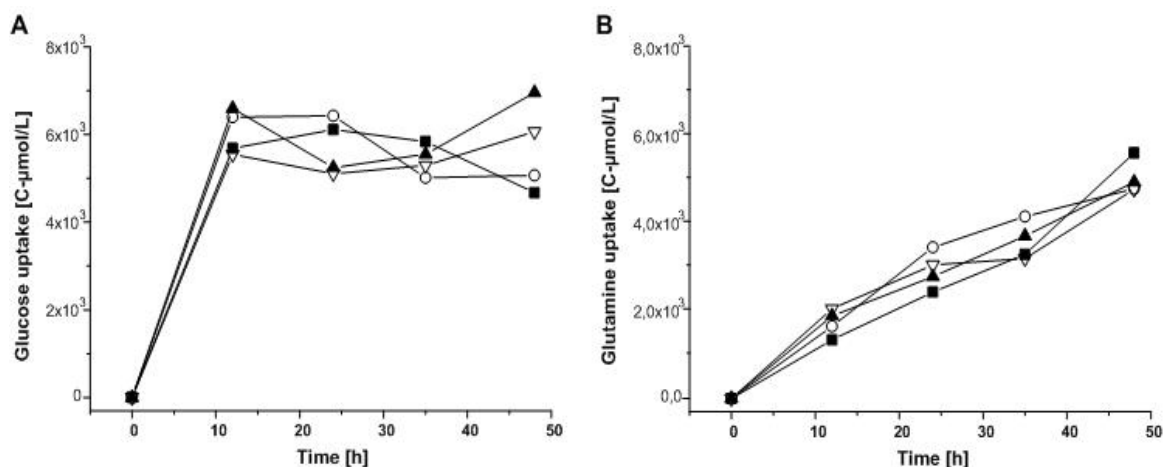
Figure 4.4.10: Carbon uptake profile of glucose **(A)** and glutamine **(B)** for primary human hepatocytes exposed to diclofenac over time. Diclofenac concentrations are denoted by: ■ control (0 µM), ○ ST1 (10 µM), ▲ (ST2, 25 µM) and ▽ (ST3, 50 µM).

Both labeled substrates could be detected by partially extensive carbon atom labeling in synthesized metabolites of the glycolysis and the TCA cycle (see Figure 4.4.11 and Figure 4.4.12). These data suggest that carbon atoms from $[U-^{13}C_6]$glucose were metabolized via glycolysis, as can be seen in the ^{13}C-metabolites of lactate, alanine, serine and glycine. Further, labeled pyruvate carbons, which are the end product of glycolysis, entered the TCA cycle, where they were degraded or used as a precursor for synthesis of metabolites. The latter is apparent in the excreted ^{13}C-metabolites glutamate, aspartate and proline, when the cells were cultured on $[U-^{13}C_6]$glucose. In addition, carbons from $[U-^{13}C_5]$glutamine were detected in the ^{13}C-metabolites of the TCA cycle. Interestingly, carbon atoms from $[U-^{13}C_5]$glutamine were also detected in lactate, alanine, serine and glycine, which are generally products of glycolysis. Thus, the data suggest an additional (gluconeogenic) flux from the TCA cycle to glycolytic metabolites.

In the following text, for primary human hepatocytes the metabolites produced from [U-^{13}C$_6$]glucose and [U-^{13}C$_5$]glutamine are discussed, regarding the pathways involved and with respect to the diclofenac exposure.

Lactate and alanine are produced from pyruvate via lactate dehydrogenase (LDH) and alanine transaminase (ALT), respectively. Since pyruvate is the end-product of glycolysis, isotopic labeled carbon atoms from [U-^{13}C$_6$]glucose can be found in lactate and alanine. However, in the lactate produced after 48 hours of cultivation (approx. 4760 C-µmol/L), carbon atoms were not only derived from glucose (approx. 2150 C-µmol/L), but also from glutamine (approx. 590 C-µmol/L). In addition, labeled carbon atoms in alanine were derived from both [U-^{13}C$_6$]glucose and [U-^{13}C$_5$]glutamine. The labeled carbon atoms from [U-^{13}C$_5$]glutamine in lactate and alanine can be explained by either gluconeogenesis or malic enzyme activity.

In detail, uniformly ^{13}C-labeled glutamine can be deaminated via glutaminase to produce uniformly labeled glutamate, which can further enter the TCA cycle (mitochondria) by conversion of glutamate to α-ketoglutarate (Bak et al., 2008) via glutamate dehydrogenase (GLUD). α-Ketoglutarate is then metabolized to uniformly labeled mitochondrial oxaloacetate (OAA). This mitochondrial OAA cannot freely diffuse to the cytosol. Thus, hepatic cells can use three pathways to shuttle the OAA into the cytosol:

- conversion of OAA to phosphoenolpyruvate (PEP), which is located in the cytosol, via mitochondrial PEP carboxykinase (PEPCK),
- transamination to aspartate, which can be transported to the cytosol where the reverse transamination occurs yielding cytosolic OAA
- reduction to malate via malate dehydrogenase (MDH) and utilization of NADH

All of these intermediate metabolites can be transported into the cytosol. If PEP is synthesized, it can be then converted to pyruvate by the enzyme pyruvate kinase (PK). As previously mentioned, pyruvate can then either be transaminated to alanine or reduced to lactate. Alternatively PEP can be used for gluconeogenic reactions.

Diclofenac exposure induced a delayed lactate synthesis in a dose-dependent manner, as shown in Figure 4.4.11. Especially, if the cells were exposed to 50 µM diclofenac, no

synthesis was observed for the first 24 hours of exposure. The overall lactate synthesis was decreased with increasing diclofenac concentrations. Lactate synthesis from either [U-^{13}C$_6$]glucose or [U-^{13}C$_5$]glutamine carbons showed the same results.

The net alanine consumption was also reduced with increasing diclofenac concentrations (Figure 4.4.11). Interestingly, labeled carbon atoms in extracellular alanine, originated both from [U-^{13}C$_6$]glucose and [U-^{13}C$_5$]glutamine carbons. Another interesting observation is, that the flux from the TCA cycle ([U-^{13}C$_5$]glutamine) to pyruvate and then to alanine appeared to be enhanced in presence of diclofenac.

Glutamate, which is synthesized from α-ketoglutarate by transamination via glutamate dehydrogenase was also found to be extensively labeled from carbons derived from [U-^{13}C$_6$]glucose and [U-^{13}C$_5$]glutamine (see Figure 4.4.11). Carbons derived from [U-^{13}C$_5$]glutamine in [U-^{13}C$_5$]glutamate can be explained by its deamination via glutaminase to glutamate (Bak et al., 2008). The formation of glutamate from carbon atoms derived from [U-^{13}C$_6$]glucose also could be accounted for by carbon atoms of pyruvate entering the TCA cycle. Pyruvate can either be transformed to OAA via pyruvate carboxylase (PC) activity, which is present in very high levels in the liver (Hasan et al., 2008), or to acetyl-CoA via pyruvate dehydrogenase (PDH) activity. In the TCA cycle OAA condenses then with acetyl-CoA to form citrate which is metabolized to α-ketoglutarate and which in turn is aminated by glutamate dehydrogenase to glutamate.

Proline is formed from glutamate and thus also has labeled carbon atoms from both universal ^{13}C-labeled substrates (see Figure 4.4.12). Labeled aspartate is directly synthesized from OAA via aspartate transaminase (AST). Both labeled substrates could be detected in aspartate carbon atoms (Figure 4.4.12), showing hereby again the glycolytic influx into the TCA cycle.

No obvious effect of diclofenac exposure was found for primary human hepatocytes for glutamate, proline or aspartate metabolism.
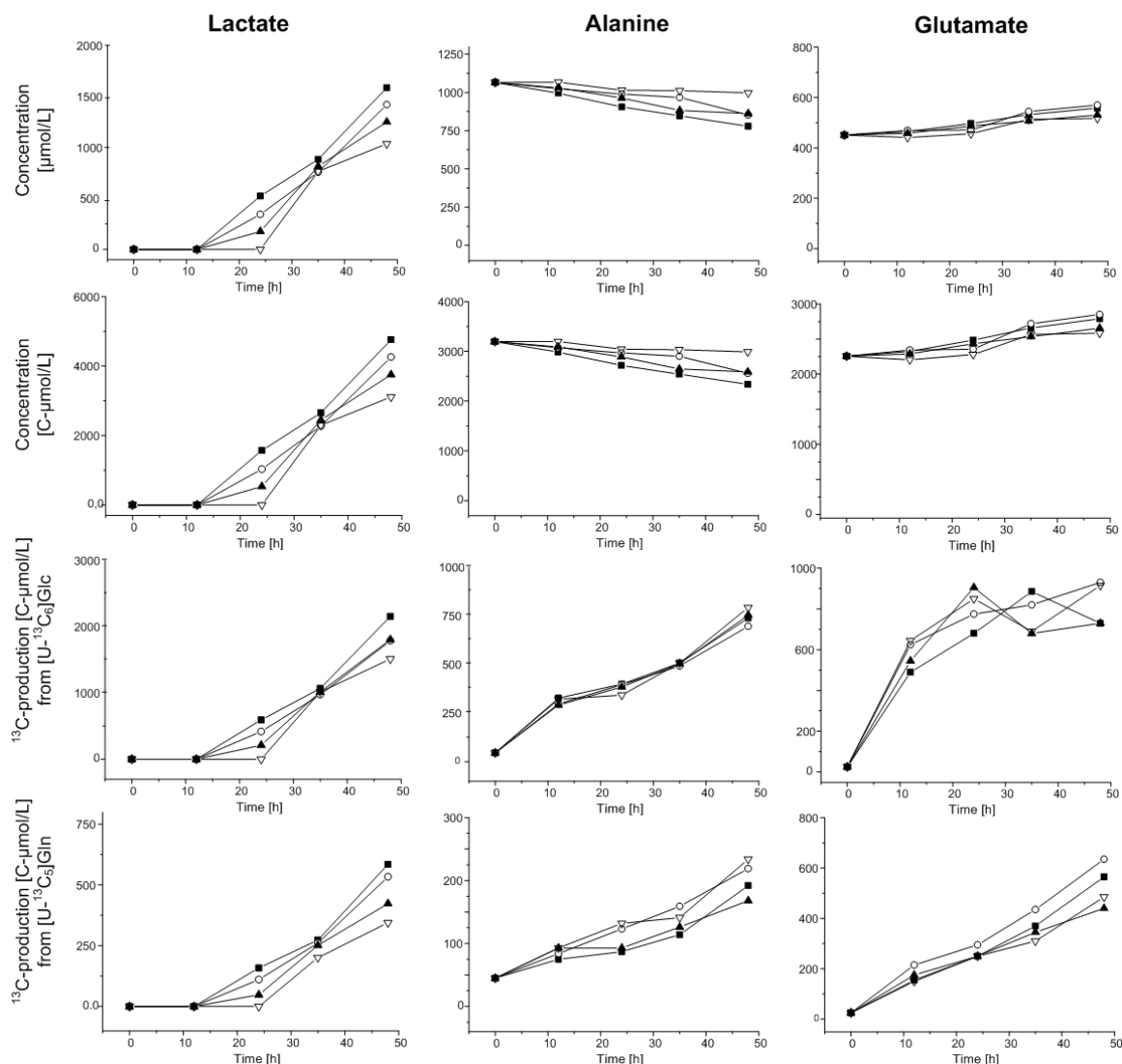
Figure 4.4.11: Carbon profiles of lactate (left column), alanine (middle column) and glutamate (right column) for primary human hepatocytes exposed to diclofenac over time [h]. Diclofenac concentrations are denoted by ■ control, ○ ST1 (10 μM), ▲ (ST2, 25 μM) and ▽ (ST3, 50 μM).

Serine, which is synthesized *de novo* from the 3-phosphoglycerate (3PG), an intermediate metabolite of the glycolysis, and is a precursor of glycine and cysteine, was synthesized (Figure 4.4.12) and excreted from the cells. Thus, carbons from [U-^{13}C$_6$]glucose were easily detected in extracellular serine and glycine. Interestingly, carbons from the uniformly labeled glutamine were also observed, thus gluconeogenic activity can also be shown here. Diclofenac treatment, however, seemed to reduce the production of serine and the consumption of glycine with increasing diclofenac concentrations, however, not significantly.
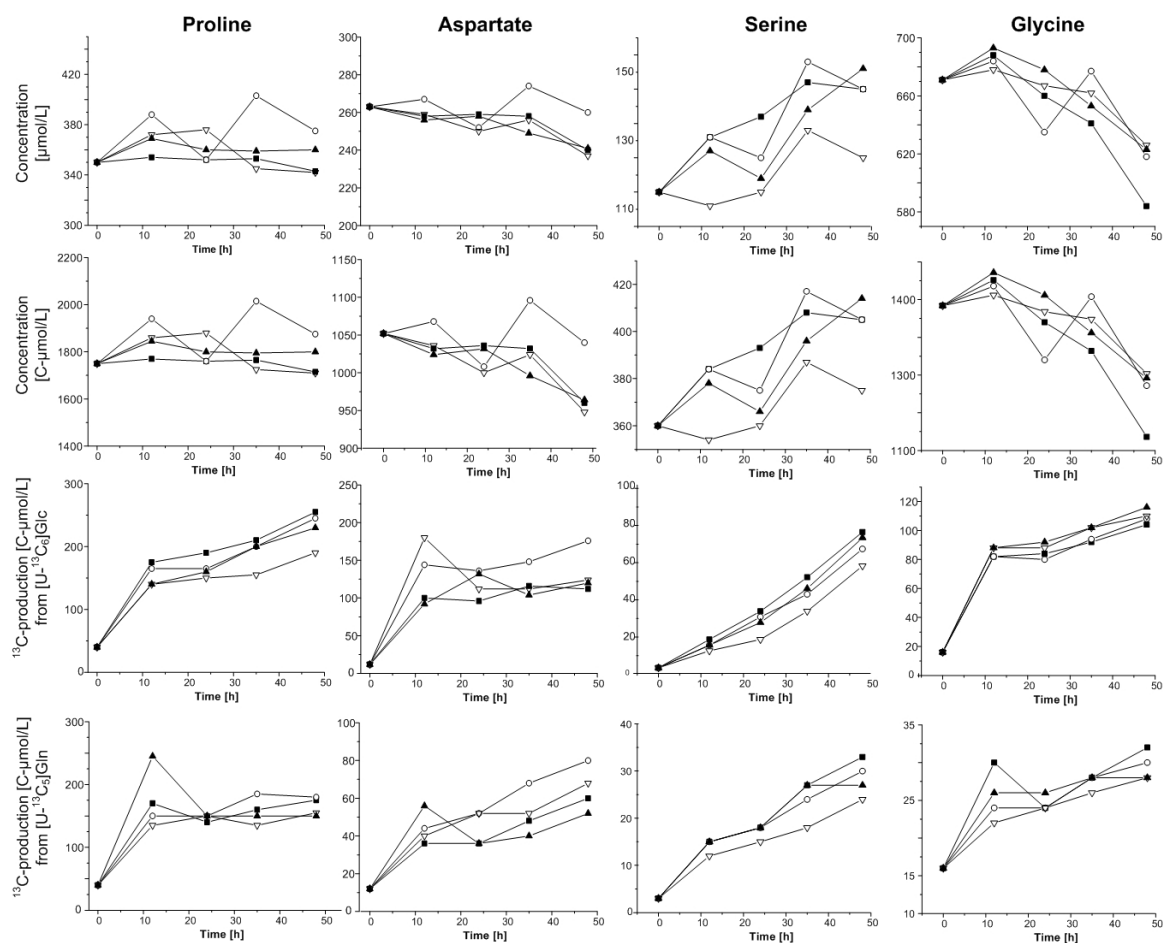
Figure 4.4.12: Carbon profiles of proline (left column), aspartate (middle left column), serine (middle right column) and glycine (right column) for primary human hepatocytes exposed to diclofenac over time [h]. Diclofenac concentrations are denoted by ■ control, ○ ST1 (10 µM), ▲ (ST2, 25 µM) and ∇ (ST3, 50 µM).

hESC derived hepatocyte-like cells

The hESC derived hepatocyte-like cells displayed higher glucose consumption and less glutamine utilization (Figure 4.4.13 A and B), compared to primary human hepatocytes (Figure 4.4.10). As previously discussed (Chapter 3.4.3.5), this high glucose demand can be considered to be due to the Warburg effect of malignant cells. Since the phenotype analysis of these cells revealed that they are to some extent mixed, it could not be ascertained which cell type is responsible for this high utilization of glucose.

Interestingly, the glutamine uptake was the highest for cells exposed to diclofenac. This can be seen in the first 24 hours of cultivation and might be induced by an energy related NADPH demand for the cytochrome P450 hydroxylation of diclofenac (since glutamine

153

degradation can be a source for NADPH (DeBerardinis et al., 2007) or a TCA cycle demand for replenishment of TCA cycle intermediates (anaplerosis). However, while the glutamine uptake was significantly enhanced for the hESC derived hepatocyte-like cells, for PHHs one could only surmise a slight trend in the first 12 hours of cultivation.
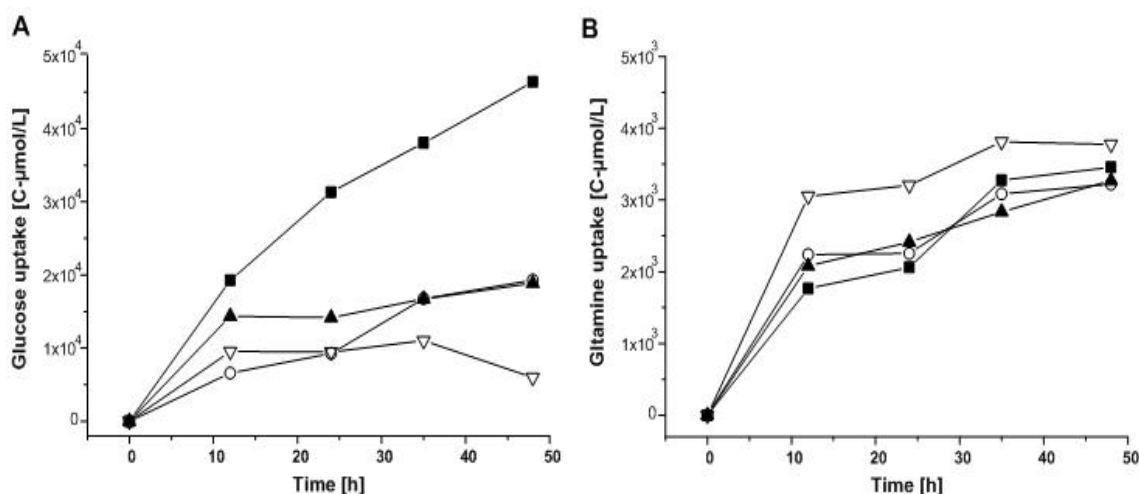
Figure 4.4.13: Carbon uptake profile of glucose (A) and glutamine (B) for human embryonic stem cell derived hepatocyte-like cells exposed to diclofenac over time [h]. Diclofenac concentrations are denoted by ■ control, ○ ST1 (100 μM), ▲ (ST2, 200 μM) and ∇ (ST3, 400 μM).

As shown in Figure 4.4.14, the lactate concentration at the end of the cultivation was considerably decreased with increasing diclofenac concentrations (ST1-ST3), mirroring the glucose uptake as shown in Figure 4.4.13. In particular the labeling from glutamine and glucose derived carbon atoms was drastically reduced, if diclofenac was supplemented close to the LC_{50} value for 48 hours (ST3). Thus, the carbon atoms of lactate did not derive from glucose.

The alanine concentrations in the supernatant for all sub-toxic drug concentrations increased, as quantified by HPLC (Figure 4.4.14). Nevertheless, the labeled carbon atoms in alanine increased to a higher extent than the actual measured net increase in the alanine concentration, pointing to reversibility of alanine synthesis and degradation. Hence, this will be discussed further below in more detail (chapter 4.4.2.3). Also interesting was that the cells showed an enhanced alanine synthesis from [U-^{13}C$_5$]glutamine and a reduced synthesis from [U-^{13}C$_5$]glucose if diclofenac was present. This is in contrast to lactate, as shown in Figure 4.4.14.
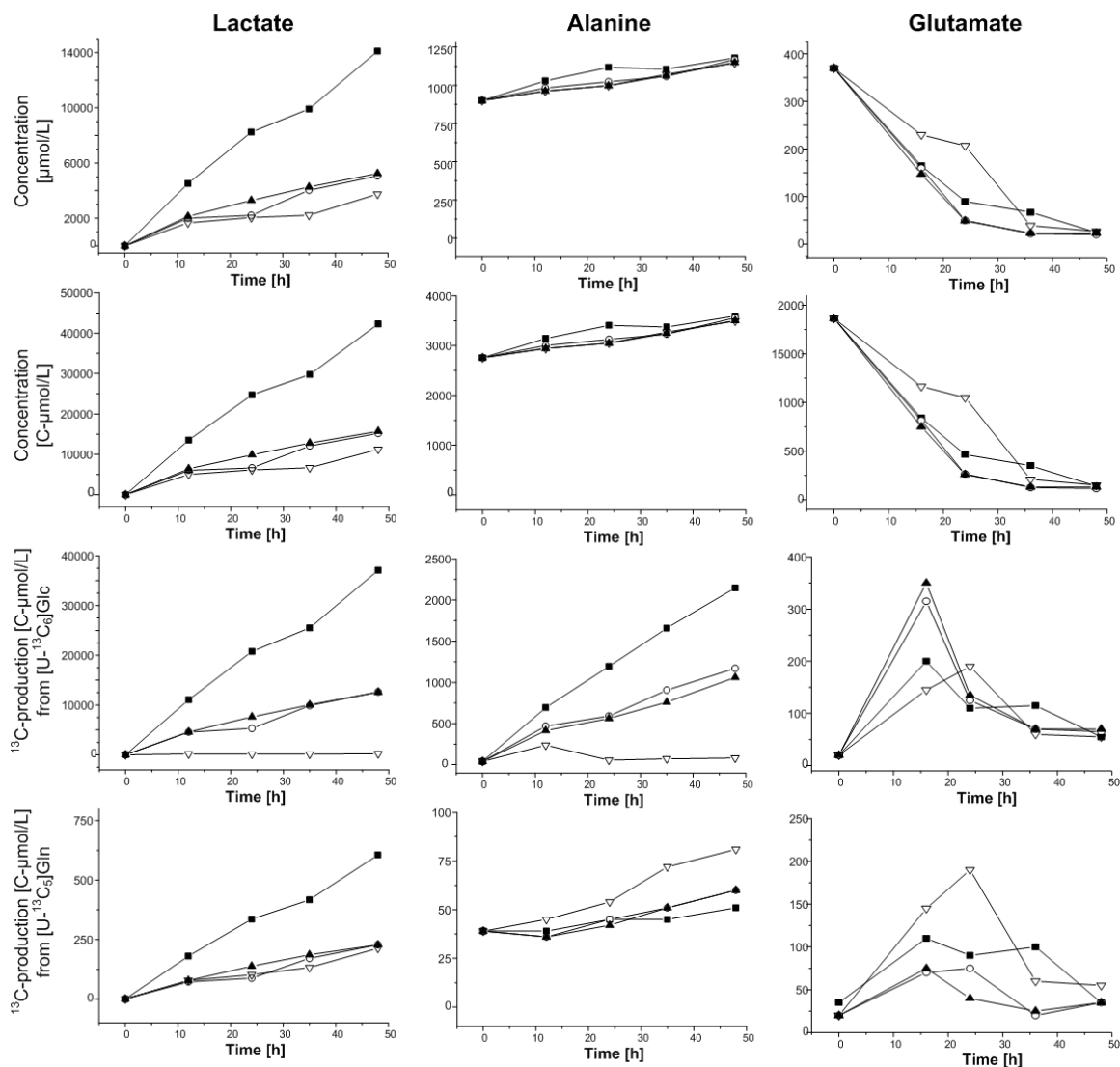
Figure 4.4.14: Carbon profile of lactate (left column), alanine (middle column) and glutamate (right column) for human embryonic stem cell derived hepatocyte-like cells exposed to diclofenac over time [h]. Diclofenac concentrations are denoted by ■ control, ○ ST1 (100 µM), ▲ (ST2, 200 µM) and ∇ (ST3, 400 µM).

Glutamate and aspartate, which feed into the TCA cycle as anaplerotic sources were almost completely degraded from the culture supernatant within 24 hours of cultivation (Figure 4.4.14 and Figure 4.4.15). Interestingly, for the highest sub-toxic concentration, the cells showed a slower metabolism of aspartate and glutamate for the first 24 hours of cultivation, however after 35 hours the cells had increased the metabolism and no difference for both metabolites was seen for control and drug-exposed cells. Similar to the overall concentrations, the labeled carbons in glutamate and aspartate from [U-^{13}C$_6$]glucose and [U-^{13}C$_5$]glutamine, which were synthesized in the beginning of the test period, were consumed at the end of the experiment. That aspartate and glutamate are

consumed, is opposite to previous observations for PHHs. Glutamate was produced and aspartate only slightly consumed by primary human hepatocytes.

Contrary to the glutamate degradation, proline, for which glutamate is the precursor, was synthesized and secreted. One possible explanation could be that increased intracellular ornithine and arginine concentrations, resulting from the urea cycle, possibly caused glutamate semialdehyde accumulation and then its cyclization to proline.
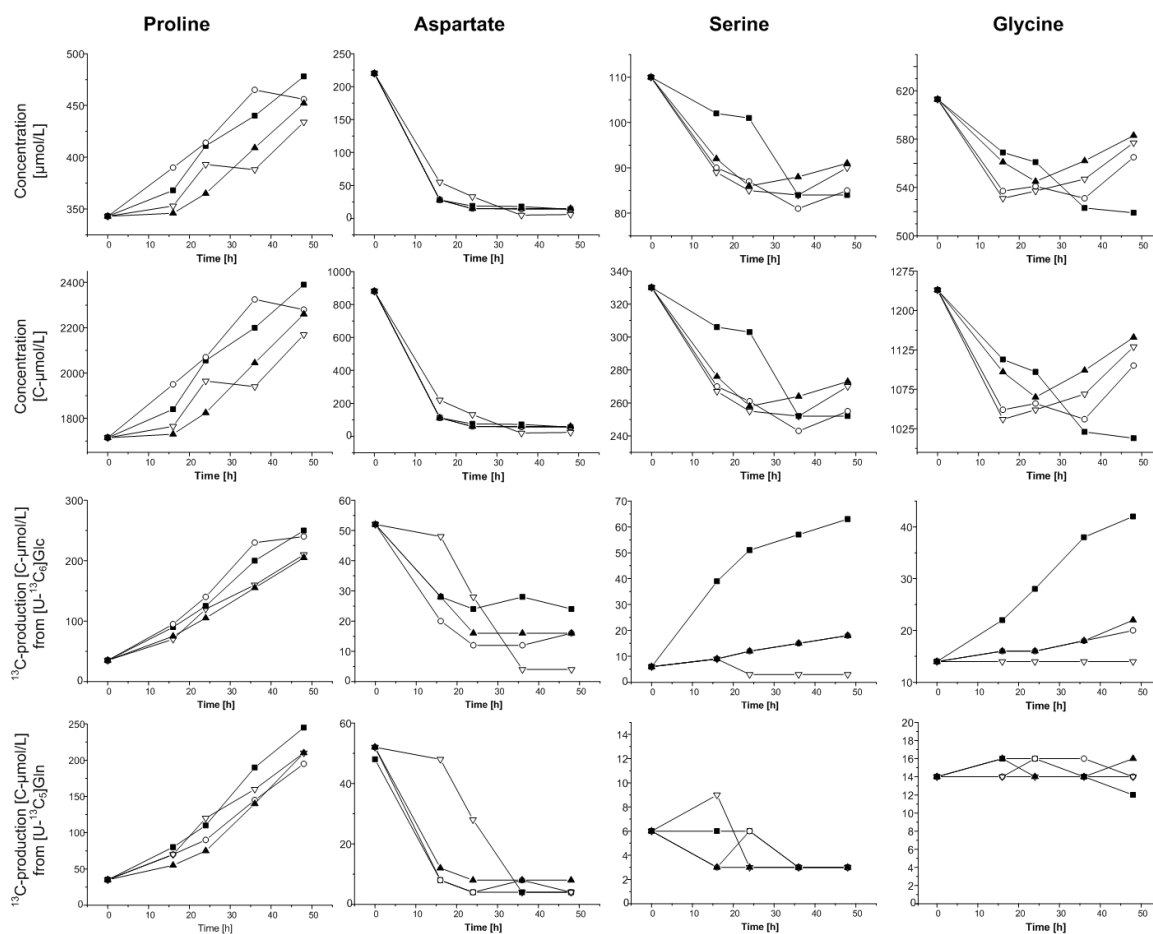
Figure 4.4.15: Carbon profiles of proline (left column), aspartate (middle left column), serine (middle right column) and glycine (right column) for human embryonic stem cell derived hepatocyte-like cells exposed to diclofenac over time. Diclofenac concentrations are denoted by ■ control, ○ ST1 (100 μM), ▲ (ST2, 200 μM) and ∇ (ST3, 400 μM).

As can be further seen in Figure 4.4.15, glycine and serine were also degraded and only small amounts of labeled carbon atoms, either derived from glucose or glutamine, were detected. Interestingly, the net decrease in extracellular serine and glycine was here seen to be enhanced for the cells exposed to diclofenac for the first 35 hours of cultivation. In

addition, if the cells were not exposed to diclofenac, serine and glycine were produced from carbons of glucose, but not from glutamine. This would imply glycolytic, but not gluconeogenic activity for these cells. However, as previously discussed (chapter 3), not all of the hESC derived hepatocyte-like cells are considered to be fully mature hepatocytes and thus, only a small gluconeogenic activity can be expected. However, this will be discussed in more detail in chapter 4.4.2.7.

4.4.2.2 Simple SFL flux model

It has been reviewed and shown by many research groups that metabolic flux estimation from stable-isotopes tracer experiments provides a key to understanding cell physiology and regulation of metabolism (Antoniewicz et al., 2007c; Stephanopoulos, 1999; Wittmann, 2007; Yoo et al., 2004). A limitation for mammalian cells for the classical method of metabolic flux analysis (MFA) is the requirement of metabolic and isotopic steady state, i.e. that labeling of the substrate and measured metabolite pools are equilibrated. Antoniewicz et al. (2007a) stated that this condition can be only approximated in continuous culture experiments after five or more residence times. As was previously shown, for primary human hepatocytes (Figure 4.4.5), no metabolic steady state was achieved. While a nearly metabolic steady state was found for the hESC derived hepatocyte-like cells, for none of the tested cell types any of the secreted metabolites showed an isotopic steady state for the culturing period of 48 hours (data not shown).

In the results presented in Figure 4.4.16, ^{13}C contribution of either [U-^{13}C$_6$]glucose (Figure 4.4.16 A & C) or [U-^{13}C$_5$]glutamine (Figure 4.4.16 B & D) carbon atoms in the secreted metabolites alanine, lactate, proline, glutamate, aspartate and serine and glycine are depicted with respect to all ^{13}C carbon atoms recovered in the secreted metabolites for PHHs (Figure 4.4.16 A & B) and hESC derived hepatocyte-like cells (Figure 4.4.16 C & D) after 48 hours of cell culture. The ^{13}C contribution of either [U-^{13}C$_6$]glucose or [U-^{13}C$_5$]glutamine carbon atoms in the secreted metabolites are given in the Appendix (Table 7.5.5 and 7.5.7) for PHHs and hESC derived hepatocyte-like cells, respectively.

For ^{13}C-balance calculations, the intracellular fluxes were normalized to glucose (Figure 4.4.16 A & C) or glutamine (Figure 4.4.16 B & C) uptake fluxes (see Table 4.4.1), which were set to 100 %. In Figure 4.4.16 the fractions of ^{13}C carbon contribution from either

[U-^{13}C$_6$]glucose or [U-^{13}C$_5$]glutamine of all carbon atoms accounted in secreted metabolites are depicted for primary human hepatocytes (Figure 4.4.16 A & B) and hESC derived hepatocyte-like cells (Figure 4.4.16 C & D), for both control cells and cells exposed to diclofenac.
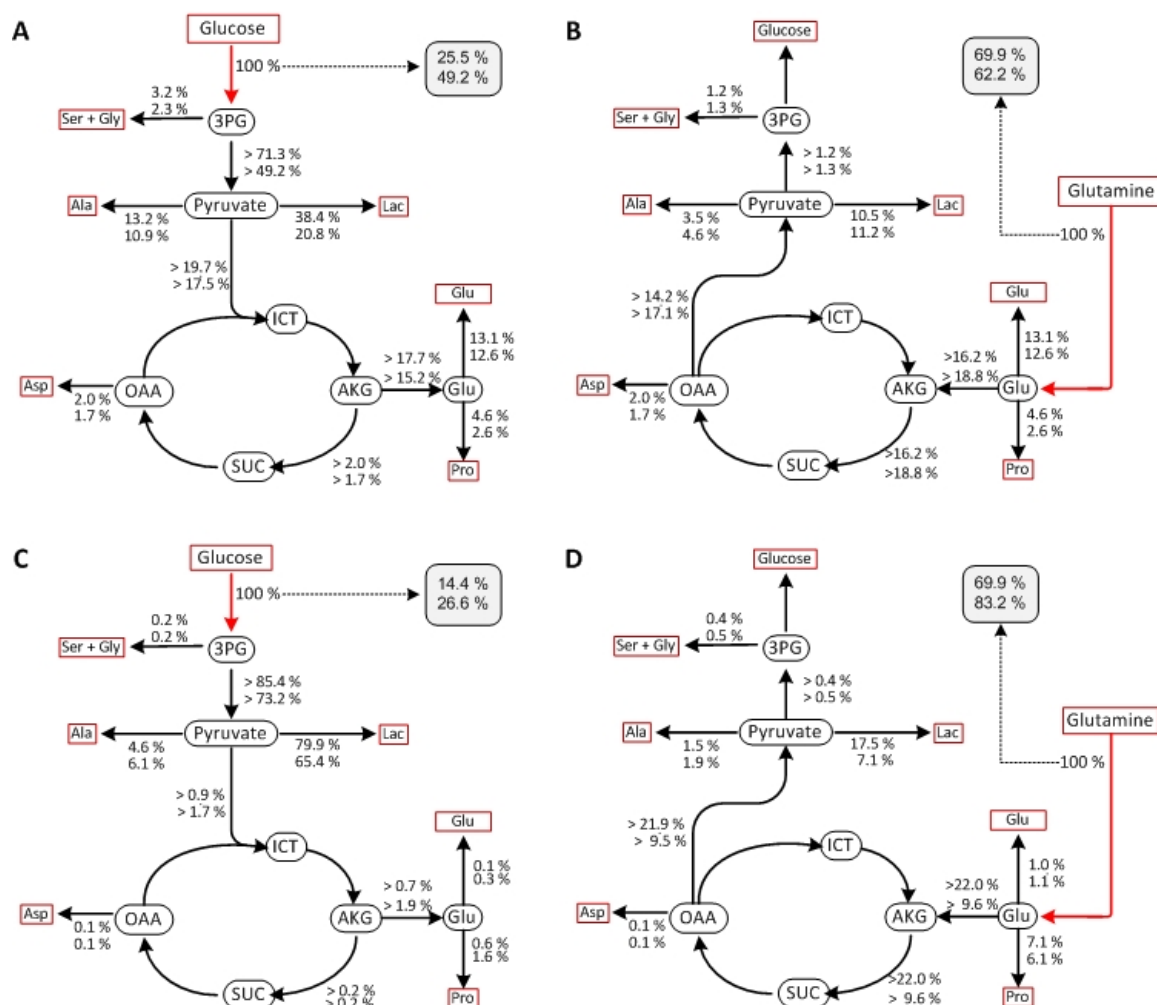
Figure 4.4.16: Simplified model for flux calculations on primary human hepatocytes (**A & B**) and SA002 cells (hESC derived hepatocyte-like cells) (**C & D**) after 48 hours of cultivation. Intracellular fluxes are normalized to glucose (**A & C**) or glutamine (**B & C**) uptake fluxes (see Table 4.4.1), set to 100 %, and depicted as fraction of ^{13}C carbon contribution from either [U-^{13}C$_6$]glucose or [U-^{13}C$_5$]glutamine of all carbon atoms accounted in secreted metabolites. The upper numbers indicate ^{13}C-fluxes for PHHs and SA002 exposed to no drug and the lower numbers indicate ^{13}C-fluxes for PHHs exposed to 50 μM and for SA002 cells to 100 μM of diclofenac. The numbers in the rounded boxes, connected by dashed arrows, indicate the percentage of not recovered carbon atoms, the rectangular boxes show extracellular metabolites and the round boxes intracellular intermediates. Abbreviations used: ICT isocitrate, OAA oxaloacetate, SUC succinate, AKG α-Ketoglutarate, Lac lactate, 3PG 3-phosphoglygerate. The amino acids have the standard 3 letter abbreviation.

As can be seen in Figure 4.4.16 A, for primary human hepatocytes, if diclofenac was present in the culture medium, the contribution of glucose carbon atoms to lactate and alanine synthesis was reduced. However, for the SA002 cells the carbon flux from glucose to lactate was reduced (Figure 4.4.16 C), whereas the flux to alanine was enhanced in presence of diclofenac. Since the hESC derived hepatocyte-like cells do not have a urea cycle as functional as PHHs (see chapter 3.4.3.1), the enhanced alanine synthesis and secretion might be an indicator of ammonia removal by the cells. While the PHHs displayed a relatively high flux into the TCA cycle (> 19.7 % for control and > 17.5 % for 50 µM diclofenac exposure), the SA002 cells metabolized the glucose carbons mainly to lactate (Warburg effect) and only few of the carbons were metabolized in the TCA cycle (> 0.9 % for control and > 1.7 % for 100 µM diclofenac exposure). Surprisingly, the influx into the TCA cycle, was enhanced in presence of diclofenac and the synthesis of glutamate and proline from glucose carbons as well (Figure 4.4.16 C).

Table 4.4.1: Glucose and glutamine uptake fluxes and glucose/glutamine ratio, calculated for primary human hepatocytes (PHH) and hESC derived hepatocyte-like cells (SA002) for control and diclofenac exposure after 48 hours of cultivation.

	Glucose Flux [C-mol/L/(10^6 cells x 48 h)]	Glutamine Flux [C-mol/L/(10^6 cells x 48 h)]	Glucose [C-mol] / Glutamine [C-mol]
PHH (0 µM Diclofenac)	32.98	32.96	0.99
PHH (50 µM Diclofenac)	42.79	33.69	1.27
SA002 (0 µM Diclofenac)	185.56	13.82	13.42
SA002 (100 µM Diclofenac)	77.12	15.10	5.10

Even though the glycolysis appeares to be decreased in primary human hepatocytes (Figure 4.4.16 A), from Table 4.4.1 one can deduce that the glycolysis actually increased if the cells are exposed to diclofenac. This is apparent from the enhanced glucose uptake flux for PHHs exposed to 50 µM diclofenac and compared to the control cells. For the hESC derived hepatocyte-like cells the glucose uptake was clearly reduced, if the cells were exposed to diclofenac. The increased glycolysis (or possibly glycogenolysis) of PHHs in response to diclofenac treatment is most probably due to ATP depletion, caused by diclofenac disturbance in the oxidative phosphorylation (Kemmelmeier and Bracht, 1989; Lim et al., 2006; Moreno-Sánchez et al., 1999; Petrescu and Tarba, 1997; Porter et al., 2000).

As shown in Figure 4.4.16 B, for primary human hepatocytes the influx of glutamine carbons into the TCA cycle was enhanced in presence of diclofenac, while for the SA002 cells this influx was reduced (see Figure 4.4.16 D and also the glucose/glutamine ratio in Table 4.4.1). Further for PHHs, the gluconeogenic flux (OAA → Pyruvate) was enhanced, if the cells were exposed to diclofenac, resulting in higher carbon atom contributions in alanine, lactate, serine and glycine. Surprisingly, even though the gluconeogenic flux in SA002 cells was reduced, if the cells were exposed to diclofenac, the glutamine contribution to alanine, serine and glycine was increased, whereas that of lactate was significantly decreased.

From the enhanced carbon atom contribution from glutamine in the metabolites, one can surmise that diclofenac interferes directly with the albumin synthesis (see chapter 3.4.3.2), since albumin synthesis was reduced in presence of diclofenac, or that diclofenac interferes with the transport of amino acids into the cells. The latter hypothesis is in accordance with observations by Kaur et al. (2010) who demonstrated a reduced amino acid uptake following treatment with a NSAID. A reduced amino acid catabolism in presence of diclofenac has been shown for both cell types in chapter 4.4.1.1. Both hypotheses would coerce the cells to synthesize these metabolites for albumin synthesis, instead of utilizing them from the culture medium. For future studies it would be interesting to analyze the contribution of synthesized and transported amino acids in synthesized and excreted albumin.

4.4.2.3 Reversibility of fluxes

As previously described, mammalian cell systems are far more complex than simple eukaryotes and prokaryotes, which has handicapped the application of metabolic flux balancing approaches. This is due to the fact that the metabolite balancing only considers overall (net) fluxes. However, mammalian cells have inter-compartmental exchange fluxes and an extensive metabolite exchange with the culture media. By applying isotope balancing, bidirectionality of pathways (reversibility reactions) must be included in the analysis, since isotope labels may be transported in the opposite direction of the net flux (Christensen and Nielsen, 2000). Reaction reversibility has been shown to complicate flux determination in certain pathways due to label redistribution. It's this regard may lead to wrong interpretation of the results and one might miss useful information on

metabolic phenomena, such as futile cycles (Christensen and Nielsen, 2000; Follstad et al., 1999; Follstad and Stephanopoulos, 1998; Wiechert and de Graaf, 1997).

The simultaneous synthesis and degradation of various amino acids was previously observed in chapter 4.4.2.1. All analyzed amino acids (alanine, aspartate, glutamate, proline, glycine and serine) showed labeling from glutamine or glucose as source, which indicates their metabolic synthesis, and were simultaneously degraded by either PHHs or SA002 cells. Thus reversible reactions for all of these metabolites take place.

This reversibility (*Rev*) is shown in Figure 4.4.17 for the metabolite alanine, which is net produced and secreted over time for the hESC derived hepatocyte-like cells (Figure 4.4.17 A). This net production is here defined as *vnet*. Previously, it was shown in chapter 4.4.2.1 (Figure 4.4.14) that ^{13}C-carbon atoms in extracellular alanine were derived from either [U-^{13}C$_6$]glucose or [U-^{13}C$_5$]glutamine as substrates. Since both cultivations were performed in parallel, one can sum the detected ^{13}C carbon atoms in alanine from [U-^{13}C$_6$]glucose and [U-^{13}C$_5$]glutamine as substrates to obtain the minimum production of ^{13}C-carbon atoms in alanine (Figure 4.4.17 B). This mass isotopomer production can be defined as flux *v1*.

The sum of the detected ^{13}C carbons in the metabolites from [U-^{13}C$_6$]glucose and [U-^{13}C$_5$]glutamine is defined as the minimum production here, since the metabolite (alanine) can also be synthesized from carbon sources other than glucose or glutamine. Other carbon sources were not isotopically labeled in this experiment, and thus the carbons of these substrates would appear as ^{12}C in secreted metabolite (alanine) carbon atoms. These, however, cannot be distinguished from the alanine supplied in the culture medium. Comparing the net carbon atom increase of alanine carbon atoms within 48 hours (840 C-µmol/L, Figure 4.4.17 A) with the amount of the produced ^{13}C carbon atoms in alanine (approx. 2200 C-µmol/L, Figure 4.4.17 B), it is apparent that the cells must have consumed alanine to account for the difference in concentration increase and ^{13}C production in alanine. The estimated minimum carbon consumption (here defined as flux *v2*) is given in Figure 4.4.17 C and was calculated according to equation 4.18.

$$v2 = v1 - vnet \qquad \text{[Eq. 4.18]}$$

From these data the reversibility (*Rev*) can be estimated as function of metabolite consumption versus ^{13}C mass isotopomer production and is given in equation 4.19.

$$Rev = \frac{v2}{v1} = \frac{v1-vnet}{v1} \qquad \text{[Eq. 4.19]}$$
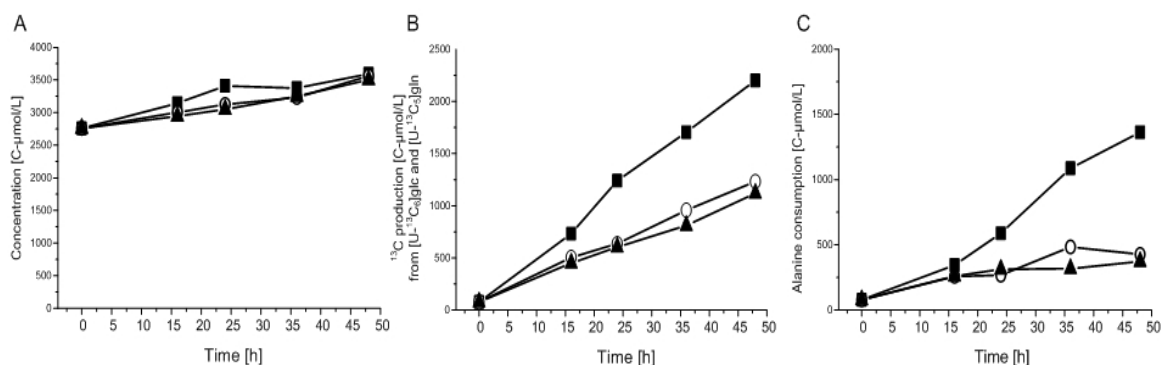
Figure 4.4.17: Carbon profiles of alanine for primary human hepatocytes exposed to diclofenac over time [h] and cultured on [U-^{13}C$_6$]glucose and [U-^{13}C$_5$]glutamine. Diclofenac concentrations are denoted by ■ control, ○ ST1 (10 μM), ▲ (ST3, 50 μM). **A)** depicts the alanine concentration [C-μmol/L] as quantified by HPLC (*vnet*). **B)** depicts the sum of produced ^{13}C carbons in alanine from [U-^{13}C$_6$]glucose and [U-^{13}C$_5$]glutamine as substrate (*v1*). **C)** depicts the estimated minimum consumption of extracellular alanine to account for the difference in concentration increase and ^{13}C production in alanine (*v2*).

The minimum ^{13}C mass isotopomer production and the minimum total consumption of alanine, serine, glycine, proline, aspartate and glutamate was determined as shown previously for alanine for primary human hepatocytes (Table 4.4.2) and the hESC derived hepatocyte-like cells (Table 4.4.3). In Figure 4.4.18 A and B, the direction of net production or consumption rate [C-μmol/L/48 hours] for each metabolite is indicated by big arrows and was further estimated and shown in Figure 4.4.18 A and B for PHHs and SA002 cells, exposed to three concentrations of diclofenac.

Table 4.4.2: Carbon concentration [C-µmol/L] over time, ^{13}C-mass isotopomer production [C-µmol/L] from [U-^{13}C$_6$]glucose or [U-^{13}C$_5$]glutamine over time [h] and total metabolite consumption [C-µmol/L] over time [h] quantified by HPLC and analyzed by GC/MS for primary human hepatocytes exposed to diclofenac.

PHH	Time [h]	Concentration [C-µmol/L]					^{13}C-mass isotopomer production [C-µmol/L] from [U-^{13}C$_5$]glucose and [U-^{13}C$_5$]glutamine					Consumption [C-µmol/L]				
		0	12	24	35	48	0	12	24	35	48	0	12	24	35	48
Alanine	*Control*	3195	2985	2715	2541	2337	90	402	486	621	930	90	612	966	1275	1788
	ST1	3195	3072	2967	2901	2559	90	381	519	651	915	90	504	747	945	1551
	ST3	3195	3198	3042	3033	2991	90	414	474	648	1026	90	411	627	810	1230
Glutamate	*Control*	2255	2325	2485	2660	2790	50	645	930	1255	1295	50	575	700	850	760
	ST1	2255	2345	2355	2720	2850	50	840	1070	1255	1565	50	750	970	790	970
	ST3	2255	2205	2280	2565	2585	50	795	1100	1000	1400	50	845	1075	690	1070
Proline	*Control*	1750	1770	1760	1765	1715	80	345	330	370	430	80	325	320	355	465
	ST1	1750	1940	1760	2015	1875	80	315	315	385	425	80	125	305	120	300
	ST3	1750	1860	1880	1725	1710	80	275	300	290	345	80	165	170	315	385
Aspartate	*Control*	1052	1032	1036	1032	960	24	136	132	164	172	24	156	148	184	264
	ST1	1052	1068	1008	1096	1040	24	188	188	216	256	24	172	232	172	268
	ST3	1052	1036	1000	1024	948	24	220	164	164	192	24	236	216	192	296
Serine	*Control*	360	384	393	408	405	6	33	51	78	108	6	9	18	30	63
	ST1	360	384	375	417	405	6	30	48	66	96	6	6	33	9	51
	ST3	360	354	360	387	375	6	24	33	51	81	6	30	33	24	66
Glycine	*Control*	1342	1376	1320	1282	1168	32	112	108	120	136	32	78	130	180	310
	ST1	1342	1368	1270	1354	1236	32	106	104	122	138	32	80	176	110	244
	ST3	1342	1356	1334	1324	1252	32	110	112	128	138	32	96	120	146	228

Table 4.4.3: Carbon concentration [C-µmol/L] over time, ^{13}C-mass isotopomer production [C-µmol/L] from [U-^{13}C$_6$]glucose or [U-^{13}C$_5$]glutamine over time [h] and total metabolite consumption [C-µmol/L] over time [h] quantified by HPLC and analyzed by GC/MS for primary human hepatocytes exposed to diclofenac. The '-' in proline consumption indicates production from other sources than glucose or glutamine.

SA002	Time [h]	Concentration [C-µmol/L]					^{13}C-mass isotopomer production [C-µmol/L] from [U-^{13}C$_5$]glucose and [U-^{13}C$_5$]glutamine					Consumption [C-µmol/L]				
		0	16	24	36	48	0	16	24	36	48	0	16	24	36	48
Alanine	*Control*	2757	3144	3408	3375	3594	78	732	1239	1704	2199	78	345	588	1086	1362
	ST1	2757	3003	3126	3231	3561	78	504	636	957	1230	78	258	267	483	426
	ST2	2757	2946	3048	3249	3504	78	450	603	810	1119	78	261	312	318	372
Glutamate	*Control*	1865	840	465	350	140	55	310	200	215	90	55	1335	1600	1730	1815
	ST1	1865	815	265	125	115	40	385	200	90	100	40	1435	1800	1830	1850
	ST2	1865	750	260	130	130	40	425	175	95	105	40	1540	1780	1830	1840
Proline	*Control*	1715	1840	2055	2200	2390	70	170	235	390	495	70	45	-105	-95	-180
	ST1	1715	1950	2070	2325	2280	70	165	230	375	435	70	-70	-125	-235	-130
	ST2	1715	1730	1825	2045	2260	70	130	180	295	415	70	115	70	-35	-130
Aspartate	*Control*	880	112	76	72	56	100	36	28	32	28	100	804	832	840	852
	ST1	880	112	60	56	56	104	28	16	20	20	104	796	836	844	844
	ST2	880	112	60	60	60	104	40	24	24	24	104	808	844	844	844
Serine	*Control*	330	306	303	252	252	12	45	57	60	66	12	69	84	138	144
	ST1	330	270	261	243	255	12	12	18	18	21	12	72	87	105	96
	ST2	330	276	258	264	273	12	12	15	18	21	12	66	87	84	78
Glycine	*Control*	1226	1138	1122	1046	1038	28	38	44	52	54	28	126	148	232	242
	ST1	1226	1074	1082	1062	1130	28	30	32	34	34	28	182	176	198	130
	ST2	1226	1122	1090	1124	1166	28	32	30	32	38	28	136	166	134	98

As can be seen in Figure 4.4.18 A and B, for PHHs and SA002 cells the metabolites serine, alanine and glutamate showed opposite net consumption/production rates. The metabolites glycine and aspartate were net consumed and proline net produced for both cell types (see Figure 4.4.18 A & B). This was previously observed for PHHs (Figure 4.4.12) and hESC derived hepatocyte-like cells (Figure 4.4.15). Interestingly, the ratio of ^{12}C carbon uptake versus ^{13}C carbon production for primary human hepatocytes was reduced for alanine and glycine in the extracellular medium, if diclofenac was supplemented. This suggests that both metabolites are distinctively produced more from non-labeled substrates in primary human hepatocytes, if diclofenac is present, even though the net uptake appears to be reduced. For the hESC derived hepatocyte-like cells the same trend was observed for glycine, when diclofenac was supplemented. However, for alanine, the net rate was here positive (production), even though the ratio of ^{12}C carbon atom uptake versus ^{13}C carbon atom production was reduced. This indicates that alanine is produced more from the non-labeled substrates also in the SA002 cells, if diclofenac is present.

For primary human hepatocytes it can be further seen in Figure 4.4.18 A, that serine and glutamate were net produced. Interestingly, here the reversibility increased with increasing diclofenac concentrations, suggesting enhanced influx of these metabolites for metabolization (Figure 4.4.18 A). Similarly it can be observed, that while the net production of serine and aspartate decreased for the SA002 cells (Figure 4.4.18 C), the total efflux of both metabolites must have also decreased with increasing diclofenac concentrations.

Surprisingly, for the hESC derived hepatocyte-like cells, while compared to control treatment the net rate of aspartate and glutamate uptake did not distinctively change due to diclofenac exposure (Figure 4.4.18 B), the reversibility decreased for glutamate and increased for aspartate. This means that glutamate was increasing its efflux ($v1$) and aspartate decreased its efflux ($v1$) in presence of diclofenac.

Since it was previously shown (Chapter 4.4.1.2) that metabolic flux balancing is not feasible for primary human hepatocytes, non-stationary models have to be applied. For these, further information on inter-compartmental exchange fluxes and metabolite exchange fluxes with the culture media can be obtained by isotope labeling experiments. For isotopomer models the knowledge of reversibility of fluxes is indispensable. Here, a

first attempt to determine existence of reversibilities and exchange fluxes with the culture medium for PHHs and SA002 cells is presented.
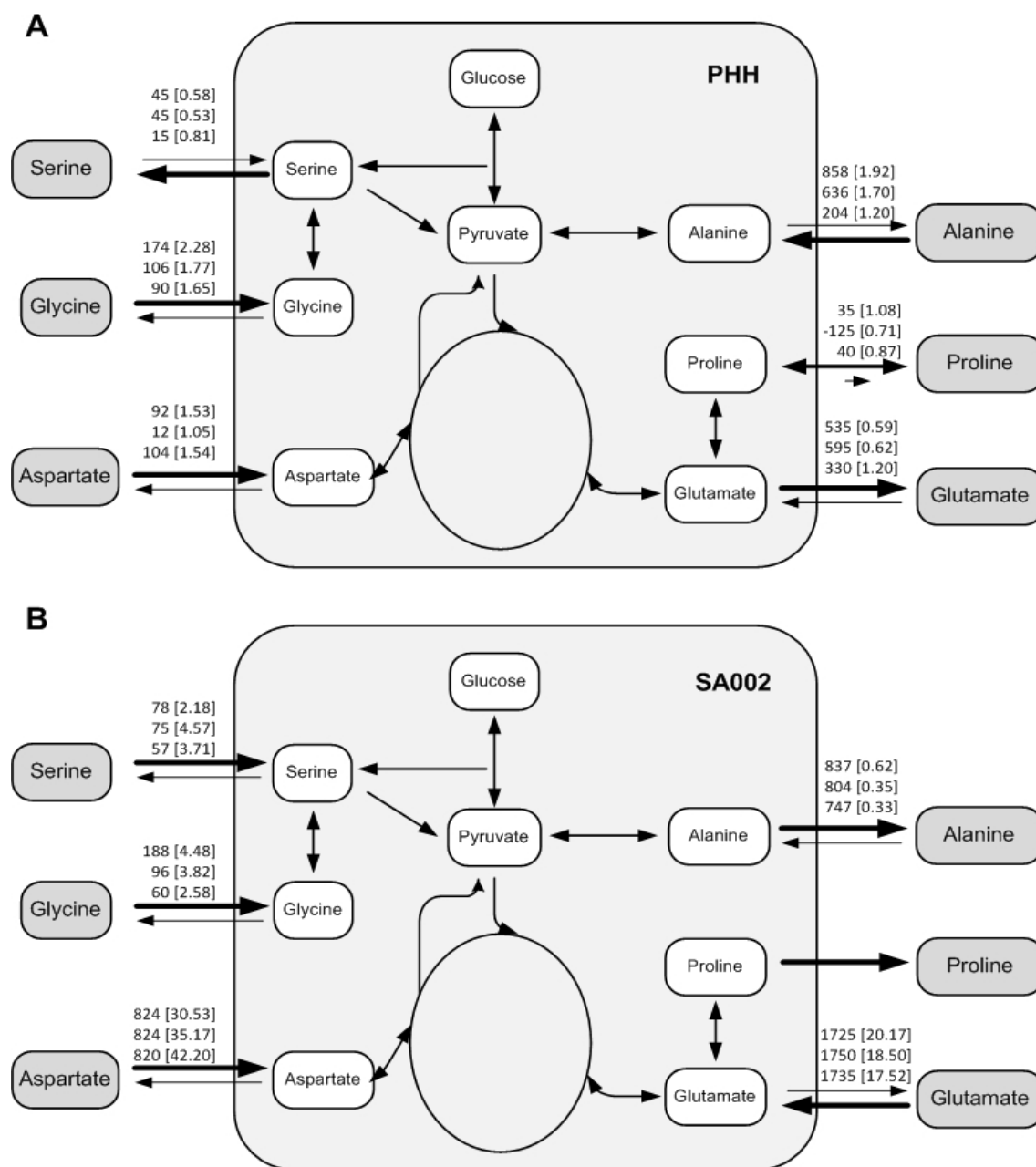
Figure 4.4.18: Net consumption/production rates with their reversibility (*Rev*), depicted in the brackets as ratio of ^{12}C carbon uptake (*v2*) versus ^{13}C carbon production (*v1*) according to equation [4.18], of the metabolites serine, glycine, aspartate, alanine, proline and glutamate for **(A)** primary human hepatocytes (PHH) and **(B)** hESC derived hepatocyte-like cells (SA002) exposed to diclofenac in three concentrations. The number on top indicates the control (0 µM diclofenac), the middle number the ST1 of both cell types (10 µM diclofenac for PHHs, 100 µM diclofenac for SA002) and the lowest number indicates 50 µM diclofenac and 200 µM diclofenac for PHHs and SA002 cells, respectively. The overall net direction is shown as big arrow for each metabolite in **(A)** and **(B)**.

4.4.2.4 Glycolysis and TCA cycle

To further investigate the interconnection of glycolysis, TCA cycle and gluconeogenesis or recycling, mass isotopomer fractions [%] and mass isotopomer concentrations [µmol/L] of the amino acids alanine, glutamate, aspartate and proline, as well as lactate from either [U-^{13}C$_6$]glucose or [U-^{13}C$_5$]glutamine were analyzed for primary human hepatocytes and hESC derived hepatocyte-like cells. In addition, possible formation of labeled metabolites was considered based on established biochemical pathways.

This chapter is subdivided into two parts. The first part deals with the analysis of lactate and alanine, which have both pyruvate as precursor. The focus of the second part is directed towards the metabolites glutamate, aspartate and proline, which are synthesized from TCA cycle intermediates.
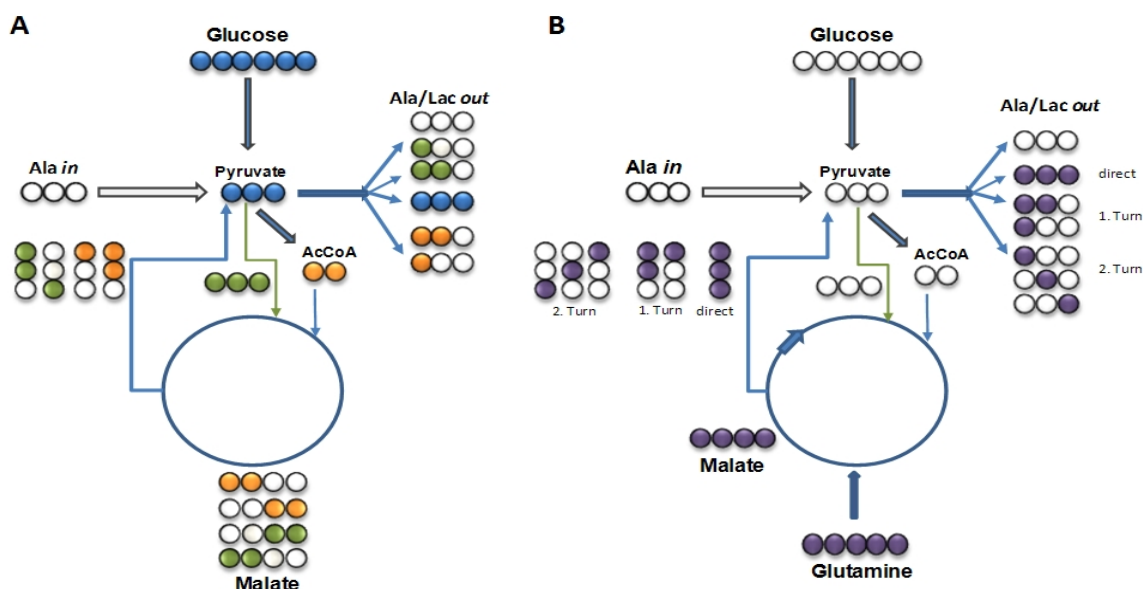
Figure 4.4.19:   Schematic depiction of labeled **(A)** glucose carbons (blue, green and orange circles) and **(B)** glutamine carbons (purple circles) metabolism by glycolysis and TCA cycle and their possible mass increase in alanine and lactate (indicated by filled dots) in primary human hepatocytes and hESC derived hepatocyte-like cells. The blue arrow from pyruvate to acetyl-CoA (ACCoA) describes pyruvate dehydrogenase (PDH), the green arrow pointing to the TCA cycle intermediate depicts the pyruvate carboxylase (PC) and the blue arrow from malate to pyruvate indicates malic enzyme (ME) activity.

As depicted in Figure 4.4.19 A, if [U-^{13}C$_6$]glucose is used as substrate, several mass isotopomers can be formed for lactate and alanine. Fully labeled mass isotopomers (*m3*) are formed, if the precursor ([U-^{13}C$_3$]pyruvate) is synthesized from [U-^{13}C$_6$]glucose via

glycolysis or the pentose phosphate pathway. The unlabeled pyruvate isotopomer fraction (*m0*) can only be synthesized from unlabeled substrates. *m1* or *m2* isotopomer fractions of pyruvate can only be formed, if $[U-^{13}C_3]$pyruvate enters the TCA cycle, either via pyruvate dehydrogenase (PDH) or pyruvate carboxylase (PC). If $[U-^{13}C_3]$pyruvate is transformed by PDH activity, it results in $[U-^{13}C_2]$acetyl-CoA. Unlabeled oxaloacetate (OAA) condenses then with $[U-^{13}C_2]$acetyl-CoA to form $[4,5-^{13}C_2]$citrate which is metabolized in the TCA cycle to $[4,5-^{13}C_2]\alpha$-ketoglutarate and then, due to scrambling, to either $[1,2-^{13}C_2]$malate or $[3,4-^{13}C_2]$malate. If $[U-^{13}C_3]$pyruvate is transformed by PC activity, also $[1,2-^{13}C_2]$malate or $[3,4-^{13}C_2]$malate is formed (Figure 4.4.19 A).

The flux towards pyruvate can be explained by two possible enzymes, namely conversion of OAA to phosphoenolpyruvate (PEP) via mitochondrial PEP carboxykinase (PEPCK), transport to the cytosol followed by conversion to pyruvate via pyruvate kinase (PK) or oxidative decarboxylation of malate to pyruvate via malate dehydrogenase (MDH, or malic enzyme ME). $[3-^{13}C]$ or $[1,2-^{13}C_2]$pyruvate is hereby formed which can be metabolized to alanine and lactate. Both pathways are active in mammalian (and human) liver cells (Brown et al., 1997; Heart et al., 2009; Wimmer et al., 1990). This recycling to pyruvate would, due to scrambling of succinate and fumarate (Bernhard and Tompa, 1990), result in a 50/50 ratio of *m1* and *m2* isotopomer fractions in alanine and lactate, regardless if $[U-^{13}C_3]$pyruvate entered the TCA cycle via PDH or PC (Figure 4.4.19 A).

If $[U-^{13}C_5]$glutamine is used as a substrate, also several mass isotopomers of lactate and alanine can be formed (Figure 4.4.19 B). $[U-^{13}C_3]$pyruvate and thus $[U-^{13}C_3]$alanine and $[U-^{13}C_3]$lactate (both *m3*) would be formed by the previously explained activity of malic enzyme or PEP carboxykinase (PEPCK). However, if $[U-^{13}C_3]$pyruvate re-enters the TCA cycle, *m1* and *m2* mass isotopomer fractions and in an additional turn, *m1* mass fractions can be formed (see Figure 4.4.19 B). The multiple turns of the TCA cycle for glutamate as synthesized metabolite have been described by Bak et al. (2008).

The measured mass isotopomer fractions and mass isotopomer concentrations of lactate and alanine for primary human hepatocytes and hESC derived hepatocyte-like cells, cultivated either on $[U-^{13}C_6]$glucose or on $[U-^{13}C_5]$glutamine as substrates are depicted in Table 4.4.4 and Table 4.4.5, respectively.

As can be seen in Table 4.4.4 A, for primary human hepatocytes, cultured for 48 hours on $[U-^{13}C_6]$glucose, the enrichment in the *m3* fraction of newly secreted lactate for the

control cells was 40.7 %. This is due to the direct synthesis of [U-^{13}C$_3$]pyruvate from [U-^{13}C$_6$]glucose and its further conversion to [U-^{13}C$_3$]lactate via LDH (see Figure 4.4.19). Interestingly, approx. 50 % of the mass isotopomer showed no labeling (*m0*). Thus, this mass isotopomer fraction must have been synthesized from other carbon sources than [U-^{13}C$_6$]glucose, since lactate was not present in the culture medium and was exclusively produced. The *m1* and *m2* fractions were however enhanced over time, which suggests [U-^{13}C$_3$]pyruvate entering the TCA cycle and being cycled back to pyruvate, which was then further converted to lactate (*m1* and *m2* fraction). Interestingly, if the PHHs were exposed to diclofenac, the *m1* and *m2* fractions were enhanced compared to control. Thus one can surmise higher recycling activity of ME or PEPCK or increased TCA cycle activity. This latter observation can be further confirmed by the mass isotopomer fractions in lactate, if the PHHs were cultured on [U-^{13}C$_5$]glutamine. Here, even though the TCA flux to pyruvate, as seen in the *m3* fraction, was reduced with increasing diclofenac concentrations, the *m2* and *m1* fractions increased, suggesting multiple turns in the TCA cycle and thus increased TCA cycling.

For the hESC derived hepatocyte-like cells, similar trends as for PHHs were observed, when cultured on either [U-^{13}C$_6$]glucose or [U-^{13}C$_5$]glutamine as substrate (Table 4.4.5 A). Interestingly, approx. 86 % of the *m3* fraction of the lactate mass isotopomer were enriched for the control cells when cultured on [U-^{13}C$_6$]glucose. This means that the cells utilized the glucose mainly for lactate synthesis. This effect has been described as Warburg effect, meaning that the cells gain their energy mainly by glycolysis, even though it is not as effective as the TCA cycle and the oxidative phosphorylation. Here, only 10 % of the mass isotopomer showed no labeling (*m0*), which means that even though glucose was the main carbon source for lactate synthesis, also other carbon sources were utilized. The *m0* fraction was increased in presence of diclofenac, which suggests that other carbon sources were then increasingly utilized for lactate synthesis and that the glycolysis was either downregulated or the flux into the TCA cycle upregulated. Since the *m1* and *m2* fractions were enhanced for diclofenac exposed cells compared to control, here also higher recycling activity of malic enzyme or PEPCK or increased TCA cycle activity can be surmised.

Table 4.4.4: Time course of mass isotopomer fractions [%] and mass isotopomer concentrations [µmol/L] of extracellular **A)** lactate and **B)** alanine, for primary human hepatocytes cultivated in parallel with the isotopic substrates [U-$^{13}C_6$]glucose and [U-$^{13}C_5$]glutamine and exposed to diclofenac in three concentrations. Isotopomer distribution (*m0-m3*) is expressed in %.

A

		Mass Isotopomer Fraction [%] from [U-$^{13}C_6$]glucose					Mass Isotopomer Concentration [µmol/L] from [U-$^{13}C_6$]glucose				
Time [h]		0	12	24	35	48	0	12	24	35	48
Control [0 µM Diclofenac]	m0	96.1	59.7	58.6	56.0	50.5	0	0	307	495	801
	m1	3.3	2.9	3.4	3.7	4.0	0	0	18	33	63
	m2	0.3	2.7	3.6	3.9	4.8	0	0	19	34	76
	m3	0.2	34.7	34.4	36.4	40.7	0	0	180	322	646
ST1 [10 µM Diclofenac]	m0	96.1	55.0	56.0	53.5	53.8	0	0	193	406	764
	m1	3.3	2.7	3.4	3.6	4.0	0	0	12	27	57
	m2	0.3	2.6	3.7	4.1	4.7	0	0	13	31	67
	m3	0.2	39.8	36.9	38.9	37.5	0	0	127	295	533
ST3 [50 µM Diclofenac]	m0	96.1	46.1	52.0	52.5	46.8	0	0	0	402	485
	m1	3.3	2.1	2.7	3.2	4.1	0	0	0	25	43
	m2	0.3	2.3	2.8	3.6	5.7	0	0	0	28	59
	m3	0.2	49.5	42.5	40.6	43.5	0	0	0	311	451

		Mass Isotopomer Fraction [%] from [U-$^{13}C_5$]glutamine					Mass Isotopomer Concentration [µmol/L] from [U-$^{13}C_5$]glutamine				
Time [h]		0	12	24	35	48	0	12	24	35	48
Control [0 µM Diclofenac]	m0	96.1	87.7	85.0	84.6	82.0	0	0	445	748	1301
	m1	3.3	4.4	4.9	5.1	5.5	0	0	26	45	87
	m2	0.3	4.0	5.0	5.2	5.9	0	0	26	46	94
	m3	0.2	3.9	5.1	5.2	6.5	0	0	27	46	103
ST1 [10 µM Diclofenac]	m0	96.1	85.9	84.1	83.3	81.8	0	0	289	633	1162
	m1	3.3	4.7	5.0	5.2	5.5	0	0	17	39	78
	m2	0.3	4.9	5.3	5.4	5.8	0	0	18	41	82
	m3	0.2	4.5	5.7	6.1	6.8	0	0	20	46	97
ST3 [50 µM Diclofenac]	m0	96.1	89.6	86.4	86.9	83.6	0	0	0	666	867
	m1	3.3	4.1	4.6	4.6	5.4	0	0	0	35	56
	m2	0.3	3.1	4.2	3.9	5.2	0	0	0	30	54
	m3	0.2	3.2	4.7	4.6	5.8	0	0	0	35	60

B

		Mass Isotopomer Fraction [%] from [U-$^{13}C_6$]glucose					Mass Isotopomer Concentration [µmol/L] from [U-$^{13}C_6$]glucose				
Time [h]		0	12	24	35	48	0	12	24	35	48
Control [0 µM Diclofenac]	m0	96.1	82.5	78.7	73.2	60.3	1023	821	712	620	470
	m1	3.5	3.6	3.6	3.8	4.1	37	36	33	32	32
	m2	0.3	12.3	12.4	13.0	16.1	3	122	112	110	125
	m3	0.0	1.5	5.2	10.0	19.5	0	15	47	85	152
ST1 [10 µM Diclofenac]	m0	96.1	84.4	80.3	76.2	64.5	1023	865	794	737	550
	m1	3.5	3.5	3.6	3.7	4.1	37	36	36	36	35
	m2	0.3	10.8	12.0	13.0	16.8	3	111	119	126	143
	m3	0.0	1.3	4.2	7.0	14.7	0	13	42	68	125
ST3 [50 µM Diclofenac]	m0	96.1	83.9	83.0	76.4	66.0	1023	894	842	772	658
	m1	3.5	3.4	3.5	3.7	4.1	37	36	35	37	41
	m2	0.3	11.4	10.4	13.3	14.5	3	121	105	134	145
	m3	0.0	1.3	3.1	6.7	15.5	0	14	31	68	155

		Mass Isotopomer Fraction [%] from [U-$^{13}C_5$]glutamine					Mass Isotopomer Concentration [µmol/L] from [U-$^{13}C_5$]glutamine				
Time [h]		0	12	24	35	48	0	12	24	35	48
Control [0 µM Diclofenac]	m0	96.1	94.5	93.6	91.9	87.0	1023	940	847	779	678
	m1	3.5	4.2	4.2	4.5	5.4	37	42	38	38	42
	m2	0.3	0.6	1.1	1.8	3.6	3	6	10	15	28
	m3	0.0	0.6	1.1	1.8	4.0	0	6	10	15	31
ST1 [10 µM Diclofenac]	m0	96.1	94.3	92.4	90.7	86.6	1023	966	914	877	738
	m1	3.5	4.1	4.4	4.6	5.3	37	42	44	44	45
	m2	0.3	0.9	1.6	2.2	3.7	3	9	16	21	32
	m3	0.0	0.8	1.7	2.5	4.3	0	8	17	24	37
ST3 [50 µM Diclofenac]	m0	96.1	94.1	92.3	91.9	87.6	1023	1003	936	929	874
	m1	3.5	4.0	4.3	4.3	5.2	37	43	44	43	52
	m2	0.3	0.9	1.6	1.7	3.4	3	10	16	17	34
	m3	0.0	0.9	1.8	2.1	3.8	0	10	18	21	38

Table 4.4.5: Time course of mass isotopomer fractions [%] and mass isotopomer concentrations [µmol/L] of extracellular A) lactate and B) alanine, for hESC derived hepatocyte-like cells, cultivated in parallel with the isotopic substrates [U-^{13}C$_6$]glucose and [U-^{13}C$_5$]glutamine and exposed to diclofenac in three concentrations. Isotopomer distribution (*m0-m3*) is expressed in %.

A

		Mass Isotopomer Fraction [%] from [U-^{13}C$_6$]glucose					Mass Isotopomer Concentration [µmol/L] from [U-^{13}C$_6$]glucose				
	Time [h]	0	16	24	36	48	0	16	24	36	48
Control [0 µM Diclofenac]	*m0*	96.8	16.8	14.7	12.9	10.9	0	760	1210	1279	1530
	m1	2.7	1.1	1.0	1.0	0.9	0	52	81	95	132
	m2	0.1	2.1	2.1	2.3	2.5	0	97	176	228	352
	m3	0.3	79.9	82.2	83.8	85.7	0	3604	6777	8312	12085
ST1 [100 µM Diclofenac]	*m0*	91.7	22.0	18.3	16.2	15.0	0	442	405	654	757
	m1	3.2	1.7	1.5	1.4	1.4	0	34	34	56	72
	m2	1.5	2.6	2.7	2.6	2.8	0	52	60	106	142
	m3	3.6	73.7	77.5	79.7	80.8	0	1480	1717	3210	4090
ST2 [200 µM Diclofenac]	*m0*	91.7	26.2	20.9	19.5	17.9	0	561	689	833	938
	m1	3.2	1.7	1.6	1.6	1.6	0	37	51	68	83
	m2	1.5	2.4	2.5	2.6	2.7	0	50	82	113	143
	m3	3.6	69.7	75.0	76.2	77.8	0	1490	2470	3250	4080

		Mass Isotopomer Fraction [%] from [U-^{13}C$_5$]glutamine					Mass Isotopomer Concentration [µmol/L] from [U-^{13}C$_5$]glutamine				
	Time [h]	0	16	24	36	48	0	16	24	36	48
Control [0 µM Diclofenac]	*m0*	96.8	96.8	96.8	96.7	96.6	0	4369	7979	9587	13621
	m1	2.7	2.7	2.7	2.8	2.9	0	122	224	275	402
	m2	0.1	0.1	0.1	0.1	0.1	0	6	12	14	20
	m3	0.3	0.3	0.4	0.4	0.4	0	15	30	38	55
ST1 [100 µM Diclofenac]	*m0*	96.8	97.0	96.8	96.7	96.5	0	1948	2146	3892	4885
	m1	2.7	2.7	2.7	2.8	2.9	0	53	60	113	148
	m2	0.1	0.1	0.1	0.2	0.2	0	1	3	6	9
	m3	0.3	0.3	0.4	0.4	0.4	0	5	8	15	20
ST2 [200 µM Diclofenac]	*m0*	96.8	96.9	96.7	96.6	96.6	0	2072	3182	4117	5064
	m1	2.7	2.7	2.8	2.9	2.9	0	58	93	123	151
	m2	0.1	0.1	0.1	0.2	0.2	0	2	5	7	9
	m3	0.3	0.3	0.4	0.4	0.4	0	6	12	17	20

B

		Mass Isotopomer Fraction [%] from [U-^{13}C$_6$]glucose					Mass Isotopomer Concentration [µmol/L] from [U-^{13}C$_6$]glucose				
	Time [h]	0	16	24	36	48	0	16	24	36	48
Control [0 µM Diclofenac]	*m0*	96.5	75.4	62.4	48.4	38.0	887	790	709	544	455
	m1	2.6	2.3	2.1	1.9	1.8	24	24	24	21	21
	m2	0.7	2.9	3.4	3.5	3.3	7	31	39	39	40
	m3	0.1	19.3	32.1	46.3	57.0	1	203	365	520	682
ST1 [100 µM Diclofenac]	*m0*	96.6	81.9	78.7	69.3	64.4	887	819	820	747	765
	m1	2.7	2.8	2.7	2.7	2.7	25	28	28	29	32
	m2	0.7	2.0	1.8	2.5	2.7	6	20	19	27	32
	m3	0.1	13.3	16.7	25.5	30.2	1	133	174	275	358
ST2 [200 µM Diclofenac]	*m0*	96.6	83.5	79.1	73.9	67.0	887	820	804	800	783
	m1	2.7	2.8	2.8	2.9	2.9	25	28	28	31	34
	m2	0.7	1.5	1.9	2.3	2.6	6	14	20	25	30
	m3	0.1	12.2	16.2	20.9	27.5	1	119	164	226	322

		Mass Isotopomer Fraction [%] from [U-^{13}C$_5$]glutamine					Mass Isotopomer Concentration [µmol/L] from [U-^{13}C$_5$]glutamine				
	Time [h]	0	16	24	36	48	0	16	24	36	48
Control [0 µM Diclofenac]	*m0*	96.5	96.6	96.6	96.6	96.6	887	1013	1097	1086	1157
	m1	2.6	3.1	3.1	3.0	3.0	24	33	35	34	36
	m2	0.7	0.1	0.1	0.1	0.1	7	1	1	1	1
	m3	0.1	0.2	0.2	0.3	0.3	1	2	3	3	4
ST1 [100 µM Diclofenac]	*m0*	96.5	96.7	96.5	96.4	96.2	887	968	1006	1038	1143
	m1	2.6	3.0	2.9	2.9	3.0	24	30	30	32	36
	m2	0.7	0.1	0.3	0.3	0.2	7	1	3	3	3
	m3	0.1	0.2	0.3	0.4	0.5	1	2	3	4	6
ST2 [200 µM Diclofenac]	*m0*	96.5	96.9	96.6	96.3	96.2	887	951	982	1043	1123
	m1	2.6	2.8	2.9	3.1	3.0	24	27	30	33	35
	m2	0.7	0.1	0.2	0.2	0.2	7	1	2	2	3
	m3	0.1	0.2	0.3	0.4	0.6	1	2	3	4	6

As can be seen in Table 4.4.4 B, for primary human hepatocytes, cultured for 48 hours on [U-^{13}C$_6$]glucose, the enrichment in the *m3* fraction of alanine for the control cells was 19.5 %. Interestingly, here the *m2* fraction was 16.1 % even though the *m1* fraction was only 4.1 % after 48 hours of cultivation. Usually one assumes scrambling of succinate and fumarate to result in a 50/50 ratio of *m1* and *m2* isotopomer fractions in alanine, regardless if [U-^{13}C$_3$]pyruvate entered the TCA cycle via PDH or PC. However, this high *m2* fraction suggests that no scrambling occurs (see Figure 4.4.19), which would mean that [U-^{13}C$_3$]pyruvate which enters the TCA cycle by PDH complex can be only measured as *m0* or *m2* fraction in alanine. Similar, it could be seen for the SA002 control cells (Table 4.4.5 B), that the *m1* fraction remained constant and the *m2* fraction increased significantly over time.

Thus, these data suggest that for primary human hepatocytes and hESC derived hepatocyte-like cells no (complete) randomization of the symmetric citric acid cycle intermediates (succinate and fumarate) occurs. Orientation conserved enzyme-to-enzyme channelling has been previously published for perfused rat livers (Sherry et al., 1994), tumoural islet cells (Malaisse et al., 1996) and yeast (Sumegi et al., 1990).

In the second part of this chapter the metabolites glutamate, aspartate and proline, which are synthesized from TCA cycle intermediates, are analyzed to gain further insights into the pathways of primary human hepatocytes and hESC derived hepatocyte-like cells.

As depicted in Figure 4.4.20 A, if [U-^{13}C$_6$]glucose was used as substrate, several mass isotopomers can be formed for glutamate, proline and aspartate. Proline however is not depicted as a separate isotopomer, since it is synthesized from glutamate and has the same carbon backbone as such. If [U-^{13}C$_6$]glucose forms [U-^{13}C$_3$]pyruvate via glycolysis, pyruvate is transformed by PDH activity to [U-^{13}C$_2$]acetyl-CoA. In the first turn unlabeled oxaloacetate (OAA) condenses then with [U-^{13}C$_2$]acetyl-CoA to form [4,5-^{13}C$_2$]citrate which is metabolized in the TCA cycle to [4,5-^{13}C$_2$]α-ketoglutarate (precursor of glutamate and proline) and then, due to scrambling, to either [1,2-^{13}C$_2$]OAA or [3,4-^{13}C$_2$]OAA (precursor of aspartate). If [U-^{13}C$_3$]pyruvate is transformed by PC activity, [1,2,3-^{13}C$_3$]OAA is formed, which condenses with unlabed acetyl-CoA to [2,3,6-^{13}C$_3$]citrate or with [U-^{13}C$_2$]acetyl-CoA to [2,3,4,5,6-^{13}C$_5$]citrate which is metabolized in the TCA cycle to [2,3-^{13}C$_2$]α-ketoglutarate or [2,3,4,5-^{13}C$_4$]α-keto-glutarate (precursor of glutamate and proline) and then, due to scrambling, to either

[1,2-^{13}C$_2$]OAA, [3,4-^{13}C$_2$]OAA or [U-^{13}C$_4$]OAA (precursor of aspartate). From both reactions the flux from malate or OAA via malic enzyme or PEPCK and PK to pyruvate can result in *m3*, *m2*, or *m1* fractional enrichment in pyruvate.
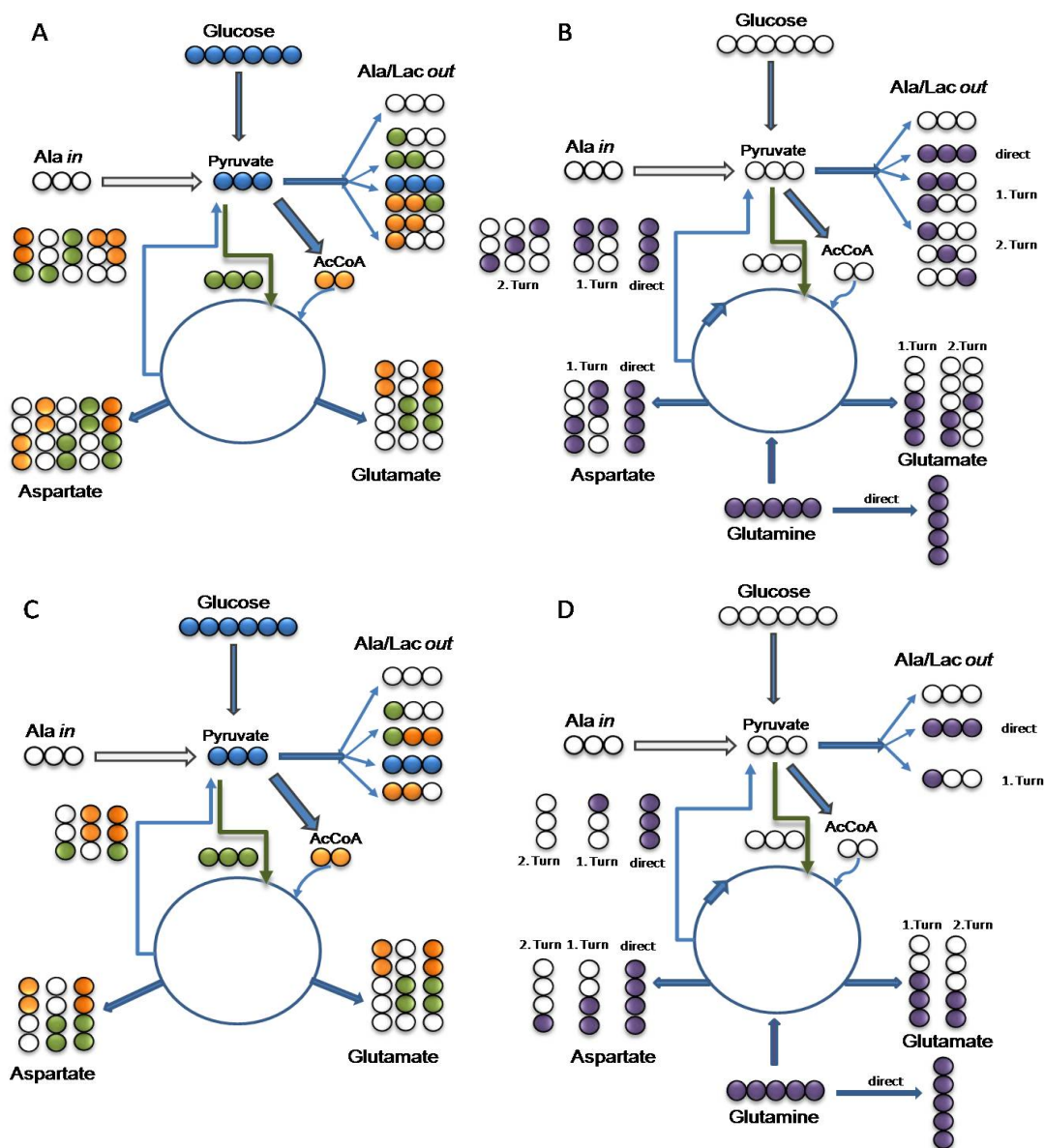
Figure 4.4.20:   Schematic depiction of labeled **(A)** glucose carbons (blue, orange and green circles) and **(B)** glutamine carbons (purple circles) metabolism by glycolysis and TCA cycle and their possible mass increase in alanine, lactate, glutamate and aspartate (indicated by filled circles). **A & B** depict the TCA cycle with scrambling of fumarate and succinate and **B & C** without scrambling. The blue arrow from pyruvate to acetyl-CoA (ACCoA) describes pyruvate dehydrogenase (PDH) and the green arrow pointing to the TCA cycle intermediate depicts the pyruvate carboxylase (PC) and the blue arrow from malate to pyruvate indicates malic enzyme and PEPCK activity.

The fractional enrichment in glutamate, proline and aspartate is depicted in Figure 4.4.20 B. [U-^{13}C$_5$]glutamine is deaminated to [U-^{13}C$_5$]glutamate and further to [U-^{13}C$_5$]α-ketoglutarate (TCA cycle) (Bak et al., 2008). This leads to [U-^{13}C$_4$]OAA, which in turn can produce [U-^{13}C$_4$]aspartate (*m4*). Oxaloacetate can then condense with non-labeled acetyl-CoA and form fourfold labeled citrate, which can then give rise to *m3* α-ketoglutarate and *m3* glutamate and *m3* proline, as well as *m2* aspartate, as depicted in Figure 4.4.20 B & D. The multiple turns of the TCA cycle for glutamate and aspartate as synthesized metabolites have been described by Bak et al. (2008).

The measured mass isotopomer fractions and mass isotopomer concentrations of glutamate, proline and aspartate for primary human hepatocytes and hESC derived hepatocyte-like cells, cultivated either on [U-^{13}C$_6$]glucose or on [U-^{13}C$_5$]glutamine as substrates are depicted in Table 4.4.6 and Table 4.4.7, respectively.

As can be seen for the glutamate and proline fractions, derived from glucose, the *m3* fraction was 39 % for primary human hepatocytes (Table 4.4.6 A & B). According to Furch et al. (2009) and Compte et al. (1997), [U-^{13}C$_3$]pyruvate is carboxylated to [1,2,3-^{13}C$_3$]OAA by PC or to [1,2,3-^{13}C$_3$]malate via malic enzyme. Then it is further converted via TCA cycle to the intermediate [2,3-^{13}C$_2$]α-ketoglutarate and thus to [2,3-^{13}C$_2$]glutamate (*m2*). Keeping in mind the reversibility of the fumarase and malate DH reactions, [2,3,4-^{13}C$_3$]OAA can be formed (Sherry et al., 2004), which would then form [1,2,3-^{13}C$_3$]α-ketoglutarate and result in [1,2,3-^{13}C$_3$]glutamate (*m3* fraction). However, if that would be the case, also a high *m2* fraction in proline and glutamate from [2,3-^{13}C$_2$]α-ketoglutarate would be expected, which is not the case regarding the collected data.

Table 4.4.6: Time course of mass isotopomer fractions [%] and mass isotopomer concentrations [μmol/L] of extracellular **A)** glutamate, **B)** proline and **C)** aspartate, for primary human hepatocytes cultivated in parallel with the isotopic substrates [U-$^{13}C_6$]glucose and [U-$^{13}C_5$]glutamine and exposed to diclofenac in three concentrations. Isotopomer distribution is expressed in %, i.e., the sum of the individual fractions equals 100 %.

A

	Time [h]	Mass Isotopomer Fraction [%] from [U-$^{13}C_6$]glucose					Mass Isotopomer Concentration [μmol/L] from [U-$^{13}C_6$]glucose				
		0	12	24	35	48	0	12	24	35	48
Control [0 μM Diclofenac]	m0	95.1	61.8	51.5	41.6	53.4	429	287	256	221	298
	m1	4.4	3.5	3.1	2.8	3.2	20	16	15	15	18
	m2	0.3	2.3	3.3	4.0	3.6	1	11	16	21	20
	m3	0.1	31.6	41.2	51.1	39.0	0	147	205	272	218
	m4	0.0	1.0	0.8	0.8	0.7	0	3	4	3	3
	m5	4.4	3.5	3.1	2.8	3.2	0	0	0	1	1
ST1 [10 μM Diclofenac]	m0	95.1	53.0	42.3	46.9	42.7	429	249	199	255	244
	m1	4.4	3.1	2.7	2.8	2.8	20	15	13	15	16
	m2	0.3	2.9	3.9	3.7	4.0	1	14	18	20	23
	m3	0.1	39.9	50.2	45.6	49.7	0	187	237	248	283
	m4	0.0	0.9	0.8	0.8	0.7	0	4	4	4	4
	m5	0.0	0.1	0.1	0.1	0.1	0	0	0	1	1
ST3 [50 μM Diclofenac]	m0	95.1	48.4	35.6	52.4	38.1	429	214	162	269	197
	m1	4.4	2.9	2.4	3.1	2.7	20	13	11	16	14
	m2	0.3	3.4	4.2	3.0	4.5	1	15	19	15	23
	m3	0.1	44.4	56.3	41.2	54.1	0	196	257	211	279
	m4	0.0	0.7	1.4	0.3	0.7	0	3	6	2	4
	m5	0.0	0.2	0.1	0.1	0.1	0	1	0	1	1

	Time [h]	Mass Isotopomer Fraction [%] from [U-$^{13}C_5$]glutamine					Mass Isotopomer Concentration [μmol/L] from [U-$^{13}C_5$]glutamine				
		0	12	24	35	48	0	12	24	35	48
Control [0 μM Diclofenac]	m0	95.1	88.5	85.0	80.6	74.1	429	411	422	429	413
	m1	4.4	4.4	4.3	4.1	4.0	20	20	21	22	22
	m2	0.3	0.6	0.7	1.1	1.5	1	3	3	6	8
	m3	0.1	2.1	2.4	3.5	3.2	0	10	12	19	18
	m4	0.0	0.5	0.7	0.9	1.4	0	2	3	5	8
	m5	0.0	3.9	7.0	9.8	15.7	0	18	35	52	88
ST1 [10 μM Diclofenac]	m0	95.1	83.2	80.4	76.7	69.2	429	390	379	417	395
	m1	4.4	4.5	4.5	4.3	4.2	20	21	21	23	24
	m2	0.3	5.1	3.5	4.1	5.9	1	24	16	22	34
	m3	0.1	2.4	2.7	3.0	3.5	0	11	13	16	20
	m4	0.0	0.6	0.9	1.1	1.5	0	3	4	6	9
	m5	0.0	4.3	7.9	10.8	15.7	0	20	37	59	90
ST3 [50 μM Diclofenac]	m0	95.1	88.1	82.3	82.4	73.7	429	389	376	423	381
	m1	4.4	4.6	4.5	4.3	4.5	20	20	21	22	23
	m2	0.3	0.6	3.0	0.9	3.7	1	3	14	5	19
	m3	0.1	2.7	3.0	3.3	3.7	0	12	14	17	19
	m4	0.0	0.5	0.8	0.8	1.4	0	2	4	4	7
	m5	0.0	3.6	6.4	8.3	13.1	0	16	29	43	68

B

	Time [h]	Mass Isotopomer Fraction [%] from [U-$^{13}C_6$]glucose					Mass Isotopomer Concentration [μmol/L] from [U-$^{13}C_6$]glucose				
		0	12	24	35	48	0	12	24	35	48
Control [0 μM Diclofenac]	m0	93.0	80.9	79.6	77.6	73.1	325	286	281	274	251
	m1	5.1	4.6	4.5	4.4	4.1	18	16	16	16	14
	m2	0.2	0.4	0.4	0.5	0.5	1	1	1	2	2
	m3	1.3	13.0	14.4	16.1	20.6	5	46	51	57	71
	m4	0.2	0.8	0.8	0.9	1.1	1	3	3	3	4
	m5	0.1	0.3	0.3	0.5	0.7	0	1	1	2	2
ST1 [10 μM Diclofenac]	m0	93.0	82.8	81.7	80.6	76.1	325	321	288	325	285
	m1	5.1	4.7	4.7	4.6	4.3	18	18	17	19	16
	m2	0.2	0.4	0.4	0.4	0.5	1	2	1	2	2
	m3	1.3	11.1	12.0	13.1	17.5	5	43	42	53	66
	m4	0.2	0.8	0.8	0.8	1.0	1	3	3	3	4
	m5	0.1	0.3	0.3	0.4	0.6	0	1	1	2	2

ST3 [50 µM Diclofenac]	m0	93.0	84.4	84.1	82.1	78.9	325	314	316	283	270
	m1	5.1	4.8	4.6	4.6	4.4	18	18	17	16	15
	m2	0.2	0.4	0.4	0.4	0.4	1	1	2	1	1
	m3	1.3	9.6	10.0	11.9	15.0	5	36	38	41	51
	m4	0.2	0.6	0.7	0.8	0.8	1	2	3	3	3
	m5	0.1	0.2	0.2	0.3	0.5	0	1	1	1	2

		Mass Isotopomer Fraction [%] from [U-^{13}C$_5$]glutamine					Mass Isotopomer Concentration [µmol/L] from [U-^{13}C$_5$]glutamine				
	Time [h]	0	12	24	35	48	0	12	24	35	48
Control [0 µM Diclofenac]	m0	93.0	81.3	83.8	82.1	80.5	325	288	295	290	276
	m1	5.1	4.7	4.7	4.7	4.5	18	17	17	17	15
	m2	0.2	0.5	0.4	0.4	0.4	1	2	1	1	1
	m3	1.3	12.5	10.2	11.7	13.2	5	44	36	41	45
	m4	0.2	0.8	0.6	0.7	0.8	1	3	2	2	3
	m5	0.1	0.3	0.3	0.4	0.7	0	1	1	1	2
ST1 [10 µM Diclofenac]	m0	93.0	84.3	83.0	82.2	81.6	325	327	292	332	306
	m1	5.1	4.8	4.7	4.6	4.7	18	19	17	19	18
	m2	0.2	0.4	0.4	0.4	0.4	1	2	1	2	1
	m3	1.3	9.7	10.9	11.6	11.9	5	38	38	47	45
	m4	0.2	0.6	0.6	0.7	0.7	1	2	2	3	3
	m5	0.1	0.3	0.4	0.5	0.7	0	1	1	2	3
ST3 [50 µM Diclofenac]	m0	93.0	84.9	83.8	84.1	82.4	325	316	315	290	282
	m1	5.1	4.7	4.6	4.6	4.6	18	17	17	16	16
	m2	0.2	0.3	0.3	0.3	0.4	1	1	1	1	1
	m3	1.3	9.3	10.3	10.1	11.4	5	35	39	35	39
	m4	0.2	0.5	0.6	0.6	0.7	1	2	2	2	2
	m5	0.1	0.2	0.3	0.3	0.5	0	1	1	1	2

C

		Mass Isotopomer Fraction [%] from [U-^{13}C$_6$]glucose					Mass Isotopomer Concentration [µmol/L] from [U-^{13}C$_6$]glucose				
	Time [h]	0	12	24	35	48	0	12	24	35	48
Control [0 µM Diclofenac]	m0	95.7	80.8	81.8	78.7	77.7	252	208	212	203	186
	m1	4.0	4.4	4.7	4.7	4.9	11	11	12	12	12
	m2	0.1	12.3	9.8	11.9	12.5	0	32	25	31	30
	m3	0.1	1.1	1.6	2.1	2.7	0	3	4	5	6
	m4	0.1	1.4	2.1	2.5	2.2	0	4	5	6	5
ST1 [10 µM Diclofenac]	m0	95.7	73.3	74.5	74.2	67.3	252	196	188	204	175
	m1	4.0	4.4	4.7	4.5	4.6	11	12	12	12	12
	m2	0.1	18.9	16.4	17.1	23.1	0	51	41	47	60
	m3	0.1	1.4	1.8	1.9	2.5	0	4	5	5	6
	m4	0.1	2.0	2.6	2.3	2.5	0	5	7	6	6
ST3 [50 µM Diclofenac]	m0	95.7	66.2	79.2	78.7	75.4	252	171	198	201	179
	m1	4.0	4.3	4.6	4.7	4.9	11	11	12	12	12
	m2	0.1	25.9	11.7	12.5	14.5	0	67	29	32	34
	m3	0.1	1.5	1.6	1.6	2.4	0	4	4	4	6
	m4	0.1	2.2	2.9	2.5	2.9	0	6	7	6	7

		Mass Isotopomer Fraction [%] from [U-^{13}C$_5$]glutamine					Mass Isotopomer Concentration [µmol/L] from [U-^{13}C$_5$]glutamine				
	Time [h]	0	12	24	35	48	0	12	24	35	48
Control [0 µM Diclofenac]	m0	95.7	92.5	92.3	90.2	88.6	252	239	239	233	212
	m1	4.0	4.6	4.4	5.2	4.7	11	12	11	13	11
	m2	0.1	0.8	0.9	1.3	1.9	0	2	2	3	5
	m3	0.1	1.1	1.2	1.7	2.5	0	3	3	4	6
	m4	0.1	1.0	1.1	1.6	2.3	0	3	3	4	6
ST1 [10 µM Diclofenac]	m0	95.7	91.6	89.8	88.6	86.5	252	245	226	243	225
	m1	4.0	4.9	5.1	5.1	5.3	11	13	13	14	14
	m2	0.1	0.9	1.4	1.7	2.3	0	2	4	5	6
	m3	0.1	1.3	1.9	2.3	2.9	0	3	5	6	8
	m4	0.1	1.3	1.9	2.3	3.0	0	3	5	6	8
ST3 [50 µM Diclofenac]	m0	95.7	91.6	90.2	90.1	87.2	252	237	226	230	207
	m1	4.0	4.7	5.0	4.7	5.5	11	12	13	12	13
	m2	0.1	1.0	1.3	1.3	2.0	0	3	3	3	5
	m3	0.1	1.3	1.7	1.9	2.6	0	3	4	5	6
	m4	0.1	1.3	1.8	2.0	2.7	0	3	5	5	6

Table 4.4.7: Time course of mass isotopomer fractions [%] and mass isotopomer concentrations [μmol/L] of extracellular **A)** glutamate, **B)** proline and **C)** aspartate, for hESC derived hepatocyte-like cells, cultivated in parallel with the isotopic substrates $[U-^{13}C_6]$glucose and $[U-^{13}C_5]$glutamine and exposed to diclofenac in three concentrations. Isotopomer distribution is expressed in %, i.e., the sum of the individual fractions equals 100 %.

A

		Mass Isotopomer Fraction [%] from $[U-^{13}C_6]$glucose					Mass Isotopomer Concentration [μmol/L] from $[U-^{13}C_6]$glucose				
Time [h]		0	16	24	36	48	0	16	24	36	48
Control [0 μM Diclofenac]	m0	95.7	57.0	57.9	43.3	31.3	357	96	54	30	9
	m1	4.0	3.5	3.9	4.1	4.0	15	6	4	3	1
	m2	0.1	8.0	11.4	18.8	21.8	0	13	11	13	6
	m3	0.1	26.3	18.0	16.9	31.7	0	44	17	12	9
	m4	0.1	4.6	7.3	13.9	6.5	0	8	7	10	2
	m5	0.0	0.6	1.5	3.0	4.6	0	1	1	2	1
ST1 [100 μM Diclofenac]	m0	95.7	34.1	18.0	9.3	8.1	357	55	9	2	2
	m1	4.0	2.3	1.8	1.4	1.4	15	4	1	0	0
	m2	0.1	6.5	9.3	8.9	8.4	0	11	5	2	2
	m3	0.1	50.5	63.3	69.9	71.2	0	82	33	17	16
	m4	0.1	6.0	6.8	9.4	9.9	0	10	4	2	2
	m5	0.0	0.6	0.8	1.2	1.0	0	1	0	0	0
ST2 [200 μM Diclofenac]	m0	95.7	21.6	12.3	7.0	7.5	357	32	6	2	2
	m1	4.0	1.7	1.5	1.2	1.3	15	3	1	0	0
	m2	0.1	5.4	7.5	7.8	8.7	0	8	4	2	2
	m3	0.1	65.7	70.9	75.3	74.8	0	99	37	20	19
	m4	0.1	5.4	6.9	7.8	6.7	0	8	4	2	2
	m5	0.0	0.2	0.9	0.8	1.0	0	0	0	0	0

		Mass Isotopomer Fraction [%] from $[U-^{13}C_5]$glutamine					Mass Isotopomer Concentration [μmol/L] from $[U-^{13}C_5]$glutamine				
Time [h]		0	16	24	36	48	0	16	24	36	48
Control [0 μM Diclofenac]	m0	95.9	81.7	69.5	37.8	57.0	358	137	65	26	16
	m1	3.1	3.9	5.6	4.9	7.1	12	7	5	3	2
	m2	0.2	1.3	6.3	44.6	15.0	1	2	6	31	4
	m3	0.7	3.3	6.2	6.6	7.1	3	5	6	5	2
	m4	0.0	1.3	2.7	2.4	3.8	0	2	3	2	1
	m5	0.0	8.6	9.8	3.7	9.9	0	14	9	3	3
ST1 [100 μM Diclofenac]	m0	95.7	86.3	46.0	63.4	30.8	357	140	24	16	7
	m1	4.0	4.6	4.4	7.6	4.1	15	8	2	2	1
	m2	0.1	0.5	33.2	19.2	53.7	0	1	18	5	12
	m3	0.1	2.0	5.9	4.9	6.3	0	3	3	1	1
	m4	0.1	0.8	3.0	2.0	2.4	0	1	2	1	1
	m5	0.0	5.8	7.6	2.8	2.7	0	9	4	1	1
ST2 [200 μM Diclofenac]	m0	95.7	85.2	79.3	69.7	49.9	357	128	41	18	13
	m1	4.0	4.4	3.5	6.4	5.4	15	7	2	2	1
	m2	0.1	0.2	1.1	2.3	26.5	0	0	1	1	7
	m3	0.1	2.1	5.2	9.5	8.4	0	3	3	2	2
	m4	0.1	0.9	2.0	3.5	2.8	0	1	1	1	1
	m5	0.0	7.1	9.0	8.6	7.1	0	11	5	2	2

B

		Mass Isotopomer Fraction [%] from $[U-^{13}C_6]$glucose					Mass Isotopomer Concentration [μmol/L] from $[U-^{13}C_6]$glucose				
Time [h]		0	16	24	36	48	0	16	24	36	48
Control [0 μM Diclofenac]	m0	93.5	87.8	85.8	80.9	78.9	321	323	353	356	378
	m1	5.1	4.7	4.8	4.8	4.8	17	17	20	21	23
	m2	0.3	4.5	5.3	7.7	8.3	1	16	22	34	40
	m3	0.7	1.7	2.3	3.0	3.2	2	6	9	13	16
	m4	0.3	0.9	1.2	2.3	2.9	1	3	5	10	14
	m5	0.1	0.5	0.7	1.4	1.8	0	2	3	6	9
ST1 [100 μM Diclofenac]	m0	93.1	87.5	84.2	79.5	78.6	320	341	349	369	358
	m1	5.1	5.1	5.2	5.1	5.2	18	20	21	24	23
	m2	0.3	4.3	6.2	7.9	7.8	1	17	26	37	36
	m3	1.0	1.7	2.1	3.1	3.3	3	6	9	14	15
	m4	0.3	1.0	1.6	2.8	3.1	1	4	6	13	14
	m5	0.2	0.5	0.7	1.6	2.0	1	2	3	7	9

ST2 [200 µM Diclofenac]	m0	93.1	88.5	86.1	83.0	80.6	320	307	315	340	364
	m1	5.1	5.2	5.1	5.3	5.3	18	18	19	21	24
	m2	0.3	3.8	5.0	6.3	7.3	1	13	18	26	33
	m3	1.0	1.3	2.0	2.5	2.9	3	5	7	10	13
	m4	0.3	0.8	1.3	1.9	2.5	1	3	5	8	11
	m5	0.2	0.3	0.6	1.0	1.3	1	1	2	4	6

		Mass Isotopomer Fraction [%] from [U-^{13}C$_5$]glutamine					Mass Isotopomer Concentration [µmol/L] from [U-^{13}C$_5$]glutamine				
	Time [h]	0	16	24	36	48	0	16	24	36	48
Control [0 µM Diclofenac]	m0	93.5	90.9	89.6	85.2	82.8	321	335	368	375	396
	m1	5.1	4.9	4.9	5.4	5.8	17	18	20	24	28
	m2	0.3	0.4	0.5	1.0	1.4	1	1	2	4	7
	m3	0.7	1.5	1.7	2.8	3.3	2	6	7	12	16
	m4	0.3	0.3	0.3	0.5	0.5	1	1	1	2	3
	m5	0.1	1.9	2.9	5.2	6.2	0	7	12	23	29
ST1 [100 µM Diclofenac]	m0	93.5	91.5	90.7	87.1	84.7	321	357	376	404	386
	m1	5.1	5.0	5.1	5.7	6.0	17	20	21	26	27
	m2	0.3	0.3	0.4	2.0	1.3	1	1	2	9	6
	m3	0.7	1.5	1.5	2.1	2.9	2	6	6	10	13
	m4	0.3	0.3	0.2	0.5	0.5	1	1	1	2	2
	m5	0.1	1.4	2.0	2.7	4.7	0	6	8	12	21
ST2 [200 µM Diclofenac]	m0	93.5	92.0	90.9	87.3	84.0	321	319	332	357	380
	m1	5.1	5.1	5.1	5.6	6.0	17	18	19	23	27
	m2	0.3	0.3	0.5	0.9	1.3	1	1	2	4	6
	m3	0.7	1.1	1.4	2.2	2.9	2	4	5	9	13
	m4	0.3	0.2	0.3	0.4	0.5	1	1	1	2	2
	m5	0.1	1.3	1.8	3.7	5.4	0	4	7	15	24

C

		Mass Isotopomer Fraction [%] from [U-^{13}C$_6$]glucose					Mass Isotopomer Concentration [µmol/L] from [U-^{13}C$_6$]glucose				
	Time [h]	0	16	24	36	48	0	16	24	36	48
Control [0 µM Diclofenac]	m0	95.7	62.3	56.9	46.1	36.2	197	18	11	8	5
	m1	4.0	9.6	8.5	5.1	7.2	9	3	2	1	1
	m2	0.1	4.2	2.9	1.9	2.6	2	1	1	0	0
	m3	0.1	16.7	27.7	44.9	51.0	2	5	5	8	7
	m4	0.1	7.2	4.0	2.0	3.1	1	2	1	0	0
ST1 [100 µM Diclofenac]	m0	95.7	72.1	70.2	62.8	54.6	198	20	10	9	8
	m1	4.0	6.7	7.2	7.1	9.1	10	2	1	1	1
	m2	0.1	3.0	2.5	2.9	4.3	3	1	0	0	1
	m3	0.1	13.0	15.6	21.8	24.5	2	4	2	3	3
	m4	0.1	5.1	4.5	5.3	7.4	1	1	1	1	1
ST2 [200 µM Diclofenac]	m0	95.7	61.8	63.8	58.9	55.0	198	17	9	9	8
	m1	4.0	10.5	8.4	9.4	10.2	10	3	1	1	2
	m2	0.1	5.2	4.9	5.5	5.5	3	1	1	1	1
	m3	0.1	11.6	14.3	16.9	20.7	2	3	2	2	3
	m4	0.1	10.9	8.6	9.4	8.6	1	3	1	1	1

		Mass Isotopomer Fraction [%] from [U-^{13}C$_5$]glutamine					Mass Isotopomer Concentration [µmol/L] from [U-^{13}C$_5$]glutamine				
	Time [h]	0	16	24	36	48	0	16	24	36	48
Control [0 µM Diclofenac]	m0	95.7	85.2	88.3	90.5	90.9	193	24	17	16	13
	m1	4.0	7.5	6.0	5.2	5.4	14	2	1	1	1
	m2	0.1	1.6	1.1	1.2	0.9	2	0	0	0	0
	m3	0.1	2.5	2.2	1.5	1.3	3	1	0	0	0
	m4	0.1	3.2	2.4	1.6	1.5	1	1	0	0	0
ST1 [100 µM Diclofenac]	m0	95.7	85.2	83.3	78.0	83.4	197	24	12	11	12
	m1	4.0	6.6	8.1	9.8	8.1	9	2	1	1	1
	m2	0.1	1.6	2.2	4.2	1.4	2	0	0	1	0
	m3	0.1	3.2	3.3	3.9	4.1	2	1	0	1	1
	m4	0.1	3.4	3.1	4.1	3.1	1	1	0	1	0
ST2 [200 µM Diclofenac]	m0	95.7	81.0	75.6	77.3	74.2	197	23	11	11	11
	m1	4.0	7.7	11.4	10.4	11.9	9	2	2	2	2
	m2	0.1	2.2	2.4	2.8	3.3	2	1	0	0	0
	m3	0.1	4.0	5.3	4.9	5.2	2	1	1	1	1
	m4	0.1	5.1	5.2	4.5	5.4	1	1	1	1	1

However, since PDH and PC are active in hepatocytes, and in addition pyruvate can be formed from OAA by malic enzyme or combined actions of PEPCK and pyruvate kinase, "pyruvate cycling" (OAA → pyruvate → OAA) and "pyruvate recycling" (OAA → pyruvate → Acetyl-CoA → → OAA) can occur (Lu et al., 2002; Sherry et al., 2004) and might be the cause for the high *m3* fractions observed. Pyruvate cycling and recycling are depicted in Figure 4.4.21.
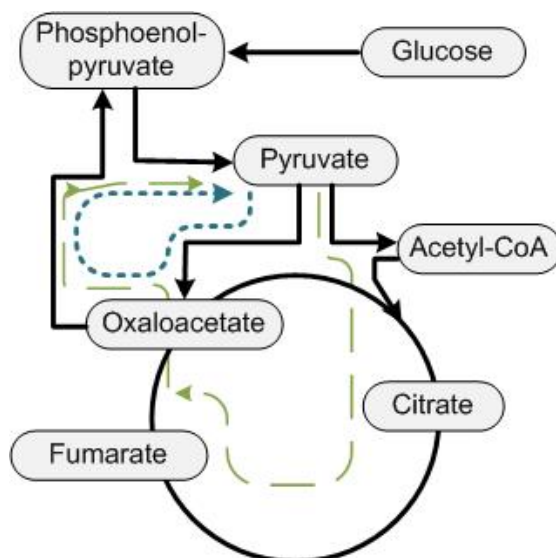
Figure 4.4.21: "Pyruvate cycling" and "pyruvate recycling" based on Sherry et al. (2004). The dotted line indicates "pyruvate cycling" and the dashed line "pyruvate recycling".

With the presence of pyruvate cycling and pyruvate recycling in primary human hepatocytes (Sherry et al., 2004), several possibilities for this high *m3* fraction in glutamate and proline exist and are discussed in the following (see also Figure 4.4.22), but with constraint for one full turn in the TCA cycle:

⇨ $^{13}CO_2$-fixation by pyruvate carboxylase (PC)
   o [U-$^{13}C_3$]pyruvate + $^{13}CO_2$ is transformed to [U-$^{13}C_4$]OAA via PC, which would be transformed to [1,2,3-$^{13}C_3$]α-ketoglutarate
      ⇨ This could, however only account for approx. 17 % of the *m3* fraction, since $^{13}CO_2$ was only abou 17 % (evaluated from the urea isotopomer mass fraction, data not shown)

⇨ No scrambling of succinate and fumarate

- o [1,2-^{13}C$_2$]OAA (formed from pyruvate recycling via PDH) condenses with [U-^{13}C$_2$]acetyl-CoA to form [3,4,5,6-^{13}C$_4$]citrate and then [3,4,5-^{13}C$_3$]α-ketoglutarate

- o [3,4-^{13}C$_2$]OAA (formed from pyruvate recycling via PC) condenses with [1-^{13}C$_1$]acetyl-CoA, which is recycled to pyruvate.

⇨ One turn in TCA cycle

- o [U-^{13}C$_2$]acetyl-CoA (PDH) condenses with [1,2,3-^{13}C$_3$]OAA, which forms [2,3,4,5,6-^{13}C$_5$]citrate and then [2,3,4,5-^{13}C$_4$]α-ketoglutarate, which is transformed to [U-^{13}C$_4$]OAA, which than can condense with non labeled acetyl-CoA to [1,2,3,6-^{13}C$_4$]citrate and then form [1,2,3-^{13}C$_3$]α-ketoglutarate

⇨ Reversibility of the fumarase and malate DH reaction

- o [U-^{13}C$_3$]pyruvate is carboxylated to [2,3,4-^{13}C$_3$]OAA, due to the reversibility of the fumarase reaction (Sherry et al., 2004), which would then form [1,2,3-^{13}C$_3$]α-ketoglutarate and result in [1,2,3-^{13}C$_3$]glutamate

It had been shown by Sherry et. al (2004), who fed ^{13}C-propionate as an anaplerotic substrate (supplies carbons to the TCA cycle via succinyl-CoA) that pyruvate cycling is very active in the liver. They estimated this cycling dependant on the PC activity to be 490 % higher than the TCA influx from pyruvate via PDH. Possibly, this can also explain, combined with the assumption of no scrambling of succinate and fumarate, the high *m3* fraction in glutamate and proline. In concordance with the high PC activity reported by Sherry et. al (2004), the *m2* fraction in asparate was also high. This can be explained by transformation of [1,2,3-^{13}C$_3$]α-ketoglutarate to [1,2-^{13}C$_2$]succinyl-CoA, which would then form [1,2-^{13}C$_2$]OAA and thus the *m2* fraction in aspartate.

Diclofenac treatment seemed to enhance the pyruvate cycling and thus the *m3* fraction in glutamate increased with increasing drug concentration. However, the *m3* fraction in proline and the *m2* fraction in aspartate decreased. This can be due to the fact that glutamate was net produced and aspartate and proline were net consumed in presence of diclofenac.
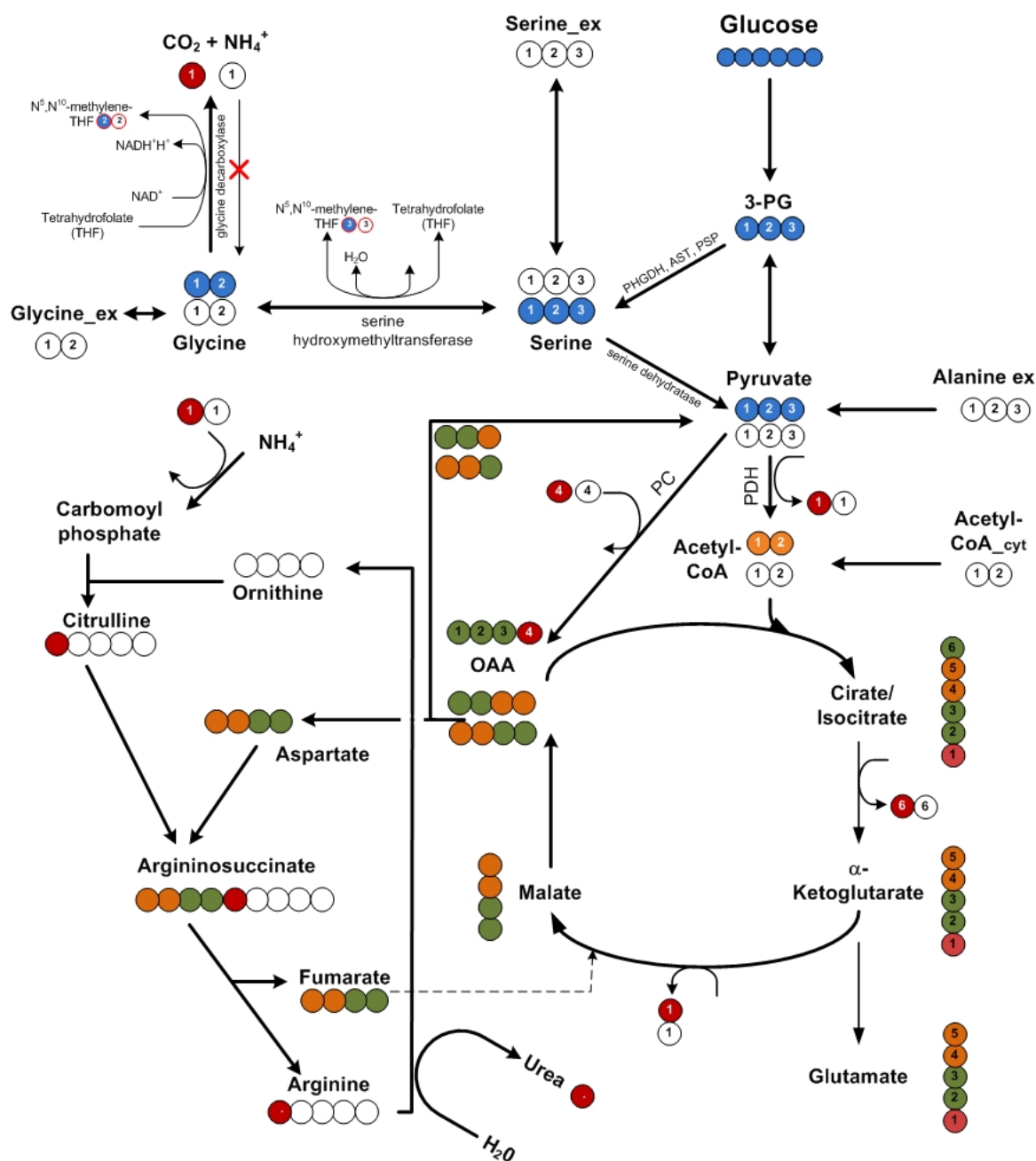
Figure 4.4.22: Schematic depiction of [U-^{13}C$_6$]glucose metabolism in hepatic cells. Labeled carbon atoms from [U-^{13}C$_6$]glucose are depicted as blue circles, labeled carbon atoms from [U-^{13}C$_3$]pyruvate in the TCA cycle (via pyruvate dehydrogenase (PDH) are depicted as orange circles, labeled carbon atoms from [U-^{13}C$_3$]pyruvate in the TCA cycle (via pyruvate carboxylase (PC) are depicted as green circles, labeled CO$_2$ as red circles and unlabeled carbon atoms as white circles.

[U-^{13}C$_5$]glutamate synthesis, derived from [U-^{13}C$_5$]glutamine via glutaminase, was detected over the test period. The measured *m5* fraction was 15.7 % after 48 hours of culture. If the glutaminase is located in the mitochondria, ^{13}C-labeled glutamine is

180

deaminated to fully labeled glutamate and further to $[U-^{13}C_5]\alpha$-ketoglutarate (Bak et al., 2008). This leads to uniformly labeled oxaloacetate, which in turn can give rise to fully labeled aspartate (*m4*). As seen in Table 4.4.6 uniformly labeled aspartate was detected only weakly (2.3 % after 48 hours of cultivation). This means, that this route was not important. $[U-^{13}C_4]$oxaloacetate can then condense with non-labeled acetyl-CoA and form fourfold labeled citrate, which can then give rise to *m3* α-ketoglutarate, *m3* glutamate and *m3* proline, as well as *m2* aspartate. Interestingly, $[U-^{13}C_5]$proline was very weakly produced, but *m3* proline very high (20.6 %, for control cells after 48 hours of cultivation). This would mean that the carbons of $[U-^{13}C_5]$glutamate are metabolized in the TCA cycle and only then proline was synthesized. The *m3* fraction of aspartate from glutamine derived carbons can only be formed, if labeled malate is transferred into the cytosol, where it is converted to pyruvate and re-enters the TCA cycle as acetyl-CoA which condenses with labeled oxaloacetate. This process is discussed as pyruvate re-cycling (Bak et al., 2007; Bak et al., 2008; Heart et al., 2009; Lu et al., 2002; Sherry et al., 2004; Stark et al., 2009). *m3* fraction enrichment (2.5 %) of aspartate from uniformly labeled glutamine carbons was identified, as shown in Table 4.4.6.

Diclofenac treatment seemed to decrease the direct synthesis of $[U-^{13}C_5]$glutamate from $[U-^{13}C_5]$glutamine with increasing concentration (Figure 4.4.6 A). However, the *m1*, *m2* and *m3* fractions were increased in the mass isotopomer fraction, when exposed to diclofenac, indicating increased cycling in the TCA cycle. In addition, the *m3* proline fraction was also decreased, when exposed to diclofenac. Interestingly, for the synthesized aspartate, increased cycling in the TCA cycle could be also found, as apparent in the increase in the *m1*, *m2*, *m3* and *m4* fractions, if the cells were exposed to increasing concentrations of diclofenac over time.

For the SA002 cells the fractional enrichment of carbons derived from fully labeled glucose in glutamate, proline and aspartate (Table 4.4.7) resulted in multiple enrichment fractions due to multiple turns in the TCA cycle, pyruvate recycling and amino acids entering the TCA cycle, as discussed previously for primary human hepatocytes.

However, enrichment from $[U-^{13}C_5]$glutamine in these TCA cycle outputs yielded some interesting new insights. Proline enrichment predominantly took place in the *m3* and *m5* fraction, indicating synthesis from the full TCA turn of glutamine carbons ($[1,2,3-^{13}C_3]\alpha$-

ketoglutarate) and transamination to glutamate, followed by synthesis of proline (*m3*) and direct synthesis from glutamate (*m5*), respectively. This is in contrast to PHHs, since the *m5* fraction in proline was not synthesized there.

Diclofenac treatment cannot be discussed for the glutamate and aspartate mass isotopomer fractions, since both metabolites were mostly depleted from the culture supernatant after 24 hours of culturing hESC derived hepatocyte-like cells.

4.4.2.5 Serine and glycine metabolism

To further investigate the interconnection of serine and glycine metabolism, their extracellular metabolites were analyzed for primary human hepatocytes and hESC derived hepatocyte-like cells, cultured on either [U-$^{13}C_6$]glucose or [U-$^{13}C_5$]glutamine, in form of mass isotopomer fractions [%] and mass isotopomer concentrations [μmol/L]. In addition, possible labeled metabolite formations were considered based on biochemistry.

In Figure 4.4.23, a schematic depiction of the metabolic pathways for serine and glycine metabolism is shown. Briefly, in mammalian cells, serine is derived from the media or is synthesized via the glycolytic intermediate 3-phosphoglycerate (3PG), which is then dehydrogenated to 3-phosphopyruvate, followed by transamination to 3-phosphoserine and final conversion to serine. In this process, the carbon skeleton of 3PG remains unaltered. Serine plays a central role in intermediary metabolism for the formation of proteins, as well is contributor to phospholipid or sphingolipid biosynthesis. Furthermore, serine is the primary source of glycine (Cook, 2000), which is the precursor of biosynthetic pathways for creatine, purines, bile acids, hemoglobin and glutathione synthesis. In addition, pyruvate can be formed from serine, via the enzyme pyruvate dehydratase. The reversible interconversion of serine and glycine is catalyzed by serine hydroxymethyltransferase (SHMT). Conversion of serine to glycine results in the removal of the C3 of serine and the formation of 5,10-methylenetetrahydrofolate from tetrahydrofolate (THF), which can be used in folate-dependent one-carbon metabolism or oxidized to CO_2 via glycine decarboxylase (Berg et al., 2003; Cook, 2000; Schlupen et al., 2003). In addition, glycine can also be synthesized from threonine via threonine aldolase and from glyoxylate via glyoxylate aminotransferase. Both glyoxylate aminotransferase and serine hydroxymethyltransferase are active in the human liver (Genolet et al., 2005; Nagata et al., 2009; Xue et al., 1999).
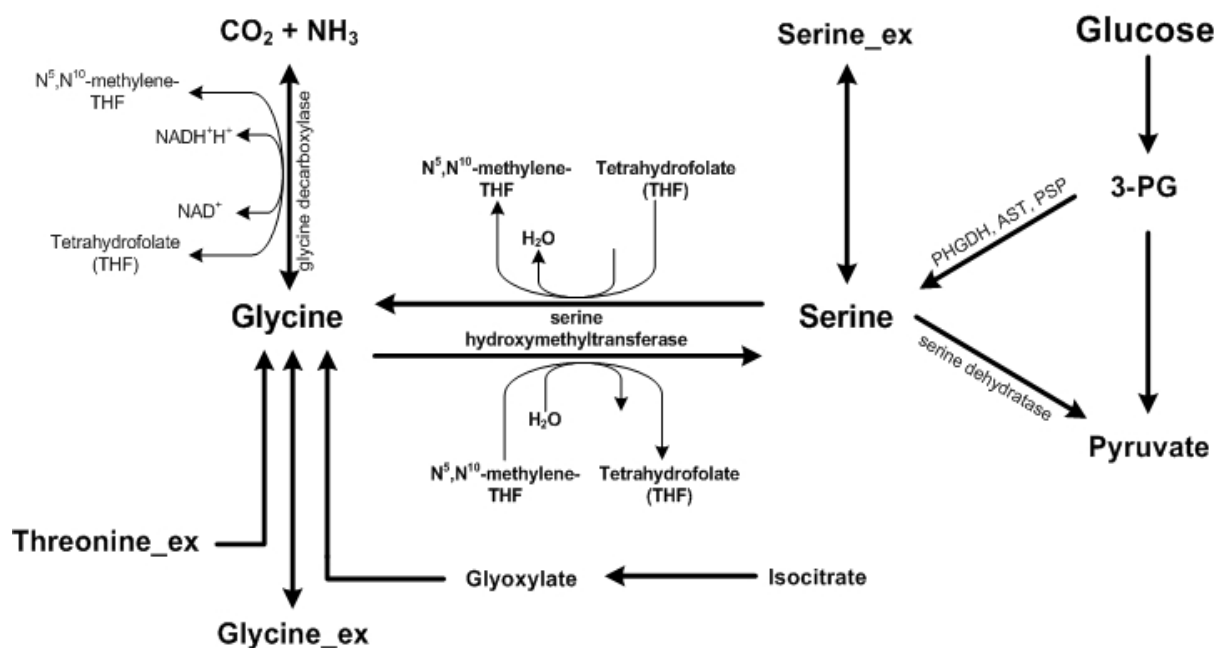
Figure 4.4.23: Schematic serine and glycine metabolic pathways of mammalian cells based on Deshpande (2007) and Schlupen et. al. (2003). Abbreviations used: PDGDH phosphoglycerate dehydrogenase, AST aminotransferase, PSP phosphoserine phosphatase. The subscript "ex" indicates extracellular metabolites.

If $[U-^{13}C_6]$glucose or $[U-^{13}C_5]$glutamine are used as substrates several mass isotopomers can be formed for serine and glycine regarding the metabolic pathways glycolysis, TCA cycle, amino acid degradation and glyoxylate cycle (Figure 4.4.24 A and B). Contrary to the model depicted in Figure 4.4.23 for this mass isotopomer model the glycine cleavage system (GCS) was assumed to be unidirectional (glycine degradation to CO_2 and NH_3) for one-carbon units production and threonine degradation was considered to be negligible, since it has been shown by House et al. (2001) that presence of 0.3 mM glycine in the culture supernatant inhibits threonine oxidation. In our study the media contained more than 0.6 mM glycine and it was observed for primary human hepatocytes and hESC derived-hepatocyte-like cells that threonine was not taken up from the culture medium (see Figure 4.4.2 and Figure 4.4.3).
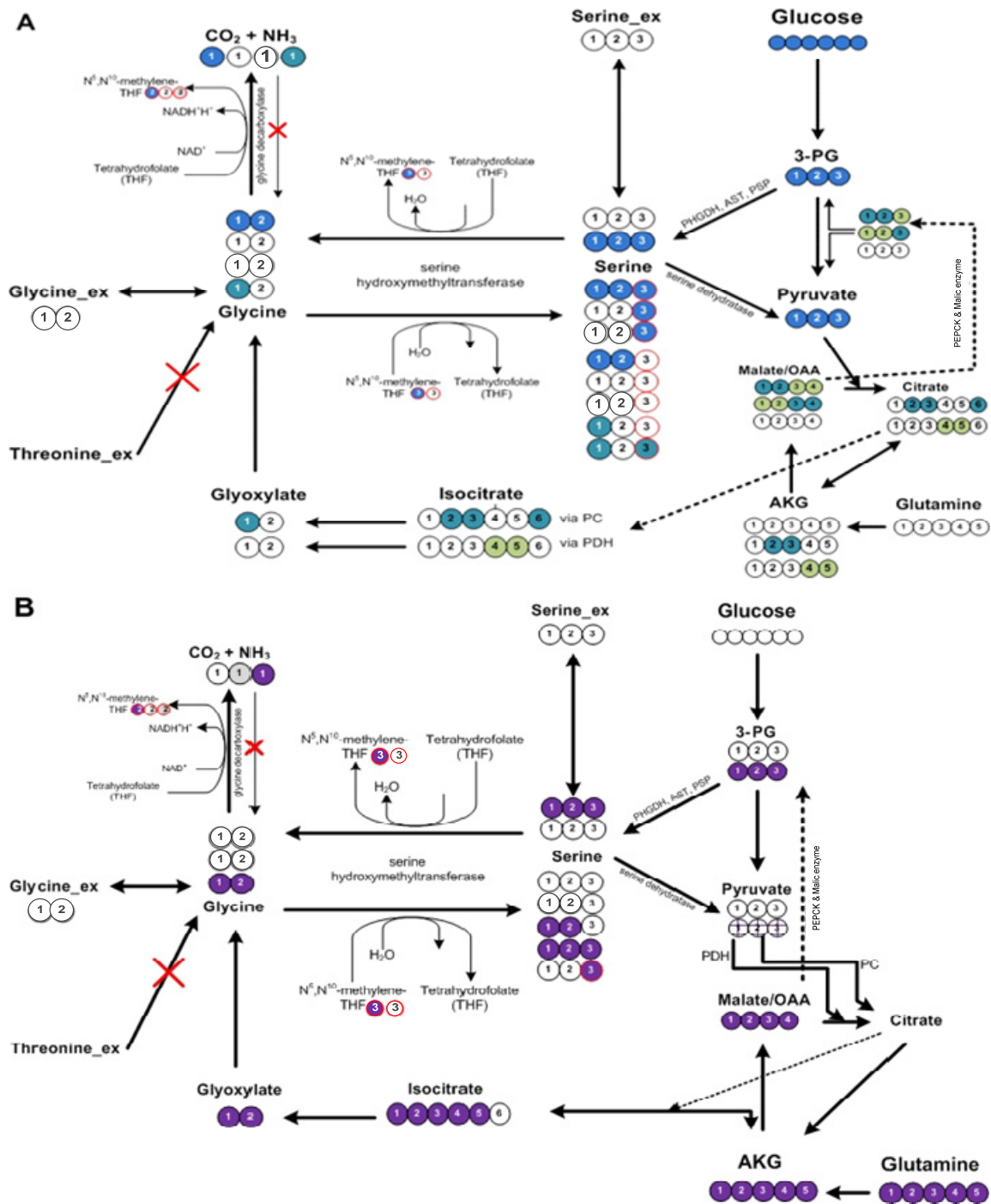
Figure 4.4.24: Schematic depiction of serine and glycine metabolic pathways. Possible formations of isotopomers are depicted for metabolites in hepatocytes, incubated with **A)** [U-^{13}C$_6$]glucose (indicated by filled blue/green circles) and **B)** [U-^{13}C$_5$]glutamine (indicated by filled purple circles) as substrates. The checked circles in pyruvate indicate all possible mass isotopomers shown for serine and 3-PG. Abbreviations: 3-PG 3-phosphoglycerate, OAA oxaloacetate, AKG α-ketoglutarate, PHGDH 3-phosphoglycerate dehydrogenase, AST aminotransaminase, PSP 3-phospho-serine phosphatase. The subscript "ex" indicates extracellular metabolites.

184

As can be seen in Figure 4.4.24 A, if [U-^{13}C$_6$]glucose is supplied as the isotopic substrate, [U-^{13}C$_3$]serine and [U-^{13}C$_2$]glycine can be formed. [U-^{13}C$_3$]serine can also be formed, if [U-^{13}C$_2$]glycine combines with a ^{13}C from THF which was released in the forward reaction of SHMT. For simplification, the reaction from serine to glycine is from here on designated as SHMT$_1$ and the back reaction as SHMT$_2$. In extracellular serine, 7.1 % and 14.9 % could be found fully labeled (*m3*) for the control cultivations of primary human hepatocytes and hESC derived-hepatocyte-like cells, cultivated for 48 hours, respectively (see Table 4.4.8 and Table 4.4.9). If the cells were exposed to increasing concentrations of diclofenac, this mass isotopomer enrichment of the extracellular serine decreased for both cell types. For primary human hepatocytes and hESC derived-hepatocyte-like cells cultivated for 48 hours the *m2* fraction in glycine was determined to be 7.2 % and 3.0 %, respectively. Glycine is formed from serine via SHMT$_1$. While the *m2* fraction in PHHs was not altered by diclofenac exposure, for the hESC derived-hepatocyte-like cells the *m2* fraction decreased with increasing diclofenac concentrations. Thus, glycine was further decarboxylated.

In extracellular serine, 7.3 % and 5.8 % could be found as *m2* fraction for the control cultivations of primary human hepatocytes and hESC derived-hepatocyte-like cells, cultivated for 48 hours, respectively (see Table 4.4.8 and Table 4.4.9). This can be explained by SHMT$_2$ activity from fully labeled glycine (*m2*), gluconeogenesis (pyruvate → Acetyl-CoA → Fumarate (no scrambling) → OAA → 3-PG → serine) and glyoxylate metabolism, where [1-^{13}C$_1$]glycine condenses with ^{13}C via SHMT$_2$ activity. Interestingly, for both cell types the *m2* fraction in serine was higher than the *m2* fraction in glycine. Thus, probably gluconeogenesis was active and the cause for the *m2* fraction in serine. However, if the cells were exposed to increasing concentrations of diclofenac, the *m2* mass isotopomer enrichment decreased for both cell types.

On [U-^{13}C$_6$]glucose the *m1* fraction for extracellular serine was found to be 18.9 % and 17.6 % for the control cultivations of primary human hepatocytes and hESC derived-hepatocyte-like cells after 48 hours. Interestingly, the *m1* fraction in glycine was increased by only 1 % for primary human hepatocytes. This high *m1* fraction in serine can thus be explained by pyruvate cycling and gluconeogenic activity of the cells (Figure 4.4.24 A), whereby only [3-^{13}C$_1$]serine can be formed here.

Table 4.4.8: Time course of mass isotopomer fractions [%] and mass isotopomer concentrations [μmol/L] of extracellular **A)** serine and **B)** glycine, for primary human hepatocytes cultivated in parallel with the isotopic substrates [U-$^{13}C_6$]glucose and [U-$^{13}C_5$]glutamine and exposed to diclofenac in three concentrations. Isotopomer distribution is expressed in %, i.e., the sum of the individual fractions equals 100 %.

A

	Time [h]	Mass Isotopomer Fraction [%] from [U-$^{13}C_6$]glucose					Mass Isotopomer Concentration [μmol/L] from [U-$^{13}C_6$]glucose				
		0	12	24	35	48	0	12	24	35	48
Control [0 μM Diclofenac]	m0	96.8	90.9	83.8	77.4	66.7	116	116	110	106	90
	m1	3.1	6.0	9.8	13.1	18.9	4	8	13	18	26
	m2	0.0	1.5	3.4	5.0	7.3	0	2	4	7	10
	m3	0.1	1.6	3.0	4.5	7.1	0	2	4	6	10
ST1 [10 μM Diclofenac]	m0	96.8	91.8	85.1	81.0	69.8	116	117	106	112	94
	m1	3.1	5.4	8.8	11.1	17.4	4	7	11	15	24
	m2	0.0	1.5	3.2	4.1	6.9	0	2	4	6	9
	m3	0.1	1.3	2.9	3.9	6.0	0	2	4	5	8
ST3 [50 μM Diclofenac]	m0	96.8	92.7	89.2	83.4	72.0	116	110	107	108	90
	m1	3.1	5.1	7.1	10.1	15.8	4	6	9	13	20
	m2	0.0	1.1	2.0	3.5	6.1	0	1	2	5	8
	m3	0.1	1.1	1.7	3.0	6.1	0	1	2	4	8
		Mass Isotopomer Fraction [%] from [U-$^{13}C_5$]glutamine					Mass Isotopomer Concentration [μmol/L] from [U-$^{13}C_5$]glutamine				
	Time [h]	0	12	24	35	48	0	12	24	35	48
Control [0 μM Diclofenac]	m0	96.8	90.9	89.8	85.9	82.2	116	116	118	117	111
	m1	3.1	6.9	7.8	10.6	13.0	4	9	10	14	18
	m2	0.0	1.0	1.5	2.4	3.2	0	1	2	3	4
	m3	0.1	1.1	0.9	1.1	1.5	0	1	1	2	2
ST1 [10 μM Diclofenac]	m0	96.8	90.7	89.0	86.8	83.6	116	116	111	121	113
	m1	3.1	7.3	8.4	9.9	12.1	4	9	10	14	16
	m2	0.0	1.2	1.6	2.1	2.9	0	2	2	3	4
	m3	0.1	0.8	1.0	1.2	1.4	0	1	1	2	2
ST3 [50 μM Diclofenac]	m0	96.8	92.2	90.1	89.8	85.0	116	109	108	116	106
	m1	3.1	6.5	7.8	8.0	11.3	4	8	9	10	14
	m2	0.0	0.7	1.3	1.4	2.5	0	1	2	2	3
	m3	0.1	0.6	0.8	0.9	1.2	0	1	1	1	1

B

	Time [h]	Mass Isotopomer Fraction [%] from [U-$^{13}C_6$]glucose					Mass Isotopomer Concentration [μmol/L] from [U-$^{13}C_6$]glucose				
		0	12	24	35	48	0	12	24	35	48
Control [0 μM Diclofenac]	m0	97.8	92.6	92.2	91.4	89.3	656	637	609	586	521
	m1	2.1	2.7	2.8	3.0	3.5	14	19	18	19	20
	m2	0.1	4.7	5.0	5.7	7.2	1	32	33	37	42
ST1 [10 μM Diclofenac]	m0	97.8	92.7	92.4	91.6	89.5	656	635	587	620	553
	m1	2.1	2.6	2.7	2.9	3.5	14	18	17	20	22
	m2	0.1	4.7	4.9	5.5	7.0	1	32	31	37	43
ST3 [50 μM Diclofenac]	m0	97.8	92.2	92.1	90.8	89.6	656	625	615	601	561
	m1	2.1	2.6	2.6	3.0	3.1	14	18	17	20	19
	m2	0.1	5.2	5.3	6.2	7.2	1	35	35	41	45
		Mass Isotopomer Fraction [%] from [U-$^{13}C_5$]glutamine					Mass Isotopomer Concentration [μmol/L] from [U-$^{13}C_5$]glutamine				
	Time [h]	0	12	24	35	48	0	12	24	35	48
Control [0 μM Diclofenac]	m0	97.8	96.5	96.8	96.4	95.4	656	664	639	618	557
	m1	2.1	2.7	2.6	2.9	3.5	14	19	17	19	20
	m2	0.1	0.9	0.5	0.7	1.1	1	6	3	4	6
ST1 [10 μM Diclofenac]	m0	97.8	96.9	96.9	96.5	95.9	656	663	616	654	593
	m1	2.1	2.6	2.6	2.8	3.2	14	18	17	19	20
	m2	0.1	0.5	0.6	0.7	0.9	1	3	4	5	6
ST3 [50 μM Diclofenac]	m0	97.8	97.1	96.9	96.7	96.3	656	658	647	640	603
	m1	2.1	2.5	2.6	2.7	3.0	14	17	17	18	19
	m2	0.1	0.4	0.5	0.5	0.7	1	3	3	3	4

Table 4.4.9: Time course of mass isotopomer fractions [%] and mass isotopomer concentrations [µmol/L] of extracellular **A)** serine and **B)** glycine, for hESC derived hepatocyte-like cells, cultivated in parallel with the isotopic substrates [U-^{13}C$_6$]glucose and [U-^{13}C$_5$]glutamine and exposed to diclofenac in three concentrations. Isotopomer distribution is expressed in %, i.e., the sum of the individual fractions equals 100 %.

A

	Time [h]	Mass Isotopomer Fraction [%] from [U-^{13}C$_6$]glucose					Mass Isotopomer Concentration [µmol/L] from [U-^{13}C$_6$]glucose				
		0	16	24	36	48	0	16	24	36	48
Control [0 µM Diclofenac]	m0	95.9	81.8	75.6	66.3	61.8	106	84	76	56	52
	m1	3.1	7.6	10.2	14.2	17.6	3	8	10	12	15
	m2	0.2	2.2	3.4	4.5	5.8	0	2	3	4	5
	m3	0.7	8.4	10.8	14.9	14.9	1	9	11	13	13
ST1 [100 µM Diclofenac]	m0	95.9	93.4	92.5	89.5	88.0	106	84	81	72	75
	m1	3.2	3.8	4.3	5.6	6.3	4	3	4	5	5
	m2	0.0	0.6	0.7	1.2	1.4	0	1	1	1	1
	m3	0.8	2.1	2.5	3.7	4.3	1	2	2	3	4
ST2 [200 µM Diclofenac]	m0	95.9	93.4	92.6	90.9	88.7	106	86	79	80	106
	m1	3.2	4.2	4.4	5.3	6.1	4	4	4	5	4
	m2	0.0	0.7	0.8	1.0	1.4	0	1	1	1	0
	m3	0.8	1.8	2.2	2.9	3.8	1	2	2	3	1
	Time [h]	Mass Isotopomer Fraction [%] from [U-^{13}C$_5$]glutamine					Mass Isotopomer Concentration [µmol/L] from [U-^{13}C$_5$]glutamine				
		0	16	24	36	48	0	16	24	36	48
Control [0 µM Diclofenac]	m0	95.9	96.0	96.0	96.1	96.1	106	98	97	80	81
	m1	3.1	3.5	3.4	3.5	3.4	3	4	3	3	3
	m2	0.2	0.2	0.2	0.2	0.2	0	0	0	0	0
	m3	0.7	0.3	0.4	0.2	0.3	1	0	0	0	0
ST1 [100 µM Diclofenac]	m0	95.9	96.0	95.2	95.6	96.0	106	87	83	77	81
	m1	3.1	3.5	4.0	3.6	3.5	3	3	3	3	3
	m2	0.2	0.2	0.4	0.4	0.2	0	0	0	0	0
	m3	0.7	0.3	0.5	0.3	0.3	1	0	0	0	0
ST2 [200 µM Diclofenac]	m0	95.9	96.0	96.3	96.0	96.1	106	88	82	84	88
	m1	3.1	3.5	3.3	3.5	3.5	3	3	3	3	3
	m2	0.2	0.2	0.1	0.2	0.2	0	0	0	0	0
	m3	0.7	0.3	0.3	0.2	0.2	1	0	0	0	0

B

	Time [h]	Mass Isotopomer Fraction [%] from [U-^{13}C$_6$]glucose					Mass Isotopomer Concentration [µmol/L] from [U-^{13}C$_6$]glucose				
		0	16	24	36	48	0	16	24	36	48
Control [0 µM Diclofenac]	m0	97.9	97.1	96.6	95.3	94.9	600	553	542	499	492
	m1	2.0	1.9	2.0	2.0	2.1	12	11	11	11	11
	m2	0.2	1.0	1.5	2.6	3.0	1	6	8	14	16
ST1 [100 µM Diclofenac]	m0	97.9	97.5	97.5	97.3	97.2	600	524	528	517	550
	m1	2.0	2.1	2.0	2.0	2.1	12	11	11	11	12
	m2	0.2	0.4	0.5	0.7	0.7	1	2	3	4	4
ST2 [200 µM Diclofenac]	m0	97.9	97.6	97.5	97.4	97.2	600	548	532	547	567
	m1	2.0	2.0	2.0	2.0	2.0	12	11	11	11	12
	m2	0.2	0.4	0.5	0.6	0.8	1	2	3	4	5
	Time [h]	Mass Isotopomer Fraction [%] from [U-^{13}C$_5$]glutamine					Mass Isotopomer Concentration [µmol/L] from [U-^{13}C$_5$]glutamine				
		0	16	24	36	48	0	16	24	36	48
Control [0 µM Diclofenac]	m0	97.9	97.6	97.6	97.7	97.9	600	556	548	511	508
	m1	2.0	2.0	2.0	2.0	1.9	12	11	11	11	10
	m2	0.2	0.4	0.3	0.3	0.3	1	2	2	2	1
ST1 [100 µM Diclofenac]	m0	97.9	97.6	97.5	97.5	97.8	600	525	528	518	553
	m1	2.0	2.0	2.0	2.1	1.9	12	11	11	11	11
	m2	0.2	0.4	0.6	0.4	0.3	1	2	3	2	2
ST2 [200 µM Diclofenac]	m0	97.9	97.7	97.7	97.7	97.7	600	548	532	549	570
	m1	2.0	2.0	2.0	2.0	2.0	12	11	11	11	12
	m2	0.2	0.4	0.3	0.3	0.3	1	2	2	2	2

Hereby, $[U-^{13}C_3]$pyruvate enters the TCA cycle via PC and forms with non-labeled acetyl-CoA $[2,3,6-^{13}C_3]$citrate, which is transformed to $[1,2-^{13}C_2]$OAA (no scrambling) and then to $[3-^{13}C_1]$3PG and finally to $[3-^{13}C_1]$serine and non-labeled glycine. In chapter 4.4.2.4 it has been previously shown that pyruvate cycling is very active and that probably no scrambling occurs. Interestingly, if the cells were exposed to increasing concentrations of diclofenac, the *m1* mass isotopomer enrichment decreased for both cell types. Thus gluconeogenesis was possibly reduced. However, other explanations for the high *m1* fraction in serine also exist; unlabeled glycine (taken up from the media) can form with ^{13}C-MTHF $[3-^{13}C_1]$serine or $[1-^{13}C_1]$glycine (from glyoxylate metabolism) forms with ^{12}C-MTHF $[1-^{13}C_1]$serine.

As can be seen in Figure 4.4.24 B, if $[U-^{13}C_5]$glutamine is supplied as the isotopic substrate, $[U-^{13}C_3]$serine and $[U-^{13}C_2]$glycine can be formed via gluconeogenesis. $[U-^{13}C_2]$glycine, however, can also be formed via reversible isocitrate dehydrogenase activity, followed by glyoxylate pathway. However, $[U-^{13}C_5]$glutamine resulted only in 1.5 % *m3* serine and 1.1 % *m2* glycine for primary human hepatocytes and only in 0.3 % *m3* serine and 0.3 % *m2* glycine for hESC derived-hepatocyte-like cells. Interestingly, the *m1* serine fraction for control cultures of primary human hepatocytes resulted in a 13.0 % fraction after 48 hours of culture. This can most likely be explained by gluconeogenesis. Hereby, $[U-^{13}C_5]$glutamine is metabolized in the TCA cycle to $[U-^{13}C_4]$OAA and forms $[1,2,3-^{13}C_3]$citrate with non-labeled acetyl-CoA, which is transformed to $[1,2-^{13}C_2]$OAA (no scrambling) and then to $[3-^{13}C_1]$3PG. Finally, from this $[3-^{13}C_1]$serine (*m1*) and non-labeled glycine can be formed via $SHMT_1$. Yet, the gluconeogenic activity was here also reduced, if the cells were exposed to diclofenac.

4.4.2.6 Pentose phosphate pathway

The pentose phosphate pathway (PPP) has two major functions; it is a source for biosynthetic carbon skeletons (e.g. supply of ribose 5-phosphate for nucleotide synthesis) and contributes to the redox potential in the cells by producing reducing equivalents in form of NADPH (Berg et al., 2003; Browne et al., 1999).

The reactions of the pentose phosphate pathway (Eq. 4.20 - Eq. 4.23) and the glycolysis (Eq. 4.24 - Eq. 4.26) with the enzymes involved can be described as followes:

188

PPP:	$G6P \rightarrow R5P + CO_2$	[Eq. 4.20]
TK:	$2 \text{ x } R5P \rightleftarrows S7P + GAP$	[Eq. 4.21]
TA:	$GAP + S7P \rightleftarrows F6P + E4P$	[Eq. 4.22]
TK2:	$E4P + R5P \rightleftarrows GAP + F6P$	[Eq. 4.23]
Gly:	$G6P \rightarrow F6P$	[Eq. 4.24]
ALD:	$F6P \rightarrow 2 \text{ x } GAP$	[Eq. 4.25]
PYK:	$GAP \rightarrow PYR$	[Eq. 4.26]
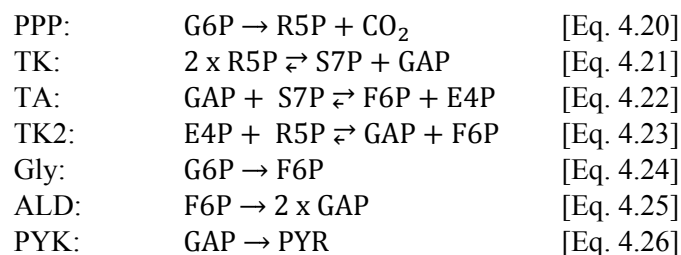
Lee et al. (1998) applied [1,2-^{13}C$_2$]glucose and calculated the PPP activity based on the model of Katz et al. (1966) and Katz and Rognstad (1967), who applied [1-^{13}C]- and [6-^{13}C]glucose. They proposed, that if [1,2-^{13}C$_2$]glucose is used as tracer, oxidative decarboxylation of [1,2-^{13}C$_2$]G6P produces [1-^{13}C]pentose phosphate, which is then converted via transketolase (TK) and transaldolase (TA) reactions to singly or doubly labeled fructose ([1-^{13}C]F6P, [1,3-^{13}C] F6P) and subsequently to other singly or doubly labeled intermediates that contribute to *m1* and *m2* abundance in mass spectra. Double-labeled [1,2-^{13}C$_2$]glucose would form, by the glycolytic pathway, the intermediates [2,3-^{13}C$_2$]triose phosphate, [2,3-^{13}C$_2$]pyruvate ([2,3-^{13}C$_2$]lactate and [2,3-^{13}C$_2$]alanine), and [1,2-^{13}C$_2$]acetyl-CoA, resulting in *m2* mass peaks. Further, recycling in the pentose phosphate pathway can lead to additional *m2* enrichment in hexoses (Figure 4.5.4 B). Thus, they included the major reactions of the pentose cycling and proposed the equation (Eq. 4.27) which can be solved for obtaining the split of the PPP from the glycolysis (Pcyc) (Eq. 4.28)

$$\frac{m1}{m2} = \frac{3 * PCyc}{1 - PCyc} \quad \text{[Eq. 4.27]} \qquad \rightarrow \qquad PCyc = \frac{\frac{m1}{m2}}{\left(3 + \frac{m1}{m2}\right)} \qquad \text{[Eq. 4.28]}$$

This method has been applied by several groups to calculate the split ratio of PPP from the glycolysis and is also applied here for the primary human hepatocytes and the hESC derived hepatocyte-like cells.

Primary human hepatocytes and the hESC derived hepatocyte-like cells were grown in media containing [1,2-^{13}C$_2$]glucose. Table 4.4.10 shows that both cell types metabolized [1,2-^{13}C$_2$]glucose over time. Mass isotopomer fractions in lactate from [1,2-^{13}C$_2$]glucose were recorded over time and are given in Table 4.4.11. The PPP split as calculated by the method described above is also given in the Table 4.4.11.

Table 4.4.10: Glucose uptake profile for hESC derived hepatocyte-like cells and primary human hepatocytes (PHH) over time [h].

	Time [h]	Concentration [C-µmol/L]					Carbon uptake [C-µmol/L]				
		0	12/16	24	36	48	0	12/16	24	36	48
PHH	*Control*	64848	58026	57510	57840	59238	0	6822	7338	7008	5610
	ST1	64848	57168	57138	58830	58764	0	7680	7710	6018	6084
	ST2	64848	56934	58554	58188	56502	0	7914	6294	6660	8346
	ST3	64848	58194	58722	58494	57570	0	6654	6126	6354	7278
SA002	*Control*	59628	40368	28284	21564	13224	0	19260	31344	38064	46404
	ST1	59628	53028	50352	42876	40332	0	6600	9276	16752	19296
	ST2	59628	45252	45480	42912	40752	0	14376	14148	16716	18876
	ST3	59628	50088	50148	48612	53640	0	9540	9480	11016	5988

While for the hESC derived hepatocyte-like cells (SA002) the PPP split did not vary over time, for primary human hepatocytes an increase over time for the participation of the pentose cycle was detected, as shown in Table 4.4.11. Further, for the hESC derived hepatocyte-like cells the PPP contribution to the metabolism of glucose increased, if the concentration of diclofenac in the media was increased. The opposite effect was observed for primary human hepatocytes.

Table 4.4.11: Mass isotoper fractions [%] in lactate from incubation with $[1,2-^{13}C_2]$glucose over time for PHH and hESC derived hepatocyte-like cells. Isotopomer distribution is expressed as molar fraction in %, i.e., the sum of the individual fractions equals 100 %. PPP activity is expressed as % glucose metabolism and calculated from *m1/m2* using Eq.4.28.

	Time [h]	Mass Isotopomer Fraction [%] in lactate From [U-$^{13}C_6$]glucose									
		Primary Hepatocytes					hESC derived hepatocyte-like cells				
		0	12	24	35	48	0	16	24	36	48
Control	*m0*	96.1	66.0	70.8	71.6	72.0	96.8	60.5	57.8	56.0	55.5
	m1	3.3	3.0	3.6	3.9	4.3	2.7	2.7	2.8	3.0	3.1
	m2	0.3	30.6	25.3	24.1	23.2	0.1	36.3	38.9	40.3	40.6
	m3	0.2	0.4	0.4	0.4	0.5	0.3	0.5	0.6	0.8	0.8
PPP [%]			3.2	4.5	5.1	5.8		2.4	2.3	2.4	2.5
ST1	*m0*	96.1	61.4	61.4	71.6	74.0	96.8	63.8	61.7	59.3	61.8
	m1	3.3	2.9	2.9	3.8	4.0	2.7	2.9	2.9	3.0	2.7
	m2	0.3	35.2	35.2	24.2	21.6	0.1	32.5	34.6	36.6	34.5
	m3	0.2	0.5	0.5	0.4	0.4	0.3	0.8	0.9	1.0	1.0
PPP [%]			2.6	2.6	4.9	5.8		2.9	2.7	2.7	2.6
ST3 (PHH) ST2 (SA002)	*m0*	96.1	47.7	64.4	67.9	67.9	96.8	61.3	60.1	58.9	59.0
	m1	3.3	2.4	3.0	3.7	4.3	2.7	2.8	2.9	2.9	2.9
	m2	0.3	49.3	32.1	28.0	27.2	0.1	34.9	35.9	37.0	37.0
	m3	0.2	0.6	0.5	0.5	0.6	0.3	1.0	1.1	1.2	1.1
PPP [%]			1.6	3.1	4.2	5.0		2.6	2.6	2.6	2.5

The above method of PPP split calculation is however not without its pitfalls. As Follstad and Stephanopoulos (1998) pointed out, that while the above mentioned conditions can be accurate under certain conditions, e.g. at low growth rates, they only represent the net fluxes through the corresponding pathways, and do not account for label redistribution due to reaction reversibility. In addition, they pointed out, that a fraction of the lactate produced, can be derived from pyruvate cycling from pyruvate via anaplerotic reactions into the TCA cycle and back to pyruvate (depicted in Figure 4.4.25 B). Thus, they concluded, one has to account for the labeling patterns in lactate due to recycling by the TCA cycle.
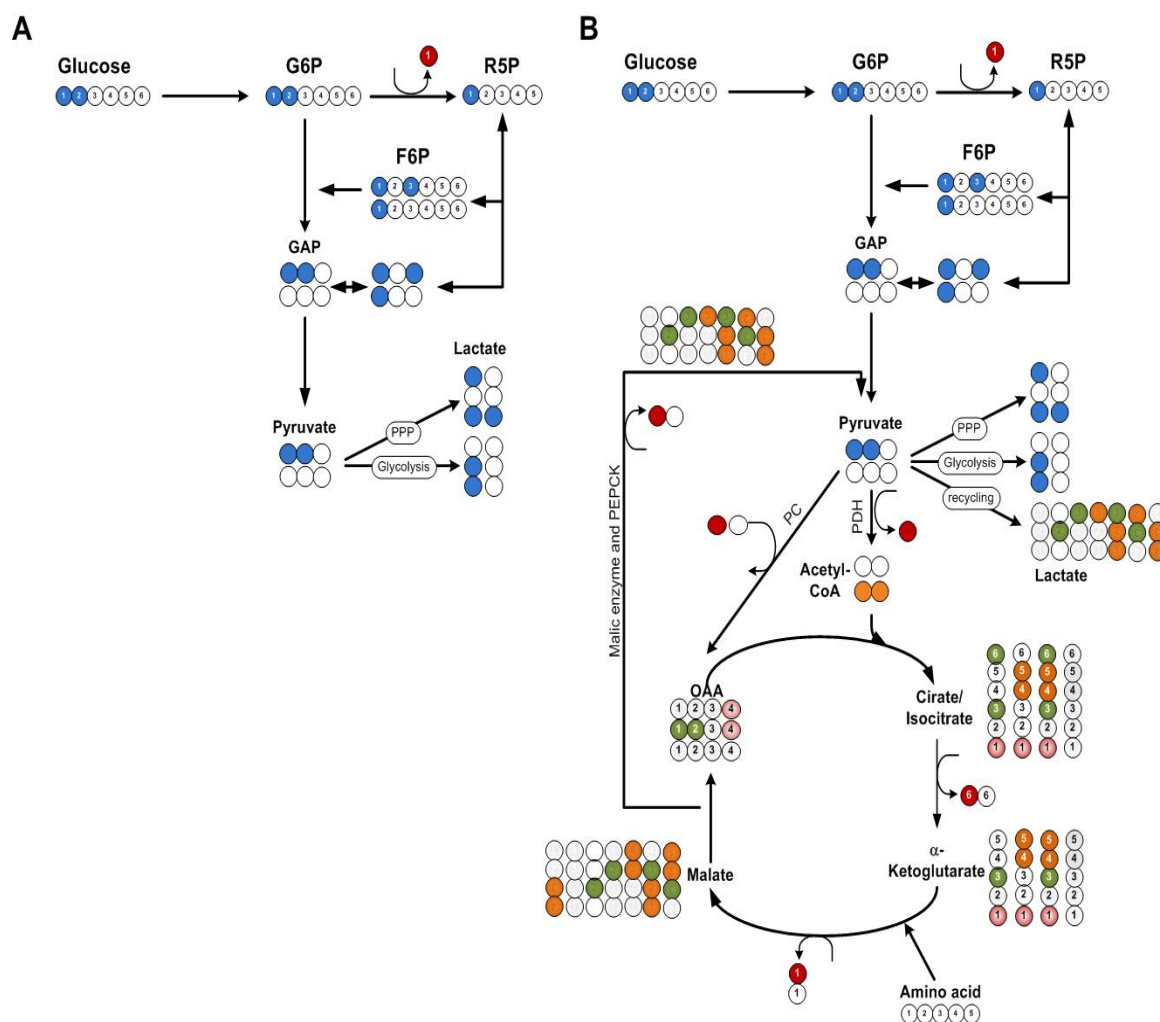
Figure 4.4.25: Schematic depiction of [1,2-$^{13}C_2$] labeled glucose metabolism by (**A**) pentose phosphate pathway and glycolysis and (**B**) pentose phosphate pathway, glycolysis and additionally with TCA cycling and the possible mass increases in lactate (indicated by filled circles).

It has been previously shown for primary human hepatocytes and hESC derived hepatocyte-like cells that recycling of pyruvate carbons, derived from [U-^{13}C$_6$]glucose, could be detected by enrichment of *m1* and *m2* fractions in lactate (chapter 4.4.2.4). A schematic depiction is presented in Figure 4.4.26 A.
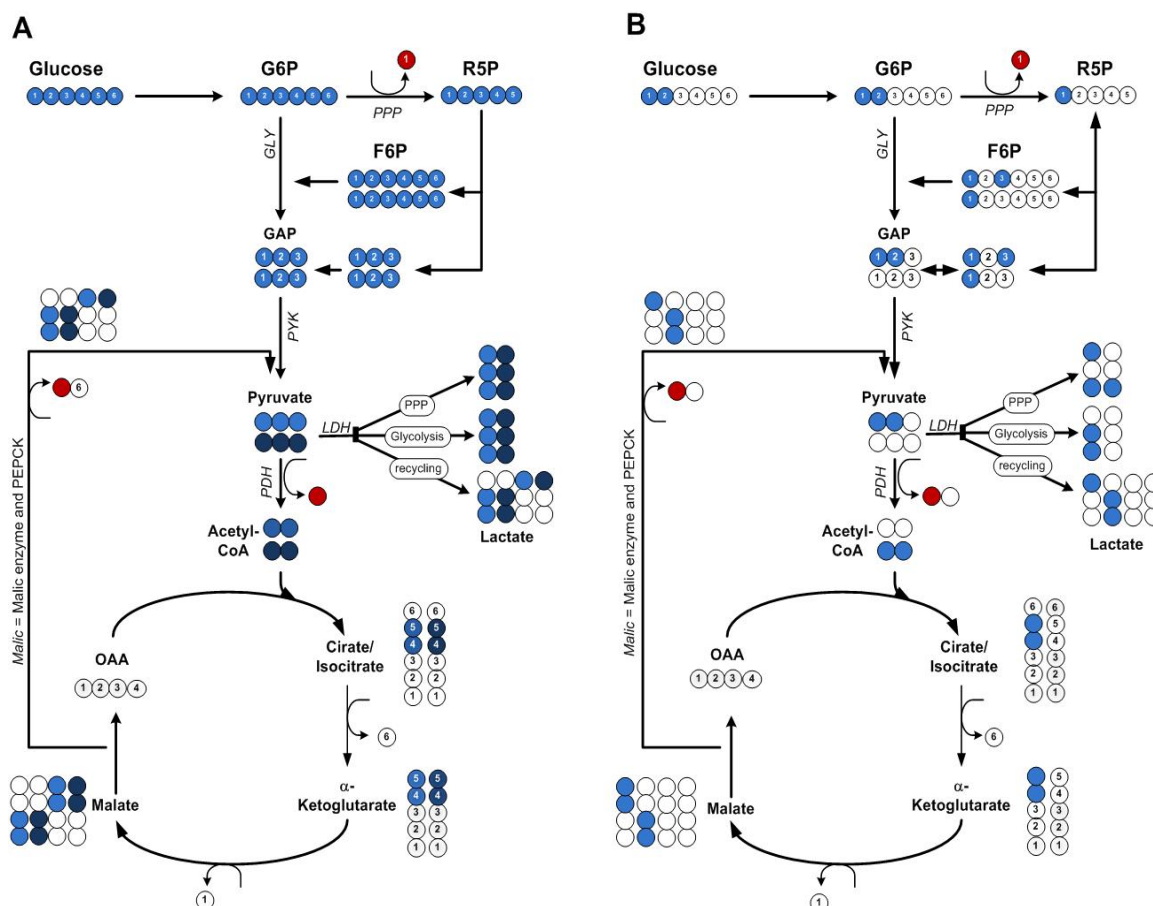
Figure 4.4.26: Schematic depiction of (**A**) [U-^{13}C$_6$]- and (**B**) [1,2-^{13}C$_2$]glucose metabolism by pentose phosphate pathway, glycolysis and TCA cycling with the possibly formed mass isotopomers in lactate (indicated by filled circles). Abbreviations used: LDH lactate dehydrogenase, GLY glycolysis, PYK pyruvate kinase, PDH pyruvate dehydrogenase, Malic malic enzyme and phosphoenolpyruvate-carboxykinase, OAA oxaloacetate.

This *m1* and *m2* fractions in lactate equals the flux from malate or OAA to pyruvate (Malic).

One can write a general balance for pyruvate

Pyruvate: $$0 = PYK + Malic - (LDH + PDH)$$ [Eq. 4.29]

where *PYK* denotes pyruvate kinase, *Malic* the flux from the TCA cycle to pyruvate via malic enzyme or phosphoenolpyruvate-carboxykinase (PEPCK), *LDH* lactate dehydrogenase and *PDH* the pyruvate dehydrogenase reaction. Further, one can write a mass balance for the *m3* mass isotopomer fraction transformed by each of the reactions.

Pyruvate_m3: $\quad 0 = PYK \cdot m3_{\_PYK} + Malic \cdot m3_{\_OAA} - (LDH + PDH) \cdot m3_{\_LAC}$

[Eq. 4.30]

Since the *m3* fraction in OAA was not measured, but OAA is the precursor of aspartate, the *m3* fraction of aspartate can be used to solve the equation. However, since the *m3* fraction in secreted aspartate was very small (< 3 % for PHH and aspartate was degraded from the culture medium for the hESC derived hepatocyte-like cells, both cultured on [U-^{13}C$_6$]glucose as substrate), one can assume the *m3* fraction of aspartate to be negligible and thus *Malic x m3_{_OAA}* to be ≈ 0. Thus equation 4.30 simplifies to

Pyruvate_m3: $\quad 0 = PYK \cdot m3_{\_PYK} - (LDH + PDH) \cdot m3_{\_LAC}$ [Eq. 4.31]

and can be resolved to $\quad (LDH + PDH) = \dfrac{PYK\, x\, m3_{\_PYK}}{m3_{\_LAC}}$

Now equation 4.31 can be implemented in equation 4.29, which is shown in Eq. 4.32

$$0 = PYK + Malic - \frac{PYK\, x\, m3_{\_PYK}}{m3_{\_LAC}}$$ [Eq. 4.32]

and one can solve for the malic enzyme activity, which is shown in equation 4.33

$$Malic = \frac{PYK\, x\, m3_{\_PYK}}{m3_{\_LAC}} - PYK$$ [Eq. 4.33]

The calculations for the malic enzyme activity are shown in Table 4.4.12, according to equation 4.33. Interestingly, while for PHHs the flux from the TCA cycle to pyruvate (Malic) and the glycolysis (PYK) increased with increasing concentrations of diclofenac, for the hESC derived cells these fluxes decreased.

Table 4.4.12: Calculation of *Malic* flux in [μmol/(L x 48 h) for primary human hepatocytes (PHH) and hESC derived hepatocyte-like cells (SA002) according to equation 4.33. [U-$^{13}C_6$]glucose was used as a substrate.

	Glucose uptake [μmol/(L x 48h)]		PYK [μmol/(L x 48h)]		m3 mass isotopomer production in lactate [μmol/(L x 48h)]		Malic [μmol/(L x 48h)]	
	PHH	SA002	PHH	SA002	PHH	SA002	PHH	SA002
Control	935	7734	1870	15468	646	12085	3543	4330
ST1	1014	3216	2028	6432	533	4090	5688	3683
ST3 (PHH)	1213	------	2426	------	451	------	10624	------
ST2 (SA002)	------	3146	------	6292	------	4080	------	3411

If one uses now [1,2-$^{13}C_2$]glucose as substrate, as shown by Lee et al. (1998), and no malic enzyme or phosphoenolpyruvate-carboxykinase (PEPCK) activity is assumed one can solve equation 4.31 for any mass isotopomer, denoted by *i* (*m1* and *m2* fractions):

PYR_m*i*:
$$0 = PYK \; x \; mi_{\_PYK} - (LDH + PDH) \; x \; mi_{\_Lac}$$
[Eq. 4.31]

However, for this, the balances around ribose-5-phosphate (R5P), fructose-6-phosphate (F6P), glyceraldehyde-3-phosphate (GAP) and glucose-6-phosphate (G6P) have to be considered and in addition, the transaldolase and the trasketolase reactions have to be assumed to be equally active.

R5P:
$$0 = PPP - 2 \; x \; TK1 - TK2$$
[Eq. 4.33]
$$0 = PPP - 3 \; x \; TK1$$
$$TK1 = \frac{PPP}{3} \implies PPP = 3 \; x \; TK1$$

FGP:
$$0 = GLY + TA + TK2 - ALD$$
[Eq. 4.34]
$$0 = GLY + 2 \; x \; \frac{PPP}{3} - ALD$$
$$\implies GLY = ALD - 2 \; x \; TK1$$

GAP:
$$0 = TK1 - TA + TK2 + 2 \; x \; ALD - PYK$$
[Eq. 4.35]
$$0 = \frac{PPP}{3} + 2 \; x \; ALD - PYK$$

G6P:
$$0 = PPP + GLY - 1$$
[Eq. 4.36]

Then Lee et al. (1998) were able to solve the pentose phosphate split ratio from the glycolysis and find an approximation, which can be expressed as *m1* and *m2* fractions in lactate (see equation 4.28).

However, if malic enzyme or phosphoenolpyruvate-carboxykinase (PEPCK) are active, additional *m1* and *m2* fractions are generated by pyruvate cycling and pyruvate recycling and have to be also considered (equation 4.37).

PYR_m_i: $0 = PYK \; x \; m_{i\_PYK} + \; Malic \; x \; m_{i\_OAA} - (LDH + PDH) \; x \; m_{i\_Lac}$ [Eq. 4.37]

For this however, one cannot compute the mass isotopomer fraction of $Malic \; x \; m_{i\_OAA}$, since the fractional enrichment in oxaloacetate and/or malate is not known. Mass balances for all possible ^{13}C mass positions would have to be written for oxaloacetate or malate. This could be done by an isotopomer model, which is however not possible here, since the metabolites of the cells were not in an isotopic steady state. However, by measuring intracellular OAA and malate mass isotopomer fractions one could learn the desired information.

Table 4.4.12:   Mass isotopomer fractions of lactate for the substrate [U-$^{13}C_6$]glucose for primary human hepatocytes and hESC derived hepatocyte-like cells exposed to diclofenac over time [h]. Isotopomer distribution is expressed as molar fraction in %, i.e., the sum of the individual fractions equals 100 %.

		Mass Isotopomer Fraction [%] in lactate from [U-$^{13}C_6$]glucose									
	Time	Primary Hepatocytes					hESC derived hepatocyte-like cells				
	[h]	0	12	24	35	48	0	16	24	36	48
Control	m0	96.1	59.7	58.6	56.0	50.5	96.8	16.8	14.7	12.9	10.9
	m1	3.3	2.9	3.4	3.7	4.0	2.7	1.1	1.0	1.0	0.9
	m2	0.3	2.7	3.6	3.9	4.8	0.1	2.1	2.1	2.3	2.5
	m3	0.2	34.7	34.4	36.4	40.7	0.3	79.9	82.2	83.8	85.7
ST1	m0	96.1	55.0	56.0	53.5	53.8	91.7	22.0	18.3	16.2	15.0
	m1	3.3	2.7	3.4	3.6	4.0	3.2	1.7	1.5	1.4	1.4
	m2	0.3	2.6	3.7	4.1	4.7	1.5	2.6	2.7	2.6	2.8
	m3	0.2	39.8	36.9	38.9	37.5	3.6	73.7	77.5	79.7	80.8
ST3/ST2	m0	96.1	46.1	52.0	52.5	46.8	91.7	26.2	20.9	19.5	17.9
	m1	3.3	2.1	2.7	3.2	4.1	3.2	1.7	1.6	1.6	1.6
	m2	0.3	2.3	2.8	3.6	5.7	1.5	2.4	2.5	2.6	2.7
	m3	0.2	49.5	42.5	40.6	43.5	3.6	69.7	75.0	76.2	77.8

4.4.2.7 Gluconeogenesis

One of the major tasks for hepatocytes is to maintain sugar homeostasis in the human body. To achieve this, the cells have to keep the blood sugar concentration in a range from 4-6 mM (mmol/L) and react to hormones (insulin and glucagon), which are released from the pancreas. In case of high sugar levels, insulin stimulates the conversion of glucose to glycogen for storage. If the concentration of glucose falls below 4 mM, glucagon is released from the pancreas, which promotes glucose synthesis from glycogen (glycogenolysis). The normal glucose levels for humans for a two day interval are depicted in Figure 4.4.27 B. If glycogen is depleted, or the glucose level decreases too fast, glucose can also be produced from lactate, glycerol or glucogenic amino acids (gluconeogenesis).
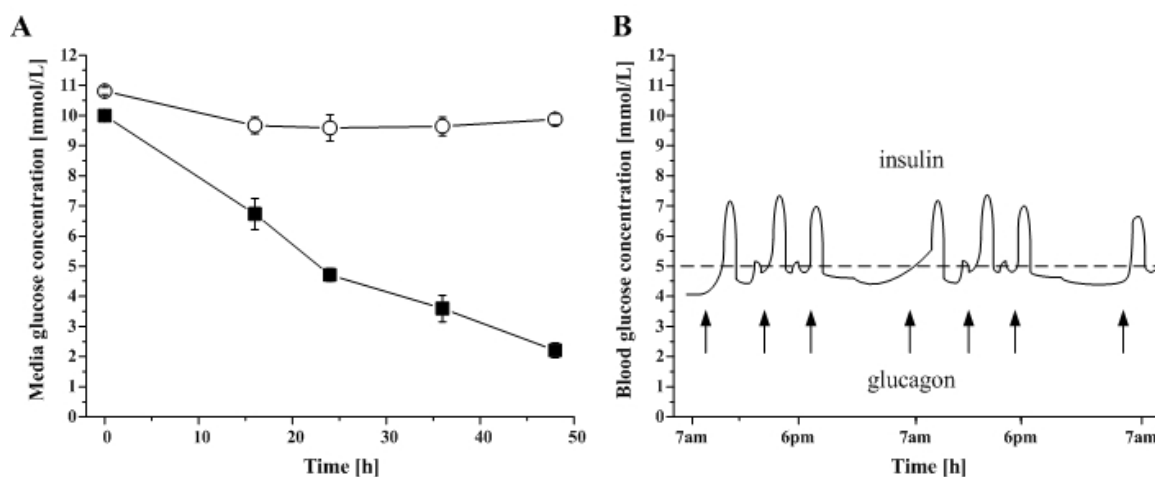
Figure 4.4.27: Glucose levels. **A)** Media glucose concentration [mmol/L] for PHH (○) and hESC derived hepatocyte-like cells (■) over time. **B)** Hypothetical blood glucose concentrations of humans for a two day interval. The arrows indicate meals during the day.

Since gluconeogenesis mostly takes place in the liver and both hormones were supplemented in the culture medium, it was of interest, if the hESC derived hepatocytes are able to synthesize new glucose and excrete it to the culture medium. For primary human hepatocytes the gluconeogenic activity has been shown and discussed by several groups (Katz and Tayek, 1999; Landau et al., 1998; Mao et al., 2002; Radziuk and Lee, 1999). As has been previously shown (Figure 4.4.10), PHH did not utilize much glucose over the culture period (Figure 4.4.27 A). However, the glucose concentration in the

medium at the beginning of the experiment was 10 mM, and many other amino acids were available for degradation. The hESC derived cells, however, metabolized approx. 8 mM glucose over a culture period of 48 hours (Figure 4.4.27 A) which would suggest that they either display the Warburg effect or that a fraction of the mixed culture was not hepatocyte-like.

Nevertheless, as discussed previously, the cells visibly decreased their uptake as soon as the concentration fell below 5 mM glucose, suggesting that they might either decrease their metabolism (not confirmed for other supplemented amino acids) or that they might have produced glucose, which would further be a typical indicator for hepatic functionality.

Table 4.4.14: Isotope enrichment [%] in glucose over time for PHH and hESC derived hepatocyte-like cells. The substrate was [U-^{13}C$_6$]glucose. Isotopomer distribution is expressed as molar fraction in %, i.e., the sum of the individual fractions (*m0-m6*) equals 100 %. SFL summed fractional labeling

		PHH					SA002				
	Time [h]	Mass Isotopomer Fraction [%] [U-^{13}C$_6$]glucose					Mass Isotopomer Fraction [%] [U-^{13}C$_6$]glucose				
		0	12	24	35	48	0	16	24	36	48
	m0	1.235	1.235	1.288	1.348	1.388	1.235	2.403	4.245	5.716	8.665
	m1	0.986	0.986	1.036	0.998	1.071	0.986	2.006	3.969	5.676	10.890
	m2	0.255	0.255	0.277	0.277	0.300	0.255	0.437	0.817	1.117	2.119
Glucose	*m3*	1.130	1.130	1.261	1.344	1.449	1.130	2.111	3.955	5.536	10.442
	m4	0.321	0.321	0.338	0.333	0.367	0.321	0.535	0.911	1.242	2.181
	m5	4.929	4.929	4.938	4.946	5.010	4.929	5.549	5.924	6.073	6.826
	m6	91.144	91.144	90.863	90.754	90.415	91.144	86.959	80.179	74.639	58.877
SFL [%]		96.28	96.28	96.10	96.03	95.84	96.28	93.48	88.63	84.61	73.76
Glc new [µM]		402	360	374	383	411	370	439	536	553	578

To study the synthesis of new glucose, the decrease of fully labeled glucose (*m6* = 91 %) was measured in the culture medium. As can be seen in Table 4.5.14, only very small decrease of [U-^{13}C$_6$]glucose was observed for primary human hepatocytes over time. However, for the hESC derived hepatocyte-like cells the summed fractional labeling (SFL) of glucose decreased by more than 20 % and even more for the *m6* fraction, which was in the beginning of the cultivation by 91 % and 59 % after 48 hours. Interestingly, the *m0, m3* and the *m1* fractions increased mostly, suggesting in case of *m3* enrichment non-labeled and fully labeled lactate, pyruvate, serine or alanine to act as gluconeogenic substrates, and in case of *m1* increased recycling from glucose carbons via the TCA

197

cycle. The increase of the *m0* fraction can be explained by non-labeled amino acids, which were supplemented in the culture media, to act as gluconeogenic substrates.

Nevertheless, this decrease in enrichment showed that hESC derived hepatocyte-like cells are capable of gluconeogenic activity, which further indicates hepatic functionality, as previously discussed (chapter 3). Here, influence of diclofenac on gluconeogenesis was not detected for primary human hepatocytes, since the primary cells did not show the activity, due to no starvation. Thus, for future studies, starved primary hepatocytes, supplemented with $[\text{U-}^{13}\text{C}_3]$alanine or $[\text{U-}^{13}\text{C}_3]$lactate in presence of diclofenac, might answer whether there is increased gluconeogenesis and glycogenolysis after diclofenac or acetaminophen exposure as proposed by Petrescu and Tarba (1997).

4.4.2.8   Concluding remarks

By analysis of fractional enrichment data of alanine and lactate, it was shown that glycolysis was the major supply of pyruvate in embryonic stem cell derived hepatocyte-like cells and was also active in primary human hepatocytes. In addition, it was shown that pyruvate enters the TCA cycle and that the carbon atoms from glucose could be detected in TCA products.

A simple metabolic flux model was generated, based on SFL data, for hESC derived hepatocyte-like cells and primary human hepatocytes. The influence of diclofenac for glycolysis and TCA cycle activity was evaluated for both cell types. While for primary human hepatocytes the glycolysis and the TCA cycle activity was enhanced, for the hESC derived hepatocyte-like cells only the TCA cycle activity was increased in presence of diclofenac.

In addition, the reversibility of synthesis and production rates was estimated and interpreted for control cells and diclofenac exposed cells.

It was shown that anaplerosis to TCA cycle intermediates took place and pyruvate cycling and pyruvate recycling is very active in the tested hepatocytes and hepatocyte-like cells. The flux from oxaloacetate or malate to pyruvate increased for primary human hepatocytes and decreased for the hESC derived hepatocyte-like cells with increasing drug concentrations. In addition, it was found that there is likely no scrambling of fumarate and succinate in the hepatocytes.

It could be shown, that it is of importance to consider TCA recycling to pyruvate to calculate pentose cycle contribution to glucose metabolism from lactate. Furthermore, it was observed that the pentose phosphate pathway was relatively inactive (less than 2 % of glycolysis).

In addition, gluconeogenesis was found to be present in hESC derived-hepatocyte-like cells, which supports their differentiation towards functional hepatocytes. Gluconeogenic activity was also detected for primary human hepatocytes, which was shown by presence of labeled carbon atoms from [U-^{13}C$_5$]glutamine in excreted serine and glycine.

4.5 Conclusions

To obtain a better insight into the fate of glucose and amino acids metabolism in hepatocytes, metabolic profile analysis, metabolic flux analysis and ^{13}C pathway analysis was used to determine the effect of diclofenac in sub-toxic concentrations on the flux distribution through the major pathways in hepatocytes. The used substrates were [U-^{13}C$_6$]glucose, [1,2-^{13}C$_2$]glucose and [U-^{13}C$_5$]glutamine. Using the new approach described above, multiple new insights of hepatic metabolism in presence of sub-toxic concentrations of diclofenac were found.

First, since the adherent cells cannot be cultured continuously, several time points were determined for analysis. The influence of diclofenac was tested by comparing medium substrates and synthesized metabolites over a time period of 48 hours for both cell types. Here dose dependent changes in the global metabolic profiles for aromatic amino acids (tryptophan, phenylalanine and tyrosine) seemed to be influenced the most by diclofenac exposure.

Second, for primary human hepatocytes, due to extensive exchange of amino acids with the surrounding culture no metabolic steady state was found. For hESC derived hepatocyte-like cells, metabolic steady state could be assumed and stationary metabolic balance analysis was performed. Here, it was observed that diclofenac increases the activity of the TCA and the urea cycle even at sub-toxic concentrations. However, the expected increase in glycolysis for balance of the ATP depletion, due to uncoupling of the oxidative phosphorylation pathway, was not observed.

Third, metabolic pathway identification was performed to elucidate activity of glycolysis, gluconeogenesis, pentose phosphate pathway and TCA cycle. Here, it was observed that diclofenac exposure increased the activity of the TCA cycle for both tested cell types and enhanced the glycolytic activity for primary human hepatocytes. It was found that the pentose phosphate pathway activity was relatively inactive and it could be shown, that it is of importance to consider TCA recycling to pyruvate to calculate pentose cycle contribution to glucose metabolism from lactate.

The observed changes could serve as indicators for hepatotoxic responses in future toxicity studies and by combining these toxicity fingerprints with drug metabolism data could help to deepen the understanding of overall toxicity.

5 Summary and Future Perspectives

The use of hepatocytes for drug metabolism studies to obtain data on biotransformation, screen for toxic effects and to elucidate the drug's mechanism of action is common in the pharmaceutical industry to ensure a safe release of new drugs into the market. Human hepatocytes are scarce and thus high-throughput toxicity assays have been developed to achieve a high data gain using as few cells as possible. Nevertheless, most assays are end-point assays which give information for a specific time point after drug exposure and do not allow further processing of the cells and/or the culture supernatant. Thus, in the first part of this thesis, a new high-throughput dynamic and non-invasive method has been introduced. The method utilizes the dissolved oxygen concentration in the media to obtain respiration data, whose change can be correlated with toxic responses in cells exposed to drugs. The degree of respiration response correlates to the toxicity caused by the drugs. The assay was shown to be applicable to immortalized, proliferating hepatoma cells and freshly isolated and non-proliferating primary rat hepatocytes. In addition, LC_{50} concentrations of the tested chemicals were in accordance with current literature data. Further, it was shown that another advantage of this assay is that the cells and the culture supernatant can also be utilized for drug metabolism studies. The assay proved to be robust, flexible and easy to adapt for adherent cell lines/types. Even though this assay decreases the demand of hepatocytes for drug studies, the demand of human hepatocytes for drug metabolism studies still exeeds the supply of liver cells. Thus, it would be of interest to further modify the microtiter plate from the current 24-well format to a 96-well or smaller format. In addition, multiple sensors (e.g. for glucose or lactate concentration in the supernatant) would improve the on-line method.

Hepatocytes, that are employed for research are mostly rejects from liver transplantation due to age, medical condition or weight of the donor or obtained from surgery. Thus, hepatocytes, derived from stem cells could provide an unlimited supply for drug studies and also for liver implantations in the future. Thus, in the second part of this thesis, hESC derived hepatocytes-like cells, which have been differentiated towards hepatocytes, were evaluated for their application in toxicity and drug metabolism studies. It was shown, that the hESC derived cells displayed typical hepatocyte morphology, that characteristic

hepatic protein expressions were present and that the cells showed hepatic functionality. The cells did not however show hepatic biotransformation functionality as high as primary human hepatocytes and thus it was concluded that the cells are not yet applicable in the pharmaceutical industry for drug metabolism studies. However, as soon as these cells become fully functional, both animal studies and demand for liver donations can be reduced. To reach this goal the efficiency of the differentiation protocols, the purity of the end-culture and their functionality should be further improved in future research studies to finally obtain a valid hepatic *in vitro* model.

In the last part of the thesis it was tested if sub-toxic concentrations of diclofenac would alter the metabolism of primary human hepatocytes and hESC-derived hepatocytes. This was done to predict possible toxicity to cells upon exposure to higher concentrations. For this, parallel cultures, using labeled substrates in the presence of diclofenac treatment, were performed and analyzed to obtain metabolic profiles. The metabolic pathways involved were defined and a stoichiometric model for metabolic flux analysis was defined. Quantification of the amino acids, pyruvate, lactate and glucose was performed by HPLC and the isotopic labeling was analyzed using GC-MS. It was shown, that diclofenac caused dose dependent changes in the global metabolic profiles for the aromatic amino acids (tryptophan, phenylalanine and tyrosine). The labeling analysis revealed that anaplerosis and pyruvate cycling and pyruvate recycling took place in the tested hepatocytes. This led to interesting new insights into TCA cycle influx and recycle capacities in regard to PC, PDH, glyoxylate shunt and isotopomer distribution in glutamate. However, these new insights were not used in the presented model, but work is currently underway for these calculations using the data generated from experiments performed in this thesis. It was also observed, that the pentose phosphate pathway was relatively inactive (less than 5 % of glucose metabolism) for the hepatocytes. It could be shown however, that it is important to consider pyruvate recycling via the TCA cycle for the pentose cycle activity split calculation in lactate, which was previously not considered. While common cytotoxicity assays do not imply any toxic response to the chosen sub-toxic diclofenac concentrations, the MFA results suggest early markers of potential toxicity in form of mitochondrial impairment, most probably in form of uncoupling of oxidative phosphorylation caused by even sub-toxic concentrations of diclofenac. Thus, in the third part of this thesis the study demonstrates that metabolic flux analysis is a powerful methodology, which allows quantification of the central

metabolism of hepatocytes and is useful to elucidate hepatic metabolic changes in response to diclofenac treatment. However, for future perspectives, dynamic modeling for multiple labeled substrates in combination with exposure to sub-toxic drug concentrations should be performed. Further, an extended metabolite quantification and isotopomer analysis, as for albumin, fatty acid, glycogen, ketone bodies and citrate synthesis, should be included to extend and improve the above presented methodology.

6 References

.

Aden DP, Fogel A, Plotkin S, Damjanov I, Knowles BB. 1979. Controlled Synthesis of Hbsag in a Differentiated Human-Liver Carcinoma-Derived Cell-Line. Nature 282(5739):615-616.

Alberts B, Johnson A, Lewis J, Raff M, Roberts P, Walter P. 2002. Molecular Biology of the Cell. fourth Edidtion ed. New York: Garland Sciences.

Alden C, Lin J, Smith P. 2003. Predictive Toxicology Technology for Avoiding Idiosyncratic Liver Injury. Preclinica May/June.

Amann T, Maegdefrau U, Hartmann A, Agaimy A, Marienhagen J, Weiss TS, Stoeltzing O, Warnecke C, Scholmerich J, Oefner PJ, Kreutz M, Bosserhoff AK, Hellerbrand C. 2009. GLUT1 expression is increased in hepatocellular carcinoma and promotes tumorigenesis. Am J Pathol 174(4):1544-1552.

Anouska D, Rebecca H, Perry L, Lionel L, Prabhas VM. 2005. E-cadherin synergistically induces hepatospecific phenotype and maturation of embryonic stem cells in conjunction with hepatotrophic factors. Biotechnology and Bioengineering 92(3):257-266.

Antoniewicz MR, Kelleher JK, Stephanopoulos G. 2007a. Accurate Assessment of Amino Acid Mass Isotopomer Distributions for Metabolic Flux Analysis. Analytical Chemistry 79(19):7554-7559.

Antoniewicz MR, Kelleher JK, Stephanopoulos G. 2007b. Elementary metabolite units (EMU): A novel framework for modeling isotopic distributions. Metabolic Engineering 9(1):68-86.

Antoniewicz MR, Kraynie DF, Laffend LA, Gonzalez-Lergier J, Kelleher JK, Stephanopoulos G. 2007c. Metabolic flux analysis in a nonstationary system: fed-batch fermentation of a high yielding strain of E. coli producing 1,3-propanediol. Metab Eng 9(3):277-292.

Arnheiter H. 1980. Primary Monolayer-Culture of Adult-Mouse Hepatocytes - Model for the Study of Hepatotropic Viruses. Archives of Virology 63(1):11-22.

Arterburn L, M. , Joanne Z, James DY, Regina MO, Aaron HH. 1995. A morphological study of differentiated hepatocytes *in vitro*. Hepatology 22(1):175-187.

Baharvand H, Hashemi SM, Ashtian SK, Farrokhi A. 2006. Differentiation of human embryonic stem cells into hepatocytes in 2D and 3D culture systems *in vitro*. International Journal of Developmental Biology 50(7):645-652.

Bai J, Cederbaum AI. 2006. Cycloheximide protects HepG2 cells from serum withdrawal-induced apoptosis by decreasing p53 and phosphorylated p53 levels. J Pharmacol Exp Ther 319(3):1435-1443.

Bailey MJ, Dickinson RG. 1996. Chemical and Immunochemical Comparison of Protein Adduct Formation of Four Carboxylate Drugs in Rat Liver and Plasma. Chemical Research in Toxicology 9(3):659-666.

Bak LK, Waagepetersen HS, Melo TM, Schousboe A, Sonnewald U. 2007. Complex glutamate labeling from [U-^{13}C]glucose or [U-^{13}C]lactate in co-cultures of cerebellar neurons and astrocytes. Neurochemical Research 32(4-5):671-680.

Bak LK, Zieminska E, Waagepetersen HS, Schousboe A, Albrecht J. 2008. Metabolism of [U-^{13}C]glutamine and [U-^{13}C]glutamate in isolated rat brain mitochondria suggests functional phosphate-activated glutaminase activity in matrix. Neurochemical Research 33(2):273-278.

REFERENCES

Balcarcel RR, Clark LM. 2003. Metabolic screening of mammalian cell cultures using well-plates. Biotechnology Progress 19(1):98-108.

Banks AT, Hyman JZ, Kamal GI, John GH. 1995. Diclofenac-associated hepatotoxicity: Analysis of 180 cases reported to the food and drug administration as adverse reactions. Hepatology 22(3):820-827.

Beckers S, Noor F, Muller-Vieira U, Mayer M, Strigun A, Heinzle E. 2010. High throughput, non-invasive and dynamic toxicity screening on adherent cells using respiratory measurements. Toxicology In Vitro 24(2):686-694.

Bennett BD, Yuan J, Kimball EH, Rabinowitz JD. 2008. Absolute quantitation of intracellular metabolite concentrations by an isotope ratio-based approach. Nature Protocols 3(8):1299-1311.

Bennett CL, Nebeker JR, Yarnold PR, Tigue CC, Dorr DA, McKoy JM, Edwards BJ, Hurdle JF, West DP, Lau DT, Angelotta C, Weitzman SA, Belknap SM, Djulbegovic B, Tallman MS, Kuzel TM, Benson AB, Evens A, Trifilio SM, Courtney DM, Raisch DW. 2007. Evaluation of serious adverse drug reactions: a proactive pharmacovigilance program (RADAR) vs safety activities conducted by the Food and Drug Administration and pharmaceutical manufacturers. Archives of Internal Medicine 167(10):1041-1049.

Berg JM, L.Tymoczko J, Stryer L. 2003. Biochemie. 5 ed. Heidelberg: Spektrum Akademeischer Verlag GmbH.

Bernhard SA, Tompa P. 1990. The mechanism of succinate or fumarate transfer in the tricarboxylic acid cycle allows molecular rotation of the intermediate. Archives of Biochemistry and Biophysics 276(1):191-198.

Boelsterli UA. 2003. Diclofenac-induced liver injury: a paradigm of idiosyncratic drug toxicity. Toxicology and Applied Pharmacology 192(3):307-322.

Bonarius HPJ, Degooijer CD, Tramper J, Schmid G. 1995. Determination of the Respiration Quotient in Mammalian-Cell Culture in Bicarbonate Buffered Media. Biotechnology and Bioengineering 45(6):524-535.

Bonarius HPJ, Timmerarends B, Gooijer CDd, Tramper J. 1998. Metabolite-balancing techniques vs. 13C tracer experiments to determine metabolic fluxes in hybridoma cells. Biotechnology and Bioengineering 58(2-3):258-262.

Bort R, Mace K, Boobis A, Gomez-Lechon MJ, Pfeifer A, Castell J. 1999a. Hepatic metabolism of diclofenac: Role of human CYP in the minor oxidative pathways. Biochemical Pharmacology 58(5):787-796.

Bort R, Ponsoda X, Jover R, Gomez-Lechon MJ, Castell JV. 1999b. Diclofenac toxicity to hepatocytes: a role for drug metabolism in cell toxicity. Journal of Pharmacology and Experimental Therapeutics 288(1):65-72.

Bova MP, Tam D, McMahon G, Mattson MN. 2005. Troglitazone induces a rapid drop of mitochondrial membrane potential in liver HepG2 cells. Toxicology Letters 155(1):41-50.

Brandon EF, Meijerman I, Klijn JS, den Arend D, Sparidans RW, Lazaro LL, Beijnen JH, Schellens JH. 2005. *In-vitro* cytotoxicity of ET-743 (Trabectedin, Yondelis), a marine anti-cancer drug, in the Hep G2 cell line: influence of cytochrome P450 and phase II inhibition, and cytochrome P450 induction. Anticancer Drugs 16(9):935-943.

Brewer JA, Tank ES. 1993. Yolk sac tumors and alpha-fetoprotein in first year of life. Urology 42(1):79-80.

Brolen G, Sivertsson L, Bjorquist P, Eriksson G, Ek M, Semb H, Johansson I, Andersson TB, Ingelman-Sundberg M, Heins N. 2010. Hepatocyte-like cells derived from human

embryonic stem cells specifically via definitive endoderm and a progenitor stage. Journal of Biotechnology 145(3):284-294.

Brown SB, Maloney M, Kinlaw WB. 1997. "Spot 14" Protein Functions at the Pretranslational Level in the Regulation of Hepatic Metabolism by Thyroid Hormone and Glucose. Journal of Biological Chemistry 272(4):2163-2166.

Browne GS, Nelson C, Nguyen T, Ellis BA, Day RO, Williams KM. 1999. Stereoselective and substrate-dependent inhibition of hepatic mitochondrial [beta]-oxidation and oxidative phosphorylation by the non-steroidal anti-inflammatory drugs ibuprofen, flurbiprofen, and ketorolac. Biochemical Pharmacology 57(7):837-844.

Bùrki C-A. 2008. Mixing and gas transfer studies in orbital shaken cylindrical vessels. Sion.

Cai J, Zhao Y, Liu YX, Ye F, Song ZH, Qin H, Meng S, Chen YZ, Zhou RD, Song XJ, Guo YS, Ding MX, Deng H. 2007. Directed differentiation of human embryonic stem cells into functional hepatic cells. Hepatology 45(5):1229-1239.

Cantelli-Forti G, Hrelia P, Paolini M. 1998. The pitfall of detoxifying enzymes. Mutation Research/Fundamental and Molecular Mechanisms of Mutagenesis 402(1-2):179-183.

Carraway ER, Demas, J.N. 1991. Luminescence Quenching Mechanism for Microheterogeneous Systems. Analytical Chemistry 63(4):332-336.

Castell JV, GomezLechon MJ, Ponsoda X, Bort R. 1997. The use of cultured hepatocytes to investigate the mechanisms of drug hepatotoxicity. Cell Biology and Toxicology 13(4-5):331-338.

Chan C, Berthiaume F, Lee K, Yarmush ML. 2003a. Metabolic flux analysis of cultured hepatocytes exposed to plasma. Biotechnology and Bioengineering 81(1):33-49.

Chan C, Berthiaume F, Lee K, Yarmush ML. 2003b. Metabolic flux analysis of hepatocyte function in hormone- and amino acid-supplemented plasma. Metabolic Engineering 5(1):1-15.

Chiao E, Elazar M, Xing Y, Xiong A, Kmet M, Millan MT, Glenn JS, Wong WH, Baker J. 2008. Isolation and transcriptional profiling of purified hepatic cells derived from human embryonic stem cells. Stem Cells 26(8):2032-2041.

Cho CH, Parashurama N, Park EYH, Suganuma K, Nahmias Y, Park J, Tilles AW, Berthiaume F, Yarmush ML. 2008. Homogeneous differentiation of hepatocyte-like cells from embryonic stem cells: applications for the treatment of liver failure. Journal of the Federation of American Societies for Experimental Biology 22(3):898-909.

Christensen B, Nielsen J. 2000. Metabolic network analysis. A powerful tool in metabolic engineering. Adv Biochem Eng Biotechnol 66:209-231.

Coakley RJ, Taggart C, O'Neill S, McElvaney NG. 2001. Alpha1-antitrypsin deficiency: biological answers to clinical questions. The American Journal of Medical Sciences 321(1):33-41.

Comte B, Vincent G, Bouchard B, DesRosiers C. 1997. Probing the origin of acetyl-CoA and oxaloacetate entering the citric acid cycle from the C-13 labeling of citrate released by perfused rat hearts. Journal of Biological Chemistry 272(42):26117-26124.

Cook RJ. 2000. Defining the steps of the folate one-carbon shuffle and homocysteine metabolism. Am J Clin Nutr 72(6):1419-1420.

Craig A, Sidaway J, Holmes E, Orton T, Jackson D, Rowlinson R, Nickson J, Tonge R, Wilson I, Nicholson J. 2006. Systems toxicology: Integrated genomic, proteomic and metabonomic analysis of methapyrilene induced hepatotoxicity in the rat. Journal of Proteome Research 5(7):1586-1601.

REFERENCES

Dambach DM, Andrews BA, Moulin F. 2005. New technologies and screening strategies for hepatotoxicity: Use of *in vitro* models. Toxicologic Pathology 33(1):17-26

Davies NM, Saleh JY, Skjodt NM. 2000. Detection and prevention of NSAID-induced enteropathy. Journal of Pharmacy and Pharmaceutical Sciences 3(1):137-155.

Davila JC, Cezar GG, Thiede M, Strom S, Miki T, Trosko J. 2004. Use and application of stem cells in toxicology. Toxicological Sciences 79(2):214-223.

DeBerardinis RJ, Mancuso A, Daikhin E, Nissim I, Yudkoff M, Wehrli S, Thompson CB. 2007. Beyond aerobic glycolysis: transformed cells can engage in glutamine metabolism that exceeds the requirement for protein and nucleotide synthesis. Proceedings of the National Academy of Sciences of the United States of America 104(49):19345-19350.

Des Rosiers C, Fernandez CA, David F, Brunengraber H. 1994. Reversibility of the mitochondrial isocitrate dehydrogenase reaction in the perfused rat liver. Evidence from isotopomer analysis of citric acid cycle intermediates. Journal of Biological Chemistry 269(44):27179-27182.

Deshpande R, Yang TH, Heinzle E. 2009. Towards a metabolic and isotopic steady state in CHO batch cultures for reliable isotope-based metabolic profiling. Biotechnol J 4(2):247-263.

Deshpande RR. 2007. Mammalian Cell Culture: High Throughput Applications of Oxygen Sensor Plates and Cellular Physiological Studies Using 13C-Labeling. Saarbrücken: Saarbrücken.

Deshpande RR, Heinzle E. 2004. On-line oxygen uptake rate and culture viability measurement of animal cell culture using microplates with integrated oxygen sensors. Biotechnology Letters 26(9):763-767.

Deshpande RR, Koch-Kirsch Y, Maas R, John GT, Krause C, Heinzle E. 2005. Microplates with integrated oxygen sensors for kinetic cell respiration measurement and cytotoxicity testing in primary and secondary cell lines. Assay and Drug Developement Technologies 3(3):299-307.

Deshpande RR, Wittmann C, Heinzle E. 2004. Microplates with integrated oxygen sensing for medium optimization in animal cell culture. Cytotechnology 46(1):1-8.

DiMasi JA, Hansen RW, Grabowski HG. 2003. The price of innovation: new estimates of drug development costs. Journal of Health Economics 22(2):151-185.

Doyle A, Griffiths J. 1997. Mammalian Cell Culture. Rickwood D, editor. Chichester, UK: Hohn Wiley & Sons.

Duan Y, Catana A, Meng Y, Yamamoto N, He S, Gupta S, Gambhir SS, Zern MA. 2007. Differentiation and enrichment of hepatocyte-like cells from human embryonic stem cells *in vitro* and *in vivo*. Stem Cells 25(12):3058-3068.

Duan Y, Ma X, Zou W, Wang C, Bahbahan IS, Ahuja TP, Tolstikov V, Zern MA. 2010. Differentiation and characterization of metabolically functioning hepatocytes from human embryonic stem cells. Stem Cells 28(4):674-686.

Ek M, Soderdahl T, Kuppers-Munther B, Edsbagge J, Andersson TB, Bjorquist P, Cotgreave I, Jernstrom B, Ingelman-Sundberg M, Johansson I. 2007. Expression of drug metabolizing enzymes in hepatocyte-like cells derived from human embryonic stem cells. Biochemical Pharmacology 74(3):496-503.

Floby E, Briem S, Terelius Y, Sohlenius-Sternbeck AK. 2004. Use of a cocktail of probe substrates for drug-metabolizing enzymes for the assessment of the metabolic capacity of hepatocyte preparations. Xenobiotica 34(11-12):949-959.

Flomenbaum NE, Goldfrank LR, Hoffmann RS, Howland MA, Lewin NA, Nelson LS. 2006. Goldfranks's Toxicologic Emergencies - 8th Ed. (2006). New York: The McGraw-Hill Companies, Inc.

REFERENCES

Follstad BD, Balcarcel RR, Stephanopoulos G, Wang DI. 1999. Metabolic flux analysis of hybridoma continuous culture steady state multiplicity. Biotechnol Bioeng 63(6):675-683.

Follstad BD, Stephanopoulos G. 1998. Effect of reversible reactions on isotope label redistribution--analysis of the pentose phosphate pathway. European Journal of Biochemistry 252(3):360-371.

Furch T, Preusse M, Tomasch J, Zech H, Wagner-Dobler I, Rabus R, Wittmann C. 2009. Metabolic fluxes in the central carbon metabolism of Dinoroseobacter shibae and Phaeobacter gallaeciensis, two members of the marine Roseobacter clade. BMC Microbiol 9:209.

Gareth JS, David CH, In-Hyun P, Judy F, Zara H, Catherine MP, Donna D, James RB, James AR, Kay S, Gang W, George QD, Je-Hyuk L, George MC, Stuart JF, John PI, Ian W. 2009. Generation of functional human hepatic endoderm from human induced pluripotent stem cells. Hepatology 9999(9999):NA.

Genolet R, Kersten S, Braissant O, Mandard S, Tan NS, Bucher P, Desvergne B, Michalik L, Wahli W. 2005. Promoter rearrangements cause species-specific hepatic regulation of the glyoxylate reductase/hydroxypyruvate reductase gene by the peroxisome proliferator-activated receptor alpha. J Biol Chem 280(25):24143-24152.

Gepstein L. 2002. Derivation and potential applications of human embryonic stem cells. Circulation Research 91(10):866-876.

Giron MC, Portolan S, Bin A, Mazzi U, Cutler CS. 2008. Cytochrome P450 and radiopharmaceutical metabolism. Quarterly Journal of Nuclear Medicine and Molecular Imaging 52(3):254-266.

Goel A, Ferrance J, Jeong J, Ataai MM. 1993. Analysis of metabolic fluxes in batch and continuous cultures of Bacillus subtilis. Biotechnology and Bioengineering 42(6):686-696.

Gomez-Lechon MJ, Ponsoda X, Bort R, Castell JV. 2001. The use of cultured hepatocytes to investigate the metabolism of drugs and mechanisms of drug hepatotoxicity. Alternatives to Laboratory Animals 29(3):225-231.

Gould GW, Holman GD. 1993. The Glucose-Transporter Family - Structure, Function and Tissue-Specific Expression. Biochemical Journal 295:329-341.

Grillo MP, Knutson CG, Sanders PE, Waldon DJ, Hua F, Ware JA. 2003. Studies on the chemical reactivity of diclofenac acyl glucuronide with glutathione: Identification of diclofenac-S-acyl-glutathione in rat bile. Drug Metabolism and Disposition 31(11):1327-1336.

Guillouzo A. 1998a. Liver cell models in in vitro toxicology. Environ Health Perspect 106 Suppl 2:511-532.

Guillouzo A. 1998b. Liver cell models in *in vitro* toxicology. Environmental Health Perspectives 106 Suppl 2:511-532.

Guo L, Zhang L, Sun Y, Muskhelishvili L, Blann E, Dial S, Shi L, Schroth G, Dragan YP. 2006. Differences in hepatotoxicity and gene expression profiles by anti-diabetic PPAR gamma agonists on rat primary hepatocytes and human HepG2 cells. Molecular Diversities 10(3):349-360.

Guzzardi MA, Vozzi F, Ahaluwalia AD. 2009. Study of the cross-talk between hepatocytes and endothelial cells using a novel multi-compartmental bioreactor: a comparison between connected cultures and co-cultures. Tissue Engineering Part A.

Haridass D, Narain N, Ott M. 2008. Hepatocyte transplantation: waiting for stem cells. Current Opinion in Organ Transplantation 13(6):627-632.

REFERENCES

Harrigan GG, Colca J, Szalma S, Boros LG. 2006. PNU-91325 increases fatty acid synthesis from glucose and mitochondrial long chain fatty acid degradation: a comparative tracer-based metabolomics study with rosiglitazone and pioglitazone in HepG2 cells. Metabolomics 2(1):21-29.

Hasan NM, Longacre MJ, Stoker SW, Boonsaen T, Jitrapakdee S, Kendrick MA, Wallace JC, MacDonald MJ. 2008. Impaired Anaplerosis and Insulin Secretion in Insulinoma Cells Caused by Small Interfering RNA-mediated Suppression of Pyruvate Carboxylase. Journal of Biological Chemistry 283(42):28048-28059.

Haymond MW, Sunehag AL. 2000. The reciprocal pool model for the measurement of gluconeogenesis by use of [U-(13)C]glucose. American Journal of Physiology - Endocrinology And Metabolism 278(1):E140-145.

Heart E, Cline GW, Collis LP, Pongratz RL, Gray JP, Smith PJ. 2009. Role for malic enzyme, pyruvate carboxylation, and mitochondrial malate import in glucose-stimulated insulin secretion. American Journal of Physiology - Endocrinology And Metabolism 296(6):E1354-1362.

Heinloth AN, Irwin RD, Boorman GA, Nettesheim P, Fannin RD, Sieber SO, Snell ML, Tucker CJ, Li L, Travlos GS, Vansant G, Blackshear PE, Tennant RW, Cunningham ML, Paules RS. 2004. Gene expression profiling of rat livers reveals indicators of potential adverse effects. Toxicology Sciences 80(1):193-202.

Heinzle E. 2006. Metabolic Engineering. Angewandte Mikrobiologie. Berlin Heidelberg: Springer. p 217-235.

Hewitt NJ, Lloyd S, Hayden M, Butler R, Sakai Y, Springer R, Fackett A, Li AP. 2002. Correlation between troglitazone cytotoxicity and drug metabolic enzyme activities in cryopreserved human hepatocytes. Chem-Biol Interact 142(1-2):73-82.

House JD, Hall BN, Brosnan JT. 2001. Threonine metabolism in isolated rat hepatocytes. Am J Physiol Endocrinol Metab 281(6):E1300-1307.

Huber C, Klimant I, Krause C, Werner T, Wolfbeis OS. 2001. Nitrate-selective optical sensor applying a lipophilic fluorescent potential-sensitive dye. Analytica Chimica Acta 449(1-2):81-93.

Hyland R, Osborne T, Payne A, Kempshall S, Logan YR, Ezzeddine K, Jones B. 2009. In vitro and in vivo glucuronidation of midazolam in humans. British Journal of Clinical Pharmacology 67(4):445-454.

Hynes J, Floyd S, Soini AE, O'Connor R, Papkovsky DB. 2003. Fluorescence-based cell viability screening assays using water-soluble oxygen probes. Journal of Biomolecular Screening 8(3):264-272.

Hynes J, Marroquin LD, Ogurtsov VI, Christiansen KN, Stevens GJ, Papkovsky DB, Will Y. 2006. Investigation of drug-induced mitochondrial toxicity using fluorescence-based oxygen-sensitive probes. Toxicological Sciences 92(1):186-200.

Hynninen VV, Olkkola KT, Leino K, Lundgren S, Neuvonen PJ, Rane A, Valtonen M, Laine K. 2007. Effect of voriconazole on the pharmacokinetics of diclofenac. Fundamental & Clinical Pharmacology 21(6):651-656.

Itskovitz-Eldor J, Schuldiner M, Karsenti D, Eden A, Yanuka O, Amit M, Soreq H, Benvenisty N. 2000. Differentiation of human embryonic stem cells into embryoid bodies comprising the three embryonic germ layers. Molecular Medicine 6(2):88-95.

Javitt NB. 1990. Hep-G2 Cells as a Resource for Metabolic Studies - Lipoprotein, Cholesterol, and Bile-Acids. The Federation of American Societies for Experimental Biology 4(2):161-168.

REFERENCES

Jensen J, Hyllner J, Bjorquist P. 2009. Human embryonic stem cell technologies and drug discovery. Journal of Cellular Physiology 219(3):513-519.

Kamiya A, Nobuhiko K, Taisei K, Yasuyuki S, Atsushi M. 2002. Maturation of fetal hepatocytes *in vitro* by extracellular matrices and oncostatin M: Induction of tryptophan oxygenase. Hepatology 35(6):1351-1359.

Kanebratt KP, Andersson TB. 2008a. Evaluation of HepaRG cells as an in vitro model for human drug metabolism studies. Drug Metabolism and Disposition 36(7):1444-1452.

Kanebratt KP, Andersson TB. 2008b. HepaRG Cells as an in Vitro Model for Evaluation of Cytochrome P450 Induction in Humans. Drug Metabolism and Disposition 36(1):137-145.

Katsura N, Ikai I, Mitaka T, Shiotani T, Yamanokuchi S, Sugimoto S, Kanazawa A, Terajima H, Mochizuki Y, Yamaoka Y. 2002. Long-Term Culture of Primary Human Hepatocytes with Preservation of Proliferative Capacity and Differentiated Functions. Journal of Surgical Research 106(1):115-123.

Katz J, Tayek JA. 1999. Recycling of glucose and determination of the Cori Cycle and gluconeogenesis. American Journal of Physiology 277(3 Pt 1):E401-407.

Katz J, Wood HG. 1960. The Use of Glucose-C14 for the Evaluation of the Pathways of Glucose Metabolism. The Journal of Biological Chemistry 235(8):2165-2177.

Kaufmann P, Torok M, Hanni A, Roberts P, Gasser R, Krahenbuhl S. 2005. Mechanisms of benzarone and benzbromarone-induced hepatic toxicity. Hepatology 41(4):925-935.

Kaur G, Kaur J, Mittal N, Nath Sanyal S. 2010. The effect of prostaglandin synthase inhibitor, aspirin on the rat intestinal membrane structure and function. Nutr Hosp 25(2):290-298.

Kelleher JK. 1999. Estimating gluconeogenesis with [U-13C]glucose: molecular condensation requires a molecular approach. American Journal of Physiology - Endocrinology And Metabolism 277(3):E395-400.

Kemmelmeier FS, Bracht A. 1989. Effects of the nonsteroidal anti-inflammatory drug mefenamic acid on energy metabolism in the perfused rat liver. Biochemical Pharmacology 38(5):823-830.

Kensy F, John GT, Hofmann B, Buchs J. 2005. Characterisation of operation conditions and online monitoring of physiological culture parameters in shaken 24-well microtiter plates. Bioprocess and Biosystems Engineering 28(2):75-81.

Kinasiewicz AJ, Kawiak J, Werynski AJ. 2006. 3D Matrigel Culture Improves Differentiated Functions of HepG2 Cells *in Vitro*. Biocybernetics and Biomedical Engineering 26(4):47-55.

King C, Tang W, Ngui J, Tephly T, Braun M. 2001. Characterization of Rat and Human UDP-Glucuronosyltransferases Responsible for the in Vitro Glucuronidation of Diclofenac. Toxicological Sciences 61(1):49-53.

King MA. 2000. Detection of dead cells and measurement of cell killing by flow cytometry. Journal of Immunological Methods 243(1-2):155-166.

Klein HH, Ullmann S, Drenckhan M, Grimmsmann T, Unthan-Fechner K, Probst I. 2002. Differential modulation of insulin actions by dexamethasone: studies in primary cultures of adult rat hepatocytes. Journal of Hepatology 37(4):432-440.

Klieber S, Hugla S, Ngo R, Arabeyre-Fabre C, Meunier V, Sadoun F, Fedeli O, Rival M, Bourrie M, Guillou F, Maurel P, Fabre G. 2008. Contribution of the N-glucuronidation pathway to the overall in vitro metabolic clearance of midazolam in humans. Drug Metabolism and Disposition 36(5):851-862.

REFERENCES

Klimant I, Wolfbeis OS. 1995. Oxygen-Sensitive Luminescent Materials Based on Silicone-Soluble Ruthenium Diimine Complexes. Analytical Chemistry 67(18):3160-3166.

Klover PJ, Mooney RA. 2004. Hepatocytes: critical for glucose homeostasis. International Journal of Biochemistry & Cell Biology 36(5):753-758.

Kocincova AS, Nagl S, Arain S, Krause C, Borisov SM, Arnold M, Wolfbeis OS. 2008. Multiplex bacterial growth monitoring in 24-well microplates using a dual optical sensor for dissolved oxygen and pH. Biotechnology and Bioengineering 100(3):430-438.

Kola I, Landis J. 2004. Can the pharmaceutical industry reduce attrition rates? Nature Reviews Drug Discovery 3(8):711-715.

Kostrubsky VE, Sinclair JF, Ramachandran V, Venkataramanan R, Wen YH, Kindt E, Galchev V, Rose K, Sinz M, Strom SC. 2000. The role of conjugation in hepatotoxicity of troglitazone in human and porcine hepatocyte cultures. Drug Metabolism and Disposition 28(10):1192-1197.

Kovacevic Z, Brkljac O, Bajin K. 1991. Control and function of the transamination pathways of glutamine oxidation in tumour cells. Biochemical Journal 273(Pt 2):271-275.

Kovacevic Z, McGivan JD. 1983. Mitochondrial metabolism of glutamine and glutamate and its physiological significance. Physiological Reviews 63(2):547-605.

Kumar S, Wittmann C, Heinzle E. 2004. Minibioreactors. Biotechnolology Letters 26(1):1-10.

Landau BR, Wahren J, Ekberg K, Previs SF, Yang D, Brunengraber H. 1998. Limitations in estimating gluconeogenesis and Cori cycling from mass isotopomer distributions using [U-13C6]glucose. American Journal of Physiology 274(5 Pt 1):E954-961.

Lavon N, Ofra Y, Nissim B. 2004. Differentiation and isolation of hepatic-like cells from human embryonic stem cells. Differentiation 72(5):230-238.

Lee JB, Lee JE, Park JH, Kim SJ, Kim MK, Roh SI, Yoon HS. 2005. Establishment and maintenance of human embryonic stem cell lines on human feeder cells derived from uterine endometrium under serum-free condition. Biology of Reproduction 72(1):42-49.

Lee K, Berthiaume F, Stephanopoulos GN, Yarmush DM, Yarmush ML. 2000. Metabolic Flux Analysis of Postburn Hepatic Hypermetabolism. Metabolic Engineering 2(4):312-327.

Lee WN, Boros LG, Puigjaner J, Bassilian S, Lim S, Cascante M. 1998. Mass isotopomer study of the nonoxidative pathways of the pentose cycle with [1,2-13C2]glucose. American Journal of Physiology 274(5 Pt 1):E843-851.

Li AP. 2001. Screening for human ADME/Tox drug properties in drug discovery. Drug Discovery Today 6(7):357-366.

Li AP. 2005. Preclinical in vitro screening assays for drug-like properties. Drug Discovery Today: Technologies 2(2):179-185.

Li AP. 2007. Human hepatocytes: Isolation, cryopreservation and applications in drug development. Chem-Biol Interact 168(1):16-29.

Li J, Ning G, Duncan SA. 2000. Mammalian hepatocyte differentiation requires the transcription factor HNF-4alpha. Genes & Development 14(4):464-474.

Li L, Sharma N, Chippada U, Jiang X, Schloss R, Yarmush ML, Langrana NA. 2008. Functional modulation of ES-derived hepatocyte lineage cells via substrate compliance alteration. Annals of Biomedical Engineering 36(5):865-876.

Liang JF, Akaike T. 1997. Dimethyl sulfoxide induces multilayer aggregates and prolongs survival of primary cultured hepatocytes. Biotechnology Techniques 11(12):869-872.

Lim MS, Lim PL, Gupta R, Boelsterli UA. 2006. Critical role of free cytosolic calcium, but not uncoupling, in mitochondrial permeability transition and cell death induced by diclofenac

REFERENCES

oxidative metabolites in immortalized human hepatocytes. Toxicology and Applied Pharmacology 217(3):322-331.

Livak KJ, Schmittgen TD. 2001. Analysis of Relative Gene Expression Data Using Real-Time Quantitative PCR and the 2-[Delta][Delta]CT Method. Methods 25(4):402-408.

Loi CM, Young M, Randinitis E, Vassos A, Koup JR. 1999. Clinical pharmacokinetics of troglitazone. Clinical Pharmacokinetics 37(2):91-104.

Lu D, Mulder H, Zhao P, Burgess SC, Jensen MV, Kamzolova S, Newgard CB, Sherry AD. 2002. 13C NMR isotopomer analysis reveals a connection between pyruvate cycling and glucose-stimulated insulin secretion (GSIS). Proceedings of the National Academy of Sciences of the United States of America 99(5):2708-2713.

Magnusson I, Chandramouli V, Schumann WC, Kumaran K, Wahren J, Landau BR. 1988. Pentose Pathway in Human Liver. Proceedings of the National Academy of Sciences 85(13):4682-4685.

Maier K. 2009. Systems Oriented Analyses of Hepatic 13C Labeling and Metabolite Dynamics Stuttgart: Stuttgart.

Malaisse WJ, Ladriere L, Zhang TM, Verbruggen I, Willem R. 1996. Enzyme-to-enzyme channelling of symmetric Krebs cycle intermediates in pancreatic islet cells. Diabetologia 39(8):990-992.

Mao CS, Bassilian S, Lim SK, Lee WN. 2002. Underestimation of gluconeogenesis by the [U-(13)C(6)]glucose method: effect of lack of isotope equilibrium. American Journal of Physiology, Endocrinology and Metabolism 282(2):E376-385.

Marín-Sanguino A, Torres NV. 2000. Optimization of Tryptophan Production in Bacteria. Design of a Strategy for Genetic Manipulation of the Tryptophan Operon for Tryptophan Flux Maximization. Biotechnology Progress 16(2):133-145.

Martens DE. 2007. Metabolic Flux Analysis of Mammalian Cells Systems Biology: Springer Netherlands. p 275-299.

Martin A, Clynes M. 1993. Comparison of 5 Microplate Colorimetric Assays for Invitro Cytotoxicity Testing and Cell-Proliferation Assays. Cytotechnology 11(1):49-58.

Masubuchi Y. 2006. Metabolic and non-metabolic factors determining troglitazone hepatotoxicity: a review. Drug Metabolism and Pharmacokinetics 21(5):347-356.

Masubuchi Y, Kano S, Horie T. 2006. Mitochondrial permeability transition as a potential determinant of hepatotoxicity of antidiabetic thiazolidinediones. Toxicology 222(3):233-239.

Masubuchi Y, Saito H, Horie T. 1998. Structural requirements for the hepatotoxicity of nonsteroidal anti-inflammatory drugs in isolated rat hepatocytes. Journal of Pharmacology and Experimental Therapeutics 287(1):208-213.

Masubuchi Y, Shintaro N, Toshiharu H. 2002. Role of mitochondrial permeability transition in diclofenac-induced hepatocyte injury in rats. Hepatology 35(3):544-551.

Masubuchi Y, Yamada S, Horie T. 2000. Possible mechanism of hepatocyte injury induced by diphenylamine and its structurally related nonsteroidal anti-inflammatory drugs. Journal of Pharmacology and Experimental Therapeutics 292(3):982-987.

Mavri-Damelin D, Damelin LH, Eaton S, Rees M, Selden C, Hodgson HJ. 2008a. Cells for bioartificial liver devices: the human hepatoma-derived cell line C3A produces urea but does not detoxify ammonia. Biotechnology and Bioengineering 99(3):644-651.

Mavri-Damelin D, Damelin LH, Eaton S, Rees M, Selden C, Hodgson HJ. 2008b. Cells for bioartificial liver devices: the human hepatoma-derived cell line C3A produces urea but does not detoxify ammonia. Biotechnol Bioeng 99(3):644-651.

REFERENCES

McCarthy TC, Pollak PT, Hanniman EA, Sinal CJ. 2004. Disruption of hepatic lipid homeostasis in mice after amiodarone treatment is associated with peroxisome proliferator-activated receptor-alpha target gene activation. Journal of Pharmacology and Experimental Therapeutics 311(3):864-873.

Mehta N, OZick L, Gbadehan E. 2008. Drug-Induced Hepatotoxicity. emedicine.

Michal G. 1999. Biochemical Pathways. Heidelberg . Berlin: Spektrum Akademischer Verlag.

Miret S, De Groene EM, Klaffke W. 2006. Comparison of *in vitro* assays of cellular toxicity in the human hepatic cell line HepG2. Journal of Biomolecular Screening 11(2):184-193.

Moreno-Sánchez R, Bravo C, Vásquez C, Ayala G, Silveira LH, Martínez-Lavín M. 1999. Inhibition and uncoupling of oxidative phosphorylation by nonsteroidal anti-inflammatory drugs: Study in mitochondria, submitochondrial particles, cells, and whole heart. Biochemical Pharmacology 57(7):743-752.

Morris GJ, Warburton S, West CML, Al-Rubeai M, Clark JB, Simione F, Doyle A. 1997. Core techniques:, In: Doyle A and Griffiths JB (eds) Mammalian Cell Culture: Essential Techniques.

Mortensen AS, Arukwe A. 2006. Dimethyl sulfoxide is a potent modulator of estrogen receptor isoforms and xenoestrogen biomarker responses in primary culture of salmon hepatocytes. Aquatic Toxicology 79(1):99-103.

Nagata M, Ichiyama A, Takayama T, Oda T, Mugiya S, Ozono S. 2009. Assay of alanine:glyoxylate aminotransferase in human liver by its serine: glyoxylate aminotransferase activity. Biomed Res 30(5):295-301.

Nahmias Y, Kramvis Y, Barbe L, Casali M, Berthiaume F, Yarmush ML. 2006. A novel formulation of oxygen-carrying matrix enhances liver-specific function of cultured hepatocytes. Faseb Journal 20(14):2531-+.

Neermann J, Wagner R. 1996. Comparative analysis of glucose and glutamine metabolism in transformed mammalian cell lines, insect and primary liver cells. Journal of Cellular Physiology 166(1):152-169.

Ngui JS, Tang W, Stearns RA, Shou M, Miller RR, Zhang Y, Lin JH, Baillie TA. 2000. Cytochrome P450 3A4-mediated interaction of diclofenac and quinidine. Drug Metabolism and Disposition 28(9):1043-1050.

Nielsen J. 1998. Metabolic engineering: Techniques for analysis of targets for genetic manipulations. Biotechnology and Bioengineering 58(2-3):125-132.

Niklas J, Noor F, Heinzle E. 2009. Effects of drugs in subtoxic concentrations on the metabolic fluxes in human hepatoma cell line Hep G2. Toxicology and Applied Pharmacology 240(3):327-336.

Nociari MM, Shalev A, Benias P, Russo C. 1998. A novel one-step, highly sensitive fluorometric assay to evaluate cell-mediated cytotoxicity. Journal of Immunological Methods 213(2):157-167.

Noh K, Wiechert W. 2006. Experimental design principles for isotopically instationary 13C labeling experiments. Biotechnology and Bioengineering 94(2):234-251.

Noor F, Niklas J, Muller-Vieira U, Heinzle E. 2009. An integrated approach to improved toxicity prediction for the safety assessment during preclinical drug development using Hep G2 cells. Toxicology and Applied Pharmacology 237(2):221-231.

Nussler AK, Wang A, Neuhaus P, Fischer J, Yuan J, Liu L, Zeilinger K, Gerlach J, Arnold PJ, Albrecht W. 2001. The suitability of hepatocyte culture models to study various aspects of drug metabolism. Altex 18(2):91-101.

O'Brien PJ, Irwin W, Diaz D, Howard-Cofield E, Krejsa CM, Slaughter MR, Gao B, Kaludercic N, Angeline A, Bernardi P, Brain P, Hougham C. 2006. High concordance of drug-induced human hepatotoxicity with *in vitro* cytotoxicity measured in a novel cell-based model using high content screening. Archives of Toxicology 80(9):580-604.

O'Connor N, Dargan PI, Jones AL. 2003. Hepatocellular damage from non-steroidal anti-inflammatory drugs. Quarterly Journal of Medicine 96(11):787-791.

O'Riordan TC, Buckley D, Ogurtsov V, O'Connor R, Papkovsky DB. 2000. A cell viability assay based on monitoring respiration by optical oxygen sensing. Analytical Biochemistry 278(2):221-227.

Owen OE, Kalhan SC, Hanson RW. 2002. The Key Role of Anaplerosis and Cataplerosis for Citric Acid Cycle Function. Journal of Biological Chemistry 277(34):30409-30412.

Papkovsky DB, Hynes J, Will Y. 2006. Respirometric screening technology for ADME-Tox studies. Expert Opinion on Drug Metabolism & Toxicology 2(2):313-323.

Park BK, Kitteringham NR, Maggs JL, Pirmohamed M, Williams DP. 2005. The role of metabolic activation in drug-induced hepatotoxicity. Annual Review of Pharmacology and Toxicology 45(1):177-202.

Pauwels B, Korst AEC, de Pooter CMJ, Pattyn GGO, Lambrechts HAJ, Baay MFD, Lardon F, Vermorken JB. 2003. Comparison of the sulforhodamine B assay and the clonogenic assay for in vitro chemoradiation studies. Cancer Chemotherapy and Pharmacology 51(3):221-226.

Pereira DA, Williams JA. 2007. Origin and evolution of high throughput screening. British Journal of Pharmacology 152(1):53-61.

Petrescu I, Tarba C. 1997. Uncoupling effects of diclofenac and aspirin in the perfused liver and isolated hepatic mitochondria of rat. Biochimica et Biophysica Acta 1318(3):385-394.

Peuhkurinen KJ, Hiltunen JK, Hassinen IE. 1983. Metabolic compartmentation of pyruvate in the isolated perfused rat heart. Biochem J 210(1):193-198.

Pfandler M-AS, Hochli M, Inderbitzin D, Meier PJ, Stieger B. 2004. Small hepatocytes in culture develop polarized transporter expression and differentiation. Journal of Cell Science 117(18):4077-4087.

Polasek TM, Elliot DJ, Miners JO. 2006. Measurement of Human Cytochrome P4501A2 (CYP1A2) Activity *In Vitro*. Current Protocols in Toxicology February, 2006.

Poon GK, Chen Q, Teffera Y, Ngui JS, Griffin PR, Braun MP, Doss GA, Freeden C, Stearns RA, Evans DC, Baillie TA, Tang W. 2001. Bioactivation of diclofenac via benzoquinone imine intermediates-identification of urinary mercapturic acid derivatives in rats and humans. Drug Metabolism and Disposition 29(12):1608-1613.

Porter SN, Howarth GS, Butler RN. 2000. Non-steroidal anti-inflammatory drugs and apoptosis in the gastrointestinal tract: potential role of the pentose phosphate pathways. European Journal of Pharmacology 397(1):1-9.

Provost A, Bastin G. 2004. Dynamic metabolic modelling under the balanced growth condition. Journal of Process Control 14(7):717-728.

Radziuk J, Lee WP. 1999. Measurement of gluconeogenesis and mass isotopomer analysis based on [U-(13)C]glucose. American Journal of Physiology 277(2 Pt 1):E199-207.

Rantanen A, Rousu J, Jouhten P, Zamboni N, Maaheimo H, Ukkonen E. 2008. An analytic and systematic framework for estimating metabolic flux ratios from C-13 tracer experiments. Bmc Bioinformatics 6(9):266.

Rehm H, Hammar F. 2008. Biochemie light. Frankfurz am Main: Harry Deutsch GmbH.

REFERENCES

Reitzer LJ, Wice BM, Kennell D. 1979. Evidence that glutamine, not sugar, is the major energy source for cultured HeLa cells. Journal of Biological Chemistry 254(8):2669-2676.

Rodriguez-Antona C, Donato MT, Boobis A, Edwards RJ, Watts PS, Castell JV, Gomez-Lechon MJ. 2002. Cytochrome P450 expression in human hepatocytes and hepatoma cell lines: molecular mechanisms that determine lower expression in cultured cells. Xenobiotica 32(6):505-520.

Rubinstein LV, Shoemaker RH, Paull KD, Simon RM, Tosini S, Skehan P, Scudiero DA, Monks A, Boyd MR. 1990. Comparison of *In vitro* Anticancer-Drug-Screening Data Generated with a Tetrazolium Assay Versus a Protein Assay against a Diverse Panel of Human Tumor-Cell Lines. Journal of the National Cancer Institute 82(13):1113-1118.

Ruepp SU, Tonge RP, Shaw J, Wallis N, Pognan F. 2002. Genomics and proteomics analysis of acetaminophen toxicity in mouse liver. Toxicological Sciences 65(1):135-150.

Ryan JA. 2008. Introduction to animal cell culture. Lowell (MA): Corning Incorporated Life Sciences.

Sancho-Bru P, Najimi M, Caruso M, Pauwelyn K, Cantz T, Forbes S, Roskams T, Ott M, Gehling U, Sokal E, Verfaillie CM, Muraca M. 2009. Stem and progenitor cells for liver repopulation: can we standardise the process from bench to bedside? Gut 58(4):594-603.

Schlupen C, Santos MA, Weber U, de Graaf A, Revuelta JL, Stahmann KP. 2003. Disruption of the SHM2 gene, encoding one of two serine hydroxymethyltransferase isoenzymes, reduces the flux from glycine to serine in Ashbya gossypii. Biochem J 369(Pt 2):263-273.

Schmidt K, Carlsen M, Nielsen J, Villadsen J. 1997. Modeling isotopomer distributions in biochemical networks using isotopomer mapping matrices. Biotechnology and Bioengineering 55(6):831-840.

Schmitz S. 2007. Zellkultur. 1. ed. München, Germany: Elsevier GmbH, München.

Schrenkhammer P. 2008. New Optical Biosensors for Uric Acid and Glucose. Regensburg: Universität Regensburg.

Schröder CR. 2006. Luminescent Planar Single and Dual Optodes for Time-Resolved Imaging of pH, pCO2 and pO2 in Marine Systems. Regensburg: Universität Regensburg.

Schuster D, Laggner C, Langer T. 2005. Why drugs fail - A study on side effects in new chemical entities. Current Pharmaceutical Design 11(27):3545-3559.

Seglen PO. 1976. Preparation of isolated rat liver cells. Methods in Cell Biology 13:29-83.

Seitz S, Boelsterli UA. 1998. Diclofenac acyl glucuronide, a major biliary metabolite, is directly involved in small intestinal injury in rats. Gastroenterology 115(6):1476-1482.

Seitz S, Kretz-Rommel A, Elferink RPJO, Boelsterli UA. 1998. Selective protein adduct formation of diclofenac glucuronide is critically dependent on the rat canalicular conjugate export pump (Mrp2). Chemical Research in Toxicology 11(5):513-519.

Sherry AD, Jeffrey FMH, Malloy CR. 2004. Analytical solutions for ^{13}C isotopomer analysis of complex metabolic conditions: substrate oxidation, multiple pyruvate cycles, and gluconeogenesis. Metabolic Engineering 6(1):12-24.

Sherry AD, Sumegi B, Miller B, Cottam GL, Gavva S, Jones JG, Malloy CR. 1994. Orientation-conserved transfer of symmetric Krebs cycle intermediates in mammalian tissue. Biochemistry 33(20):6268-6275.

Sibson NR, Mason GF, Shen J, Cline GW, Herskovits AZ, Wall JM, Behar KL, Rothman DL, Shulman RG. 2001. In vivo13C NMR measurement of neurotransmitter glutamate cycling, anaplerosis and TCA cycle flux in rat brain during [2-13C]glucose infusion. Journal of Neurochemistry 76(4):975-989.

REFERENCES

Skehan P, Storeng R, Scudiero D, Monks A, McMahon J, Vistica D, Warren JT, Bokesch H, Kenney S, Boyd MR. 1990. New colorimetric cytotoxicity assay for anticancer-drug screening. Journal of National Cancer Institute 82(13):1107-1112.

Slater K. 2001. Cytotoxicity tests for high-throughput drug discovery. Current Opinion in Biotechnology 12(1):70-74.

Snykers S, De Kock J, Rogiers V, Vanhaecke T. 2009. In vitro differentiation of embryonic and adult stem cells into hepatocytes: state of the art. Stem Cells 27(3):577-605.

Soderdahl T, Kuppers-Munther B, Heins N, Edsbagge J, Bjorquist P, Cotgreave I, Jernstrom B. 2007. Glutathione transferases in hepatocyte-like cells derived from human embryonic stem cells. Toxicology In Vitro 21(5):929-937.

Soto-Gutierrez A, Basma H, Navarro-Alvarez N, Uygun B, Yarmush M, Kobayashi N, Fox I. 2008. Differentiating stem cells into liver. Biotechnology and Genetic Engineering Reviews 25:149-164.

Spaniol M, Bracher R, Ha HR, Follath F, Krahenbuhl S. 2001. Toxicity of amiodarone and amiodarone analogues on isolated rat liver mitochondria. Journal of Hepatology 35(5):628-636.

Stark R, Pasquel F, Turcu A, Pongratz RL, Roden M, Cline GW, Shulman GI, Kibbey RG. 2009. Phosphoenolpyruvate cycling via mitochondrial phosphoenolpyruvate carboxykinase links anaplerosis and mitochondrial GTP with insulin secretion. Journal of Biological Chemistry 284(39):26578-26590.

Stephanopoulos G. 1999. Metabolic Fluxes and Metabolic Engineering. Metabolic Engineering 1(1):1-11.

Stephanopoulos G, Aristidou AA, Nielsen JH. 1998. Metabolic engineering : Principles and Methodologies. San Diego: Academic Press.

Stumvoll M, Perriello G, Meyer C, Gerich J. 1999. Role of glutamine in human carbohydrate metabolism in kidney and other tissues. Kidney International 55(3):778-792.

Sumegi B, Sherry AD, Malloy CR. 1990. Channeling of TCA cycle intermediates in cultured Saccharomyces cerevisiae. Biochemistry 29(39):9106-9110.

Swagell CD, Morris CP, Henly DC. 2006. Effect of fatty acids, glucose, and insulin on hepatic glucose uptake and glycolysis. Nutrition 22(6):672-678.

Szafranek J, Pfaffenberger CD, Horning EC. 1974. The mass spectra of some per-O-acetylaldononitriles. Carbohydrate Research 38:97-105.

Tanaka Y, Yoshikawa M, Kobayashi Y, Kuroda M, Kaito M, Shiroi A, Yamao J-i, Fukui H, Ishizaka S, Adachi Y. 2003. Expressions of hepatobiliary organic anion transporters and bilirubin-conjugating enzyme in differentiating embryonic stem cells. Biochemical and Biophysical Research Communications 309(2):324-330.

Tang W, Stearns RA, Bandiera SM, Zhang Y, Raab C, Braun MP, Dean DC, Pang J, Leung KH, Doss GA, Strauss JR, Kwei GY, Rushmore TH, Chiu SH, Baillie TA. 1999. Studies on cytochrome P-450-mediated bioactivation of diclofenac in rats and in human hepatocytes: identification of glutathione conjugated metabolites. Drug Metabolism and Disposition 27(3):365-372.

Tanimizu N, Miyajima A, Mostov KE. 2007. Liver progenitor cells develop cholangiocyte-type epithelial polarity in three-dimensional culture. Molecular Biology of the Cell 18(4):1472-1479.

Thews EM, Vaupel P.:. 1999. Anatomie, Physiologie, Pathophysiologie des Menschen. 5. Auflage ed. Stuttgart: Wissenschaftliche Verlagsgesellschaft GmbH.

Thibault N, Claude JR, Ballet F. 1992. Actin filament alteration as a potential marker for cholestasis: a study in isolated rat hepatocyte couplets. Toxicology 73(3):269-279.

Thomson JA, Itskovitz-Eldor J, Shapiro SS, Waknitz MA, Swiergiel JJ, Marshall VS, Jones JM. 1998. Embryonic stem cell lines derived from human blastocysts. Science 282(5391):1145-1147.

Tirmenstein MA, Hu CX, Gales TL, Maleeff BE, Narayanan PK, Kurali E, Hart TK, Thomas HC, Schwartz LW. 2002. Effects of troglitazone on HepG2 viability and mitochondrial function. Toxicological Sciences 69(1):131-138.

Touboul T, Nicholas RFH, Sébastien C, Amélie M, Clémence M, Sophie B, Sylvie M, Hélène S-M, Roger P, James Di S, Anne W, Ludovic V. 2010. Generation of functional hepatocytes from human embryonic stem cells under chemically defined conditions that recapitulate liver development. Hepatology 51(5):1754-1765.

Toyoda Y, Tsuchida A, Iwami E, Miwa I. 2001. Toxic effect of troglitazone on cultured rat hepatocytes. Life Sciences 68(16):1867-1876.

Tzanakakis ES, Hess DJ, Sielaff TD, Hu WS. 2000. Extracorporeal tissue engineered liver-assist devices. Annual Review of Biomedical Engineering 2:607-632.

Uehara T, Kiyosawa N, Shimizu T, Omura K, Hirode M, Imazawa T, Mizukawa Y, Ono A, Miyagishima T, Nagao T, Urushidani T. 2008. Species-specific differences in coumarin-induced hepatotoxicity as an example toxicogenomics-based approach to assessing risk of toxicity to humans. Human and Experimental Toxicology 27(1):23-35.

Vallino JJ, Stephanopoulos G. 1993. Metabolic flux distributions in Corynebacterium glutamicum during growth and lysine overproduction. Biotechnology and Bioengineering 67(6):872-885.

Van der Valk J. 2004. The humane collection of fetal bovine serum and possibilities for serum-free cell and tissue culture. Toxicol In Vitro(18):1-12.

Verma P, Verma V, Ray P, Ray AR. 2007. Formation and characterization of three dimensional human hepatocyte cell line spheroids on chitosan matrix for in vitro tissue engineering applications. In Vitro Cellular & Developmental Biology - Animal 43(10):328-337.

Vesey DA, Cunningham JM, Selden AC, Woodman AC, Hodgson HJF. 1991. Dimethyl-Sulfoxide Induces a Reduced Growth-Rate, Altered Cell Morphology and Increased Epidermal-Growth-Factor Binding in Hep G2 Cells. Biochemical Journal 277:773-777.

Viau CJ, Curren RD, Wallace K. 1993. Cytotoxicity of tacrine and velnacrine metabolites in cultured rat, dog and human hepatocytes. Drug and Chemical Toxicology 16(3):227-239.

Vichai V, Kirtikara K. 2006. Sulforhodamine B colorimetric assay for cytotoxicity screening. Nature Protocols 1(3):1112-1116.

Vickers AE. 2009. Tissue slices for the evaluation of metabolism-based toxicity with the example of diclofenac. Chemico-Biological Interactions 179(1):9-16

Waagepetersen H, Døring S, Schousboe A. 2008. Metabolism of [1,6-^{13}C]Glucose and [U-^{13}C]Glutamine and Depolarization Induced GABA Release in Superfused Mouse Cerebral Cortical Mini-slices. Neurochemical Research 33(8):1610-1617.

Wahl SA. 2002. Statistische Untersuchungen von Messmodellen für die Metabolische Stoffflussanalyse mit 13C Markierungsexperimenten. Dresden: Technische Universität Dresden.

Waldhauser KM, Torok M, Ha HR, Thomet U, Konrad D, Brecht K, Follath F, Krahenbuhl S. 2006. Hepatocellular toxicity and pharmacological effect of amiodarone and amiodarone derivatives. Journal of Pharmacology and Experimental Therapeutics 319(3):1413-1423.

REFERENCES

Wang AG, Xia T, Yuan J, Yu RA, Yang KD, Chen XM, Qu W, Waalkes MP. 2004a. Effects of phenobarbital on metabolism and toxicity of diclofenac sodium in rat hepatocytes in vitro. Food and Chemical Toxicology 42(10):1647-1653.

Wang K, Shindoh H, Inoue T, Horii I. 2002. Advantages of in vitro cytotoxicity testing by using primary rat hepatocytes in comparison with established cell lines. Journal of Toxicological Sciences 27(3):229-237.

Wang YJ, Liu HL, Guo HT, Wen HW, Liu J. 2004b. Primary hepatocyte culture in collagen gel mixture and collagen sandwich. World Journal of Gastroenteroly 10(5):699-702.

Wanson JC, Drochmans P, Mosselmans R, Ronveaux MF. 1977. Adult rat hepatocytes in primary monolayer culture. Ultrastructural characteristics of intercellular contacts and cell membrane differentiations. The Journal of Cell Biology 74(3):858-877.

Washizu T, Azakami D, Bonkobara M, Washizu M, Arai T. 2005. Changes in activities of enzymes related to energy metabolism in canine lymphoma cells. Journal of Veterinary Medical Science 67(6):615-616.

Westmacott A, Burke ZD, Oliver G, Slack JM, Tosh D. 2006. C/EBPalpha and C/EBPbeta are markers of early liver development. International Journal of Developmental Biology 50(7):653-657.

Wiechert W. 2001. ^{13}C metabolic flux analysis. Metabolic Engineering 3(3):195-206.

Wiechert W, de Graaf AA. 1997. Bidirectional reaction steps in metabolic networks: I. Modeling and simulation of carbon isotope labeling experiments. Biotechnology and Bioengineering 55(1):101-117.

Wiechert W, Noh K. 2005. From stationary to instationary metabolic flux analysis. Advances in Biochemical Engineering/Biotechnology 92:145-172.

Wilkening S, Stahl F, Bader A. 2003. Comparison of primary human hepatocytes and hepatoma cell line HEPG2 with regard to their biotransformation properties. Drug Metabolism and Disposition 31(8):1035-1042.

Wimmer M, Luttringer C, Colombi M. 1990. Enzyme activity patterns of phosphoenolpyruvate carboxykinase, pyruvate kinase, glucose-6-phosphate-dehydrogenase and malic enzyme in human liver. Histochemistry 93(4):409-415.

Wittmann C. 2002. Metabolic Flux Analysis Using Mass Spectrometry. Advances in Biochemical Engineering/Biotechnology-Springer-Verlag Berlin Heidelberg 2002 74.

Wittmann C. 2007. Fluxome analysis using GC-MS. Microbial Cell Factories 6(6).

Wittmann C, Heinzle E. 1999. Mass spectrometry for metabolic flux analysis. Biotechnology and Bioengineering 62(6):739-750.

Wodnicka M, Guarino RD, Hemperly JJ, Timmins MR, Stitt D, Pitner JB. 2000. Novel fluorescent technology platform for high throughput cytotoxicity and proliferation assays. Journal of Biomolecular Screening 5(3):141-152.

Xing JZ, Zhu L, Jackson JA, Gabos S, Sun XJ, Wang XB, Xu X. 2005. Dynamic monitoring of cytotoxicity on microelectronic sensors. Chemical Research in Toxicology 18(2):154-161.

Xu J, Purcell WM. 2006. Energy metabolism and biotransformation as endpoints to pre-screen hepatotoxicity using a liver spheroid model. Toxicology and Applied Pharmacology 216(2):293-302.

Xue H-H, Sakaguchi T, Fujie M, Ogawa H, Ichiyama A. 1999. Flux of the l-Serine Metabolism in Rabbit, Human, and Dog Livers. Journal of Biological Chemistry 274(23):16028-16033.

REFERENCES

Yan Z, Li J, Huebert N, Caldwell GW, Du Y, Zhong H. 2005. Detection of A Novel Reactive Metabolite of Diclofenac: Evidence for CYP2C9-mediated Bioactivation via Arene Oxides. Drug Metabolism and Disposition 33(6):706-713.

Yang H, Roth CM, Ierapetritou MG. 2009. A rational design approach for amino acid supplementation in hepatocyte culture. Biotechnology and Bioengineering 103(6):1176-1191.

Yoo H, Stephanopoulos G, Kelleher JK. 2004. Quantifying carbon sources for de novo lipogenesis in wild-type and IRS-1 knockout brown adipocytes. J Lipid Res 45(7):1324-1332.

Young JD, Jason LW, Maciek RA, Hyuntae Y, Gregory S. 2008. An elementary metabolite unit (EMU) based method of isotopically nonstationary flux analysis. Biotechnology and Bioengineering 99(3):686-699.

Zhu B, Bush D, Doss GA, Vincent S, Franklin RB, Xu SY. 2008. Characterization of 1 '-hydroxymidazolam glucuronidation in human liver microsomes. Drug Metabolism and Disposition 36(2):331-338.

Zitova A, O'Mahony FC, Cross M, Davenport J, Papkovsky DB. 2009. Toxicological profiling of chemical and environmental samples using panels of test organisms and optical oxygen respirometry. Environmental Toxicology 24(2):116-127.

Zupke C, Stephanopoulos G. 1994. Modeling of Isotope Distributions and Intracellular Fluxes in Metabolic Networks Using Atom Mapping Matrixes. Biotechnology Progress 10(5):489-498.

7 Appendix

7.1 Symbols and Abbreviations

A1AT	alpha-1-Antitrypsin
Phe	phenylalanine
#	pseudo inverse of a matrix
[O2]	concentration of oxygen
2D	two dimensions
3PG	3-phosphoglycerate
A	*m x n* stoichiometric matrix
AAM	atom mapping matrices
ABC	ATP-binding cassette
ABU	α-aminobutyric acid
ABU	α-aminobutyric acid
ACCoA	Acetyl-CoA
Acetyl-CoA	Acetyl-Coenzyme A
ADMET	Absorption, Distribution, Metabolism, Excretion and Toxicity
ADP	adenosine diphosphate
ADR	adverse drug reactions
AFP	α-Fetoprotein
Ala	alanine
ALB	albumin
ALT	alanine transaminase
ar(t)	m-dimensional metabolite accumulation rate vector
Arg	arginine
$ar_{met}(t)$	accumulation rate of metabolite met
ASCs	adult stem cells
Asn	asparagine
Asp	aspartic acid (aspartate)
AST	aspartate aminotransferase
AST	aspartate transaminase
ATP	adenosine-5'-triphosphate
AUC	area under the curve
BCAAs	branched-chain amino acids
bFGFs	basic fibroblast growth factors
BSA	bovine serum albumin
BSEP	bile-salt export pump
CIT	citrate
CK	cytokeratin

CYP450	cytochrome P450
Cys	cysteine
DMF	dimethylformamide
DMSO	dimethyl sulfoxide
DNA	deoxyribonucleic acid
DO	dissolved oxygen concentration
E4P	erythrose 4-phosphate
EBs	embryoid bodies
ECVAM	European Center for the Validation of Alternative Methods
EI	electron impact ionization
ELISA	enzyme-linked immunosorbent assay
EMU	elementary metabolite unit
ES cells	embryonic stem cells
EST	estrogen sulfotransferase
f	weighting factor
F6P	fructose 6-phosphate
FADH2	flavin adenine dinucleotide
FCS	fetal calf serum
FGF	fibroblast growth factor
FMOC	N-(9-fluorenyl) methoxycarbonyl
fmod	modulation frequency of the excitation light
G6PDH	glucose-6-phosphate dehydrogenase
GABA	γ-aminobutyrate
GAP	glyceraldehyde 3-phosphate
GC-MS	gas chromatography-mass spectroscopy
GCS	glycine cleavage system
Gln	glutamine
Glu	glutamic acid (glutamate)
GLUD	glutamate dehydrogenase
Gly	glycine
GNG	gluconeogenesis
GSH	glutathione
GST	gluthathione-S-transferase
h	hour
HCS	high content screening
hESC	human embryonic stem cells
HGF	hepatocyte growth factor
His	histidine
HK	hexokinase
HNF	hepatocyte nuclear factor
HTS	high throughput screening
HTS	high troughput screening
I	quenched luminescence intensity

II

I_0	unquenched luminescence intensity
ICM	inner cell mass
ICT	isocitrate
IDV	isotopomer distribution vector
IFCC	International Federation of Clinical Chemistry
Ile	isoleucine
IMM	isotopomer mapping matrice
IST	insulin-transferin-sodium selenite
KSV	Stern-Volmer constant
Lac	lactate
LC_{50}	lethal concentration, 50%
LCT	liver cell transplantation
LDA	low density array
LDH	lactate dehydrogenase
Leu	leucine
Lys	lysine
m	measurable reaction rates
m/z	mass to charge
MABs	monoclonal antibodies
MAPCs	multipotent adult progenitor cells
MAV	metabolite activity vector
MBDSTFA	N-(t-butyldimethylsilyl)-N-methyltrifluoroacetamide
MDH	malate dehydrogenase
MDH	malate dehydrogenase, malic enzyme
ME	molar enrichment
MEF	mouse embryonic fibroblast
MEF-CM	MEF-conditioned culture media
met	metabolite
Met	methionine
MFA	metabolic flux analysis
min	minute
mM	millimolar
MPT	mitochondrial permeability transition
MRM	multiple reaction monitoring
mRNA	mitochondrial RNA
MRP2	multidrug resistance protein 2
MS	mass spectrometry
MSCs	mesenchymal stem cells
MTHF	5,10-methylenetetrahydrofolate
MTP	microtiter plates
MTT	3-(4,5-Dimethylthiazol-2-yl)-2,5-diphenyltetrazolium bromide
MTX	methotrexate
NAC	N-acetylcysteine

NADH	nicotinamide adenine dinucleotide
NADPH	nicotinamide adenine dinucleotide phosphate
NAPQI	N-acetyl-p-benzoquinoneimine
NDA	new drug application
nm	non-measurable reaction rates
NMR	nuclear magnetic resonance
ns	nanosecond
NSAID	non steroidal anti inflammatory drugs
OAA	oxaloacetate
OPA	o-phtaldialdehyde
OSM	oncostatin M
OTC	ornithine transcarbamylase
PBS	phosphate buffered saline
PBST	PBS with 0.2 % Triton X-100
PC	pyruvate carboxylase
PCR	polymerase chain reaction
Pcyc	pentose cycle activity
PDC	pyruvate dehydrogenase complex
PDH	pyruvate dehydrogenase
PEP	phosphoenealpyruvate
PEPCK	phosphoenealpyruvate carboxykinase
PFA	paraformaldehyde
PH hepatocytes	primary human hepatocytes
PHH	primary human hepatocytes
PK	pyruvate kinase
pO_2	oxygen partial pressure
PPP	pentose phosphate pathway
PRH	primary rat hepatocytes
Pro	proline
PSS	pseudo-steady-state
PST	phenol sulfotransferase
PYK	pyruvate kinase
qRT-PCR	quantitative Real-Time PCR
rDNA	recombinant DNA
RI	refraction indexes
$r_{i,in(t)}$	flux towards the metabolite through reaction i
RNA	ribonucleic acid
$r_{o,out(t)}$	flux from the metabolite through reaction o
ROS	reactive oxygen species
RP-HPLC	reversed phase high performance liquid chromatography
s	stoichiometric coefficient
S7P	sedoheptulose 7-phosphate
SDR	SensorDish® Reader

SDS	sodium dodecyl sulphate
Ser	serine
SFL	summed fractional labeling
SHMT	serine hydroxymethyltransferase
SIM	selected ion monitoring
SRB	Sulforhodamine B
SRM	selected reaction monitoring
ST	sub-toxic concentration
STREP	Specific Target Research Project
T	transpose of a matrix
TA	transaldolase
TCA	tricarboxylic acid
TCA	trichloroacetic acid
THF	tetrahydrofolate
Thr	threonine
TK	transketolase
TO	tyrosine oxygenase
TP	triose phosphate
Trp	tryptophan
Tyr	tyrosine
UDP	uridine diphosphate
UGT	UDP -dependent glucuronosyl transferase
UV	ultraviolet
Val	valine
w/o	without
WME	Williams Medium E
WST-1	4-[3-(4-Iodophenyl)-2-(4-nitrophenyl)- 2H-5-tetrazolio]-1,3-benzene disulfonate
x(t)	n-dimensional flux vector
XTT	2,3-bis(2-methoxy-4-nitro-5-sulfophenyl)-2H-tetrazolium-5-carbox-anilide
γ	isotope yield
$\Delta\Psi m$	mitochondrial inner transmembrane potential
τ	luminescence decay time (Oxygen present)
τ_0	luminescence decay time (Oxygen absent)
Φ	phase angle
μ	growth rate

7.2 List of Tables

7.3 List of Figures

7.4 Embryonic Stem Cells Derived Hepatocyte-like Cells

7.4.1 LDA - Heat map

Genes		PHH	HepG2	SA461 not differentiated	SA461 (3 x)	SA002 not differentiated	SA002 (3x)
Cytochrome P450s	CYP1A1	0.516	1	0.005	0.011	0.147	0.078
	CYP1A2	⇑	N.D.	N.D.	N.D.	N.D.	N.D.
	CYP1B1	⇑	N.D.	⇑	⇑	⇑	⇑
	CYP2A6	119.165	1	2.038	1.0997	5.715	0.539
	CYP2B6	⇑	N.D.	⇑	N.D.	⇑	⇑
	CYP2C19	⇑	N.D.	N.D.	⇑	N.D.	⇑
	CYP2C8	⇑	N.D.	N.D.	N.D.	N.D.	N.D.
	CYP2C9	⇑	N.D.	N.D.	⇑	N.D.	N.D.
	CYP2D6	5.826	1	0.001	0.012	0.279	0.002
	CYP2E1	1977.144	1	0.104	4.285	0.014	1.422
	CYP3A4	92.997	1	0.023	0.167	0.020	0.083
	CYP3A7	2.151	1	0.007	0.093	0.002	0.148
UGTs	UGT1A	80.443	1	0.015	0.119	0.0003	0.0904
	UGT1A3	146.266	1	0.009	0.023	0.0005	0.002
	UGT1A6	⇑	N.D.	N.D.	⇑	N.D.	⇑
	UGT1A8	⇑	N.D.	N.D.	N.D.	N.D.	N.D.
	UGT2B7	32.282	1	0.0001	0.377	0.00003	0.202
Transporters	BSEP	⇑	N.D.	N.D.	N.D.	N.D.	N.D.
	MDR1	0.312	1	0.001	0.007	0.003	0.008
	MDR3	0.449	1	0.005	0.009	0.009	0.021
	MRP2	0.442	1	0.00001	0.015	0.0001	0.008
	NTCP	⇑	N.D.	N.D.	⇑	N.D.	⇑
	OATP-A	N.D.	N.D.	⇑	⇑	⇑	⇑
	OATP-C	⇑	N.D.	⇑	⇑	⇑	⇑
	OCT1	52.807	1	0.003	0.301	0.148	0.309
Transcription factors	CAR	5.920	1	0.009	0.389	0.003	0.358
	FXR	1.235	1	0.00003	0.036	0.00001	0.021
	PXR	0.795	1	0.022	0.017	0.00002	0.002
	RXRa	1.712	1	0.278	1.133	0.529	0.813
	RXRb	0.333	1	0.112	1.823	0.158	0.756
	RXRg	⇑	N.D.	N.D.	⇑	⇑	⇑
	HNF1a	0.347	1	0.00005	0.201	0.00002	0.152
	HNF3a	0.243	1	0.0001	1.499	0.004	1.581
	HNF3b	0.474	1	0.002	0.960	0.052	0.904
	HNF4a	0.362	1	0.00002	0.279	0.00001	0.181
	HNF6	2.472	1	0.0003	0.131	0.003	0.238
	C/EBP A	0.180	1	0.022	0.569	0.014	0.423
	C/EBP B	1.040	1	0.085	0.214	0.103	0.084
Other genes	Albumin	4.656	1	0.00001	0.046	0.00001	0.010
	Alcoholdehydrogenase	⇑	N.D.	N.D.	⇑	N.D.	⇑
	Alpha-1-antitrypsin	8.639	1	0.0000005	0.910	0.0001	0.315
	Apolipoprotein E	0.593	1	0.201	0.415	0.166	0.372
	Cholesterol 7 alpha-hydroxylase	0.248	1	0.015	0.037	0.002	0.007
	Glucose-6-phosphate	8.137	1	0.001	0.016	0.0006	0.009
	P450 reductase	0.244	1	0.137	0.423	0.148	0.247

N.D.	<0.001	0.001-0.01	0.01-0.1	0.1-0.9	0.9-1.1	1.1-10.0	>10.0	⇑

Figure 7.4.1: Relative gene expression for liver related genes as measured by LDA assay. All samples were run on LDA cards containing different genes associated with liver drug metabolism. The expression for all genes is normalized against the expression of HPRT in each sample. The expression levels in each sample are compared to the expression levels in Hep G2 cells, which are set to 1.0 for all genes. UGTs: UDP-glucuronosyltransferases, N.D.: not detected, ↑: detected.

7.4.2 LC-MS/MS Chromatograms

7.4.2.1 Diclofenac

A
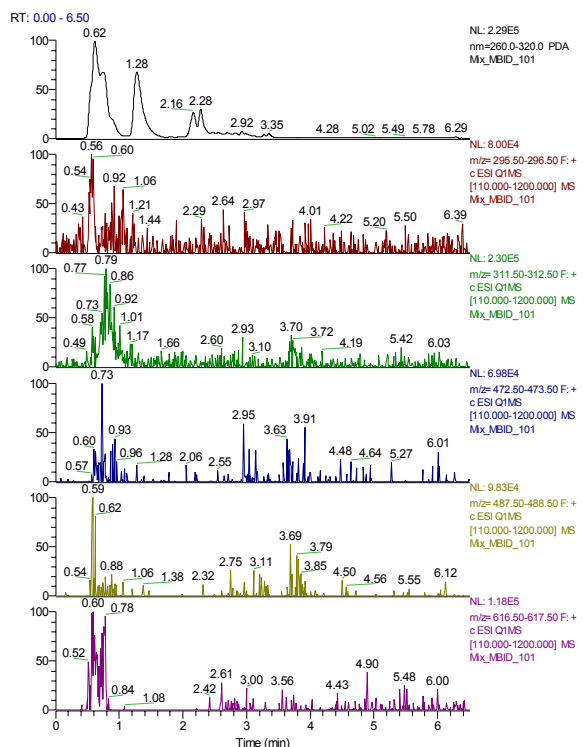
B
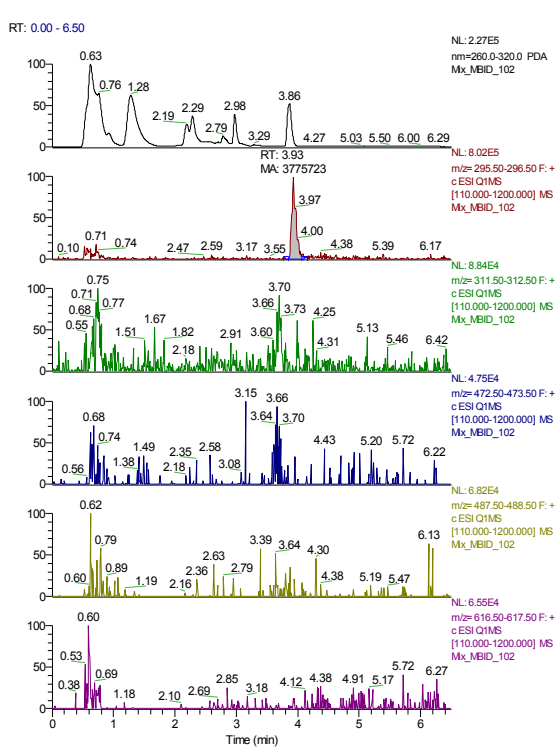
C
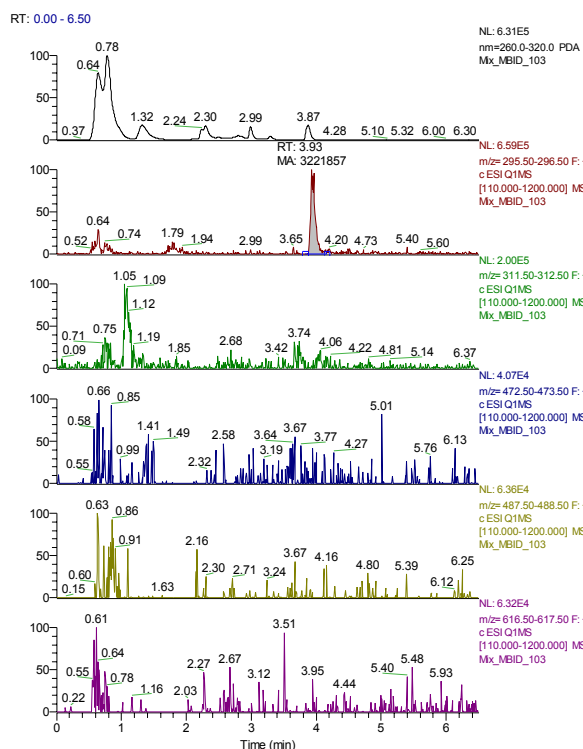
D
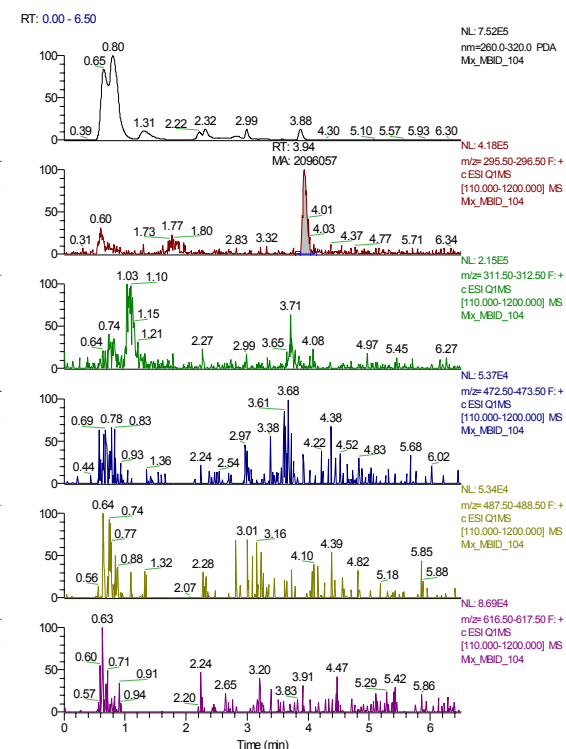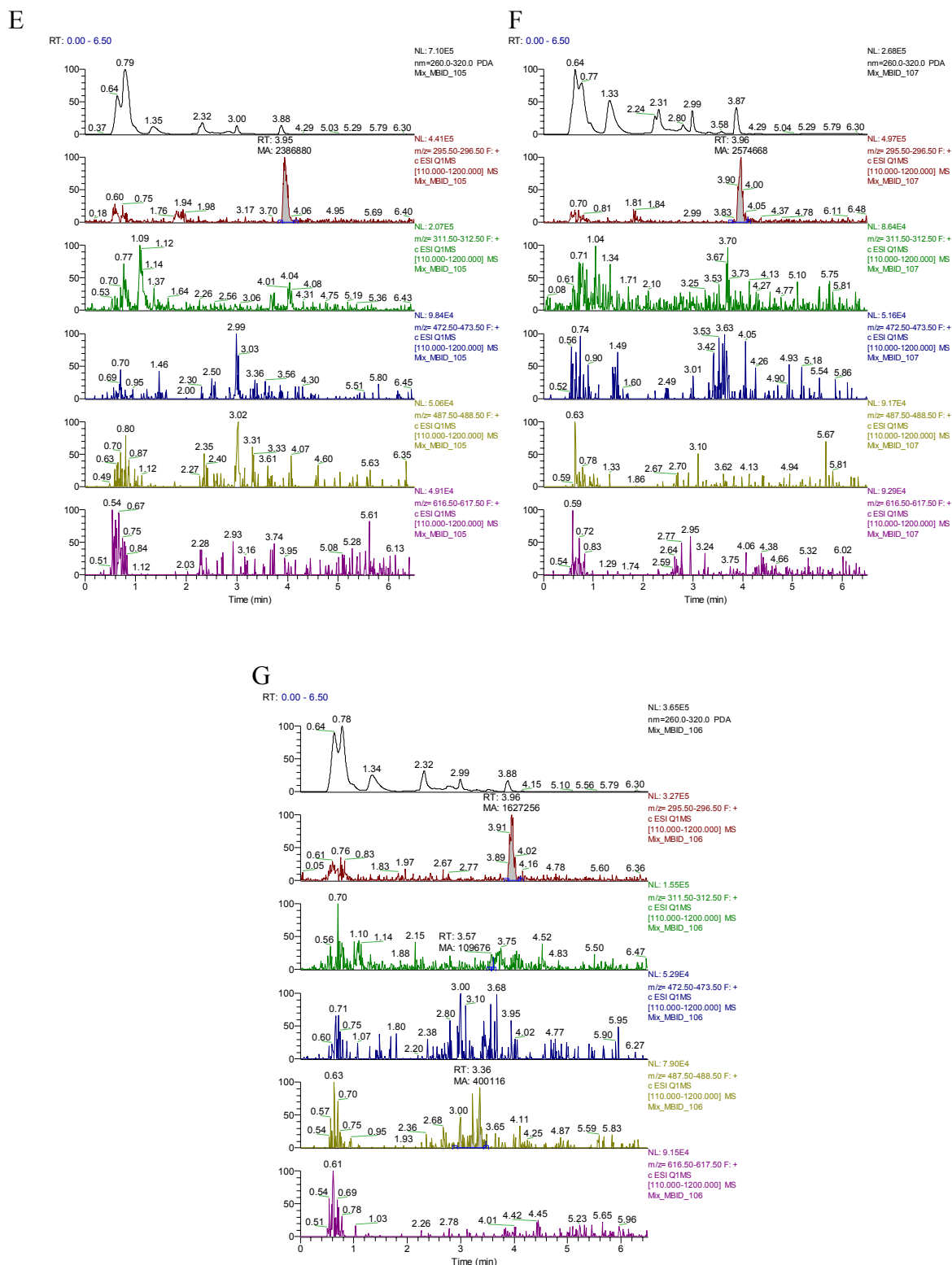
Figure 7.4.2: LC-MS/MS chromatograms of diclofenac, its metabolites and controls. **A)** Control media without cells and without diclofenac, phenacetin and midazolam, **B)** activity assay media without cells, diclofenac metabolized by **C)** SA002 **D)** SA167, **E)** SA461, **F)** Hep G2 cells and **G)** Primary human hepatocytes. Chromatograms are depicted in colors, indicating metabolites, namely: red = diclofenac, green = OH-diclofenac, blue = Acylglucuronide, olive = O-glucuronide and purple = Glutathione, Retention times are indicated and Areas under the curve (AUC, here MA) are filled in grey.

7.4.2.2 Phenacetin

A
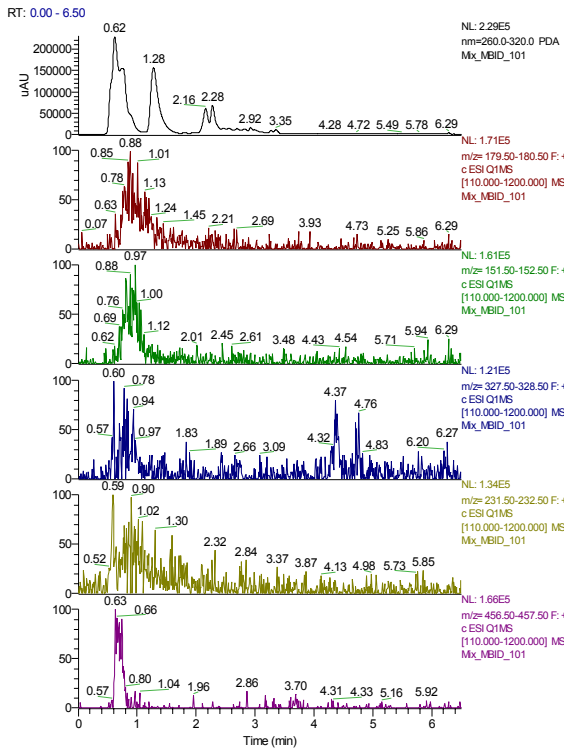
B
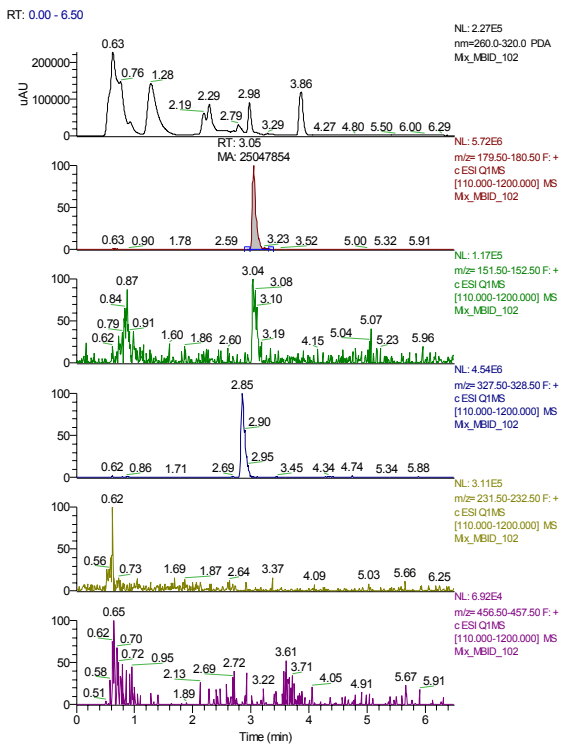
C
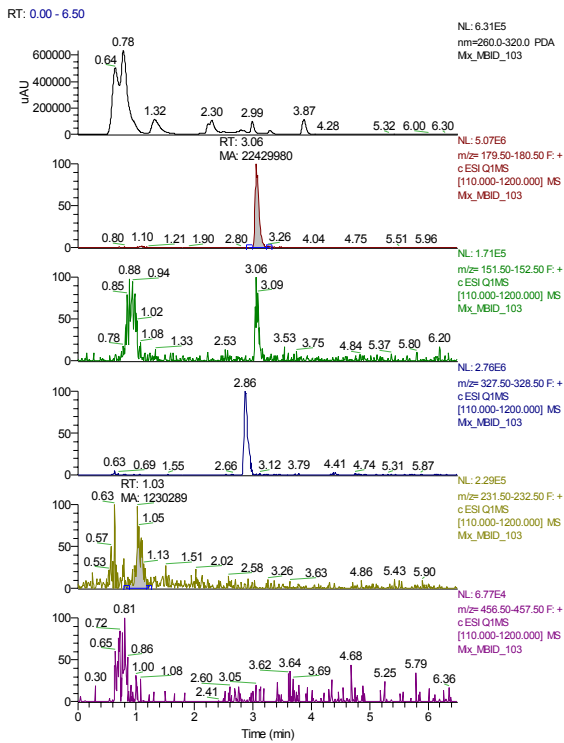
D
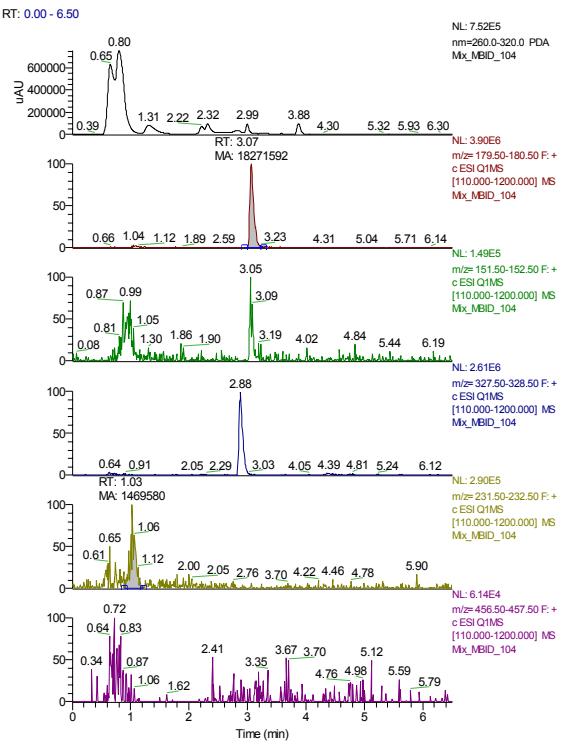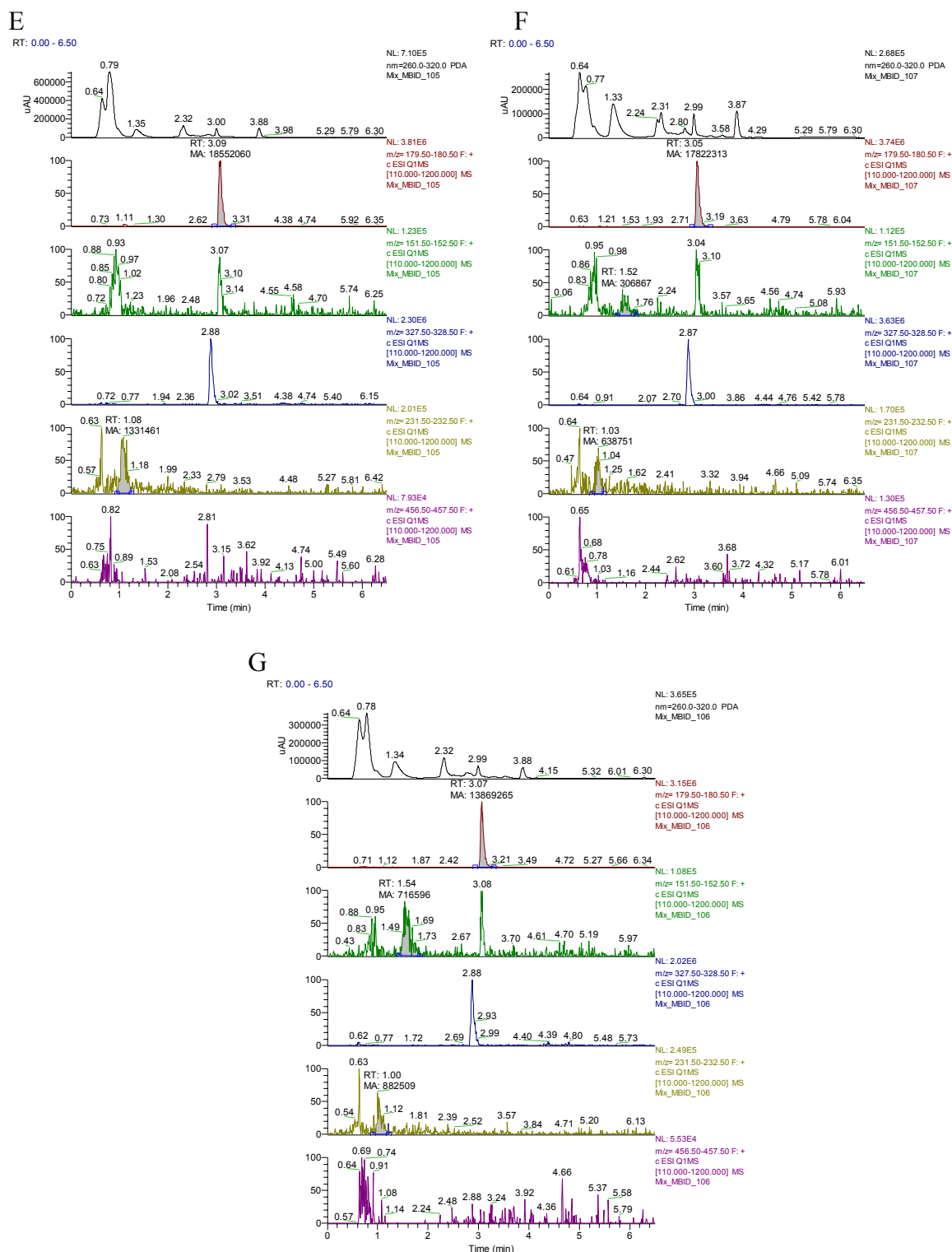
Figure 7.4.3: LC-MS/MS chromatograms of phenacetin, its metabolites and controls. **A)** Control media without cells and without diclofenac, phenacetin and midazolam, **B)** activity assay media without cells, phenacetin metabolized by **C)** SA002 **D)** SA167, **E)** SA461, **F)** Hep G2 cells and **G)** Primary human hepatocytes. Chromatograms are depicted in colors, indicating metabolites, namely: red = phenacetin, green = Acetaminophen (APAP), blue = APAP-glucuronide, olive = APAP-sulfate and purple = APAP-Glutathione, Retention times are indicated and Areas under the curve (AUC, here MA) are filled in grey.

7.4.2.3 Midazolam

A

B

C

D

XX
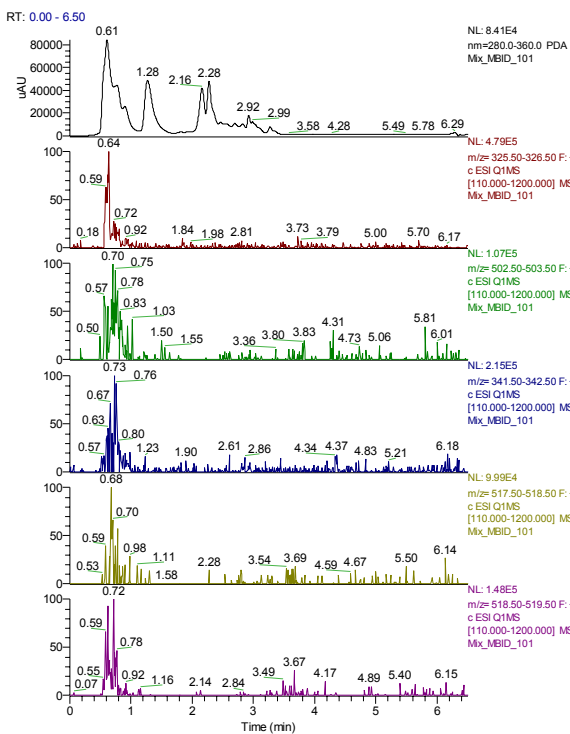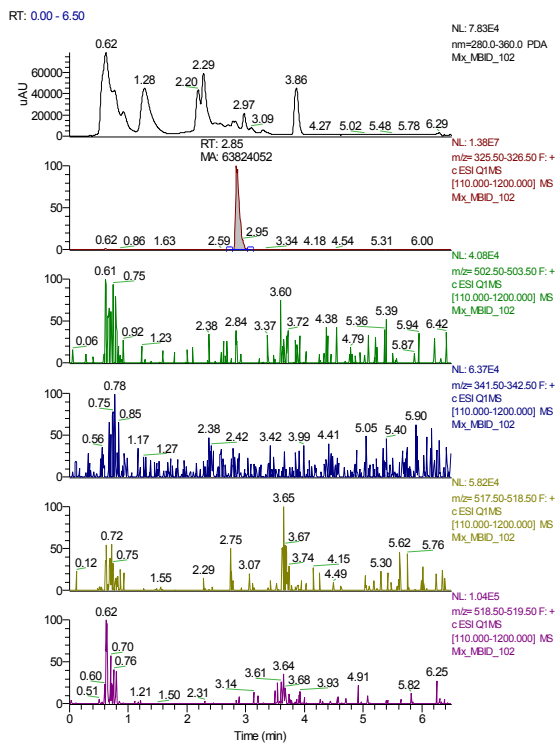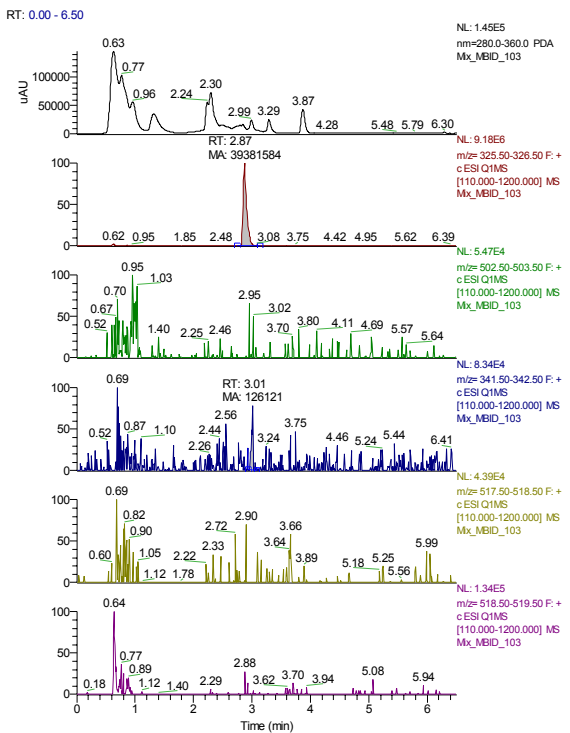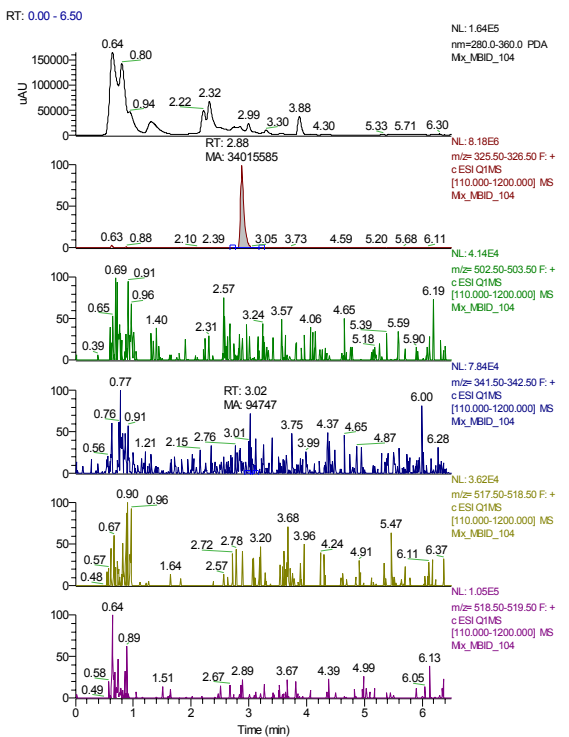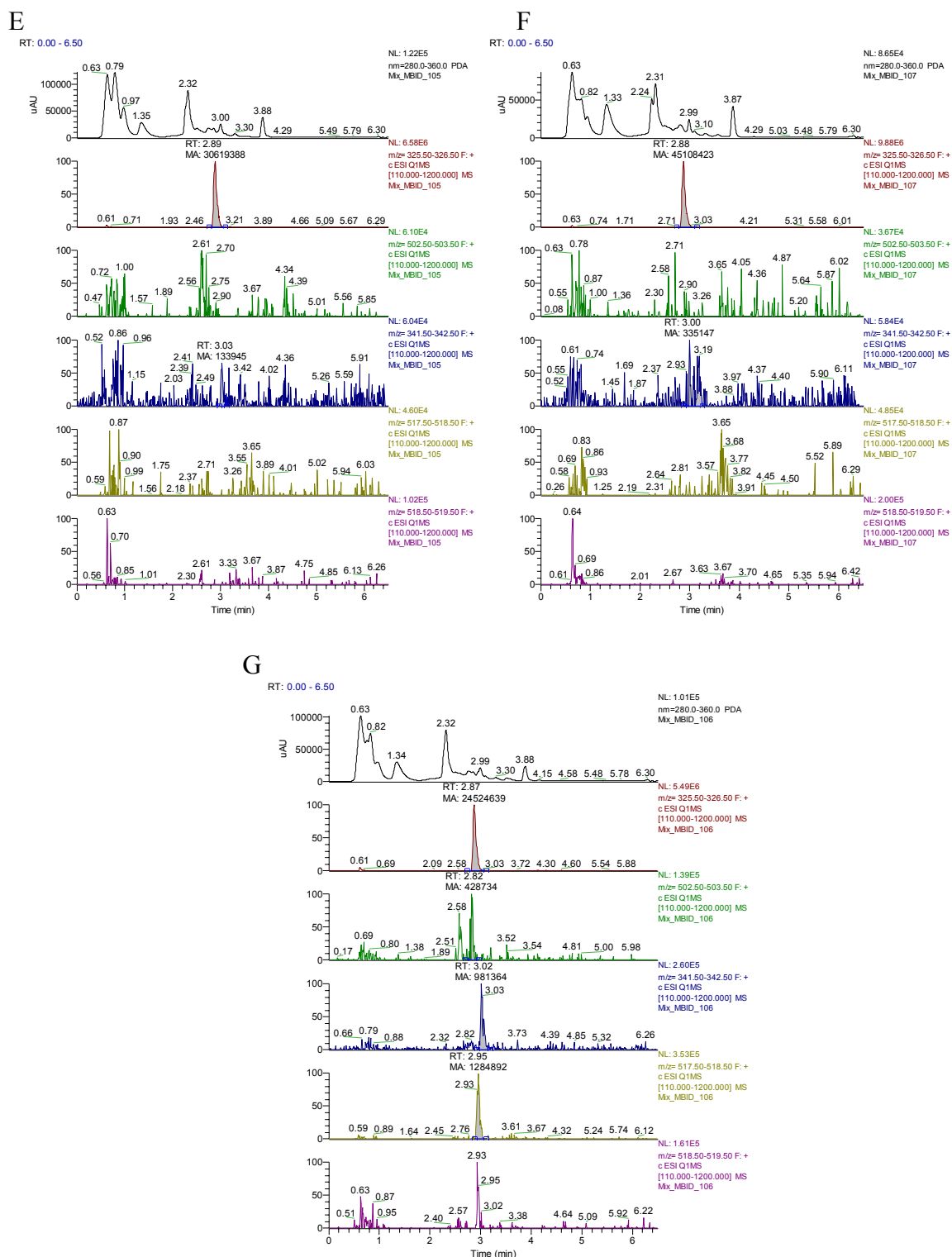
Figure 7.4.4: LC-MS/MS chromatograms of midazolam, its metabolites and controls. **A)** Control media without cells and without diclofenac, phenacetin and midazolam, **B)** activity assay media without cells, midazolam metabolized by **C)** SA002 **D)** SA167, **E)** SA461, **F)** Hep G2 cells and **G)** Primary human hepatocytes. Chromatograms are depicted in colors, indicating metabolites, namely: red = midazolam, green = midazolam-N-glucuronide, blue = OH-midazolam, olive = OH-midazolam-O-glucuronide and purple = OH-midazolam-N-glucuronide, Retention times are indicated and Areas under the curve (AUC, here MA) are filled in grey.

7.5 Physiological Studies Applying Sub-toxic Drug Concentrations

7.5.1 Definitions for pseudo-steady-state metabolic network

The stoichiometric network, which was constructed, was based knowledge contained in databases (e.g. KEGG, Roche Table…) and on previous observations, obtained from the metabolic profile, to obtain a working mathematical description of the hepatic metabolism. Thus, pathways included were, glycolysis, the TCA cycle, the urea cycle, amino acid oxidation and albumin synthesis. However, glycogen synthesis production was not considered, since it was not quantified. In addition, since SA002 cells do not proliferate, certain other definitions, regarding the pseudo-steady-state metabolic network were defined as follows:

1) Pseudo-steady-state for the hepatic metabolic network can be assumed, since the rate of intracellular composition change is very small compared to their turnover rate (Marín-Sanguino and Torres, 2000; Yang et al., 2009). To ensure this, several metabolites were measured over the course of experiment to evaluate the changes in the rate of uptake or release and were found to be constant (see Figure 4.4.6).

2) Protein degradation as source of amino acids was neglected, since the medium was devoid of proteins.

3) Albumin synthesis was used for calculations of the anabolic demand (see reaction 4.17), since the cells do not proliferate and albumin is the major protein product of hepatocytes (Chan et al., 2003a). Its release was further found to be constant over time (data not shown).

4) Transport processes were included in the model to distinguish between cytosolic pools and mitochondrial pools; however the mechanism was not included, since active transport consumes energy, however, does not affect the carbons structure. The energy balance was not included.

5) The non-oxidative branch of the pentose phosphate pathway was not considered. The demand for ribose 5-phosphate for nucleotide synthesis is negligible, since the cells do not proliferate (Chan et al., 2003a). However, the NADPH generating branch was also not considered, since it only accounts for approximately of 2-6 % of glucose metabolism (Magnusson et al., 1988) and may be less due to pyruvate cycling.

7.5.2 Stoichiometric network for metabolic flux analysis of hepatocytes
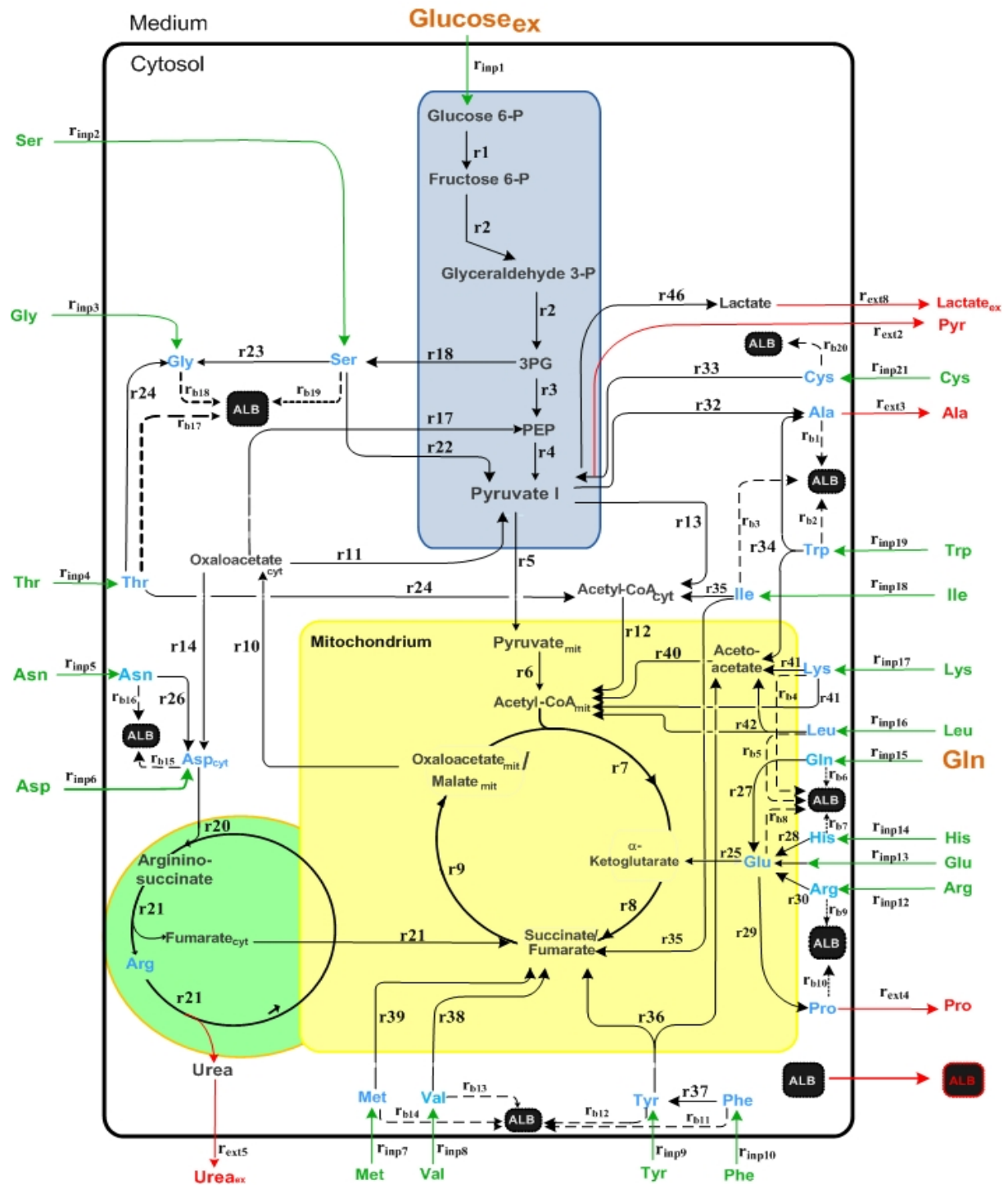
Figure 7.5.1: Mammalian cell metabolism. The network is comprised of intracellular metabolite balances, extracellular fluxes (22 uptake fluxes of amino acids, pyruvate and glucose, indicated by green arrows), 3 fluxes which indicate secretion (red arrows)) and 20 anabolic fluxes (albumin synthesis, dashed arrows). Arrows indicate the direction of reaction assumed in the model. Abbreviations used: CIT citrate, ICT isocitrate, ALB albumin. The amino acids have the standard 3 letter abbreviation. The subscripts "mit" indicate mitochondrial metabolites and "cyt" cytosolic. The subscripts "inp" and "ext" indicate input and export fluxes, respectively.

The stoichiometric balances for the intracellular metabolites are defined as depicted in Table 7.5.1:

Table 7.5.1: Stoichiometric balances for the intracellular metabolites of primary human hepatocytes and hESC derived hepatocyte-like cells. The subscripts "mit" indicate mitochondrial metabolites and "cyt" cytosolic. The subscripts "inp" and "ext" indicate input and export fluxes, respectively. The letter "L" indicates minimum labeled concentration of metabolites, which are excreted.

Metabolite	Balance equation
Glucose 6-P	$0 = r_{inp1} - r1$
Fructose 6-P	$0 = r1 - r2$
3PG	$0 = 2 \cdot r2 - r3 - r18$
PEP	$0 = r3 - r4 + r17$
Pyruvate I	$0 = r4 - r5 + r22 + r11 - r13 - r32 + r33 - r46 - r_{ext2}$
Pyruvate$_{mit}$	$0 = r5 - r6$
Acetyl-CoA$_{mit}$	$0 = r6 - r7 + r12 + 2 \cdot r40 + r41 + r42$
Acetyl-CoA$_{cyt}$	$0 = r13 + r24 + r35 - r12$
α-Ketoglutarate	$0 = r7 - r8 + r25$
Succinate/Fumarate	$0 = r8 - r9 + r21 + r35 + r36 + r38 + r39$
Oxaloacetate$_{mit}$/Malate$_{mit}$	$0 = r9 - r7 - r10$
Oxaloacetate$_{cyt}$	$0 = r10 - r11 - r14 - r17$
Acetoacetate	$0 = r34 + r41 + r42 - r40 + r36$
Urea	$0 = r21 - r_{ext5}$
Lactate	$0 = r46 - r_{ext1}$
Cys	$0 = r_{inp21} - r_{b20} - r33$
Ala	$0 = -r_{ext3} - r_{b1} + r32 + r34$
Trp	$0 = r_{inp19} - r_{b2} - r34$
Ile	$0 = r_{inp18} - r_{b3} - r35$
Lys	$0 = r_{inp17} - r_{b4} - r41$
Leu	$0 = r_{inp16} - r_{b5} - r42$
Gln	$0 = r_{inp15} - r_{b6} - r27$
Glu	$0 = r_{inp13} - r_{b8} - r25 + r28 + r30 + r27 - r29$
His	$0 = r_{inp14} - r_{b7} - r28$
Arg	$0 = r_{inp12} - r_{b9} - r30$
Pro	$0 = r_{ext4} - r_{b10} + r29$
Phe	$0 = r_{inp10} - r_{b11} - r37$
Tyr	$0 = r_{inp9} - r_{b12} - r36 + r37$
Val	$0 = r_{inp8} - r_{b13} - r38$
Met	$0 = r_{inp7} - r_{b14} - r39$
Asp$_{cyt}$	$0 = r_{inp6} - r_{b15} - r20 + r26 + r14$
Argininosuccinate	$0 = r20 - r21$
Urea	$0 = r21 - r_{ext5}$
Asn	$0 = r_{inp5} - r_{b16} - r26$
Thr	$0 = r_{inp4} - r_{b17} - r24$
Gly	$0 = r_{inp3} - r_{b18} + r23 + r24$
Ser	$0 = r_{inp2} - r_{b19} - r22 - r23 + r18$

Intracellular fluxes were calculated using a script, adapted from A. Strigun, using average yields with their standard deviation and applying Monte-Carlo-simulation. The script for use in Matlab® was as followed:

```
%%%%%%%%%%%%%%%%%%%%%%%%%%%%%%%%%%%%%%%%%%%%%%%%%%%%%%%%%%%%%%%%%%%%%%%%%%%
%%%%%%%%%%%%%%%%%%%%%%%%%%%%%%%%%%%%%%%%%%%%%%%%%%%%%%%%%%%%%%%%%%%%%%%%%%%
% Script for calculation of intracellular fluxes using average yields
% obtained by Monte Carlo random numbers with standard deviation of input
% data (several time point available).

%please define qm (measured rates), qm_error (measured
%standard deviations) and S_M (Measured Matrix) S_C (Calculated Matrix)
nMonteCarlo = 10    ;                  %number of Monte-Carlo runs
load Matrices;
c = [];
for i = 1: nMonteCarlo;
  D = normrnd(qm, qm_error);
  b = (-pinv(S_C)*S_M*D)';
  c = [c; b];
end
qc=(mean(c)');
qc_error=abs(std(c)');
qm=qm';
qm_error=qm_error';
```

The data used in Matlab® are shown next. Hereby, *S_M* denotes the matrix of measured fluxes, *S_C* the matrix of calculable fluxes, *qc* the calculated flux vector and *qc_error* the standard deviation for each flux of *qc*.

S_M =

S_C

	r1	r2	r3	r4	r5	r6	r7	r8	r9	r10	r11	r12	r13	r14	r17	r18	r20	r21	r22	r23	r24	r25	r26	r27	r28	r29	r30	r32	r33	r34	r35	r36	r37	r38	r39	r40	r41	r42	r46
Glucose 6-P	-1	0	0	0	0	0	0	0	0	0	0	0	0	0	0	0	0	0	0	0	0	0	0	0	0	0	0	0	0	0	0	0	0	0	0	0	0	0	0
Fructose 6-P	1	-1	0	0	0	0	0	0	0	0	0	0	0	0	0	0	0	0	0	0	0	0	0	0	0	0	0	0	0	0	0	0	0	0	0	0	0	0	0
3PG	0	2	-1	0	0	0	0	0	0	0	0	0	0	0	0	-1	0	0	0	0	0	0	0	0	0	0	0	0	0	0	0	0	0	0	0	0	0	0	0
PEP	0	0	1	-1	0	0	0	0	0	0	0	0	0	0	1	0	0	0	0	0	0	0	0	0	0	0	0	0	0	0	0	0	0	0	0	0	0	0	0
Pyruvate I	0	0	0	1	-1	0	0	0	0	0	1	0	-1	0	0	0	0	0	0	0	1	0	0	0	0	0	0	-1	1	0	0	0	0	0	0	0	0	0	-1
Pyruvate_mit	0	0	0	0	1	-1	0	0	0	0	0	0	0	0	0	0	0	0	0	0	0	0	0	0	0	0	0	0	0	0	0	0	0	0	0	0	0	0	0
Acetyl-CoA_mit	0	0	0	0	0	1	-1	0	0	0	0	1	0	0	0	0	0	0	0	0	0	0	0	0	0	0	0	0	0	0	0	0	0	0	0	2	1	1	0
Acetyl-CoA_cyt	0	0	0	0	0	0	0	0	0	0	0	0	-1	1	0	0	0	0	0	0	0	0	0	1	0	0	0	0	0	0	0	1	0	0	0	0	0	0	0
α-Ketoglutarate	0	0	0	0	0	0	1	-1	0	0	0	0	0	0	0	0	0	0	0	0	0	0	1	0	0	0	0	0	0	0	0	0	0	0	0	0	0	0	0
Succinate/Fumarate	0	0	0	0	0	0	0	1	-1	0	0	0	0	0	0	0	1	0	0	0	0	0	0	0	0	0	0	0	0	0	0	0	0	1	0	1	1	0	0
Oxaloacetate_mit	0	0	0	0	0	0	-1	0	1	-1	0	0	0	0	0	0	0	0	0	0	0	0	0	0	0	0	0	0	0	0	0	0	0	0	0	0	0	0	0
Oxaloacetate_cyt	0	0	0	0	0	0	0	0	0	1	-1	0	0	-1	-1	0	0	0	0	0	0	0	0	0	0	0	0	0	0	0	0	0	0	0	0	0	0	0	0
Acetoacetate	0	0	0	0	0	0	0	0	0	0	0	0	0	0	0	0	0	0	0	0	0	0	0	0	0	0	0	0	0	0	1	0	1	0	0	0	-1	1	1
Urea	0	0	0	0	0	0	0	0	0	0	0	0	0	0	0	0	0	0	0	0	0	1	0	0	0	0	0	0	0	0	0	0	0	0	0	0	0	0	0
Lactate	0	0	0	0	0	0	0	0	0	0	0	0	0	0	0	0	0	0	0	0	0	0	0	0	0	0	0	0	0	0	0	0	0	0	0	0	0	0	1
Cys	0	0	0	0	0	0	0	0	0	0	0	0	0	0	0	0	0	0	0	0	0	0	0	0	0	0	-1	0	0	0	0	0	0	0	0	0	0	0	0
Ala	0	0	0	0	0	0	0	0	0	0	0	0	0	0	0	0	0	0	0	0	0	0	0	0	1	0	1	0	0	0	0	0	0	0	0	0	0	0	0
Trp	0	0	0	0	0	0	0	0	0	0	0	0	0	0	0	0	0	0	0	0	0	0	0	0	-1	0	0	0	0	0	0	0	0	0	0	0	0	0	0
Ile	0	0	0	0	0	0	0	0	0	0	0	0	0	0	0	0	0	0	0	0	0	0	0	0	0	0	0	0	0	-1	0	0	0	0	0	0	0	0	0
Lys	0	0	0	0	0	0	0	0	0	0	0	0	0	0	0	0	0	0	0	0	0	0	0	0	0	0	0	0	0	0	0	0	0	0	0	0	0	-1	0
Leu	0	0	0	0	0	0	0	0	0	0	0	0	0	0	0	0	0	0	0	0	0	0	0	0	0	0	0	0	0	0	0	0	0	0	0	0	0	-1	0
Gln	0	0	0	0	0	0	0	0	0	0	0	0	0	0	0	0	0	0	0	0	-1	0	0	0	0	0	0	0	0	0	0	0	0	0	0	0	0	0	0
Glu	0	0	0	0	0	0	0	0	0	0	0	0	0	0	0	0	0	0	-1	0	1	1	-1	1	0	0	0	0	0	0	0	0	0	0	0	0	0	0	0
His	0	0	0	0	0	0	0	0	0	0	0	0	0	0	0	0	0	0	0	0	0	0	0	-1	0	0	0	0	0	0	0	0	0	0	0	0	0	0	0
Arg	0	0	0	0	0	0	0	0	0	0	0	0	0	0	0	0	0	0	0	0	0	0	0	0	-1	0	0	0	0	0	0	0	0	0	0	0	0	0	0
Pro	0	0	0	0	0	0	0	0	0	0	0	0	0	0	0	0	0	0	0	0	0	0	0	1	0	0	0	0	0	0	0	0	0	0	0	0	0	0	0
Phe	0	0	0	0	0	0	0	0	0	0	0	0	0	0	0	0	0	0	0	0	0	0	0	0	0	0	0	0	0	0	0	0	0	0	0	-1	0	0	0
Tyr	0	0	0	0	0	0	0	0	0	0	0	0	0	0	0	0	0	0	0	0	0	0	0	0	0	0	0	0	0	0	0	0	0	0	-1	1	0	0	0
Val	0	0	0	0	0	0	0	0	0	0	0	0	0	0	0	0	0	0	0	0	0	0	0	0	0	0	0	0	0	0	-1	0	0	0	0	0	0	0	0
Met	0	0	0	0	0	0	0	0	0	0	0	0	0	0	0	0	0	0	0	0	0	0	0	0	0	0	0	0	0	-1	0	0	0	0	0	0	0	0	0
Asp_cyt	0	0	0	0	0	0	0	0	0	0	0	0	1	0	0	-1	0	0	0	0	0	0	0	0	1	0	0	0	0	0	0	0	0	0	0	0	0	0	0
Argininosuccinate	0	0	0	0	0	0	0	0	0	0	0	0	0	0	1	-1	0	0	0	0	0	0	0	0	0	0	0	0	0	0	0	0	0	0	0	0	0	0	0
Urea	0	0	0	0	0	0	0	0	0	0	0	0	0	0	0	0	1	0	0	0	0	0	0	0	0	0	0	0	0	0	0	0	0	0	0	0	0	0	0
Asn	0	0	0	0	0	0	0	0	0	0	0	0	0	0	0	0	0	0	0	0	0	0	-1	0	0	0	0	0	0	0	0	0	0	0	0	0	0	0	0
Thr	0	0	0	0	0	0	0	0	0	0	0	0	0	0	0	0	0	0	0	0	0	0	0	0	0	0	-1	0	0	0	0	0	0	0	0	0	0	0	0
Gly	0	0	0	0	0	0	0	0	0	0	0	0	0	0	0	0	0	0	0	1	1	0	0	0	0	0	0	0	0	0	0	0	0	0	0	0	0	0	0
Ser	0	0	0	0	0	0	0	0	0	0	0	0	0	0	1	0	0	-1	-1	0	0	0	0	0	0	0	0	0	0	0	0	0	0	0	0	0	0	0	0

qm and *qm_error* =

		r [µmol/(mg Albumin x 24 hours)]					
		0 µM Diclofenac		100 µM Diclofenac		200 µM Diclofenac	
		mean	STD	mean	STD	mean	STD
rext1	Lactate	1822.860	31.610	1574.005	118.050	1630.597	122.295
rext2	Pyruvate	25.343	2.060	12.438	0.933	15.547	1.166
rext3	Alanine	36.000	9.000	83.400	6.255	77.440	5.808
rext4	Proline	17.455	5.275	34.800	2.610	33.700	2.528
rext5	Urea	78.743	3.139	111.940	8.396	103.545	7.766
rinp1	Glucose	1000.000	64.244	1000.000	75.000	1000.000	60.000
rinp2	Serine	3.400	0.605	7.900	0.593	5.800	0.435
rinp3	Glycine	12.200	5.564	15.000	1.125	9.500	0.713
rinp4	Threonine	5.895	1.291	2.815	0.211	1.424	0.107
rinp5	Asparagine	1.885	1.130	0.010	0.001	0.010	0.001
rinp6	Aspartate	26.600	0.195	60.000	4.500	63.700	4.778
rinp7	Methionine	2.473	0.300	2.065	0.155	0.983	0.074
rinp8	Valine	10.844	2.102	1.173	0.088	0.000	0.000
rinp9	Tyrosine	3.406	1.033	1.726	0.129	0.270	0.020
rinp10	Phenylalanine	3.349	0.846	2.255	0.169	0.577	0.043
rinp12	Arginine	8.679	1.069	8.238	0.618	4.689	0.352
rinp13	Glutamate	44.600	0.849	108.900	8.168	108.100	8.108
rinp14	Histidine	1.922	0.800	2.301	0.173	1.540	0.116
rinp15	Glutamine	89.348	27.412	162.962	12.222	164.819	12.361
rinp16	Leucine	19.511	4.475	9.626	0.722	4.684	0.351
rinp17	Lysine	8.349	3.405	10.314	0.774	5.668	0.425
rinp18	Isoleucine	13.875	2.633	5.302	0.398	3.046	0.228
rinp19	Tryptophane	1.456	0.062	0.034	0.003	0.000	0.000
rinp21	Cysteine	0.001	0.001	0.001	0.000	0.398	0.030
rb9	ARGinALB	0.080	0.004	0.175	0.009	0.144	0.007
rb15	cASPinALB	0.107	0.005	0.233	0.012	0.192	0.010
rb1	ALAinALB	0.204	0.010	0.444	0.022	0.366	0.018
rb19	SERinALB	0.080	0.004	0.175	0.009	0.144	0.007
rb20	CYSinALB	0.117	0.006	0.255	0.013	0.210	0.010
rb8	GLUinALB	0.190	0.010	0.415	0.021	0.342	0.017
rb18	GLYinALB	0.057	0.003	0.124	0.006	0.102	0.005
rb12	TYRinALB	0.070	0.004	0.153	0.008	0.126	0.006
rb17	THRinALB	0.110	0.006	0.240	0.012	0.198	0.010
rb4	LYSinALB	0.117	0.006	0.255	0.013	0.210	0.010
rb11	PHEinALB	0.087	0.004	0.189	0.009	0.156	0.008
rb6	GLNinALB	0.083	0.004	0.182	0.009	0.150	0.007
rb10	PROinALB	0.100	0.005	0.218	0.011	0.180	0.009
rb7	HISinALB	0.050	0.003	0.109	0.005	0.090	0.004
rb14	METinALB	0.020	0.001	0.044	0.002	0.036	0.002
rb16	ASNinALB	0.067	0.003	0.146	0.007	0.120	0.006
rb2	TRPinALB	0.003	0.000	0.007	0.000	0.006	0.000
rb13	VALinALB	0.117	0.006	0.255	0.013	0.210	0.010
rb3	ILEinALB	0.043	0.002	0.095	0.005	0.078	0.004
rb5	LEUinALB	0.187	0.009	0.408	0.020	0.336	0.017

Since albumin is the major protein produced in hepatocytes and the cells did not proliferate, for the anabolic demand, amino acids consumption for albumin synthesis, was used according to Chan et al. (2003a).

24 ARG + 32 ASP + 61 ALA + 24 SER + 35 CYS + 57 GLU + 17 GLY + 21 TYR
+ 33 THR + 53 LYS + 26 PHE + 25 GLN + 30 PRO + 15 HIS + 6 MET
+ 20 ASN + TRP + 35 VAL + 13 ISO + 56 LEU + 2332 ATP
= albumin + 2332 ADP + 2332 P_i

By multiplication of the anabolic demand of amino acids for the albumin synthesis [$\text{mmol}_{\text{amino acid}} \cdot \text{mg}_{\text{Albumin}}^{-1}$] with the yield [$\text{mg}_{\text{Albumin}} \cdot \text{mmol}_{\text{substrate}}$] the values were normalized to the defined glucose uptake and implemented into the stoichiometric flux model (see Table 7.1.2 and Table 7.1.3.

Table 7.5.2: Albumin concentration and glucose uptake after 24 hours of exposure to diclofenac for hESC derived hepatocyte-like cells.

	SA002 (24 hours)		
	Control	ST1 [100 µM]	ST2 [100 µM]
Albumin (g/L)	0.86	0.78	0.63
Albumin (mmol/L)	2.61×10^{-5}	2.34×10^{-5}	1.89×10^{-5}
Glucose uptake (mmol/L)	3.91	1.61	1.57

Table 7.5.3: Anabolic demand for the production of albumin and normalized to glucose uptake for hESC derived hepatocyte-like cells exposed to diclofenac for 24 hours.

		Control		ST1		ST2	
AS	Albumin Composition (mmol)	Anabolic demand (mmol AS / mmol Albumin)	Anabolic demand (mmol AS/mmol Albumin / mmol Glucose)	Anabolic demand (mmol AS / mmol Albumin)	Anabolic demand (mmol AS/mmol Albumin / mmol)	Anabolic demand (mmol AS / mmol Albumin)	Anabolic demand (mmol AS/mmol Albumin / mmol)
Arg	24	0.00031317	0.0000200	0.00028086	0.000044	0.0002265	0.000036
Asp	32	0.00041756	0.0000267	0.00037448	0.000058	0.000302	0.000048
Ala	61	0.00079597	0.0000509	0.00071385	0.000111	0.00057569	0.000091
Ser	24	0.00031317	0.0000200	0.00028086	0.000044	0.0002265	0.000036
Cys	35	0.00045671	0.0000292	0.00040959	0.000064	0.00033031	0.000052
Glu	57	0.00074378	0.0000476	0.00066704	0.000104	0.00053794	0.000085
Gly	17	0.00022183	0.0000142	0.00019894	0.000031	0.00016044	0.000025
Tyr	21	0.00027402	0.0000175	0.00024575	0.000038	0.00019819	0.000031
Thr	33	0.00043061	0.0000276	0.00038618	0.000060	0.00031144	0.000049
Lys	35	0.00045671	0.0000292	0.00040959	0.000064	0.00033031	0.000052
Phe	26	0.00033927	0.0000217	0.00030427	0.000047	0.00024538	0.000039
Gln	25	0.00032622	0.0000209	0.00029256	0.000045	0.00023594	0.000037
Pro	30	0.00039146	0.0000250	0.00035108	0.000055	0.00028313	0.000045
His	15	0.00019573	0.0000125	0.00017554	0.000027	0.00014156	0.000022
Met	6	7.8292E-05	0.0000050	7.0215E-05	0.000011	5.6625E-05	0.000009
Asn	20	0.00026097	0.0000167	0.00023405	0.000036	0.00018875	0.000030
Trp	1	1.3049E-05	0.0000008	1.1703E-05	0.000002	9.4375E-06	0.000001
Val	35	0.00045671	0.0000292	0.00040959	0.000064	0.00033031	0.000052
Iso	13	0.00016963	0.0000109	0.00015213	0.000024	0.00012269	0.000019
Leu	56	0.00073073	0.0000468	0.00065534	0.000102	0.0005285	0.000084

7.5.3 Studies of central carbon metabolism employing ^{13}C isotopes

Table 7.5.4: [U-^{13}C$_6$]glucose and [U-^{13}C$_5$]glutamine supplemented as substrates. The carbon profile for primary human hepatocytes is shown over time [h]. The sub-toxic concentrations are abbreviated as ST1-ST3, being 10 µM, 25 µM and 50 µM diclofenac, respectively.

Substrate	Time [h]	Concentration [C-µmol/L]					Uptake [C-µmol/L]				
		0	12	24	35	48	0	12	24	35	48
Glucose	Control	64848	58026	57510	57840	59238	0	6822	7338	7008	5610
	ST1	64848	57168	57138	58830	58764	0	7680	7710	6018	6084
	ST2	64848	56934	58554	58188	56502	0	7914	6294	6660	8346
	ST3	64848	58194	58722	58494	57570	0	6654	6126	6354	7278
Glutamine	Control	21495	20155	19065	18205	15890	0	1340	2430	3290	5605
	ST1	21495	19845	18045	17340	16710	0	1650	3450	4155	4785
	ST2	21495	19610	18715	17785	16555	0	1885	2780	3710	4940
	ST3	21495	19445	18445	18300	16720	0	2050	3050	3195	4775

Table 7.5.5: Concentrations [µmol/L], carbon concentration [C-µmol/L] over time, ^{13}C-mass isotopomer concentration [C-µmol/L] from [U-^{13}C$_6$]glucose or [U-^{13}C$_5$]glutamine over time [h], quantified by HPLC and analyzed by GC/MS for primary human hepatocytes exposed to diclofenac in four concentrations.

Metabolite	Time [h]	Concentration [µmol/L]					Concentration [C-µmol/L]				
		0	12	24	35	48	0	12	24	35	48
Lactate	Control	0	0	523	884	1587	0	0	1569	2652	4761
	ST1	0	0	344	759	1421	0	0	1032	2277	4263
	ST2	0	0	177	816	1251	0	0	531	2448	3753
	ST3	0	0	0	766	1037	0	0	0	2298	3111
Alanine	Control	1065	995	905	847	779	3195	2985	2715	2541	2337
	ST1	1065	1024	989	967	853	3195	3072	2967	2901	2559
	ST2	1065	1030	963	882	862	3195	3090	2889	2646	2586
	ST3	1065	1066	1014	1011	997	3195	3198	3042	3033	2991
Glutamate	Control	451	465	497	532	558	2255	2325	2485	2660	2790
	ST1	451	469	471	544	570	2255	2345	2355	2720	2850
	ST2	451	458	487	507	531	2255	2290	2435	2535	2655
	ST3	451	441	456	513	517	2255	2205	2280	2565	2585
Proline	Control	350	354	352	353	343	1750	1770	1760	1765	1715
	ST1	350	388	352	403	375	1750	1940	1760	2015	1875
	ST2	350	369	360	359	360	1750	1845	1800	1795	1800
	ST3	350	372	376	345	342	1750	1860	1880	1725	1710
Aspartate	Control	263	258	259	258	240	1052	1032	1036	1032	960
	ST1	263	267	252	274	260	1052	1068	1008	1096	1040
	ST2	263	256	258	249	241	1052	1024	1032	996	964
	ST3	263	259	250	256	237	1052	1036	1000	1024	948
Serine	Control	120	128	131	136	135	360	384	393	408	405
	ST1	120	128	125	139	135	360	384	375	417	405
	ST2	120	126	122	132	138	360	378	366	396	414
	ST3	120	118	120	129	125	360	354	360	387	375
Glycine	Control	671	688	660	641	584	1342	1376	1320	1282	1168
	ST1	671	684	635	677	618	1342	1368	1270	1354	1236
	ST2	671	693	678	653	623	1342	1386	1356	1306	1246
	ST3	671	678	667	662	626	1342	1356	1334	1324	1252

Metabolite	Time [h]	^{13}C-mass isotopomer concentration [C-µmol/L] from [U-^{13}C$_6$]glucose					^{13}C-mass isotopomer concentration [C-µmol/L] from [U-^{13}C$_5$]glutamine				
		0	12	24	35	48	0	12	24	35	48
Lactate	Control	0	0	594	1068	2154	0	0	159	273	585
	ST1	0	0	417	975	1788	0	0	111	261	534
	ST2	0	0	213	1017	1803	0	0	48	252	423
	ST3	0	0	0	1014	1512	0	0	0	201	345

Substrate		0	16	24	36	48	0	16	24	36	48
Alanine	*Control*	45	327	399	507	738	45	75	87	114	192
	ST1	45	297	396	492	696	45	84	123	159	219
	ST2	45	291	384	504	753	45	93	93	126	168
	ST3	45	321	342	507	792	45	93	132	141	234
Glutamate	*Control*	25	490	680	885	730	25	155	250	370	565
	ST1	25	625	775	820	930	25	215	295	435	635
	ST2	25	545	905	680	730	25	175	250	345	440
	ST3	25	645	850	690	915	25	150	250	310	485
Proline	*Control*	40	175	190	210	255	40	170	140	160	175
	ST1	40	165	165	200	245	40	150	150	185	180
	ST2	40	140	160	200	230	40	245	150	150	150
	ST3	40	140	150	155	190	40	135	150	135	155
Aspartate	*Control*	12	100	96	116	112	12	36	36	48	60
	ST1	12	144	136	148	176	12	44	52	68	80
	ST2	12	92	132	104	120	12	56	36	40	52
	ST3	12	180	112	112	124	12	40	52	52	68
Serine	*Control*	3	18	33	51	75	3	15	18	27	33
	ST1	3	15	30	42	66	3	15	18	24	30
	ST2	3	15	27	45	72	3	15	18	27	27
	ST3	3	12	18	33	57	3	12	15	18	24
Glycine	*Control*	16	82	84	92	104	16	30	24	28	32
	ST1	16	82	80	94	108	16	24	24	28	30
	ST2	16	88	92	102	116	16	26	26	28	28
	ST3	16	88	88	102	110	16	22	24	26	28

Table 7.5.6: [U-^{13}C$_6$]glucose and [U-^{13}C$_5$]glutamine supplemented as substrates. The carbon profile for hESC derived hepatocyte-like cells is shown over time [h]. The sub-toxic concentrations are abbreviated as ST1-ST3, being 100 µM, 200 µM and 400 µM diclofenac, respectively.

Substrate	Time [h]	Concentration [C-µmol/L]					Uptake [C-µmol/L]				
		0	16	24	36	48	0	16	24	36	48
Glucose	*Control*	59628	40368	28284	21564	13224	0	19260	31344	38064	46404
	ST1	59628	53028	50352	42876	40332	0	6600	9276	16752	19296
	ST2	59628	45252	45480	42912	40752	0	14376	14148	16716	18876
	ST3	59628	50088	50148	48612	53640	0	9540	9480	11016	5988
Glutamine	*Control*	17960	16200	15905	14685	14505	0	1765	2060	3275	3455
	ST1	17960	15720	15705	14875	14740	0	2240	2255	3085	3220
	ST2	17960	15885	15545	15125	14695	0	2080	2415	2835	3270
	ST3	17960	14910	14755	14150	14185	0	3050	3205	3810	3775

Table 7.5.7: Concentrations [µmol/L], carbon concentration [C-µmol/L] over time, ^{13}C-mass isotopomer concentration [C-µmol/L] from [U-^{13}C$_6$]glucose or [U-^{13}C$_5$]glutamine over time [h], quantified by HPLC and analyzed by GC/MS for hESC derived hepatocyte-like cells exposed to diclofenac in four concentrations.

Metabolite	Time [h]	Concentration [µmol/L]					Concentration [C-µmol/L]				
		0	16	24	36	48	0	16	24	36	48
Lactate	Control	0	4512	8244	9914	14098	0	13536	24732	29742	42294
	ST1	0	2008	2216	4026	5062	0	6024	6648	12078	15186
	ST2	0	2138	3292	4264	5244	0	6414	9876	12792	15732
	ST3	0	1672	2050	2224	3754	0	5016	6150	6672	11262
Alanine	Control	919	1048	1136	1125	1198	2757	3144	3408	3375	3594
	ST1	919	1001	1042	1077	1187	2757	3003	3126	3231	3561
	ST2	919	982	1016	1083	1168	2757	2946	3048	3249	3504
	ST3	919	980	1017	1091	1165	2757	2940	3051	3273	3495
Glutamate	Control	373	168	93	70	28	1865	840	465	350	140
	ST1	373	163	53	25	23	1865	815	265	125	115
	ST2	373	150	52	26	26	1865	750	260	130	130
	ST3	373	233	210	42	30	1865	1165	1050	210	150
Proline	Control	343	368	411	440	478	1715	1840	2055	2200	2390
	ST1	343	390	414	465	456	1715	1950	2070	2325	2280
	ST2	343	346	365	409	452	1715	1730	1825	2045	2260
	ST3	343	353	393	388	434	1715	1765	1965	1940	2170
Aspartate	Control	220	28	19	18	14	880	112	76	72	56
	ST1	220	28	15	14	14	880	112	60	56	56
	ST2	220	28	15	15	15	880	112	60	60	60
	ST3	220	55	33	5	6	880	220	132	20	24
Serine	Control	110	102	101	84	84	330	306	303	252	252
	ST1	110	90	87	81	85	330	270	261	243	255
	ST2	110	92	86	88	91	330	276	258	264	273
	ST3	110	89	85	84	90	330	267	255	252	270
Glycine	Control	613	569	561	523	519	1226	1138	1122	1046	1038
	ST1	613	537	541	531	565	1226	1074	1082	1062	1130
	ST2	613	561	545	562	583	1226	1122	1090	1124	1166
	ST3	613	531	537	547	577	1226	1062	1074	1094	1154

Metabolite	Time [h]	^{13}C-mass isotopomer concentration [C-µmol/L] from [U-^{13}C$_6$]glucose					^{13}C-mass isotopomer concentration [C-µmol/L] from [U-^{13}C$_5$]glutamine				
		0	16	24	36	48	0	16	24	36	48
Lactate	Control	0	11055	20766	25488	37089	0	180	336	417	606
	ST1	0	4578	5307	9897	12627	0	72	87	171	228
	ST2	0	4608	7623	10044	12609	0	78	138	186	228
	ST3	0	150	135	132	213	0	78	102	132	213
Alanine	Control	39	693	1194	1659	2148	39	39	45	45	51
	ST1	39	468	591	906	1170	39	36	45	51	60
	ST2	39	414	561	759	1059	39	36	42	51	60
	ST3	39	237	54	72	81	39	45	54	72	81
Glutamate	Control	20	200	110	115	55	35	110	90	100	35
	ST1	20	315	125	70	65	20	70	75	20	35
	ST2	20	350	135	70	70	20	75	40	25	35
	ST3	20	145	190	60	55	20	145	190	60	55
Proline	Control	35	90	125	200	250	35	80	110	190	245
	ST1	35	95	140	230	240	35	70	90	145	195
	ST2	35	75	105	155	205	35	55	75	140	210
	ST3	35	70	120	160	210	35	70	120	160	210
Aspartate	Control	52	28	24	28	24	48	8	4	4	4
	ST1	52	20	12	12	16	52	8	4	8	4
	ST2	52	28	16	16	16	52	12	8	8	8
	ST3	52	48	28	4	4	52	48	28	4	4
Serine	Control	6	39	51	57	63	6	6	6	3	3
	ST1	6	9	12	15	18	6	3	6	3	3
	ST2	6	9	12	15	18	6	3	3	3	3
	ST3	6	9	3	3	3	6	9	3	3	3
Glycine	Control	14	22	28	38	42	14	16	16	14	12
	ST1	14	16	16	18	20	14	14	16	16	14
	ST2	14	16	16	18	22	14	16	14	14	16
	ST3	14	14	14	14	14	14	14	14	14	14

XXX